“Visible light photoredox catalysis: a versatile tool for the activation and formation of aromatic compounds”

Dissertation

Zur Erlangung des Doktorgrades der Naturwissenschaften

Dr. rer. nat.

an der Fakultät für Chemie und Pharmazie

der Universität Regensburg

vorgelegt von

Michael Neumeier

aus Friedberg

Regensburg 2019

The experimental part of this work was performed from February 2016 to March 2018 at the Institute of Organic Chemistry, University of Regensburg and from April 2018 to July 2019 at the Institute of Inorganic and Applied Chemistry, University of Hamburg under the supervision of Prof. Dr. Axel Jacobi von Wangelin.

Date of thesis submission:		11.09.2019
Date of thesis defense:		11.10.2019
Board of examiners:	Chairman:	Apl. Prof. Dr. Rainer Müller
	1st Referee:	Prof. Dr. Axel Jacobi von Wangelin
	2nd Referee:	Prof. Dr. Julia Rehbein
	Examiner:	Prof. Dr. Arno Pfitzner

Meiner Familie

1 Introduction

Solar radiation is by far the most ubiquitous, persistent and sustainable source of energy on our planet. From the earliest days of the Earth, nature itself has capitalized from sunlight as the driving force for evolution. Natural processes regarding light have been noticed and studied by human kind ever since. Some selected examples are the light induced bleaching of paintings and textiles observed by the Egypts even before Christ, the report on fluorescence of lignum nephriticum by Niccolo Monardes in the 16th century or the first photographs on silver paper by Davy and Wedgewood around 1800.[1] With the ongoing progress in science during the 19th and early 20th century, chemists discovered most of the nowadays well-known photochemical textbook reactions, such as Paterno-Büchi reaction, Norrish-fragmentation, photoisomerizations and radical halogenations.[2] A name that deserves special credit during these days is Giacomo Luigi Ciamician, an Italian researcher, who was one of the first people at the time to actively screen and target photochemical reactions by exposing his reaction mixture to the Italian sunshine (Figure 1-1).[3]

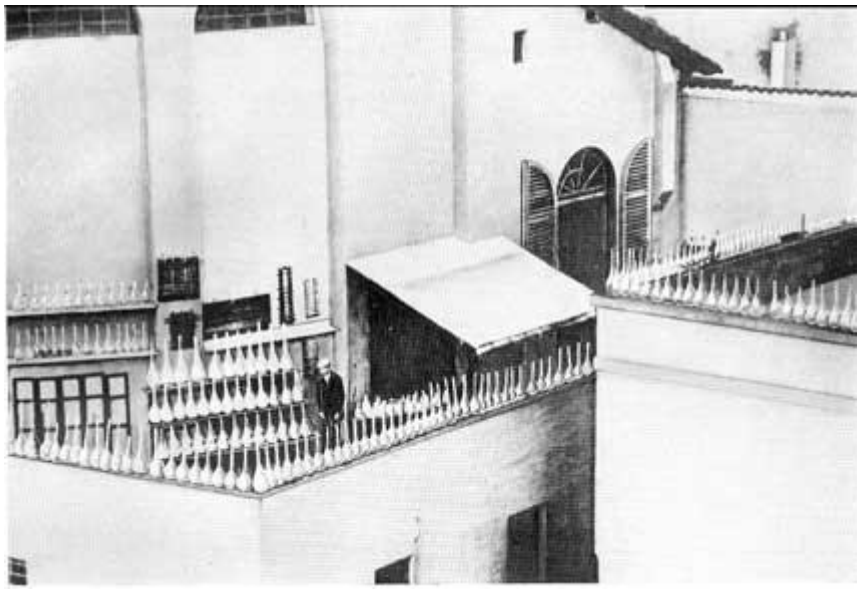

Figure 1-1. Giacomo Ciamician surveying his collection of tubes and flasks being exposed to the sun on the roof of his laboratory.[3a]

The UV part of solar radiation is filtered to a great extend by the atmosphere. Hence, this “oldschool” photochemistry features some issues with reproducibility and mostly predictability in selectivity. A lot of modern photochemical researchers turned their focus from the rather unselective UV-light catalyzed reactions to transformations enabled by the visible section of the solar spectrum. This new approach had one distinct problem to face, namely most organic molecules being colourless and thus lacking the ability to absorb visible light. A solution was provided by the employment of colourful organic and inorganic dyes (photocatalysts) as additives. These compounds can either transfer energy or an electron to another (substrate) molecule

(Scheme 1-1).[4] By absorption of a photon in the ground-state (S_0) the photocatalyst is excited into its singlet excited state (S_1) and after intersystem-crossing (ISC) reaches the triplet excited state (T_1). By looking at the electronic situation in the HOMO and LUMO of these states, it becomes clear that the former empty HOMO of S_0 transforms into a HOMO occupied with a single electron in S_1 or T_1 and the former fully occupied LUMO of S_0 transforms into a LUMO occupied with a single electron in S_1 or T_1. Overall, this leads to a higher oxidation as well as reduction power in the excited states compared to the ground state or in other words, the excited photocatalyst can serve as a better electron donor and acceptor for different kind of substrates than the ground state (Scheme 1-1).[5] One of the most commonly employed dyes is $Ru(bpy)_3Cl_2$.[6]

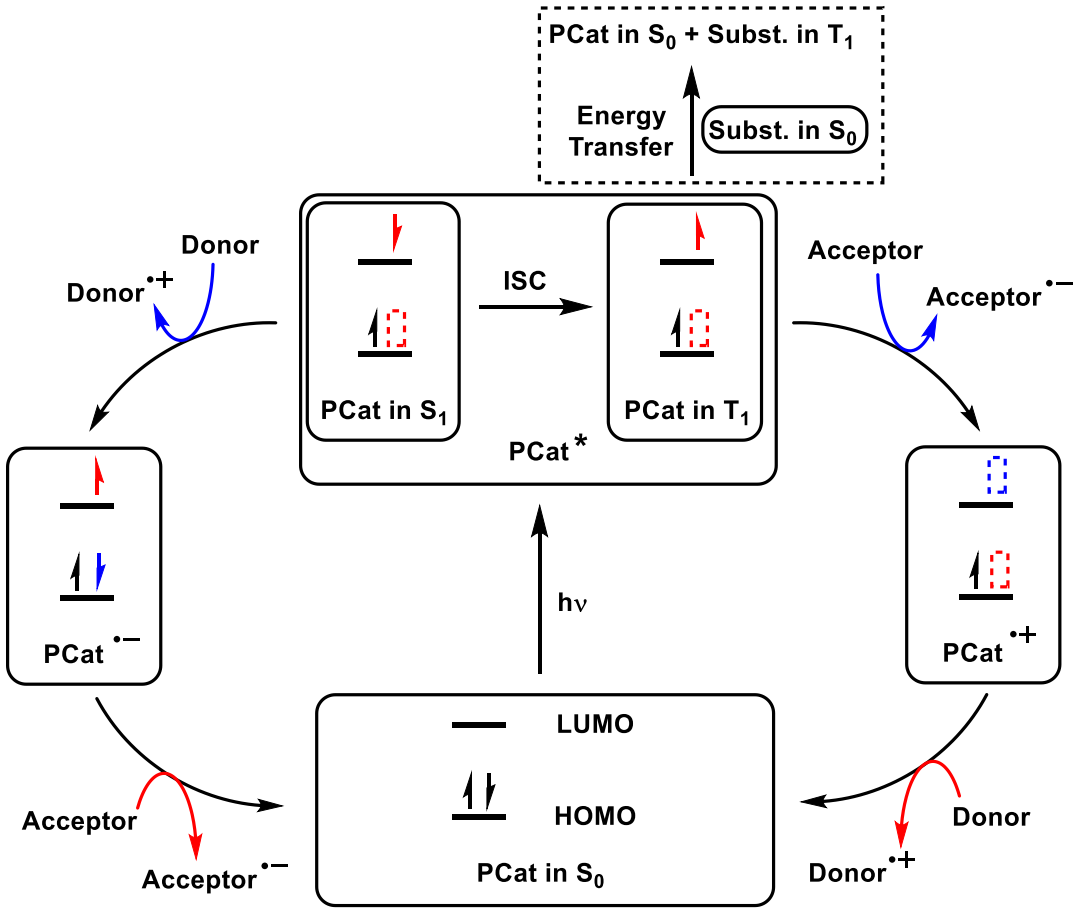

Scheme 1-1. The concept of photoredox catalysis focusing on the conceptual HOMO-LUMO situations in different states of the photocatalyst (PCat).

A prominent example and an early milestone in the field of socalled “photoredox-catalysis” was the photocatalytic “Pschorr-Reaction” reported by Cano-Yelo and Deronzier in 1984.[7] Technical progress (cheap and easily handable LED’s) and changing morals in society (endeavor towards sustainability) have initiated a veritable hype of photo(redox)catalysis over the last decade.[4-6] Science became aware of the great potential that lies in the unthinkable amount of unexploited energy of solar radiation and the new transformations that could be enabled by visible-light driven photo(redox)catalysis. In 2008 the MacMillan group published a seminal report on the

combination of an organo- and a photoredox-catalytic cycle.[8] This was the kickstart for a huge amount of publications on the field of dual catalysis.[9] Organic photoredox catalysis and photocatalytic arylations are two chapters that have prospered around 2010.[10] A couple of years later, the MacMillan group proved their pioneering status in photochemical research again with the introduction of a new dual catalytic branch called “metallaphotoredox catalysis”.[11] A great amount of people hopped on the train of merging photoredox with transition metal catalysis which led to numerous high impact publications on this specific field.[12] Activation of bonds exceeding the energy provided by a single visible photon still exhibits a great challenge for photochemists and has drawn quite some attention of the community lately.[13]

The scope of this work was directed towards the development of new methodologies in the flourishing fields of classical photoredox catalysis,[14] multiple photon (upconversion) processes[15] and metallaphotoredox catalysis.[16] These concepts served as a versitale tool for the exemplary activation and formation of aromatic compounds.

---

[1] I. Plutnikov, *Allgemeine Photochemie*, 2nd Ed., Walter de Gruyter, Berlin, **1936**.

[2] a) E. Paterno, *Gazz. Chim. Ital.* **1909**, 39, 237-250; b) R. G. W. Norrish, F. W. Kirkbride, *J. Chem. Soc.* **1932**, 1518-1530; c) W. H. Perkin, *J. Chem. Soc.* **1881**, *39*, 409-452; d) J. Schramm, *Ber. Dtsch. Chem. Ges.* **1884**, *17*, 2922-2925.

[3] a) Figure 1-1 is copied from: G. Nebbia, G. B. Kauffman, *Chem. Educator* **2007**, *12*, 362-369; b) G. Ciamician, *Science* **1912**, *36*, 385-394.

[4] a) A. G. Griesbeck, M. Oelgemoeller, F. Ghetti, *CRC Handbook of Organic Photochemistry and Photobiology*, 3rd ed., CRC Press, Boca Raton, **2012**; b) V. Balzani, P. Ceroni, A. Juris, *Photochemistry and Photophysics: Concepts, Research, Applications*, Wiley-VCH, Weinheim, **2014**.

[5] K. Zeitler, *Angew. Chem. Int. Ed.* **2009**, *48*, 9785-9789.

[6] C. K. Prier, D. A. Rankic, D. W. C. MacMillan, *Chem. Rev.* **2013**, *113*, 5322-5363.

[7] H. Cano-Yelo, A. Deronzier, *J. Chem. Soc. Perkin Trans. II* **1984**, 1093-1098.

[8] D. A. Nicewicz, D. W. C. MacMillan, *Science* **2008**, *322*, 77-80.

[9] a) M. N. Hopkinson, B. Sahoo, J.-L. Li, F. Glorius, *Chem. Eur. J.* **2014**, *20*, 3874-3886; b) K. L. Skubi, T. R. Blum, T. P. Yoon, *Chem. Rev.* **2016**, *116*, 10035-10074.

[10] a) M. Majek, A. Jacobi von Wangelin, *Acc. Chem. Res.* **2016**, *49*, 2316-2327; b) I. Gosh, L. Marzo, A. Das, R. Shaikh, B. König, *Acc. Chem. Res.* **2016**, *49*, 1566-1577.

[11] Z. Zuo, D. T. Ahneman, L. Chu, J. A. Terrett, D. W. C. MacMillan, *Science* **2014**, *345*, 437-440.

[12] J. Twilton, C. Le, P. Zhang, M. H. Shaw, R. W. Evans, D. W. C. MacMillan, *Nature Reviews Chemistry* **2017**, *1*, 0052.

[13] a) B. D. Ravetz, A. B. Pun, E. M. Churchill, D. N. Congreve, T. Rovis, L. M. Campos, *Nature* **2019**, *565*, 343-346; b) I. Gosh, B. König, *Angew. Chem. Int. Ed.* **2016**, *55*, 7676-7679.

[14] see chapter 3.

[15] see chapter 2 and 4.

[16] see chapter 5.

2 Capturing and harnessing the energy of multiple photons for photoredox catalysis[i,ii]

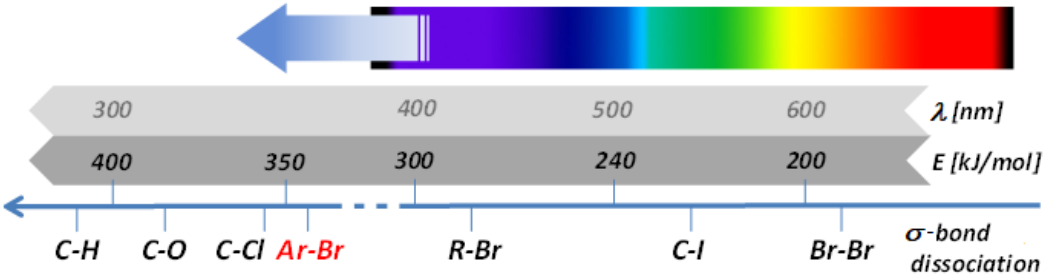

Photocatalytic transformations are generally limited by the photon energy. Traditional photoredox catalysis tries to overcome this issue by the use of activated substrates. A great potential for challenging bond activations keep photophysically well-established upconversion processes. Highly energetic intermediates, such as excited doublet states, can be generated via different excitation sequences (photon/photon, photon/electron/photon). Employment of the latter for synthethic organic transformations has received remarkable attention over the last few years. This chapter aims to summarize the recent advances in this field.

[i] This chapter will be published as a minireview: “Capturing and harnessing the energy of multiple photons for photoredox catalysis”, M. Neumeier, A. Jacobi von Wangelin in an appropriate peer-review journal. Schemes, tables and text may differ from published version.

[ii] Author contributions: M.N. performed the literature research and wrote the manuscript. A.J.v.W. guided the project and contributed to the writing of the manuscript.

2.1 Introduction

Over the past decade, photoredox catalysis has significantly expanded the toolbox of modern organic synthesis for the construction of structural complexity and diversity in natural products, fine chemicals and polymeric materials.[1] However, most of the photocatalytic protocols are premised on the formation of carbon centered radicals adjacent to heteroatomic substituents (amines/ imines/enamines, carbonyls, malonates, etc.) and aryl moieties,[1] or alternatively rely on irreversible reaction steps.[2] Non-activated substrates have received less attention, primarily due to the intrinsic limitation that their activation by visible light through “traditional” photoredox catalysis is not feasible. The energy provided by a single visible photon (170-300 kJ mol^{-1}) is merely sufficient for the cleavage of weak C-I, C(sp^3)-Br and π-bonds. Activation of stronger Ar-Br (bond dissociation energy of Ph-Br: 346 kJ mol^{-1}), C-Cl, C-O or even C-H bonds either requires the use of UV-irradiation,[3] or elaborate dual activation mechanisms such as the combination of photoredox and transition metal catalysis.[4] However, low-energy irradiation and mild reaction conditions lie at the heart of ensuring broad functional group tolerances as well as high stability of the photocatalyst. Thus, upconversion processes have recently attracted increased attention from the synthetic community as they carry the potential of bypassing the energy limitations of a visible light photon. In the following minireview we provide insights into the recent developments in organic chemistry that make use of triplet-triplet annihilation (TTA), excited doublet states and photoionizations as new methodologies for the utilization of multiple visible light photons for the activation of challenging substrates such as aryl halides. These three concepts, by no means encompass the complete range of possibilities for energy upconversion technologies, however, they are the only ones to find themselves in synthetic organic laboratories, thus far.

2.2 Application of triplet-triplet annihilation (TTA) upconversion to photoredox catalysis

Triplet-triplet annihilation (TTA) upconversion (UC) is a photo-chemical process discovered by Parker and Hatchard dating back to the 1960s that describes the generation of a single high energy photon (from a highly energetic excited state) by the investment of two lower-energy photons.[5] In recent years, this methodology has found various applications in the form of upconverting nanoparticles or via solid state TTA-UC in solar cells,[6] bioimaging,[7] phototherapy,[8] displays,[9] and data storage technology.[10] While mechanistic and photochemical details in solution are well-investigated,[11] examples for synthetic chemical applications using TTA-UC have been scarce until today. A generalized mechanism (Scheme 2-1) starts with the long-wavelength selective excitation of a sensitizer ^{1}[Sen], followed by intersystem crossing (ISC) to its triplet state ^{3}[Sen]*. This molecule then undergoes a triplet-triplet energy transfer (TTET) to a ground-state emitter molecule ^{1}[Em]. The TTET process proceeds via a Dexter-type mechanism, regenerates the ground-state sensitizer and converts the emitter to its triplet state ^{3}[Em]*. If two of these ^{3}[Em]* molecules collide,

spin-allowed TTA leads to disproportionation of the emitter pair in one highly energetic singlet state molecule ^{1}[Em]* and one ground-state molecule ^{1}[Em]. With respect to the quantum mechanical tensor product of the initial spin states in ^{3}[Em]*, their encounter complex can only dissociate in 1 out of 9 cases (9 Eigenstates of the encounter complex are possible) into ^{1}[Em]*, thus limiting the TTA efficiency to ca. 11%, regardless of further deactivation processes and energy losses.[12] ^{1}[Em]* features a characteristic anti-Stokes shifted delayed fluorescence $h\nu_2$ of an intensity that displays a quadratic dependence on the excitation light power as TTA is a biphotonic process between two ^{3}[Em]* molecules. The excited singlet emitter can further undergo classical energy or single electron transfer chemistry in the presence of a substrate molecule.

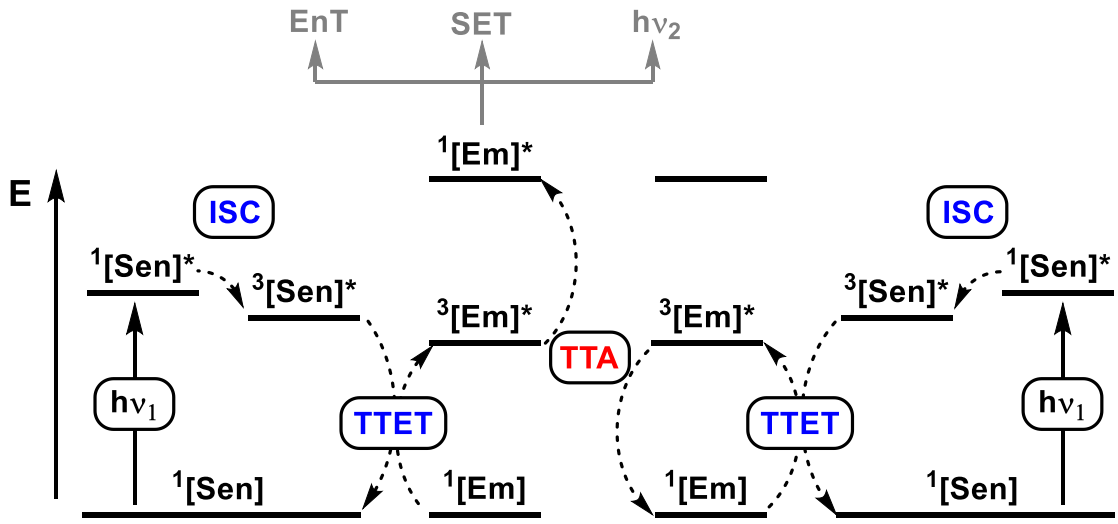

Scheme 2-1. Simplified mechanism of TTA-UC; Sen = sensitizer; Em = emitter; ISC = intersystem crossing; TTET = triplet-triplet energy transfer; EnT = energy transfer; SET = single electron transfer; $h\nu_2$ = delayed fluorescence.

Versatile sensitizer molecules should feature an absorption in the range of visible or NIR light and possess a relatively long triplet excited state lifetime (up to microseconds). Furthermore, the energy of ^{3}[Sen]* has to lie higher than the energy of ^{3}[Em]* to allow for a favorable TTET process. The energy level of ^{1}[Em]* must be lower or equal to the double ^{3}[Em]* energy, thus leading to an energetic leveling of ^{1}[Em]* > ^{1}[Sen]* > ^{3}[Sen]* > ^{3}[Em]*. A broad range of sensitizers and emitters have been shown to be viable for TTA upconversion.[7] Transition metal complexes such as Pd or Pt porphyrin derivates are widely applied sensitizers due to their increased spin-orbit-coupling that leads to a highly efficient ISC and relatively long triplet lifetimes in these complexes. [7] Suitable emitters are usually represented by small organic molecules with an absorption in the UV-A or UV-B range of the electromagnetic spectrum and an emission in the blue or UV-A respectively.[7] Another class of emitters that has recently attracted a lot of attention recently are BODIPY chromophores.[7] To date, suitable sensitizer/emitter pairs for almost any wavelength upconversion in the

visible spectrum are known (selected examples are shown in Figure 2-1), including systems approaching 1 eV of upconversion energy.[7]

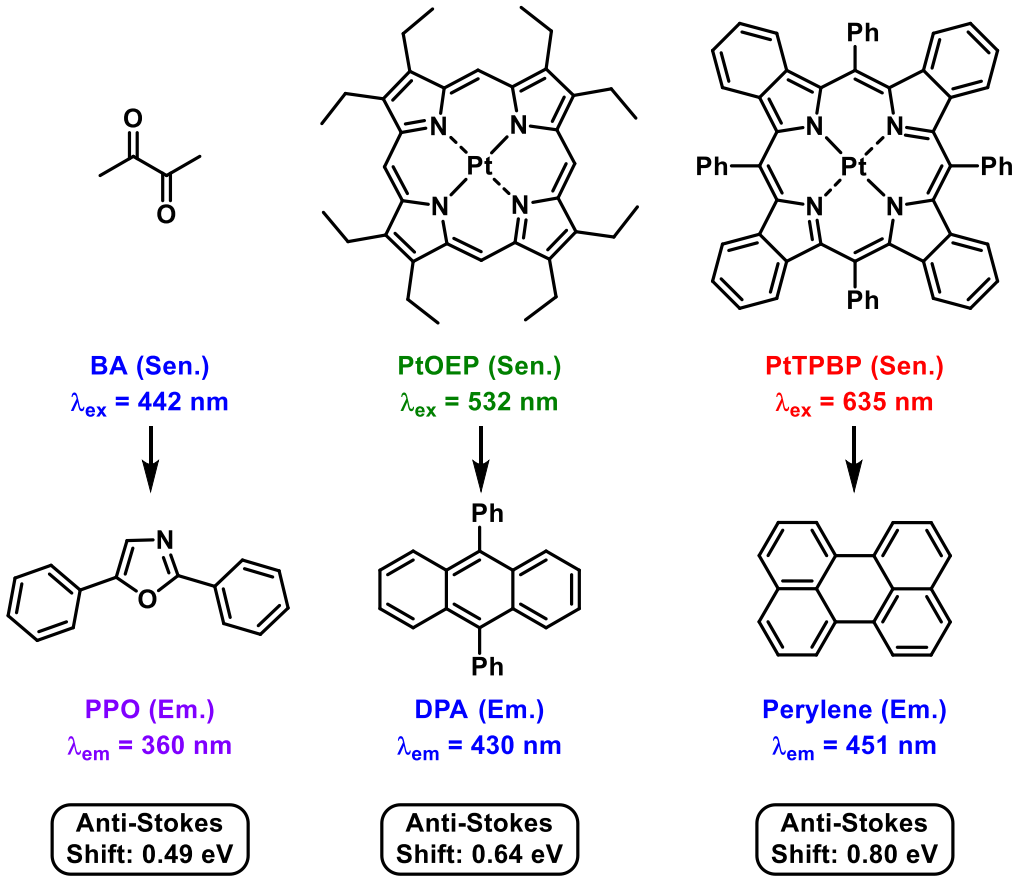

Figure 2-1. Selected examples of sensitizer/emitter pairs and their respective excitation wavelength (λ_{ex}), emission wavelength (λ_{em}) and anti-Stokes shifts of the delayed fluorescence; PPO = 2,5-diphenyloxazole; PtOEP = platinum(II) octaethylporphyrin; PtTPBP = platinum(II)-tetraphenyltetrabenzoporphyrin; BA = biacetyl; DPA = 9,10-diphenylanthracene.

In 2015 our group published the first report of a TTA-UC process employed for chemical bond activation in a photoredox catalytic protocol.[13] We made use of the previously established sensitizer/emitter pair BA/PPO to promote the dehalogenation of aryl bromides under blue laser pulse irradiation (Scheme 2-2a).[9] Transient spectroscopy, quenching studies, and DFT calculations provided strong indications for the formation of highly reducing ^{1}PPO* (-2.14 V vs. SCE) and its subsequent SET to the aryl bromide. Fragmentation of Ar-Br$^{\bullet-}$ to an aryl radical,[14] followed by hydrogen atom transfer from the solvent afforded the reduced benzene. Thereafter, we were able to achieve similar photoreduction of several aryl bromides by the use of a green-to-blue TTA-UC system (PtOEP/DPA) in a confined gel matrix under aerobic conditions.[15] Considering the inclination of oxygen towards the quenching of triplet excited states, performing TTA-UC under air is still a big challenge today. Two years later, Perez-Ruiz et al. extended the established aryl bromide activation towards C-C coupling reactions between several aryl halides and *N*-methyl pyrrole.[16] Under blue light irradiation with a simple laser pointer, highly reducing ^{1}DPA* was generated via

TTA-UC sensitized by a diiodoBOPHY-like derivative. Without the need for a complex and expensive pulsed laser setup this work paves the way for TTA-UC applications in standard laboratories. More recently, Rovis and Campos demonstrated the versatility and flexibility that was long anticipated, but, until their seminal report, was unachieved by TTA-UC.[17] By using a porphyrine based near infrared (NIR) sensitizer combined with furanyldiketopyrrolo-pyrrole (FDPP) as an emitter (λ_{em} = 530 nm) they were able to employ the TTA system as an internal light source for common photoredox catalyst such as Eosin Y or Rose Bengal in well-established photoreactions like aliphatic hydride-halogenations, oxidations (Scheme 2-2b) and radical cyclizations.[17]

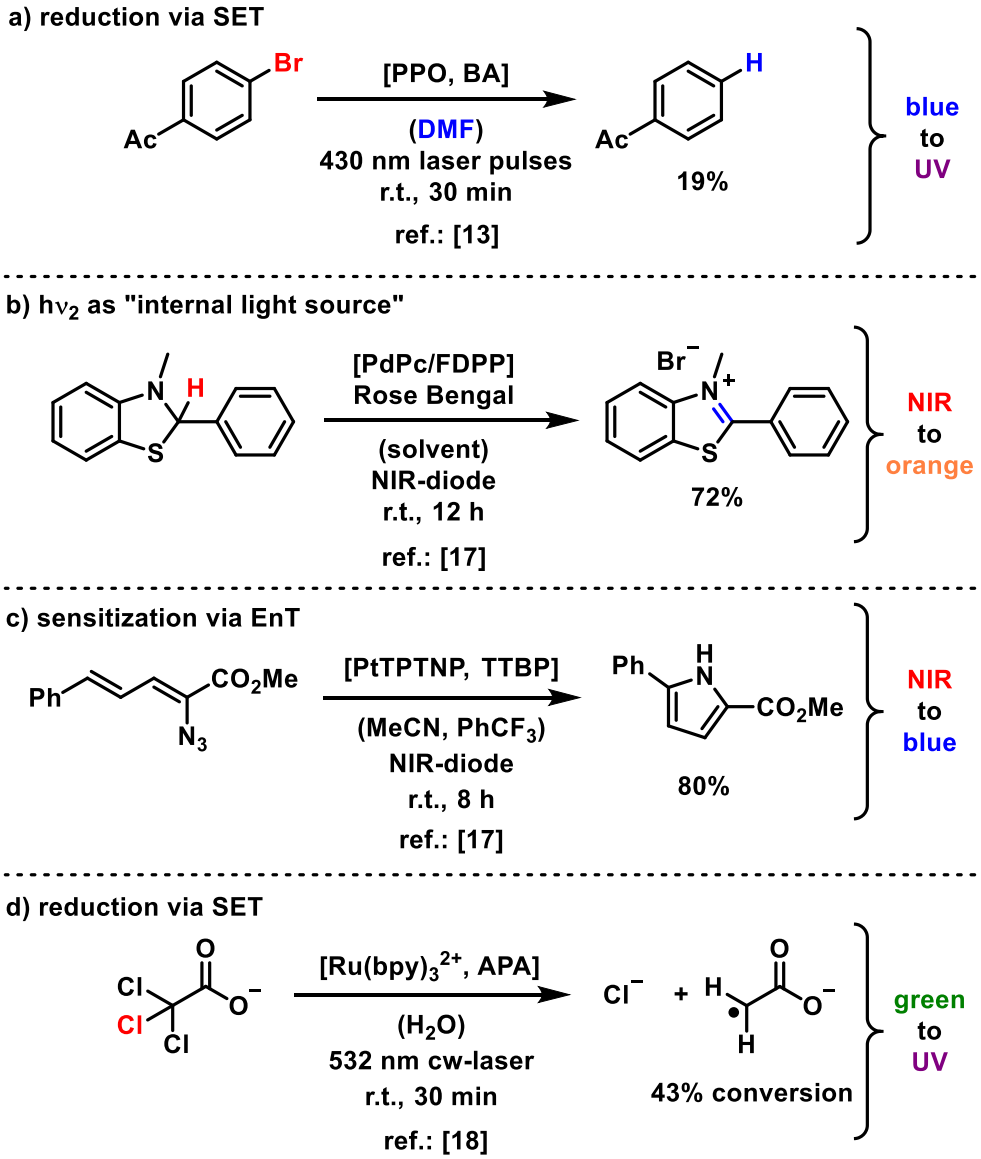

Scheme 2-2. Selected examples for synthetical applications of TTA-UC.

As the employed NIR-diode is 100-1000 times weaker in terms of lamp power than direct illumination of Rose Bengal, the authors proposed a large increase of net illumination area by formation of internal “light-bulbs” deep inside the reaction

mixture.[17] With slight changes to the sensitizer/emitter pair (PtTPTNP, TTBP), NIR-to-blue upconversion was achieved and classical photo-sensitization chemistry from ^{1}TTBP* on the example of vinylazides was demonstrated (Scheme 2-2c).[17] Additionally, a major advantage of NIR-to-visible upconversion was demonstrated in the case of photoinduced radical polymerization of methyl methacrylate (MMA) via C-Br bond reduction of the initiator. Several filter materials, such as an haemoglobin solution or pig skin, were tested in the polymerization (gel formation) of MMA, revealing a penetration power of the NIR-to-blue upconversion system that is 300 times higher than direct irradiation with blue light, thus addressing one of the biggest issues for industrial photochemical applications: scale-up limitations due to illumination penetration issues in consequence of the Beer-Lambert law.[17]

In 2018 Wenger and Kerzig demonstrated that TTA-UC for synthetic applications is not only limited to organic solvents, but can also be employed in water as the most environmentally friendly solvent.[18] $Ru(bpy)_3^{2+}$ and anthracenepropionate (APA) as a water-soluble sensitizer/emitter pair for green-to-UV upconversion were employed for the dechlorination of trichloroacetate under irradiation with a green continuous wave laser (Scheme 2-2d). To complete this section on TTA-UC, a report by the Koenig group from 2017, which was initially proposed to operate via sensitization-initiated electron transfer and was later also under discussion to be operating via TTA-UC activation, has to be mentioned.[19]

2.3 Photoredox catalysis with excited doublet states by consecutive photoinduced SET cascades

Excited doublet states provide another reservoir of high energy intermediates inaccessible via single photon absorption from the neutral ground state. While the (photo-)physical properties of organic doublet states have been fairly well investigated since the 1980s,[20] their excited state applications and understanding of the mechanistic progress in organic synthesis is still limited. A simplified graphical representation of the process for reductive substrate activation is expected to appear as follows: after absorption of the first photon the photocatalyst (PC) is excited to PC* and the first single-electron transfer (SET) from a donor-molecule D to PC* generates the radical ion pair $PC^{\bullet-}$ and $D^{\bullet+}$ (Figure 2-2, top). If the radical anion of the photocatalyst in the ground state is reasonably stable it can absorb a second photon and generate a superreducing excited doublet state $PC^{\bullet-}$*. In a second photo-induced SET from $PC^{\bullet-}$*, substrates can be activated and the photocatalyst is regenerated in its ground state to close the catalytic cycle. The key feature for the biphotonic generation of such high energy states, is the storage of the first photon's energy in a radical ion. While the chemical and photocatalytic generation of radical anions of common photocatalysts and their ground-state lifetime is well known,[20,2] their excited state lifetimes as well as the absorption of PC and $PC^{\bullet-}$ are the crucial factors for application in synthetic laboratories. A variety of commercial dyes that fulfill these criteria via visible light irradiation are available e.g.: perylenediimines, rhodamine 6G and 9,10-dicyanoanthracene (Figure 2-2, bottom).

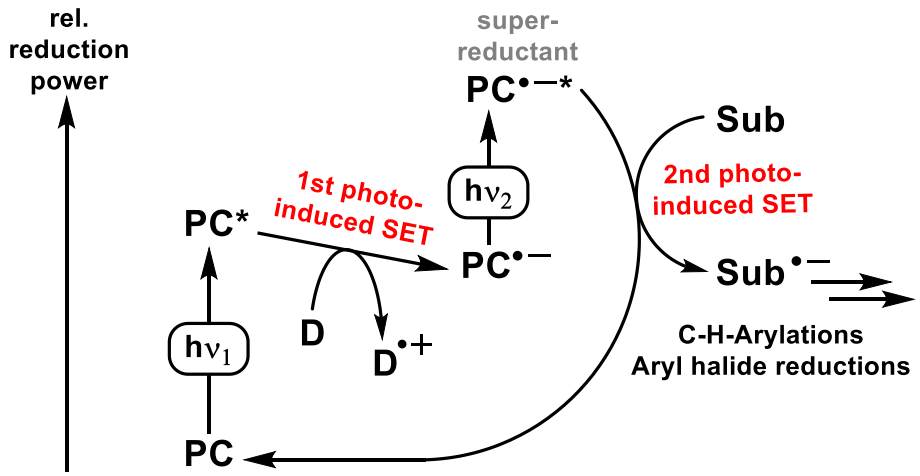

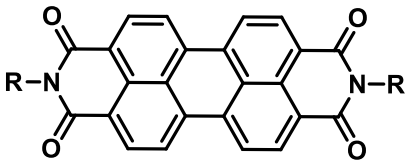

Perylenediimines (PDIs)

R = dipp :

λ_{max} (PDI) = ca. 520 nm

λ_{max} (PDI$^{\bullet-}$) = ca. 700 nm

E_{ox} (PDI$^{\bullet-}$*) = ca. -2.2 V

τ (PDI$^{\bullet-}$*) = ca. 145 ps

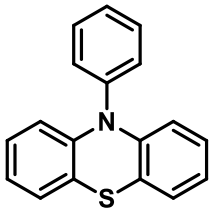

10-Phenyl-10*H*-phenotiazine (PTZ)

λ_{max} (PTZ) = ca. 321 nm

λ_{max} (PTZ$^{\bullet+}$) = ca. 514 nm

E_{ox} (PTZ$^{\bullet+}$*) = ca. +2.1 V

τ (PTZ$^{\bullet+}$*) = ca. 32 ps

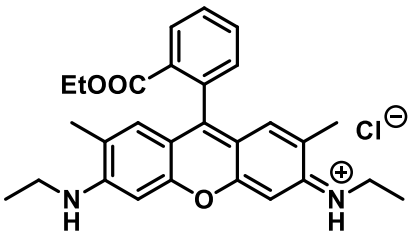

Rhodamine 6G (Rh6G)

λ_{max} (Rh6G) = ca. 530 nm

λ_{max} (Rh6G$^{\bullet-}$) = ca. 425 nm

E_{ox} (Rh6G$^{\bullet-}$*) = ca. -2.4 V

E_{ox} (Rh6G$^{\bullet-}$* + LnI_2) = ca. -3.1 V

τ (Rh6G$^{\bullet-}$*) = ca. 8 ns

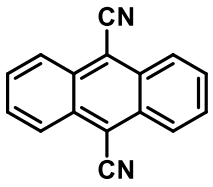

9,10-Dicyanoanthracene (DCA)

λ_{max} (DCA) = ca. 420 nm

λ_{max} (DCA$^{\bullet-}$) = ca. 510 nm

E_{ox} (DCA$^{\bullet-}$*) = ca. -2.5 V

τ DCA$^{\bullet-}$*) = ca. 5 ns

Figure 2-2. General mechanistic proposal (top) for reductive substrate activation; selected photocatalysts and their properties for substrate activations from excited doublet states; redox potentials are given vs. SCE.

In 2014, the group of Koenig published a seminal report on the reduction of aryl halides by an excited doublet state of perylenediimine (PDI).[21] Under blue light irradiation and in presence of NEt_3, several challenging aryl iodides, -bromides, and even -chlorides could be activated. After the second photo-induced SET and consecutive fragmentation of the $Ar\text{-}X^{\bullet-}$,[14] an aryl radical is formed that can either undergo hydrogen abstraction from triethylamine or the solvent (DMF) to form the reduced benzene product, or in the presence of a high excess of pyrrole derivatives participates in a C-C coupling reaction to generate arene-substituted pyrroles (Scheme 2-3, top).[21] Poor solubility, a strong tendency for aggregation and self-quenching are intrinsic limitations of the homogeneous PDI system, which were overcome by a heterogeneous approach employing the incorporation of PDI into a metal-organic polymer Zn-PDI by Duan et al..[22] In 2018, Lin et al. investigated the influence of substituents on the crucial bay position of regular PDI towards its photocatalytic reactivity, as well as optical and redox properties.[23] With the scope and reaction conditions adapted from Koenig's paper, they showed that electron-withdrawing substituents enhance reactivity while electron-donating substituents decrease the reaction rate.[23] As promising as the original Koenig protocol appears, the key features of $PDI^{\bullet-}$/ $PDI^{\bullet-*}$ (λ_{max} = 700 nm, τ = 145 ps)[20b] and their inconsistencies (455 nm irradiation) with the established procedure encouraged the scientific community for detailed investigations on the reaction mechanism. During these studies, an alternate active catalyst species could not be identified, however, the researchers provide data indicating that $PDI^{\bullet-*}$ may not be the ultimate reducing species, but some of its degradation products may overtake this role.[24] Two years after their pioneering article, the Koenig group discovered Rhodamine 6G (Rh6G) to be similarly active in analogous chemical transformations like those of PDI.[25] With absorption maxima of 530 nm (for Rh6G) and 425 nm (for $Rh6G^{\bullet-}$), a lifetime of ca. 8 ns in the excited doublet state $Rh6G^{\bullet-*}$ and an estimated oxidation potential of E_{ox} ($Rh6G^{\bullet-*}$) = -2.4 V vs. SCE,[26] Gosh and Koenig were able to adjust the reduction potential of Rh6G and thus chromoselectively cleave multiple C-Br bonds in 1,3,5-tribromo-benzene depending on the employed LED's.[25] Using 530 nm irradiation only electron poor aryl bromides (E_{ox} ($Rh6G^{\bullet-}$) = -1.0 V vs. SCE) were activated in the presence of DIPEA as sacrificial donor and a large excess of pyrrole derivative to form the C-C coupling product. With 455 nm irradiation, the lamp emission fitted both the absorption of the ground-state Rh6G as well as its radical anion and hence the superreducing $Rh6G^{\bullet-*}$ allowed for use of non-activated aryl bromides for C-H arylation reactions.[25] The Koenig group applied their rhodamine protocol to several different substrate classes (Scheme 2-3, middle) such as bromoheteroarenes,[27] halogenated nucleobases,[28] and 1-(2-bromophenyl)-1*H*-pyrrole derivatives (trapped with terminal alkynes form pyrrolo[1,2-*a*]quinoline and ullazines).[29] A selection of these substrates was subjected to the same protocol substituting pyrroles as trapping agent by trialkyl phosphites, thus generating aryl phosphonates.[30] Addition of Lewis acidic lanthanide ions (DyI_2) further enhanced the overall oxidation potential in a proposed excited radical complex $[Rh6G^{\bullet}]/Dy^{3+}$ to such an amount that non-activated aryl chlorides (potentials ca. -3 V vs. SCE) became accessible to the photocatalytic C-H arylation chemistry.[31] In an elaborate effort towards the detailed aryl halide activation mechanism by $Rh6G^{\bullet-*}$, the

Koenig group teamed up with physicists from the Lupton group to monitor the reactivity and fate of Rh6G$^{\bullet-*}$ on a molecular level and supported the possibility of the proposed mechanism by simple model systems.[32] Additionally, they performed C-H arylations of aryl iodides and -bromides using 1,8-dihydroxyanthraquinone as the photocatalyst.[33] However, for this protocol, mechanistic details are more complex and the overall procedure is less efficient regarding yields and atom economy.

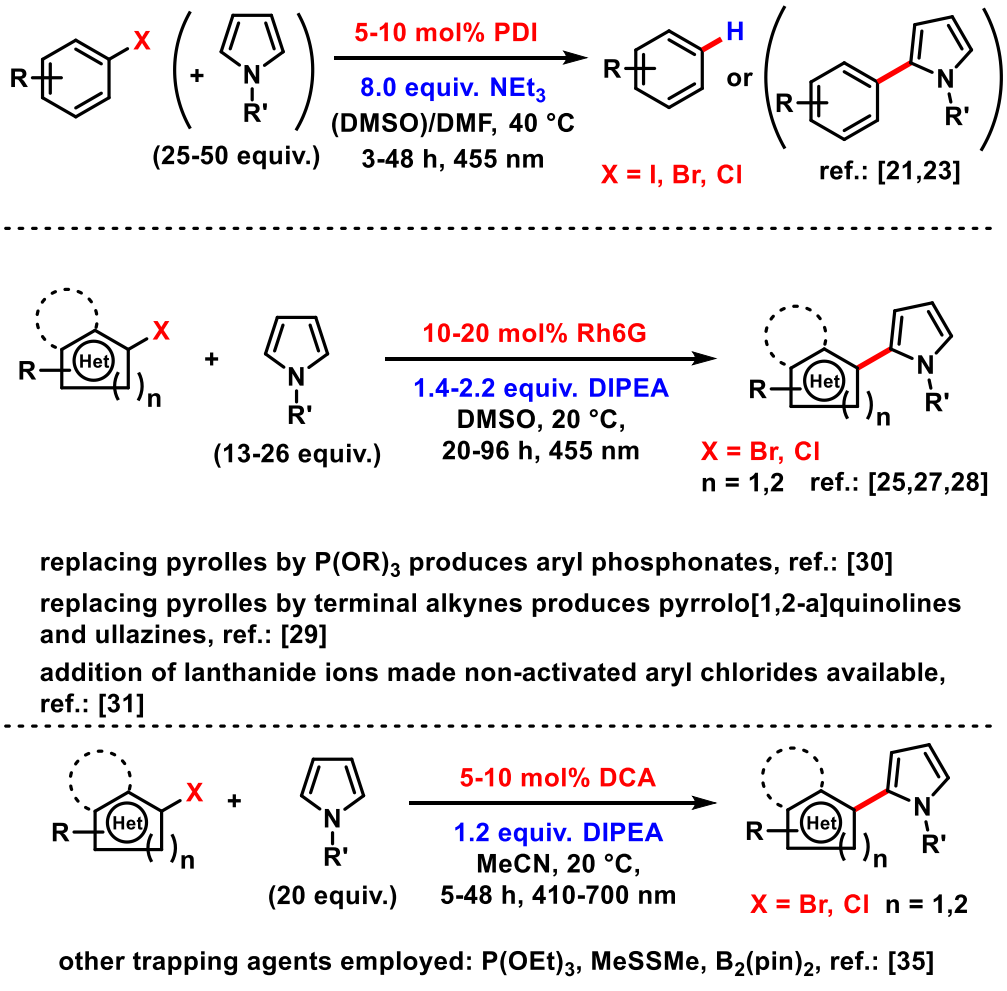

Scheme 2-3. Overview of reduction and cross coupling chemistry employing excited doublet states of PDI (top), Rh6G (middle) and DCA (bottom) as superreductants.

Another photocatalyst for this class of aryl halide activation, that has gained the attention of our group in 2018 is represented by 9,10-dicyanoanthracene (DCA) featuring absorption maxima of 420 nm (for DCA) and 510 nm (for DCA$^{\bullet-}$) and ca. 5 ns of lifetime of DCA$^{\bullet-*}$.[34,35] The biphotonic activation of DCA/ DCA$^{\bullet-}$ was achieved by employing a simple cold white LED setup and a catalytic amount of sacrificial donor DIPEA (10 mol%, 1eq. DIPEA required for Br^- trapping). Key features of our system were reduced catalyst loadings and shorter reaction times compared to the established Rh6G protocols as well as the expansion towards B- and S-based trapping agents (Scheme 2-3, bottom).[35] Furthermore, we provided a thermodynamic and kinetic

analysis towards the electron transfer from $DCA^{\bullet -*}$ to Ar-X based on DFT calculations.[35]

In all of the previously reported examples, bleaching of the organic photocatalyst and long reaction times due to catalyst deactivation are major issues, that have been overcome by relatively high catalyst loadings or even additions of second catalyst portions over time. Recently, Eosin Y was identified to suffer minor deactivation/decomposition in such a minimalistic Z-scheme approach for the generation of a superreductant and holds the potential to be more efficient in synthetic applications.[36]

This chapter has exclusively dealt with excited radical anions and reductive substrate activation so far. However, there is one sole example to date of a synthetic application for an excited radical cation employing 10-phenyl-10*H*-phenothiazine (PTZ) as the photocatalyst in an oxidative activation of styrene derivatives. With absorption maxima of 321 nm (PTZ) and 514 nm ($PTZ^{\bullet +}$), the experimental setup of Rombach and Wagenknecht required simultaneous irradiation with 365 nm and 525 nm LED's.[37] After absorption of a UV-A photon, PTZ is excited to PTZ*, which undergoes its first photo-induced oxidative SET to sulfur hexafluoride generating $PTZ^{\bullet +}$ and $SF_6^{\bullet -}$ (Scheme 2-4). Absorption of a green photon leads to superoxidizing $PTZ^{\bullet +*}$ (E_{red} = 2.1 V vs. SCE)[38] that is quenched by 1,1-diphenylethylene to regenerate groundstate PTZ and a 1,1-diphenylethylene radical cation. Fragmentation of $SF_6^{\bullet -}$ into $SF_5^{\bullet}$ and a fluoride anion and subsequent recombination with the 1,1-diphenylethylene radical cation leads to the pentafluorosulfonated product.

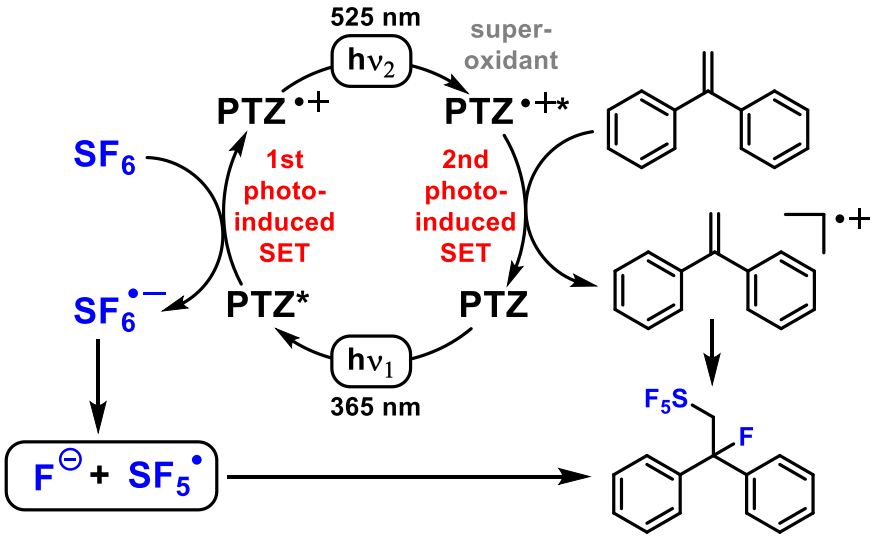

Scheme 2-4. Proposed mechanism for the pentafluorosulfonation of stryrenes as an example for a superoxidizing excited radical cation.

2.4 Chemistry of the hydrated electron generated by biphotonic photoionizations

Contrary to the previously described methods that operate mostly in organic media, synthetic protocols involving multiphoton processes in aqueous solution are rather scarce. One promising option is the generation of a hydrated electron $e^{\bullet-}_{aq.}$ via biphotonic photoionization. $e^{\bullet-}_{aq}$ features a high standard potential (-2.9 V vs. NHE) comparable to the reducing power of alkali metals and a lifetime of up to 1 µs, that is much longer than the lifetime of most excited states.[39] Hence, the hydrated electron fulfills the two crucial criteria for chemical reactivity in terms of thermodynamics and kinetics, and carries the intrinsic promise of highly reducing chemistry in water. Biphotonic photoionization is a well-investigated, yet poorly understood method in terms of factors that govern its efficiency for the generation of $e^{\bullet-}_{aq}$.[40] However, the typical procedures feature severe limitations regarding efficiency, selectivity, and experimental operability (mostly radiolysis or UV-C radiation required; high photon energies from low-intensity sources).[41] Pioneering contributions in this field towards organic synthesis in standard laboratories were achieved by the group of Goez. The typical sequential mechanism for the direct photoionization of organic compounds with visible or near UV-light (Scheme 2-5, red) involves the absorption of the first photon by the ground-state of a photoactive dye X to the excited (triplet) state X*. The second photon is absorbed by X* and leads to its direct ionization into $e^{\bullet-}_{aq}$ and $X^{\bullet+}$.[42] In the late 1990s, Goez et al. established a new ionization pathway in the presence of an electron donor D (Scheme 2-5, blue).[43] By absorption of the first photon, X is excited to X* which does not absorb another photon, but rather undergoes a fast SETwith D generating $D^{\bullet+}$ and $X^{\bullet-}$. As there exists no photophysical deactivation for $X^{\bullet-}$, it is supposed to be better suited for the absorption of a second photon in order to trigger the photoionization to $e^{\bullet-}_{aq}$ and X rather than photophysically excited states.

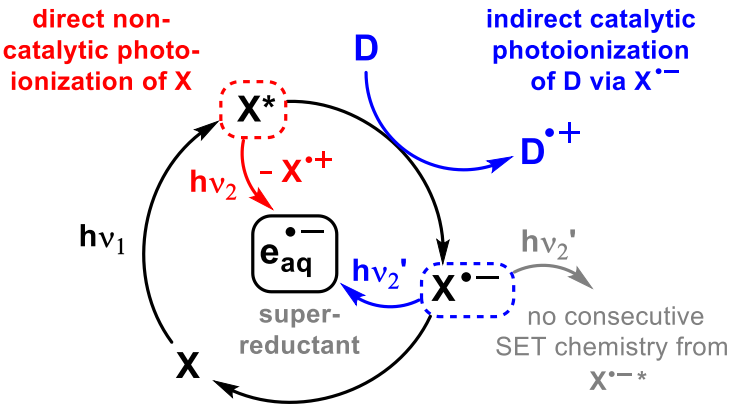

Scheme 2-5. Release of a superreducing solvated electron by direct non-catalytic photoionization of a photoactive dye X (red) or indirect catalytic photoionization of a non-absorbing electron donor D (blue).

Overall, X could be viewed as a two-photon absorption shuttle in a catalytic cycle for the net photoionization of the non-photoactive donor. Important to note here is, that

under the selected reaction conditions (low photon energies from high intensity laser irradiation) and according to the properties of X, absorption of a photon by $X^{\bullet-}$ does not lead to the previously described reduction chemistry directly from $X^{\bullet-*}$ but to the distinct liberation of a hydrated electron, which can be identified by transient absorption spectroscopy, and its follow-up reactions. However, the general concept of storing the first photon energy in a rather stable radical anion before the absorption of a second photon is similar to section 2-3.

In 2004 Goez et al. investigated the generation of $e^{\bullet-}_{aq}$ by photoionization with xanthone in the presence and absence of DABCO as the donor molecule at consecutive UV-A and green laser pulses. Significantly higher electron yields and the ubiquity of quencher molecules in nature (e.g. amino acids, etc.) made the catalytic version via the radical anion $X^{\bullet-}$ a promising model system for biologically relevant systems and set the go-ahead signal for synthetical applications.[42] 10 years later, the Goez laboratory could transfer this knowledge to the green-light ionization of the 1,5-naphtalene disulfonate radical anion generated with the help of sodium ascorbate under physiological conditions featuring an ionization quantum yield comparable to the most efficient UV ionizations.[44] In the same year, they published a seminal report on the first “all-green” production of hydrated electrons via a sustainable, homogeneous and catalytical photoionization system.[45] The role of the photon absorption shuttle was represented by ruthenium (tris)bipyridine which features an extraordinarily high lifetime in aqueous solution after the reduction with a sacrificial donor (e.g. sodium ascorbate or 4-methoxy phenolate), due to the localization of the radical anion at the bipyridine ligand.[46]

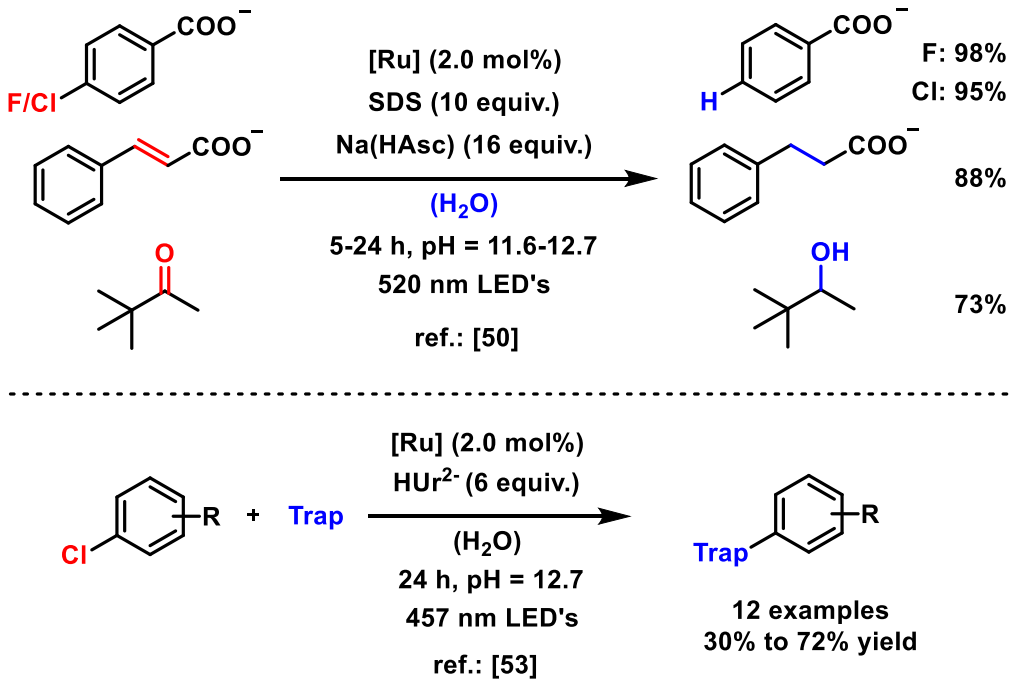

Scheme 2-6. Chemical reductions (top) and cross-couplings (bottom) enabled by the release of $e^{\bullet-}_{aq}$ with similar photocatalytic systems in presence (top) and absence (bottom) of micelles.

SDS: sodiumdodecylsulfate; $HAsc^-$: ascorbate anion; HUr^{2-}: uric acid dianion; yields were being calculated from NMR.

Their laser flash photolysis studies resolved a mechanism equal to scheme 2-5 with $h\nu_1$ and $h\nu_2$' being superimposed, independently triggered 532 nm laser pulses. They were able to extend the 2014 system by substitution of the metal- with an organo catalyst or an energy transfer (sensitization) system.[47,48] Simplifying the operational setup to a single green laser[49] or even simple LED's[50] by enhancing the reactivity and photoionization efficiency through spatial separations via micellar environments was a breakthrough on all areas that enabled unprecedented reduction chemistry in the field of visible light photoredox catalysis (Scheme 2-6, top).[51] Aromatic dehalogenations, olefin hydrogenations, and carbonyl reductions are impressive reactions (single photon energy of 520 nm = 2.33 eV; standard potentials of substrates revolve around -2.2 V to -2.7 V) achieved by this operationally simple, cheap and non-hazardous photocatalytic system for the lab-scale release of superreducing $e^{\bullet-}_{aq}$. Even strong aliphatic C-Cl bonds (in e.g. chloroacetate) can be cleaved,[49-51] and non-activated aryl chlorides can be subjected to cross-coupling chemistry.[51,52] By modifying the ruthenium catalyst and equipping it with carboxylate groups Naumann and Goez were able to get rid of the necessary compartmentalization featured by the SDS micelles while conserving the same reactivity in aromatic dehalogenations and cross-couplings (Scheme 2-6, bottom).[53]

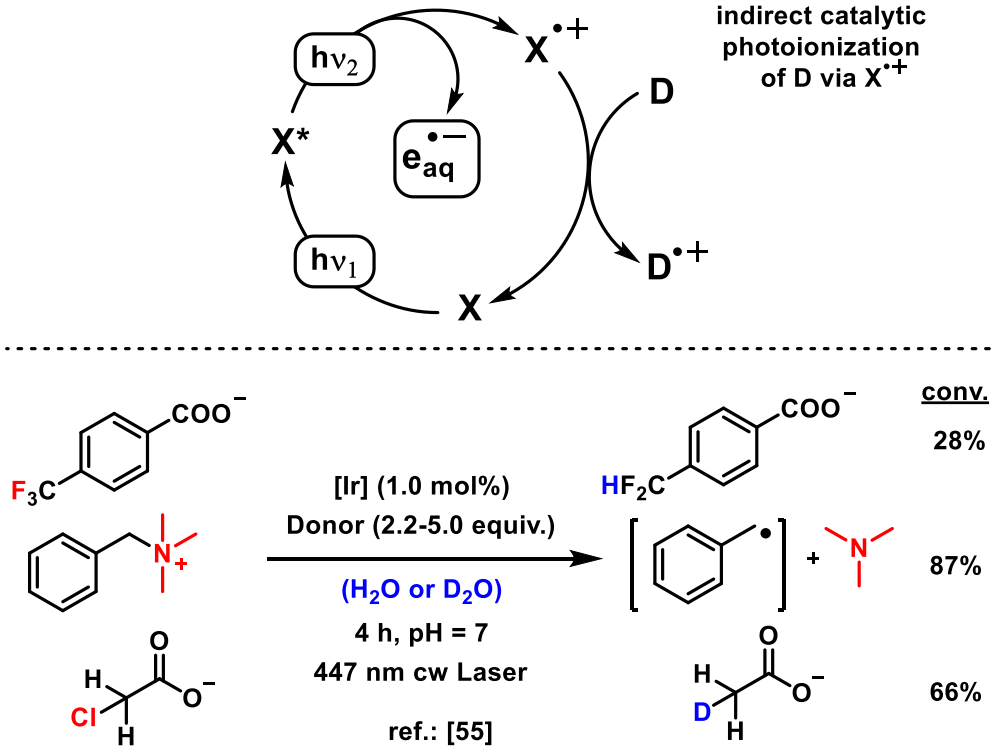

Scheme 2-7. Concept of the indirect catalytic photoionization of a non-absorbing electron donor D (top) and chemical transformations enabled by such a system (bottom).

Depending on the redox potential of the photocatalyst and its absorption behavior in the excited state, a biphotonic ionization of X* to $X^{\bullet+}$, according to scheme 5 (red), with a consecutive electron transfer by a donor molecule to close the catalytic cycle and to generate the photoionized $D^{\bullet+}$ similar to scheme 2-5 (blue) would constitute another alternative pathway in the context of photoionizations (Scheme 2-7, top). Kerzig and Goez investigated and realized such a system in 2015 on the example of 9-anthrolate under near-UV irradiation.[54] Just recently, this concept was extended by Kerzig et al. towards visible light irradiatation, a simpler setup and synthetic applications (Scheme 2-7, bottom).[55] With the aid of a water-soluble *fac*-Ir(ppy)$_3$ analogue, the hydrated electron can be generated by a cheap continuous wave laser (447 nm, 1W) under mild conditions without the need for micelles. This concept was successfully applied to the monodefluorination of a CF_3 group, the degradation of a benzyltrimethylammonium cation and the dechlorination of 2-chloroacetic acid.[55]

2.5 Conclusion and outlook

Over the last decades, former borders between different scientific fields started to melt down and pave ways for experts that unite the theory knowledge and challenging application-oriented issues. With this overview of recent advances in the synthetic utilization of multiple visible-light photons via upconversion methods, we highlight a comprehensive field of photophysics, photochemistry, catalysis and organic synthesis. TTA upconversion, exited doublet states and the hydrated electron contain great potential for the construction of structural complexity and diversity. Unprecedented photoredox catalytic transformations and substrate activations that rely on complex photophysical studies on simple model system using high intensity lasers, could be realized in standard synthetic laboratory using simple LED's. To date, the scope of these reactions is still limited to mostly reductive activation of aryl halides with little information about the occurring sophisticated physical processes under the synthetic conditions. For that we like to highlight the need for further collaborations in order to promote this promising new field of photoredox catalysis.

2.6 References

[1] a) C. K. Prier, D. A. Rankic, D. W. C. MacMillan, *Chem. Rev.* **2013**, *113*, 5322-5363; b) N. A. Romero, D. A. Nicewicz, *Chem. Rev.* **2016**, *116*, 10075-10166; c) J. W. Beatty, C. R. J. Stephenson, *Acc. Chem. Res.* **2015**, *48*, 1474-1484; d) D. Ravelli, S. Protti, M. Fagnoni, *Chem. Rev.* **2016**, *116*, 9850–9913; e) D.M. Schultz, T.P. Yoon, *Science* **2014**, *343*, 1239176; f) K. Nakajima, Y. Miyake, Y. Nishibayashi, *Acc. Chem. Res.* **2016**, *49*, 1946-1956.

[2] a) M. Majek, A. Jacobi von Wangelin, *Acc. Chem. Res.* **2016**, *49*, 2316-2327; b) I.Ghosh, L. Marzo, A. Das, R. Shaikh, B. König, *Acc. Chem. Res.* **2016**, *49*, 1566-1577; c) Y. Jin, H. Fu, *Asian J. Org. Chem.* **2017**, *6*, 368-385; d) J. Xuan, Z.-G. Zhang, W.-J. Xiao, *Angew. Chem. Int. Ed.* **2015**, *54*, 15632-15641.

[3] E. Abitelli, S. Protti, M. Fagnoni, A. Albini, *J. Org. Chem.* **2012**, *77*, 3501-3507.

[4] a) K. L. Skubi, T. R. Blum, T. P. Yoon, *Chem. Rev.* **2016**, *116*, 10035-10074; b) J. C.Tellis, C. B. Kelly, D. N. Primer, M. Jouffroy, N. R. Patel, G. A. Molander, *Acc. Chem. Res.* **2016**, *49*, 1429-1439; Selected examples: c) J. Twilton, C. Le, P. Zhang, M. H. Shaw, R. W. Evans, D. C. W. MacMillan, *Nat. Rev. Chem.* **2017**, *1*, 0052.

[5] a) C.A. Parker, C.G. Hatchard, *Proc. Chem. Soc.* **1962**, 386; b) C. A. Parker, C. G. Hatchard, *Proc. Royal Soc. A* **1962**, *269*, 574; c) C.A. Parker, C.G. Hatchard, T.A. Joyce, *Nature* **1965**, *205*, 1282-1284.

[6] T. F. Schulze, T. W. Schmidt, *Energy Environ. Sci.* **2015**, *8*, 103–125.

[7] Y. I. Park, K. T. Lee, Y. D. Suh, T. Hyeon, *Chem. Soc. Rev.* **2015**, *44*, 1302-1317.

[8] M. E. Lim, Y.-L. Lee, Y. Zhang, J. J. H. Chu, *Biomaterials* **2012**, *33*, 1912-1920.

[9] T. Miteva, V. Yakutkin, G. Nelles, S. Baluschev, *New J. Phys.* **2008**, *10*, 103002.

[10] Zhou, Y. et al. *Nat. Commun.* **2014**, *5*, 4720.

[11] a) T. N. Singh-Rachford, F. N. Castellano, *Coord. Chem. Rev.* **2010**, *254*, 2560-2573; b) M. P. Rauch, R. R. Knowles, *Chimia* **2018**, *72*, 501-507.

[12] a) J. L. Charlton, R. Dabestani, J. Saltiel, *J. Am. Chem. Soc.* **1983**, *105*, 3473-3476; b) S. M. Bachilo, R. B. Weisman, *J. Phys. Chem. A* **2000**, *104*, 7711-7714; c) J. Saltiel, B. Atwater, *Advances in Photochemistry*; Wiley, New York, **1988**.

[13] M. Majek, U. Faltermeier, B. Dick, R. Pérez-Ruiz, A. Jacobi von Wangelin, *Chem. Eur. J.* **2015**, *21*, 15496-15501.

[14] C. Costentin, M. Robert, J.-M. Saveant, *J. Am. Chem. Soc.* **2004**, *126*, 16051-16057.

[15] M. Häring, R. Pérez-Ruiz, A. Jacobi von Wangelin, D. D. Díaz, *Chem. Commun.* **2015**, *51*, 16848-16851.

[16] C. G. Lopez-Calixto, M. Liras, V. A. de la Pena O'Shea, R. Perez-Ruiz, *Applied Catalysis B: Environmental* **2018**, *237*, 18-23.

[17] B. D. Ravetz, A. B. Pun, E. M. Churchill, D. N. Congreve, T. Rovis, L. M. Campos, *Nature* **2019**, *565*, 343-346.

[18] C. Kerzig, O. S. Wenger, *Chem. Sci.* **2018**, *9*, 6670-6678.

[19] a) I. Ghosh, R. S. Shaikh, B. König, *Angew. Chem. Int. Ed.* **2017**, *56*, 8544-8549; b) M. Marchini, G. Bergamini, P. G. Cozzi, P. Ceroni, V. Balzani, *Angew. Chem. Int. Ed.* **2017**, *56*, 12820-12821; c) I. Ghosh, J. I. Bardagi, B. König, *Angew. Chem. Int. Ed.* **2017**, *56*, 12822-12824.

[20] a) M. A. Fox, *Chem. Rev.* **1979**, *79*, 253-273. b) D. Gosztola, M. P. Niemczyk, W. Svec, A. S. Lukas, M. R. Wasielewski, *J. Phys. Chem. A* **2000**, *104*, 6545-6551 and references therein.

[21] I. Ghosh, T. Ghosh, J. I. Bardagi, B. König, *Science* **2014**, *346*, 725-728.

[22] L. Zeng, T. Liu, C. He, D. Shi, F. Zhang, C. Duan, *J. Am. Chem. Soc.* **2016**, *138*, 3958-3961.

[23] H.-X. Gong, Z. Cao, M.-H. Li, S.-H. Liao, M.-J. Lin, *Org. Chem. Front.* **2018**, *5*, 2296-2302.

[24] M. Marchini, A. Gualandi, L. Mengozzi, P. Franchi, M. Lucarini, P. G. Cozzi, V. Balzani, P. Ceroni, *Phys. Chem. Chem. Phys.* **2018**, *20*, 8071-8076.

[25] I. Ghosh, B. König, *Angew. Chem. Int. Ed.* **2016**, *55*, 7676-7679.

[26] a) S. van de Linde, A. Löschberger, T. Klein, M. Heidbreder, S. Wolter, M. Heilemann, M. Sauer, *Nat. Protoc.* 2011, *6*, 991-1009; b) S. van de Linde, I. Krstic ´, T. Prisner, S. Doose, M. Heilemann, M. Sauer, *Photochem. Photobiol. Sci.* 2011, *10*, 499-506. c) T. Slanina, T. Oberschmid, *ChemCatChem* 2018, *10*, 4182-4190.

[27] L. Marzo, I. Ghosh, F. Esteban, B. König, *ACS Catal.* **2016**, *6*, 6780-6784.

[28] A. Graml, I. Gosh, B. König, *J. Org. Chem.* **2017**, *82*, 3552-3560.

[29] A. Das, I. Gosh, B. König, *Chem. Commun.* **2016**, *52*, 8695-8698.

[30] R. S. Shaikh, S. J. S. Düsel, B. König, *ACS Catal.* **2016**, *6*, 8410-8414.

[31] A. U. Meyer, T. Slanina, A. Heckel, B. König, *Chem. Eur. J.* **2017**, *23*, 7900-7904.

[32] a) J. M. Haimerl, I. Gosh, B. König, J. M. Lupton, J. Vogelsang, *J. Phys. Chem. B* **2018**, *122*, 10728-10735; b) J. M. Haimerl, I. Gosh, B. König, J. Vogelsang, J. M. Lupton, *Chem. Sci.* **2019**, *10*, 681-687.

[33] J. I. Bardagi, I. Gosh, M. Schmalzbauer, T. Gosh, B. König, *Eur. J. Org. Chem.* **2018**, 34-40.

[34] a) M. Fujita, A. Ishida, T. Majima, S. Takamuku, *J. Phys. Chem.* **1996**, *100*, 5382-5387; b) J.-C. Gumy, E. Vauthey, *J. Phys. Chem. A* **1997**, *101*, 8575-8580; c) T. Shida, *Electronic Absorption Spectra of Radical Ions*, Elsevier, Amsterdam, **1988**, pp. 246.

[35] M. Neumeier, D. Sampedro, M. Májek, V. de la Pena O'Shea, A. Jacobi von Wangelin, R. Pérez-Ruiz, *Chem. Eur. J.* **2018**, *24*, 105-108.

[36] A. Aguirre-Soto, K. Kaastrup, S. Kim, K. Ugo-Beke, H. D. Sikes, *ACS Catalysis* **2018**, *8*, 6394-6400.

[37] D. Rombach, H.-J. Wagenknecht, *ChemCatChem* **2018**, *10*, 2955-2961.

[38] J. A. Christensen, B. T. Phelan, S. Chaudhuri, A. Acharya, V. S. Batista, M. R. Wasielewski, *J. Am. Chem. Soc.* **2018**, *140*, 5290-5299.

[39] G. V. Buxton, C. L. Greenstock, W. P. Helman, A. B. Ross, *J. Phys. Chem. Ref. Data* **1988**, *17*, 513-886.

[40] a) P. Natarajan, R. W. Fessenden, *J. Phys. Chem.* **1989**, *93*, 6095–6100; b) N. Ishiwata, H. Murai, K. Kuwata, *J. Phys. Chem.* **1993**, *97*, 7129–7131; c) P. Jacques, X. Allonas, A. Sarbach, E. Haselbach, E. Vauthey, *Chem. Phys. Lett*. **2003**, *378*, 185–191.

[41] Y. Hirata, N. Mataga, *Prog. React. Kinet.* **1993**, *18*, 273–308.

[42] M. Goez, B. H. M. Hussein, *Phys. Chem. Chem. Phys.* **2004**, *6*, 5490-5497.

[43] a) M. Goez, V. Zubarev, *Angew. Chem. Int. Ed.* **1997**, *36*, 2664-2666; b) M. Goez, V. Zubarev, *J. Phys. Chem. A* **1999**, *103*, 9605-9613; c) M. Goez, V. Zubarev, G. Eckert, *J. Am. Chem. Soc.* **1998**, *120*, 5347-5348; d) M. Goez, V. Zubarev, *Chem. Phys.* **2000**, *256*, 107-116.

[44] C. Kerzig, M. Goez, *Phys. Chem. Chem. Phys.* **2014**, *16*, 25342-25349.

[45] M. Goez, C. Kerzig, R. Naumann, *Angew. Chem. Int. Ed.* **2014**, *53*, 9914-9916.

[46] Q. G. Mulazzani, S. Emmi, P. G. Fuochi, M. Z. Hoffman, M. Venturi, *J. Am. Chem. Soc.* **1978**, *100*, 981-983.

[47] T. Kohlmann, R. Naumann, C. Kerzig, M. Goez, *Photochem. Photobiol. Sci.* **2017**, *16*, 1613-1622.

[48] C. Kerzig, M. Goez, *Chem. Sci.* **2016**, *7*, 3862-3868.

[49] R. Naumann, C. Kerzig, M. Goez, *Chem. Sci.* **2017**, *8*, 7510-7520.

[50] R. Naumann, F. Lehmann, M. Goez, *Angew. Chem. Int. Ed.* **2018**, *57*, 1078-1081.

[51] R. Naumann, F. Lehmann, M. Goez, *Chem. Eur. J.* **2018**, *24*, 13259-13269.

[52] R. Naumann, M. Goez, *Chem. Eur. J.* **2018**, *24*, 9833-9840.

[53] R. Naumann, M. Goez, *Chem. Eur. J.* **2018**, *24*, 17557-17567.

[54] C. Kerzig, M. Goez, *Phys. Chem. Chem. Phys.* **2015**, *17*, 13829-13836.

[55] C. Kerzig, X. Guo, O. Wenger, *J. Am. Chem. Soc.* **2019**, *141*, 2122-2127.

3 Aromatic chlorosulfonylation by photoredox catalysis[i,ii]

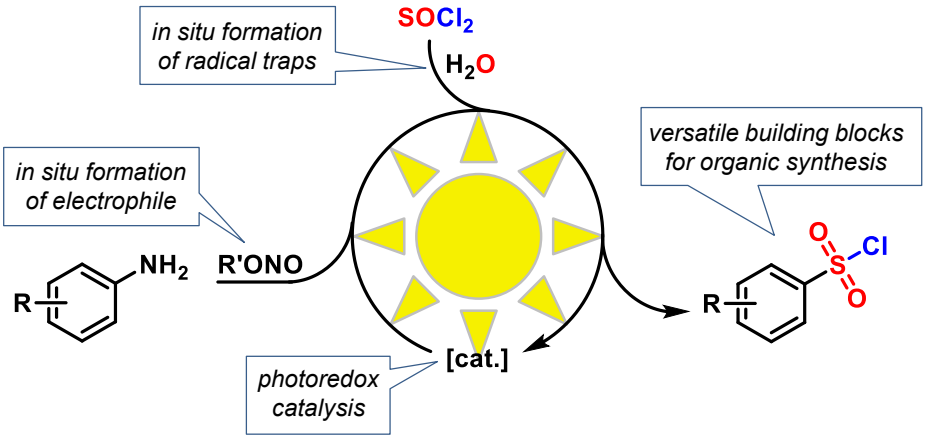

Abstract: Visible light photoredox catalysis enables the efficient synthesis of arenesulfonyl chlorides from anilines. The presented protocol involves the convenient *in situ* preparations of arenediazonium salts (from anilines) and the reactive gases SO_2 and HCl (from aqueous thionyl chloride). The photocatalytic chlorosulfonylation operates at mild conditions (room temperature, acetonitrile/water) with low catalyst loading (0.5 mol% $Ru(bpy)_3Cl_2$). Various functional groups are being tolerated (e.g. halides, azide, nitro, CF_3, SF_5, esters, heteroarenes). Theoretical and experimental studies support a photoredox catalysis mechanism (Φ = 0.027).

[i] Reproduced from M. Májek, M. Neumeier, A. Jacobi von Wangelin, *ChemSusChem* **2017**, *10*, 151-155 with permission of Wiley-VCH. Schemes, tables and text may differ from published version.

[ii] Author contributions: M.M. performed theoretical calculations, spectroscopic measurements and initiated the project. M.N. performed experimental and analytical work. A.J.v.W. guided the project. All authors contributed to the writing of the manuscript.

3.1 Introduction

Sulfonyl chlorides constitute key intermediates in the preparation of numerous organosulfur compounds such as sulfones, sulfonates, and sulfonamides (Scheme 3-1).[1] Industrial processes via sulfonyl chlorides include the manufacture of fine chemicals, herbicides, pharmaceuticals, and dyes.[1] 17 of the 200 most frequently prescribed drugs in the U.S. contained sulfonamide linkages (Scheme 3-2).[2] Sulfonylations of alcohols and amines are among the five most widely applied reactions in pharmaceutical research endeavours.[2] Sulfonyl chlorides are also used in functional group protection strategies[3] and the activation of unreactive entities[4] (reactive esters such as triflates, tosylates, mesylates) and the chemical identification of amines (Hinsberg test).[5] Many protocols for the construction of the arenesulfonyl chloride function have been reported (Scheme 3-1). The direct chlorosulfonation with $ClSO_3H$ has a wide range of applications with simple aromatic substrates but exhibits severe limitations with highly functionalized arenes, when harsh conditions are required, or low regioselectivity is observed.[6] Sulfonyl chlorides can be obtained from the parent sulfonic acids with mild chlorination reagents (e.g. cyanuric chloride) but the preparation of sulfonic acids is governed by the same criteria as the chlorosulfonation.[7] Oxidative chlorinations of thiols allow the preparation of acid-sensitive sulfonyl chlorides. Various combinations of chlorinating agents and oxidant can be used (e.g. aqueous Cl_2, NaOCl/HCl, TMSCl/KNO_3, oxone/KCl or H_2O_2/$SOCl_2$).[8] These methods require the facile access to thiophenols, e.g. by reduction of sulfonyl chlorides or from arenediazonium salts and thiourea (or similar sulfur sources).[9] The first synthesis of arenesulfonyl chlorides from arenediazonium salts by Meerwein was a variation of the Sandmeyer reaction.[10] The protocol was performed in aqueous solution with SO_2 gas and gave mostly low to moderate yields. Arenediazonium salts exhibit very low solubility under these conditions which results in the formation of thick aqueous slurries that exhibit high hazard potential due to poor mixing, local overheating, and run-away reactions. The addition of organic co-solvents afforded slightly improved yields (~50%) but explosive run-away reactions were still observed.[11]

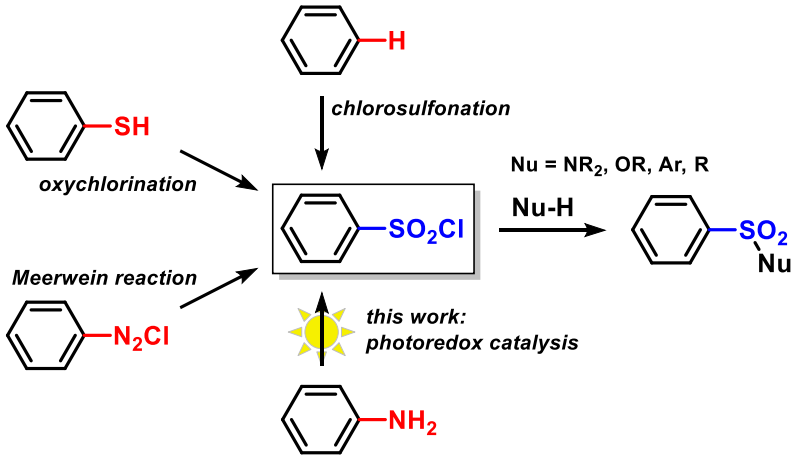

Scheme 3-1. Methods of arenesulfonyl chloride preparations.

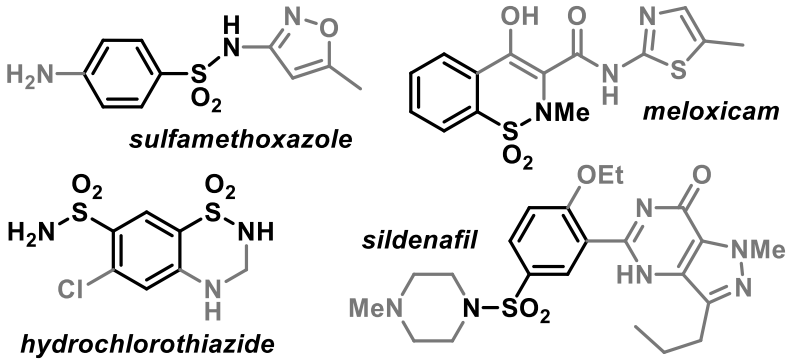

Scheme 3-2. Top-selling pharmaceuticals containing arenesulfonamide linkages.

We aimed to develop a photoredox-catalyzed chlorosulfonylation reaction which is driven by visible light in the presence of a photocatalyst and operates in standard reaction vessels under mild conditions. We wished to use organic solvents and avoid the handling of hazardous materials but rather embed the *in situ* generation of all reagents from available starting materials within an overall one-pot reaction protocol (Scheme 3-3). The use of the irritating and toxic gas SO_2 is impractical under lab-scale conditions. The common solid and liquid surrogates (i.e. sulfite salts, sulfolene, amine-SO_2 adducts, thionyl chloride) are easier to handle and less hazardous.[12] For our purpose, the use of $SOCl_2$ was especially suitable as it is a commercially available liquid, it is soluble in organic solvents, and undergoes rapid hydrolysis by addition of equimolar amounts of water to release two building blocks for the construction of the sulfonyl chloride moiety: SO_2 and HCl.[13] The aromatic electrophile should be generated by diazotization of abundantly available anilines under similar conditions. Polar organic solvents such as acetonitrile exhibit high solubility of anilines, arenediazonium salts, SO_2 and HCl, are miscible with minor amounts of water (for *in situ* hydrolysis of $SOCl_2$) and therefore warrant a homogeneous reaction without the limitations of earlier reports.[11],[14]

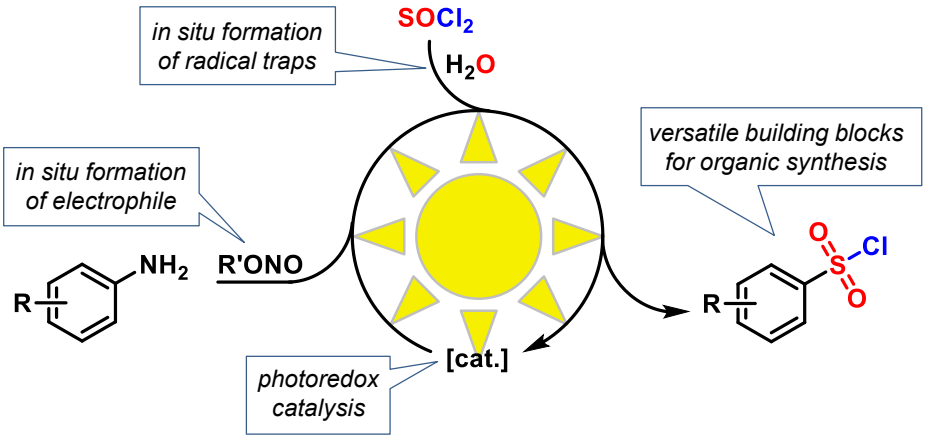

Scheme 3-3. The concept of our photoredox-catalyzed chlorosulfonylation and *in situ* preparation of reagents.

3.2 Results and discussion

We initially focused on the development of the photoredox-catalyzed chlorosulfonylation of arenediazonium salts by SO_2 and HCl, with the latter two being formed *in situ* from equimolar $SOCl_2$/water in acetonitrile. The model substrate 4-anisole-diazonium tetrafluoroborate (**1**) was chosen since electron-rich arenediazonium salts were unreactive in a recently reported Meerwein protocol.[13] Optimization of the chlorosulfonylation of **1** in the presence of 0.5 mol% of the photocatalyst tris(2,2'-bipyridine)ruthenium(II)dichloride and blue light afforded 4-anisole-sulfonyl chloride (**2**) in excellent yield (Table 3-1).[15]

Table 3-1. Selected optimization experiments.[a]

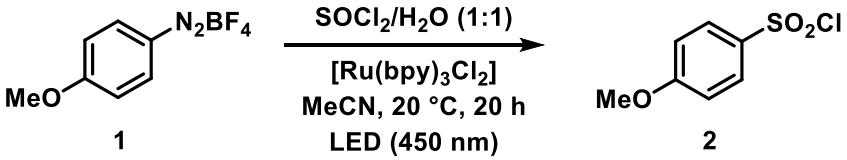

1 **2**

Entry	c [1] in M	Equiv. $SOCl_2/H_2O$	Cat. load. in mol%	Yield in %
1	0.17	5	5	18
2	0.17	5	1	29
3	0.17	5	0.5	48
4	0.17	10	0.5	16
5	0.67	2.5	0.5	69
6	**0.67**	**5**	**0.5**	**96 (83)[b]**
7	1	5	0.5	95
8[c]	0.17	5	2.5	5
9[d]	0.67	5	0.5	<1
10	0.67	5	-	<2

[a] General procedure: A solution of 4-anisolediazonium tetrafluoroborate (**1**, 0.5 mmol), $SOCl_2$/water (1/1), and $Ru(bpy)_3Cl_2 \cdot 6H_2O$ in acetonitrile was irradiated with a blue LED (450 nm, 3.8 W) for 20 h at 20°C. Yields of **2** were determined after aqueous quench and phase separation by GC-FID vs. 1-dodecanenitrile; [b] *in situ* formation of diazonium salt from 4-methoxy-aniline and 1.1 equiv. *i*-amyl nitrite; [c] Eosin Y·Na_2 instead of $Ru(bpy)_3Cl_2$, green LED (535 nm); [d] dark reaction.

With higher catalyst concentrations, hydrodefunctionalization was observed (Entries 1 and 2, Table 3-1).[16] Higher excess amounts of $SOCl_2/H_2O$ led to low yields, possibly due to the strongly acidic conditions and/or the interference of single-electron transfer (SET) with SO_2 (Entry 4, Table 3-1). Interestingly, the reaction could also be performed in combination with the *in situ* generation of the anisolediazonium salt in a one-pot

procedure (Entry 6, Table 3-1, in parentheses). The use of eosin Y, with similar redox properties,[17] resulted in very low conversion (Entry 8, Table 3-1) which is a consequence of dye protonation to the photo-inactive state.[18]

A set of 20 arenediazonium salts were then subjected to the optimized reaction conditions (Scheme 3-4, isolated yields are given).[15] It is important to note that the arenesulfonyl chlorides are volatile compounds so that precautions have to be taken when isolating the products. The conditions exhibited exceptionally high functional group tolerance; substrates with halide, azide, ester, nitro, CF_3, SF_5, and thiophene substituents were cleanly reacted. This protocol is a significant expansion of earlier methods which were not applicable to electron-rich and halide-bearing arenediazonium salts, respectively.[10],[11],[13] However, pyridine-bearing substrates gave complex product mixtures which is in accordance with the generally low stability of pyridinediazonium salts.[19]

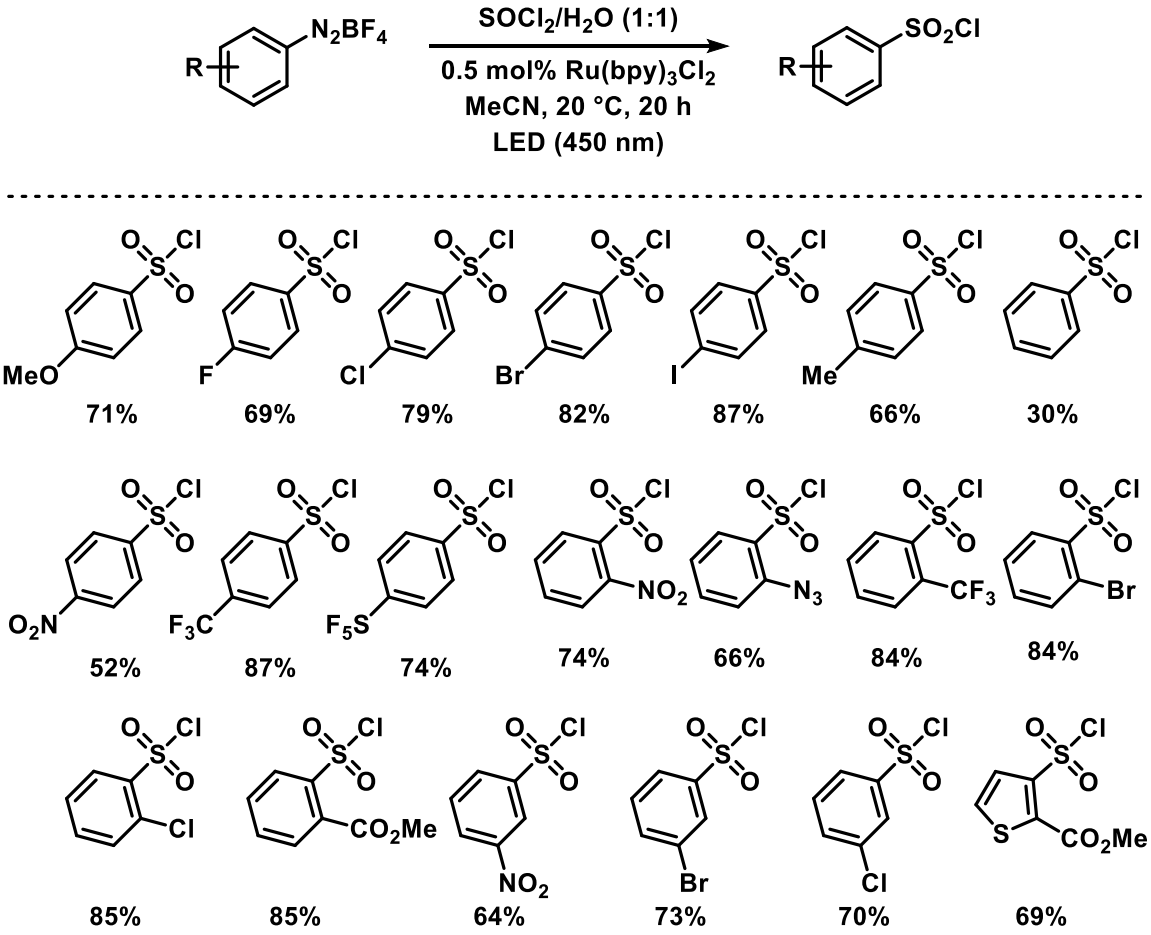

Scheme 3-4. Photocatalytic chlorosulfonylation of arenediazonium tetrafluoroborates (isolated yields are given).

The high stability of the formed arenesulfonyl chlorides toward further photocatalytic single-electron transfer is remarkable in view of their significant electrophilicity and the redox potential of excited $[Ru(bpy)_3]^{2+}$.[20] Prolonged reaction times showed only slight

erosion of the yields of the arenesulfonyl chlorides by hydrodechlorosulfonylation. For example, 4-anisolesulfonyl chloride (**2**) slowly underwent defunctionalization under the photocatalytic reaction conditions with less than 5% of anisole being formed from **2** after 30 h.[15] Similarly high chemoselectivity was observed with the 4-iodo derivative which was not susceptible to reductive SET-activation under photocatalysis conditions.[21]

We then combined the standard procedure with the generation of arenediazonium salts under the reaction conditions.[22] The resultant three-step one-pot protocol involves the *in situ* preparation of all three components (arenediazonium salt, SO_2 and HCl) and their photoredox-catalyzed reaction to give arenesulfonyl chlorides (Scheme 3-5).[15] Interestingly, most of the one-pot reactions starting from anilines gave higher yields than the corresponding protocols starting from arenediazonium salts (Scheme 3-4). The low yield of the 2-nitrobenzenesulfonyl chloride is due to a sluggish diazotation reaction between the deactivated 2-nitroaniline and the mild nitrosonium source *iso*-amylnitrite.

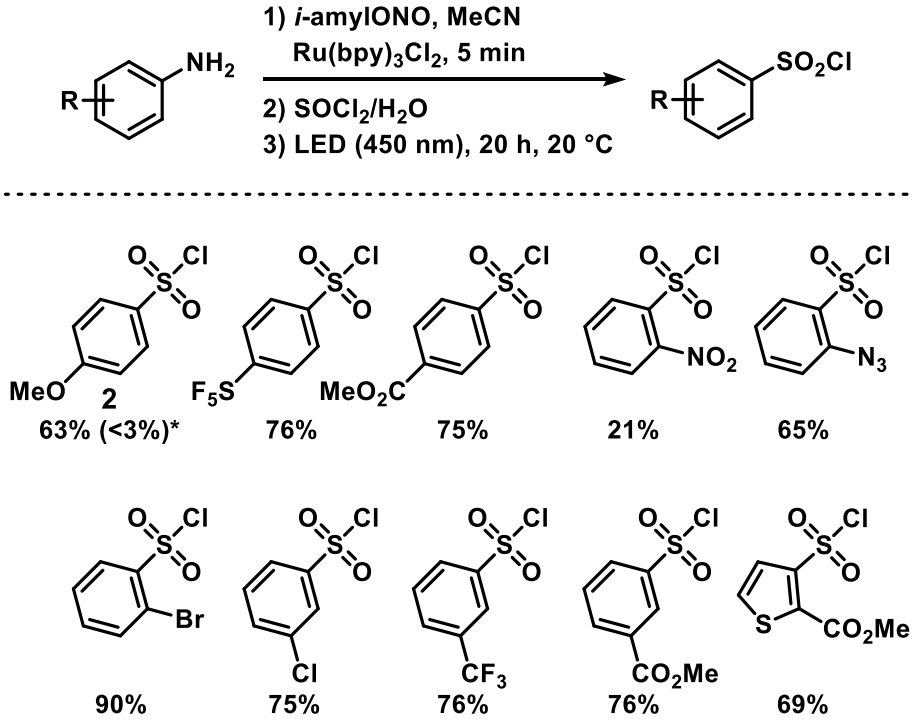

Scheme 3-5. Synthesis of chlorosulfonates from anilines by *in situ* diazotation-chlorosulfonation (isolated yields are given; * reactions without catalyst and light, without catalyst with light, with catalyst without light afforded **2** in GC yields of <3%, respectively).

The great utility of arenesulfonyl chlorides for further chemical manipulation was probed with the synthesis of saccharin.[23] The photocatalytic chlorosulfonylation of 2-aminocarbonylbenzene-diazonium tetrafluoroborate afforded saccharin as single isolable product in 70% yield after intramolecular sulfoxamidation. Surprisingly, a one-pot procedure starting from the commercial fluorescent label anthranilamide without

isolation of the arenediazonium intermediate gave quantitative conversion to saccharin (>98% yield, Scheme 3-6).

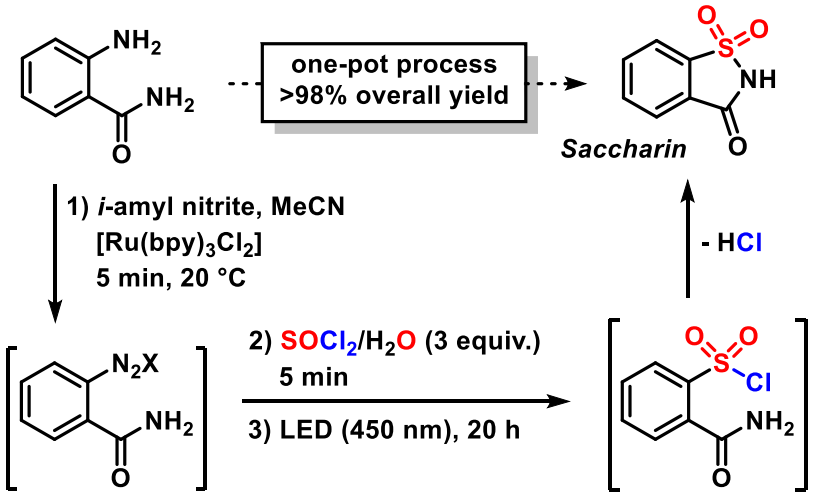

Scheme 3-6. First photoredox-catalyzed one-pot synthesis of saccharin.

Based on our previous works on related photoredox-catalyzed reactions of arenediazonium salts,[17],[24] we have proposed a mechanism of this chlorosulfonation (Scheme 3-7):

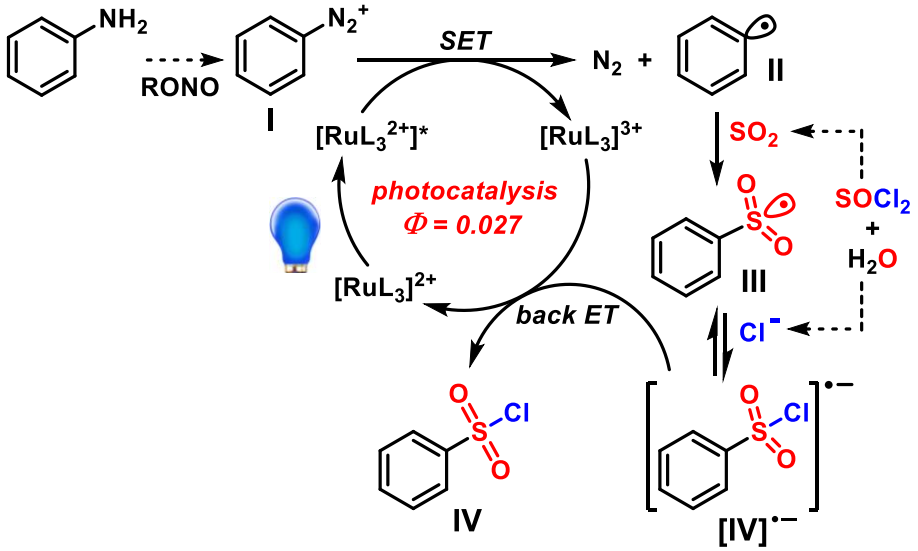

Scheme 3-7. Postulated reaction mechanism of the photoredox-catalyzed chlorosulfonylation. For quantum yield determination, see below and experimental part.

The arenediazonium salt **I** undergoes facile SET-reduction with the excited photocatalyst to the reactive aryl radical (**II**) which is rapidly trapped by the good *n*-donor SO_2. The resultant stabilized *S*-centered sulfonyl radical **III** reacts with the chloride anion to give the radical anion $[\mathbf{IV}]^{\bullet-}$. Back-electron transfer with the oxidized form of the catalyst, $[Ru(bpy)_3]^{3+}$, affords the neutral arenesulfonyl chloride **IV**. Only with very unstable diazonium salts and/or at elevated temperatures, minor amounts of

the aryl chloride were detected. Reductive activation of the arenesulfonyl chlorides does not occur under the reaction conditions. Nucleophilic substitution at the sulfonyl chloride was also not observed.

DFT calculations were performed to rationalize the key steps of the proposed reaction mechanism (Scheme 3-8).[15] These suggest a high thermodynamic driving force of the radical trapping of **II** with SO_2 to give arenesulfonyl radical **III** which is irreversible under the reaction conditions (stabilization greater than 100 kJ/mol). This is consistent with our observation that rapid aryl radical trapping proceeded with relatively low amounts of the trapping reagent SO_2 in comparison with literature reports of other electron-donor traps.[25] The competing pathway is H atom abstraction from the solvent.[16] Moreover, the high stability of arenesulfonyl radicals vs. aryl radicals is also documented by the recent development of a photocatalytic sulfoxide synthesis by reaction of arylsulfenium ions with π-electron donors.[26] Our calculations show that the addition of the chloride anion onto the sulfur-centered radical **III** is energetically neutral and barrierless. Even if a slow back-electron transfer from the radical anion **[IV]**$^{\bullet-}$ to the catalyst would not impair the overall reaction selectivity. Both intermediates **III** and **[IV]**$^{\bullet-}$ are the global thermodynamic sinks of the reaction and do not undergo side reactions. The predicted redox potential of the couple **IV** / **[IV]**$^{\bullet-}$ is 0.49 V vs. SCE which is fully consistent with the experimental value.[27]

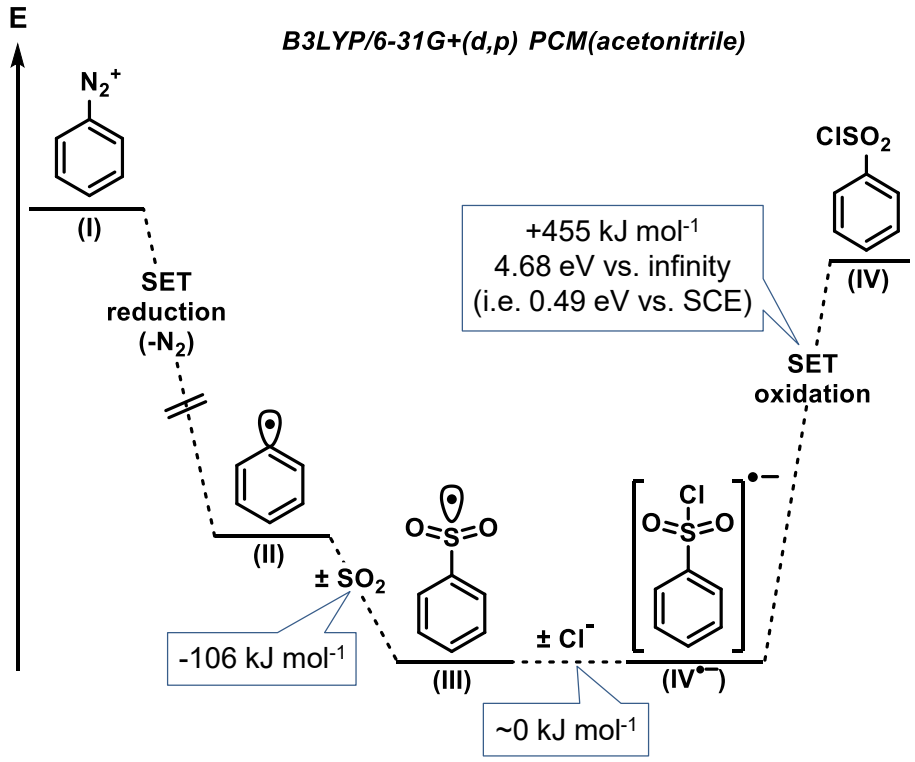

Scheme 3-8. Thermodynamic reaction profile obtained from DFT calculations.

We have analyzed the thermodynamics of the half-reactions of the redox couples present in the standard reaction mixture (Scheme 3-9). The excited catalyst $[Ru^{2+}]^*$ can easily reduce the arenediazonium salt in a highly exergonic process ($\Delta G = -zF\Delta E$).

On the other hand, the radical anion [**IV**]$^{\bullet-}$ is not sufficiently reducing to convert the arenediazonium salt (ΔE -0.49 V). The only species capable of oxidation of [**IV**]$^{\bullet-}$ is the oxidized form of the photocatalyst [Ru^{3+}]. This back-electron transfer is required for a closed photocatalytic cycle. We have determined a reaction quantum yield of Φ = 2.7%[15] using a modified setup of the total photon flux counter by Riedle et al.,[28] which suggests that radical chain processes are not operating.

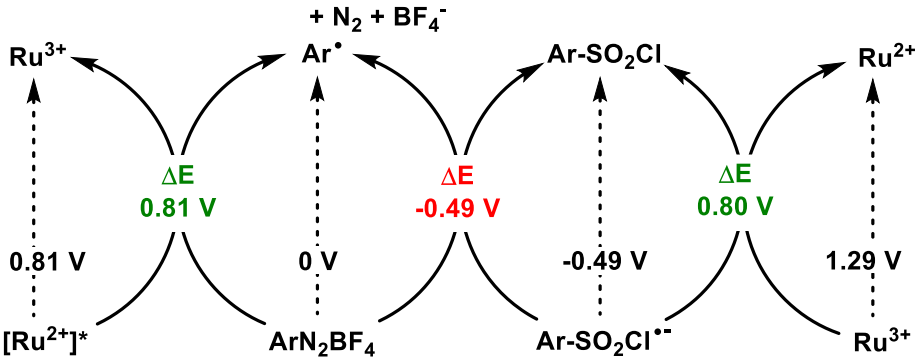

Scheme 3-9. Reaction potentials of the half-reactions (vs. SCE). Redox potentials of $Ru(bpy)_3Cl_2$ and arenediazonium salts were taken from ref. [15].

3.3 Conclusions

We have developed a methodology which allows efficient transformations of anilines to sulfonyl chlorides upon the sequential combination of *in situ* preparations of the three reagents arenediazonium salt, sulfur dioxide, and HCl with a photoredox-catalyzed three-component reaction. Equimolar thionyl chloride and water were employed as liquid sources of SO_2 and HCl; the mild nitrosonium reagent *i*-amyl nitrite afforded the arenediazonium intermediates. The three-component assembly of arenesulfonyl chlorides is driven by visible light in the presence of 0.5 mol% $Ru(bpy)_3Cl_2$ as photocatalyst at room temperature. The proposed mechanism has been corroborated by DFT calculations and photochemical studies. This method is another example of the potential of chemical synthesis at the interfaces of three distinct physical entities: visible light, a liquid and gaseous phase.[24b],[29] Future efforts in our group will aim at the development of related multi-component photocatalyses with easily available gaseous reagents.

3.4 Experimental Section

3.4.1 Materials and methods

Chemicals and solvents: All reagents and solvents were purchased from commercial suppliers (Acros, Alfa Aesar, Fisher, Fluka, Merck, Sigma Aldrich, Sojuz-Chimexport and TCI) and used as received. Diazonium salts were prepared by synthetic routes (*vide infra*), with the respective aniline precursors used without further purification as obtained from the vendors.

Reaction setup: The reactions were carried out in Rotilabo®-sample vials (6 mL, Ø 22 mm, Roth) sealed with Rotilabo®-aluminium caps with septum (Ø 20 mm, Roth). Irradiation was performed with a blue high-power LED (Luxeon Rebel, Canada, P = 3.8 W, λ_{max} = 450 nm) through the plain bottom side of the reaction vials.

Nuclear magnetic resonance (NMR) spectroscopy: ^{1}H NMR, ^{13}C NMR and ^{19}F NMR spectroscopy were used for purity and structure confirmation/determination of products. NMR spectral data were collected on a Bruker Avance 300 (300 MHz for ^{1}H; 75 MHz for ^{13}C, 282 MHz for ^{19}F) spectrometer and a Bruker Avance 400 (400 MHz for ^{1}H; 100 MHz for ^{13}C) spectrometer at 20 °C. Chemical shifts are reported in δ/ppm, coupling constants *J* are given in Hertz. Solvent residual peaks were used as internal standard for all NMR measurements. The quantification of ^{1}H cores was obtained from integrations of appropriate resonance signals. Abbreviations used in NMR spectra: s – singlet, d – doublet, t – triplet, q – quartet, m – multiplet, bs – broad singlet, dd – doublet of doublet, ddd – doublet of doublet of doublet.

Gas chromatography (GC-FID and GC-MS): GC-FID measurements on an Agilent 7820A GC-system with N_2 as carrier gas were used for quantification purposes in reaction optimization screenings and kinetic experiments. 1-Dodecanenitrile was used as internal standard; the yield-% was calculated from a linear calibration curve that was set up from at least three data points of various concentrations of authentic product material. Low-resolution mass spectrometry (LRMS) was carried out on an Agilent 6890N GC-System coupled with a 5975 MS mass detector (EI ionization source) and H_2 as carrier gas. LRMS was used for reaction control purposes and structure determination of literature-known products

High resolution mass spectrometry (HRMS): HRMS was carried out by the Central Analytics at the department of chemistry, University of Regensburg. Abbreviations used in MS spectra: M – molar mass of target compound, EI – electron impact ionization, ESI – electrospray ionization.

Column (CC) and thin layer (TLC) chromatography: TLC was performed on commercial SiO_2-coated aluminium plates (DC60 F254, Merck). Visualization was done by UV light (254 nm). Column chromatography was performed using silica gel (Acros Organics, mesh 35-70, 60 Å pore size) as the stationary phase.

3.4.2 General procedures

General procedure for the synthesis of arenediazonium salts:

Most of the arenediazonium salts were prepared according to the following literature procedure: M. Májek, A. Jacobi von Wangelin, *Chem. Commun*. **2013**, *49*, 5507-5509.

The parent aniline (4.5 mmol) was dissolved in glacial acetic acid (3.0 mL) and aqueous tetrafluoroboric acid (2.0 mL, 32%) at room temperature. Then, a solution of *tert*-butyl nitrite (0.95 mL) or *iso*-amyl nitrite (1.0 mL) in glacial acetic acid (2.0 mL) was slowly added at room temperature over 5 min. Diethylether (15 mL) was added, and the reaction mixture was cooled until crystals started to form. The crystals were filtered off, washed with cold diethylether (2 x 10 mL) and dried on air. If necessary, the solid was recrystallized from acetone by addition of diethyl ether to give analytically pure arenediazonium salts.

For methoxy- and nitro-substituted arenediazonium tetrafluoroborates an alternative procedure was used:

The parent aniline (40 mmol) was dissolved in aqueous tetrafluoroboric acid (25 mL, 32%) at room temperature. Then, an aqueous solution of sodium nitrite (4.3 M, 43 mmol) in water (10 mL) was added at 0 °C over 5 min. The solid was filtered off, washed with cold water (10 mL) and recrystallized from acetone by addition of diethyl ether to give analytically pure arenediazonium salts.

General procedure for the chlorosulfonylation of arenediazonium tetrafluoroborates:

A vial (6 mL) was charged with a magnetic stir bar, the arenediazonium salt (1.0 mmol), and $[Ru(bpy)_3]Cl_2 \cdot 6\ H_2O$ (3.7 mg, 0.5 mol%). The vial was sealed with an aluminium-capped septum. Acetonitrile (1.5 mL) was added and the solution was purged with N_2 for 5 min. Then, water (90 µL, 5.0 mmol) and thionyl chloride (0.36 mL, 5.0 mmol), were added (Careful! Exothermic reaction!). The solution was irradiated with an external LED (455 nm, 3.8 W) at 20 °C. After 20 h, water (10 mL) was added and the mixture was extracted with ethyl acetate (3 x 15 mL). The combined organic phases were washed with brine (10 mL) and dried ($MgSO_4$). The solvent was evaporated and the residue purified by column chromatography over silica gel in *n*-pentane/ethyl acetate.

General procedure for the chlorosulfonylation of anilines:

A vial (6 mL) was charged with a magnetic stir bar, the parent aniline (1.0 mmol), and $[Ru(bpy)_3]Cl_2 \cdot 6\ H_2O$ (3.7 mg, 0.5 mol%). The vial was sealed with an aluminium-capped septum. Acetonitrile (1.5 mL) was added and the solution was purged with N_2 for 5 min. *Iso*-Amyl nitrite (0.16 mL, 1.2 mmol) was added and the reaction mixture was stirred for 5 min at 20 °C. Then, water (90 µL, 5.0 mmol) and thionyl chloride (0.36 mL, 5.0 mmol) were added (Careful! Exothermic reaction!). The reaction was irradiated with an external LED (455 nm, 3.8 W) at 20 °C. After 20 h, water (10 mL) was added and the mixture was extracted with ethyl acetate (3 x 15 mL). The combined organic phases were washed with brine (10 mL) and dried ($MgSO_4$). The solvent was evaporated and

the residue purified by column chromatography over silica gel in *n*-pentane/ethyl acetate.

Procedure for the quantum yield determination:

The setup developed by Riedle et. al.[30] was used for the determination of the photon flux. A high power LED (Osram OSLON SSL80, LD-CQ7P-1U3U, λ_{max}=455 nm ± 21 nm) served as the irradiation source; the light beam was concentrated by a photographic lens with f = 50 mm; as the PS19Q power sensor from Coherent served as the power meter.

A vial (6 mL) was charged with a magnetic stir bar, the *p*-methoxybenzenediazonium tetrafluoroborate (1.68 mmol), and $[Ru(bpy)_3]Cl_2 \cdot 6\ H_2O$ (6.2 mg, 0.5 mol%). The vial was sealed with an aluminum cap with a septum. Acetonitrile (2.5 mL) was added and the solution was purged with nitrogen gas stream for 5 minutes. Then water (150 µL, 8.4 mmol), and thionyl chloride (0.60 mL, 8.4 mmol), were added to the solution (careful! exothermic reaction between water and thionyl chloride). The reaction was irradiated in the irradiation apparatus for 4 hours to keep the conversion sufficiently low. At the given concentration of catalyst, total absorption of light was observed. After the irradiation was discontinued, brine (10 mL) and ethyl acetate (15 mL) were added. Dodecanenitrile (20 µL) was added as an internal standard. An aliquot from the organic phase (cca. 2 mL) was dried oved magnesium sulfate, and the amount of the product (*p*-methoxybenzenesulfonyl chloride) was determined by GC-FID. We have determined the absorbed light power by measuring the power of transmitted light by a vial of the same geometry containing pure acetonitrile.

The average light power was ***P = 61.4 mW***.

The photon flux was determined according to the following formulae:

$$E_P = h \cdot \nu = h \cdot \frac{c}{\lambda}$$

$$E_t = P \cdot t = h \cdot N_{phot} \cdot \frac{c}{\lambda} \Rightarrow \frac{N_{phot}}{t} = \frac{P \cdot \lambda}{h \cdot c}$$

$$\Phi = \frac{n_{phot}}{t} = \frac{N_{phot}}{N_A \cdot t} = \frac{P \,.\lambda}{N_A \cdot h \cdot c} = \frac{61.4 \cdot 10^{-3} \cdot 455 \cdot 10^{-9}}{6.022 \cdot 10^{23} \cdot 6.63 \cdot 10^{-34} \cdot 3 \cdot 10^{8}}\,\mathrm{E/s} = \mathbf{0.23\ \mu E/s}$$

where E_p is the energy of a single photon of wavelength λ; E_t is the energy of photons of wavelength λ, which were emitted over a time period *t* by the light source, which has a radiative power *P*; n_{phot} and N_{phot} are respectively the molar amount and the amount of photons emitted in the period of time *t*. Φ is the radiative flux of the light source (amount of photons emitted per time); N_A is the Avogadro's constant, *h* is the Planck's constant and *c* is the speed of light.

After 4 h of irradiation, we have determined the amount of product to be $\boldsymbol{n_{prod}}$ **= 0.088 mmol**, which corresponds to the conversion of 5%, a value low enough to consider a constant amount of starting materials over the course of 4 h.

The quantum yield was determined as:

$$\phi = \frac{n_{prod}}{n_{phot}} = \frac{n_{prod}}{\Phi \cdot t} = \frac{0.088 \cdot 10^{-3}}{0.23 \cdot 10^{-6} \cdot 4 \cdot 3600} = \mathbf{2.7}\%$$

3.4.3 Kinetics

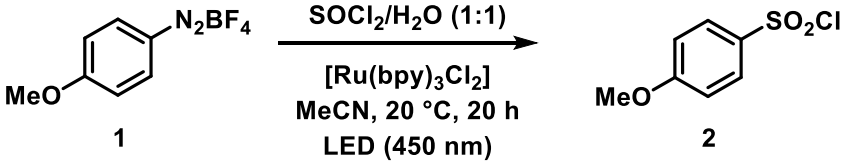

The reaction kinetics were studied using GC-FID analysis with an internal standard to determine the yields. The following conditions were used: 0.5 mmol of *p*-methoxybenzenediazonium tetrafluoroborate (**1**), 5 equiv. of thionylchloride/water (1/1), 0.5 mol% of photocatalyst ($[Ru(bpy)_3]Cl_2 \cdot 6\ H_2O$), concentration of the arene-diazonium salt in acetonitrile was set to 0.17 M. Irradiation was performed in the same setup as used for the preparative reactions. A linear increase of yield was observed until 20 h, when slow degradation of the product commenced.

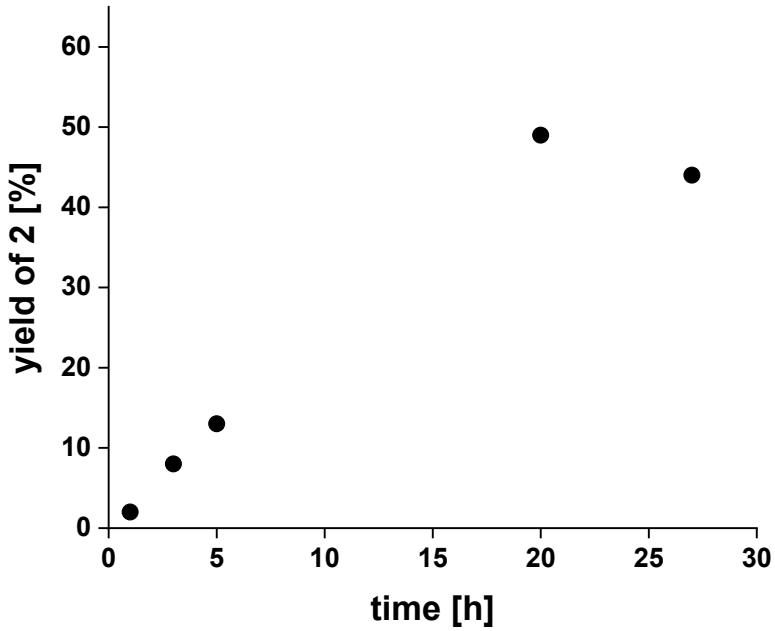

Figure 3-1. Kinetic profile of the model reaction.

3.4.4 Detailed overview of optimization reactions

Table 3-2. Further optimization reactions.[a]

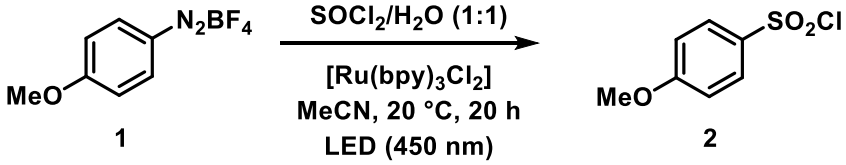

Entry	c [1] in M	Equiv. $SOCl_2/H_2O$	Cat. load. in mol%	Yield in %
1[b]	0.17	5	0.5 mol%	15
2[c]	0.17	5	0.5 mol%	0
3[d]	0.17	5	0.5 mol%	2
4[e]	0.17	5	0.5 mol%	2
5	0.17	5	0.5 mol%	48
6	0.17	5	5 mol%	18
7	0.17	5	2 mol%	24
8	0.17	5	1 mol%	29
9	0.17	5	0.25 mol%	29
10	0.17	5	0.1 mol%	4
11	0.17	10	0.5 mol%	16
12	0.17	20	0.5 mol%	14
13	0.17	2	0.5 mol%	44
14	0.1	5	0.5 mol%	45
15	0.5	5	0.5 mol%	77
16	1.0	5	0.5 mol%	95
17	0.67	5	0.5 mol%	96
18	0.67	2.5	0.5 mol%	69
19	0.67	1.5	0.5 mol%	55

[a] General procedure: A solution of 4-anisolediazonium tetrafluoroborate (**1**, 0.5 mmol), $SOCl_2$/water (1/1), and $Ru(bpy)_3Cl_2 \cdot 6H_2O$ in acetonitrile was irradiated with a blue LED (450 nm, 3.8 W) for 20 h at 20°C. Yields of **2** were determined after aqueous quench and phase separation by GC-FID vs. 1-dodecanenitrile; [b] reaction THF [c] reaction in DMSO [d] reaction in DMF [e] reaction in CH_2Cl_2.

3.4.5 Analytical data of compounds

Analytical data of arenediazonium salts:

2-Azidophenyldiazonium tetrafluoroborate

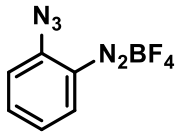

^{1}H NMR (400 MHz, DMSO-d^{6}): δ = 8.61-8.56 (m, 1H), 8.27-8.20 (m, 1H), 8.03-7.97 (m, 1H), 7.67-7.61 (m, 1H).

^{19}F NMR (376 MHz, DMSO-d^{6}): δ = −147.8 ($^{10}BF_4$), −147.9 ($^{11}BF_4$).

2-Carbamoylbenzoldiazonium tetrafluoroborate

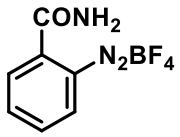

^{1}H NMR (300 MHz, DMSO-d^{6}): δ = 9.00-8.88 (m, 1H), 8.88 (bs, 1H), 8.51 (bs, 1H), 8.43-8.29 (m, 2H), 8.21-8.10 (m, 1H).

^{19}F NMR (282 MHz, DMSO-d^{6}): δ = −147.6 ($^{10}BF_4$), −147.7 ($^{11}BF_4$).

Analytical data of arenesulfonyl chlorides:

4-Methoxybenzenesulfonyl chloride

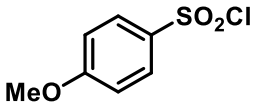

^{1}H NMR (300 MHz, $CDCl_3$): δ = 8.02-7.94 (m, 2H), 7.09-7.01 (m, 2H), 3.93 (s, 3H).

^{13}C NMR (75 MHz, $CDCl_3$): δ = 165.0 (C), 136.2 (C), 129.7 (2CH), 114.8 (2CH), 56.1 (CH_3).

GC-MS (EI): *m/z* (relative intensity) = 206 (25), 171 (100), 107 (49).

Spectral data were consistent with S. Madabhushi, R. Jillella, V. Sriramojua, R. Singh, *Green Chem.* **2014**, *16*, 3125-3131.

4-Fluorobenzenesulfonyl chloride

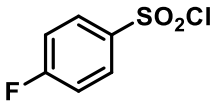

^{1}H NMR (300 MHz, $CDCl_3$): δ = 8.13-8.04 (m, 2H), 7.35-7.26 (m, 2H).

^{13}C NMR (75 MHz, $CDCl_3$): δ = 166.5 (d, *J* = 259.9 Hz, CF), 140.4 (d, *J* = 3.2 Hz, C), 130.3 (d, *J* = 10.1 Hz, 2CH), 114.8 (d, *J* = 23.2 Hz, 2CH).

^{19}F NMR (282 MHz, $CDCl_3$): δ = −100.0.

GC-MS (EI): *m/z* (relative intensity) = 194 (13), 159 (81), 95 (100).

Spectral data were consistent with S. Madabhushi, R. Jillella, V. Sriramojua, R. Singh, *Green Chem.* **2014**, *16*, 3125-3131.

4-Chlorobenzenesulfonyl chloride

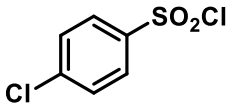

^{1}H NMR (300 MHz, $CDCl_3$): δ = 8.02-7.95 (m, 2H), 7.65-7.57 (m, 2H).

^{13}C NMR (75 MHz, $CDCl_3$): δ = 142.7 (C), 142.3 (C), 130.2 (2CH), 128.6 (2CH).

GC-MS (EI): *m/z* (relative intensity) = 212 (15), 210 (21), 177 (29), 175 (80), 113 (32), 111 (100).

Spectral data were consistent with S. Madabhushi, R. Jillella, V. Sriramojua, R. Singh, *Green Chem.* **2014**, *16*, 3125-3131.

4-Bromobenzenesulfonyl chloride

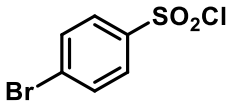

^{1}H NMR (300 MHz, $CDCl_3$): δ = 7.94-7.88 (m, 2H), 7.81-7.74 (m, 2H).

^{13}C NMR (75 MHz, $CDCl_3$): δ = 143.2 (C), 133.2 (CH), 131.0 (2C), 128.5 (2CH).

GC-MS (EI): *m/z* (relative intensity) = 256 (40), 254 (29), 221 (100), 219 (95), 157 (94), 155 (95).

Spectral data were consistent with G. K. S. Prakash, T. Mathew, C. Panja, and G. A. Olah, *J. Org. Chem.* **2007**, *72*, 5847-5850.

4-Iodobenzenesulfonyl chloride

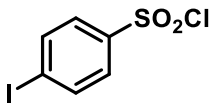

^{1}H NMR (300 MHz, $CDCl_3$): δ = 8.03-7.96 (m, 2H), 7.78-7.71 (m, 2H).

^{13}C NMR (75 MHz, $CDCl_3$): δ = 143.9 (C), 139.1 (2CH), 128.2 (2CH), 103.9 (C).

GC-MS (EI): *m/z* (relative intensity) = 302 (77), 267 (100), 203 (84).

Spectral data were consistent with J. R. DeBergh, N. Niljianskul, S. L. Buchwald, *J. Am. Chem. Soc.* **2013**, *135*, 10638-10641.

4-(Trifluoromethyl)benzenesulfonyl chloride

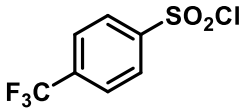

^{1}H NMR (300 MHz, $CDCl_3$): δ = 8.20 (d, *J* = 8.2 Hz, 2H), 7.91 (d, *J* = 8.2 Hz, 2H).

^{13}C NMR (75 MHz, $CDCl_3$): δ = 147.2 (C), 136.8 (q, *J* = 33.5 Hz, C), 127.8 (2CH), 127.1 (q, *J* = 3.6 Hz, 2CH), 122.9 (q, *J* = 273.4 Hz, CF_3).

^{19}F NMR (282 MHz, $CDCl_3$): δ = −63.9.

GC-MS (EI): *m/z* (relative intensity) = 244 (8.8), 225 (9.8), 209 (78), 145 (100).

Spectral data were consistent with J. R. DeBergh, N. Niljianskul, S. L. Buchwald, *J. Am. Chem. Soc.* **2013**, *135*, 10638-10641.

Methyl 4-(chlorosulfonyl)benzoate

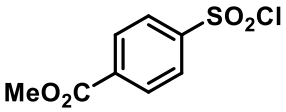

^{1}H NMR (400 MHz, $CDCl_3$): δ = 8.27 (d, *J* = 8.7 Hz, 2H), 8.12 (d, *J* = 8.7 Hz, 2H).

^{13}C NMR (100 MHz, $CDCl_3$): δ = 165.0 (COO), 147.6 (C), 136.2 (C), 131.0 (2CH), 127.2 (2CH), 53.1 (CH_3).

GC-MS (EI): *m/z* (relative intensity) = 234 (16), 203 (61), 199 (100), 135 (78).

Spectral data were consistent with J. R. DeBergh, N. Niljianskul, S. L. Buchwald, *J. Am. Chem. Soc.* **2013**, *135*, 10638-10641.

4-(Pentafluoro-λ^{6}-sulfanyl)benzenesulfonyl chloride

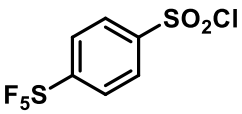

^{1}H NMR (300 MHz, $CDCl_3$): δ = 8.18 (d, *J* = 9.1 Hz, 2H), 8.07-8.00 (m, 2H).

^{13}C NMR (75 MHz, $CDCl_3$): δ = 158.3 (quintet, *J* = 19.0 Hz, C), 146.6 (C), 128.0 (quintet, *J* = 4.9 Hz, 2CH) 127.9 (2CH).

^{19}F NMR (282 MHz, $CDCl_3$): δ = 80.1 (quintet, 1F), 61.9 (d, *J* = 150.8 Hz, 4F).

GC-MS (EI): *m/z* (relative intensity) = 302 (6.5), 267 (100), 203 (70).

Spectral data were consistent with M. V. Westphal, B. T. Wolfstädter, J.-M. Plancher, J. Gatfield, E. M. Carreira, *ChemMedChem* **2015**, *10*, 461-469.

4-Methylbenzenesulfonyl chloride

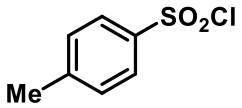

^{1}H NMR (300 MHz, $CDCl_3$): δ = 7.96-7.89 (m, 2H), 7.45-7.37 (m, 2H), 2.49 (s, 3H).

^{13}C NMR (75 MHz, $CDCl_3$): δ = 147.0 (C), 141.8 (C), 130.4 (2CH), 127.2 (2CH), 22.0 (CH_3).

GC-MS (EI): *m/z* (relative intensity) = 190 (16), 155 (46), 91 (100).

Spectral data were consistent with S. Madabhushi, R. Jillella, V. Sriramojua, R. Singh, *Green Chem.* **2014**, *16*, 3125-3131.

4-Nitrobenzenesulfonyl chloride

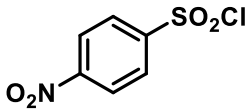

^{1}H NMR (300 MHz, $CDCl_3$): δ = 8.53-8.44 (m, 2H), 8.31-8.21 (m, 2H).

^{13}C NMR (75 MHz, $CDCl_3$): δ = 151.4 (C), 148.7 (C), 128.7 (2CH), 125.2 (2CH).

GC-MS (EI): *m/z* (relative intensity) = 221 (7.4), 186 (100), 122 (45).

Spectral data were consistent with G. K. S. Prakash, T. Mathew, C. Panja, and G. A. Olah, *J. Org. Chem.* **2007**, *72*, 5847-5850.

Benzenesulfonyl chloride

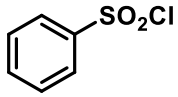

^{1}H NMR (300 MHz, $CDCl_3$): δ = 8.09-8.01 (m, 2H), 7.79-7.71 (m, 1H), 7.68-7.58 (m, 2H).

^{13}C NMR (75 MHz, $CDCl_3$): δ = 144.5 (C), 135.4 (CH), 129.8 (2CH), 127.1 (2CH).

GC-MS (EI): *m/z* (relative intensity) = 176 (12), 141 (45), 77 (100).

Spectral data were consistent with G. K. S. Prakash, T. Mathew, C. Panja, and G. A. Olah, *J. Org. Chem.* **2007**, *72*, 5847-5850.

2-Chlorobenzenesulfonyl chloride

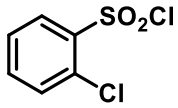

^{1}H NMR (300 MHz, $CDCl_3$): δ = 8.19-8.12 (m, 1H), 7.71-7.63 (m, 2H), 7.56-7.45 (m, 1H).

^{13}C NMR (75 MHz, $CDCl_3$): δ = 141.4 (C), 136.1 (CH), 133.1 (C), 133.0 (CH), 130.6 (CH), 127.5 (CH).

GC-MS (EI): *m/z* (relative intensity) = 212 (18), 210 (26), 177 (27), 175 (76), 113 (31), 111 (100).

HRMS (EI): *m/z* = calculated for $C_6H_4O_2SCl_2^{+\bullet}$: 209.9304, found: 209.9304.

2-Bromobenzenesulfonyl chloride

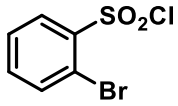

^{1}H NMR (300 MHz, $CDCl_3$): δ = 8.24-8.16 (m, 1H), 7.91-7.83 (m, 1H), 7.60-7.52 (m, 2H).

^{13}C NMR (75 MHz, $CDCl_3$): δ = 143.1 (C), 136.6 (CH), 136.0 (CH), 130.9 (CH), 128.2 (CH), 120.9 (C).

GC-MS (EI): *m/z* (relative intensity) = 256 (50), 254 (37), 221 (92), 219 (89), 157 (98), 155 (100).

Spectral data were consistent with J. R. DeBergh, N. Niljianskul, S. L. Buchwald, *J. Am. Chem. Soc.* **2013**, *135*, 10638-10641.

2-(Trifluoromethyl)benzenesulfonyl chloride

^{1}H NMR (300 MHz, $CDCl_3$): δ = 8.41-8.34 (m, 1H), 8.02-7.95 (m, 1H), 7.93-7.82 (m, 2H).

^{13}C NMR (75 MHz, $CDCl_3$): δ = 142.5 (C), 135.5 (CH), 133.3 (CH), 131.5 (CH), 129.0 (q, *J* = 6.2 Hz, CH), 122.1 (q, *J* = 274.4 Hz, CF_3). Aromatic carbon next to the CF_3-group was not observed.

^{19}F NMR (282 MHz, $CDCl_3$): δ = −57.8.

GC-MS (EI): *m/z* (relative intensity) = 244 (6.7), 209 (77), 145 (100).

Spectral data were consistent with Y.-M. Pu, A. Christesen, Y.-Y. Ku, *Tetrahedron Lett.* **2010**, *51*, 418-421.

Methyl 2-(chlorosulfonyl)benzoate

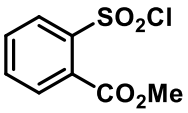

^{1}H NMR (300 MHz, $CDCl_3$): δ = 8.20-8.15 (m, 1H), 7.84-7.68 (m, 3H), 3.99 (s, 3H).

^{13}C NMR (75 MHz, $CDCl_3$): δ = 166.4 (COO), 141.8 (C), 135.3 (CH), 132.5 (C), 131.6 (CH), 130.2 (CH), 129.2 (CH), 53.6 (CH_3).

GC-MS (EI): *m/z* (relative intensity) = 234 (4.5), 203 (71), 199 (100), 135 (27).

Spectral data were consistent with J. Waser, B. Gaspar, H. Nambu, E. M. Carreira, *J. Am. Chem. Soc.* **2006**, *128*, 11693-11712.

2-Azidobenzenesulfonyl chloride

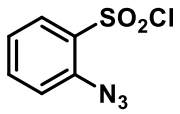

^{1}H NMR (300 MHz, $CDCl_3$): δ = 8.05 (dd, *J* = 8.1 Hz, 1.5 Hz, 1H), 7.75 (ddd, *J* = 8.1 Hz, 7.5 Hz, 1.5 Hz, 1H), 7.41 (dd, *J* = 8.1 Hz, 1.0 Hz, 1H), 7.32 (ddd, *J* = 8.1 Hz, 7.5 Hz, 1.0 Hz, 1H).

^{13}C NMR (75 MHz, $CDCl_3$): δ = 139.7 (C), 136.6 (CH), 133.7 (C), 130.2 (CH), 124.8 (CH), 120.8 (CH).

HRMS (EI): *m/z* = calculated for $C_6H_4N_3O_2SCl^{+\bullet}$: 216.9707, found: 216.9711.

2-Nitrobenzenesulfonyl chloride

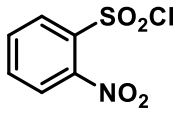

^{1}H NMR (300 MHz, $CDCl_3$): δ = 8.27 (dd, *J* = 7.7 Hz, 1.4 Hz, 1H), 7.99-7.81 (m, 3H).

^{13}C NMR (75 MHz, $CDCl_3$): δ = 136.7 (CH), 136.0 (C), 133.1 (CH), 133.1 (C), 130.6 (CH), 125.4 (CH).

GC-MS (EI): *m/z* (relative intensity) = 221 (3.5), 186 (100).

HRMS (EI): *m/z* = calculated for $C_6H_4NO_4SCl^{+\bullet}$: 220.9544, found: 220.9540.

3-Chlorobenzenesulfonyl chloride

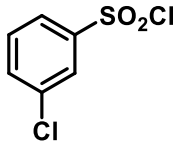

^{1}H NMR (300 MHz, $CDCl_3$): δ = 8.03 (dd, *J* = 1.9 Hz, 1H), 7.94 (ddd, *J* = 8.0 Hz, 1.9 Hz, 1.1 Hz, 1H), 7.72 (ddd, *J* = 8.0 Hz, 1.9 Hz, 1.1 Hz, 1H), 7.59 (dd, *J* = 8.0 Hz, 1H).

^{13}C NMR (75 MHz, $CDCl_3$): δ = 145.5 (C), 136.0 (C), 135.5 (CH), 131.1 (CH), 127.2 (CH), 125.2 (CH).

GC-MS (EI): *m/z* (relative intensity) = 212 (16), 210 (23), 177 (20), 175 (55), 113 (31), 111 (100).

Spectral data were consistent with Y.-M. Pu, A. Christesen, Y.-Y. Ku, *Tetrahedron Lett.* **2010**, *51*, 418-421.

3-Bromobenzenesulfonyl chloride

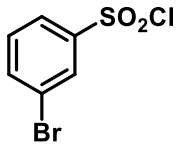

^{1}H NMR (300 MHz, $CDCl_3$): δ = 8.18 (dd, *J* = 1.9 Hz, 1H), 7.99 (ddd, *J* = 8.0 Hz, 1.9 Hz, 1.0 Hz, 1H), 7.88 (ddd, *J* = 8.0 Hz, 1.9 Hz, 1.0 Hz, 1H), 7.52 (dd, *J* = 8.0 Hz, 1H).

^{13}C NMR (75 MHz, $CDCl_3$): δ = 145.6 (C), 138.4 (CH), 131.3 (CH), 130.0 (CH), 125.6 (CH), 123.6 (C).

GC-MS (EI): *m/z* (relative intensity) = 256 (46), 254 (34), 221 (84), 219 (82), 157 (99), 155 (100).

HRMS (EI): *m/z* = calculated for $C_6H_4O_2SClBr^{+\bullet}$: 253.9798, found: 253.8791.

3-(Trifluoromethyl)benzenesulfonyl chloride

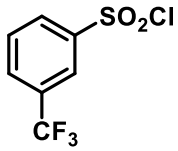

^{1}H NMR (300 MHz, $CDCl_3$): δ = 8.31 (s, 1H), 8.26 (d, *J* = 8.0 Hz, 1H), 8.02 (d, *J* = 8.0 Hz, 1H), 7.82 (dd, *J* = 8.0 Hz, 1H).

^{13}C NMR (75 MHz, $CDCl_3$): δ = 145.2 (C), 132.7 (q, *J* = 34.4 Hz, C), 132.0 (q, *J* = 3.3 Hz, CH), 130.9 (CH), 130.3 (CH), 124.3 (q, *J* = 3.9 Hz, CH), 122.8 (q, *J* = 273.3 Hz, CF_3).

^{19}F NMR (282 MHz, $CDCl_3$): δ = −63.4.

GC-MS (EI): *m/z* (relative intensity) = 244 (7.8), 225 (14), 209 (77), 145 (100).

Spectral data were consistent with Y.-M. Pu, A. Christesen, Y.-Y. Ku, *Tetrahedron Lett.* **2010**, *51*, 418-421.

Methyl 3-(chlorosulfonyl)benzoate

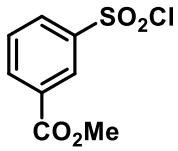

^{1}H NMR (300 MHz, $CDCl_3$): δ = 8.69 (dd, *J* = 1.9 Hz, 1H), 8.41 (ddd, *J* = 7.9 Hz, 1.9 Hz, 1.0 Hz, 1H), 8.22 (ddd, *J* = 7.9 Hz, 1.9 Hz, 1.0 Hz, 1H), 7.74 (dd, *J* = 7.9 Hz, 1H), 4.00 (s, 3H).

^{13}C NMR (75 MHz, $CDCl_3$): δ = 164.8 (COO), 144.9 (C), 136.1 (CH), 132.2 (C), 130.9 (CH), 130.2 (CH), 128.3 (CH), 53.1 (CH_3).

GC-MS (EI): *m/z* (relative intensity) = 234 (16), 203 (73), 199 (100), 135 (88).

Spectral data were consistent with A. Freitag, P. Prajwal, A. Shymanets, C. Harteneck, B. Nürnberg, C. Schächtele, M. Kubbutat, F. Totzke, S. A. Laufer, *J. Med. Chem.* **2015**, *58*, 212-221.

3-Nitrobenzenesulfonyl chloride

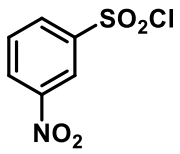

^{1}H NMR (300 MHz, $CDCl_3$): δ = 8.89 (dd, *J* = 2.0 Hz, 1H), 8.62 (ddd, *J* = 8.1 Hz, 2.0 Hz, 1.0 Hz, 1H), 8.39 (ddd, *J* = 8.1 Hz, 2.0 Hz, 1.0 Hz, 1H), 7.91 (dd, *J* = 8.1 Hz, 1H).

^{13}C NMR (75 MHz, $CDCl_3$): δ = 148.5 (C), 145.6 (C), 132.4 (CH), 131.5 (CH), 129.7 (CH), 122.6 (CH).

GC-MS (EI): *m/z* (relative intensity) = 221 (6.9), 186 (100), 122 (46).

Spectral data were consistent with P. J. Hogan, B. G. Cox, *Org. Process Res. Dev.* **2009**, *13*, 875-879.

Methyl 3-(chlorosulfonyl)thiophene-2-carboxylate

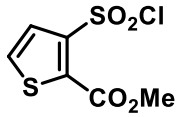

^{1}H NMR (300 MHz, $CDCl_3$): δ = 7.66 (d, *J* = 5.4 Hz, 1H), 7.60 (d, *J* = 5.4 Hz, 1H), 3.99 (s, 3H).

^{13}C NMR (75 MHz, $CDCl_3$): δ = 159.0 (COO), 144.1 (C), 136.1 (C), 130.0 (CH), 130.0 (CH), 53.5 (CH_3).

GC-MS (EI): *m/z* (relative intensity) = 240 (27), 209 (47), 205 (100).

Spectral data were consistent with C. Corral, J. Lissavetzky, A. S. Alvarez-Insúa, A. M. Valdeolmillos, *Org. Prep. Proc. Int.* **1985**, *17*, 163.

Saccharin/Benzo[d]isothiazol-3(2H)-one 1,1-dioxide

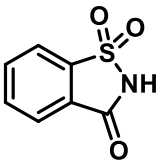

^{1}H NMR (300 MHz, DMSO-d_6): δ = 10.10 (bs, 1H), 8.22-8.14 (m, 1H), 8.07-7.90 (m, 3H).

^{13}C NMR (75 MHz, DMSO-d_6): δ = 160.8 (CO), 139.2 (C), 135.7 (CH), 134.9 (CH), 127.4 (C), 124.9 (CH), 121.3 (CH).

GC-MS (EI): *m/z* (relative intensity) = 183 (72), 119 (92), 92 (68), 76 (100).

Spectral data were consistent with E. Kleinpeter, D. Ströhl, G. Jovanovski, B. Soptrajanov, *J. Mol Struc.* **1991**, *246*, 185-188.

3.4.6 Selected NMR spectra

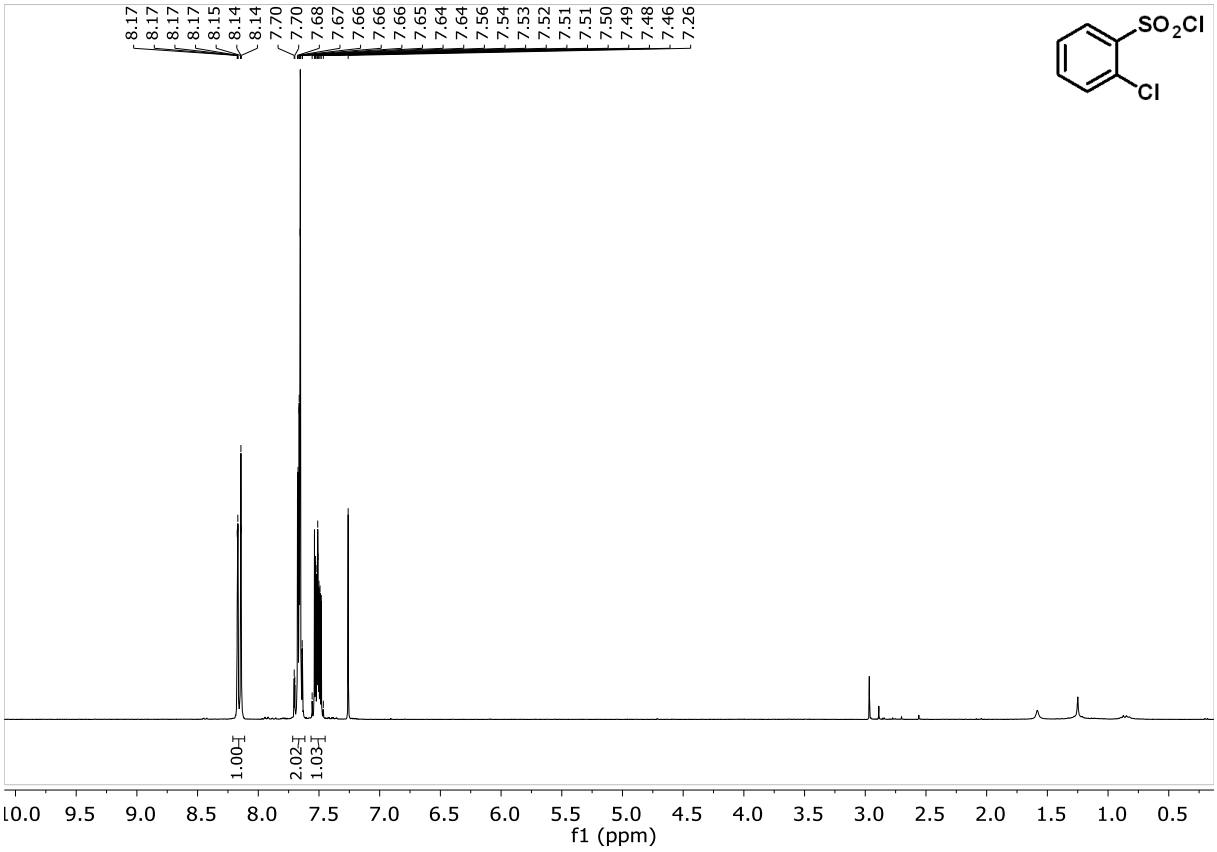

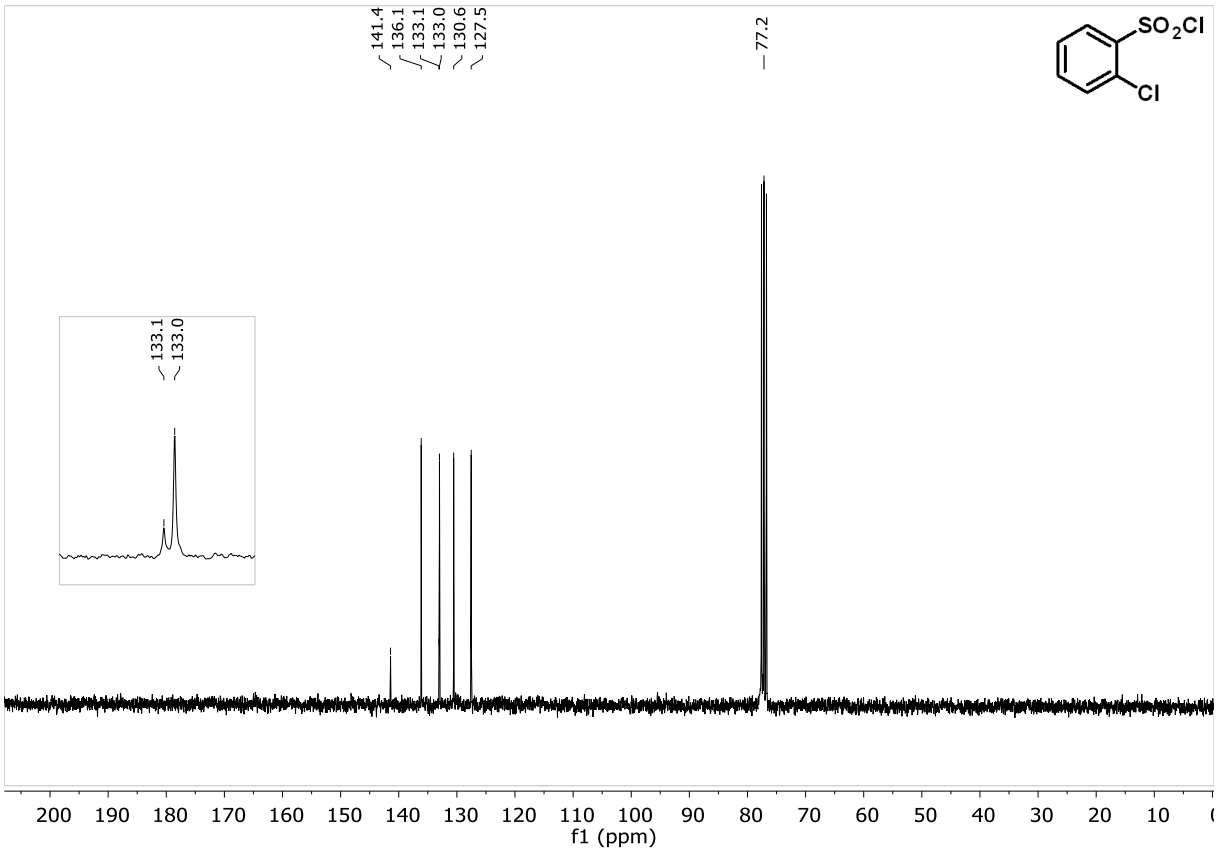

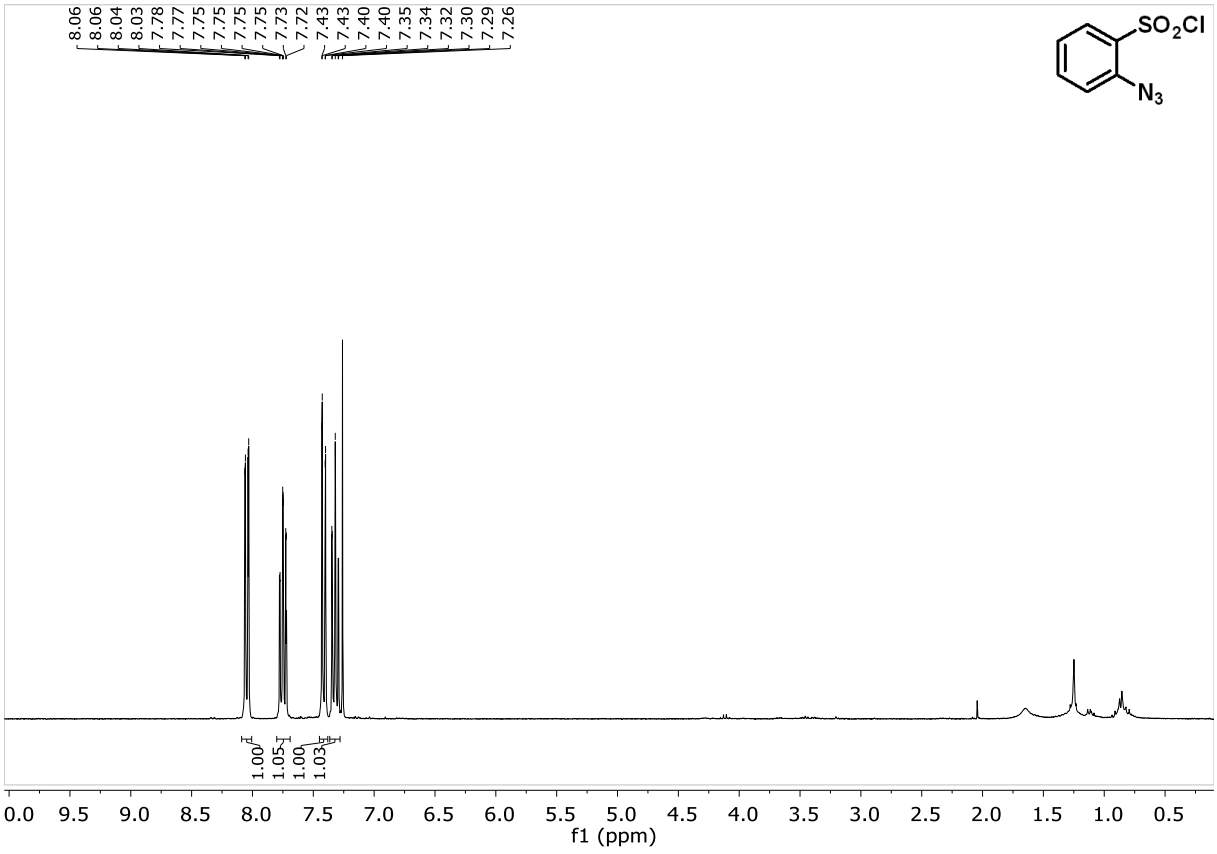
8.06
8.06
8.04
8.03
7.78
7.77
7.75
7.75
7.75
7.75
7.73
7.72
7.43
7.43
7.40
7.40
7.35
7.34
7.32
7.30
7.29
7.26
SO2Cl
N3
1.00
1.05
1.00
1.03
0.0 9.5 9.0 8.5 8.0 7.5 7.0 6.5 6.0 5.5 5.0 4.5 4.0 3.5 3.0 2.5 2.0 1.5 1.0 0.5
f1 (ppm)

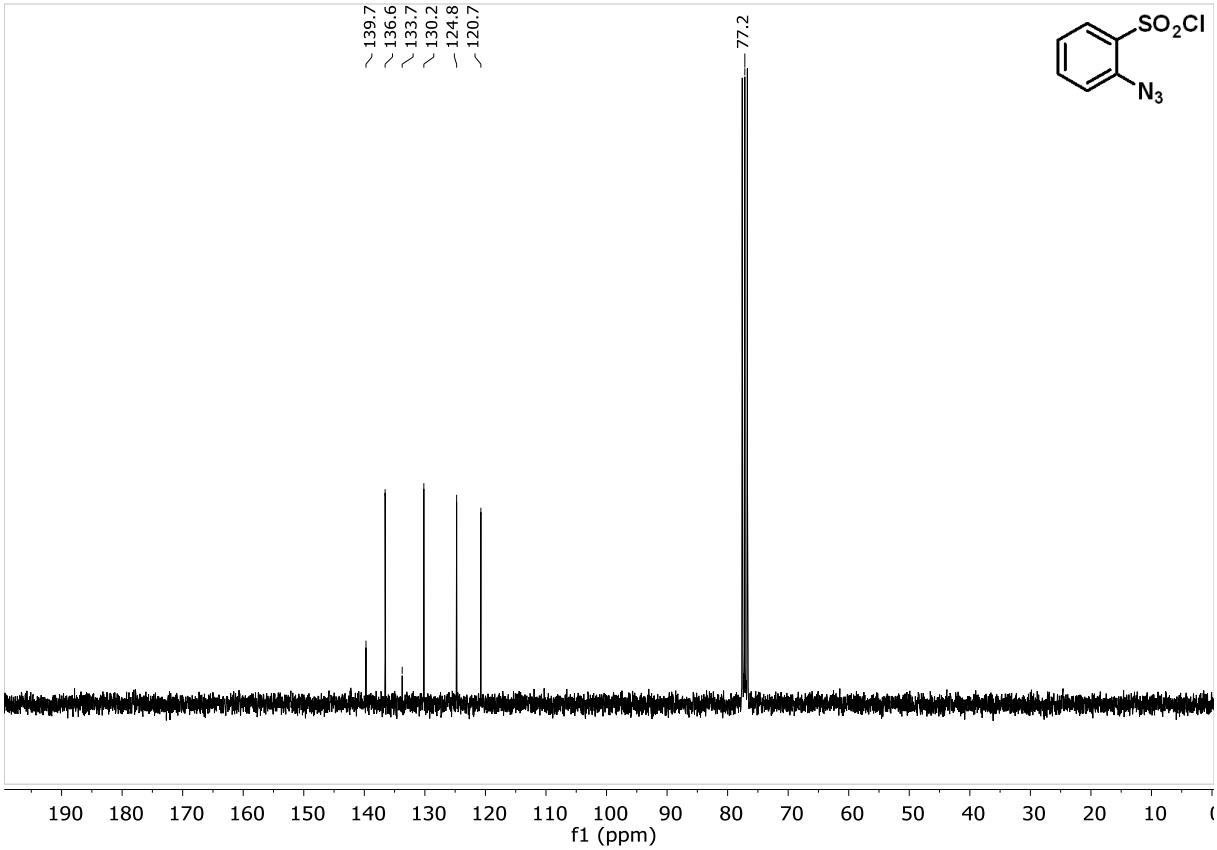
139.7
136.6
133.7
130.2
124.8
120.7
77.2
SO2Cl
N3
190 180 170 160 150 140 130 120 110 100 90 80 70 60 50 40 30 20 10
f1 (ppm)

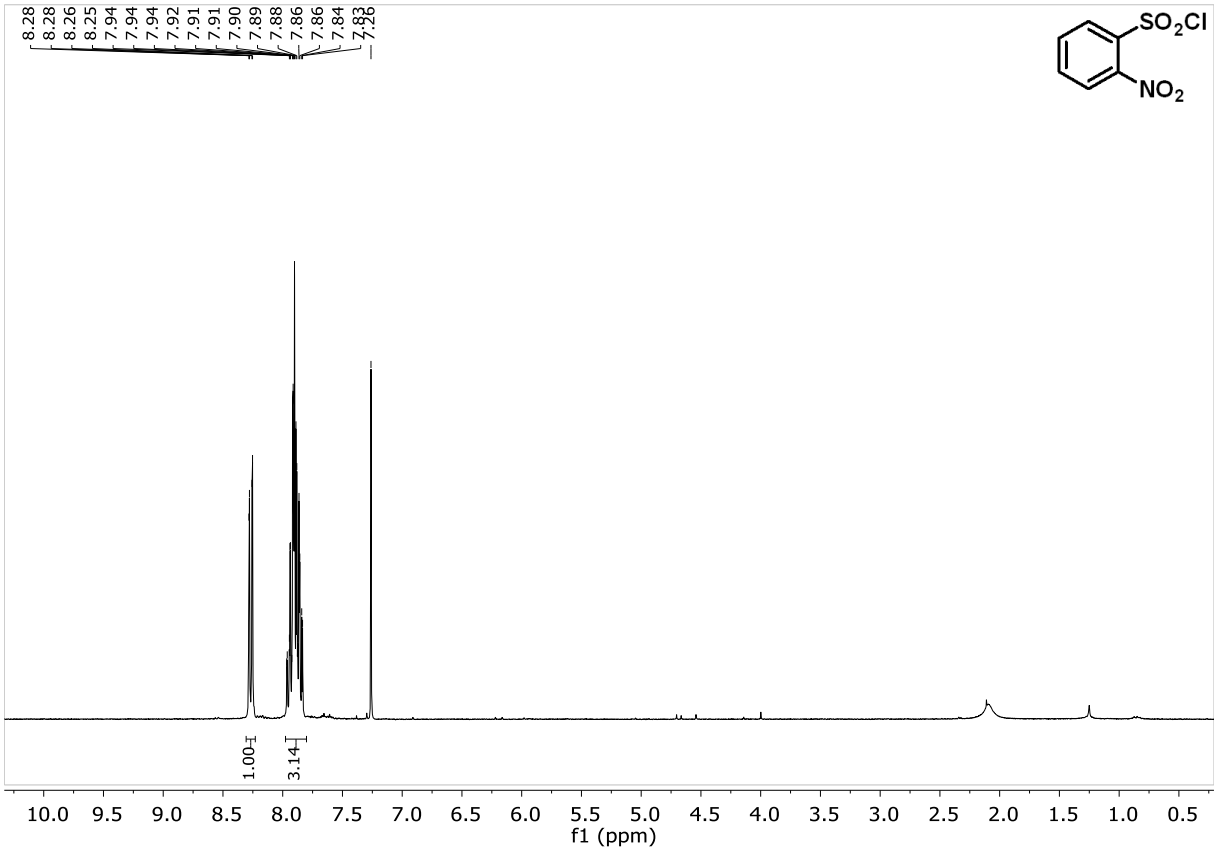
8.28
8.28
8.26
8.25
7.94
7.94
7.94
7.92
7.91
7.91
7.90
7.89
7.88
7.86
7.86
7.84
7.83
7.80
SO2Cl
NO2
1.00
3.14
10.0 9.5 9.0 8.5 8.0 7.5 7.0 6.5 6.0 5.5 5.0 4.5 4.0 3.5 3.0 2.5 2.0 1.5 1.0 0.5
f1 (ppm)

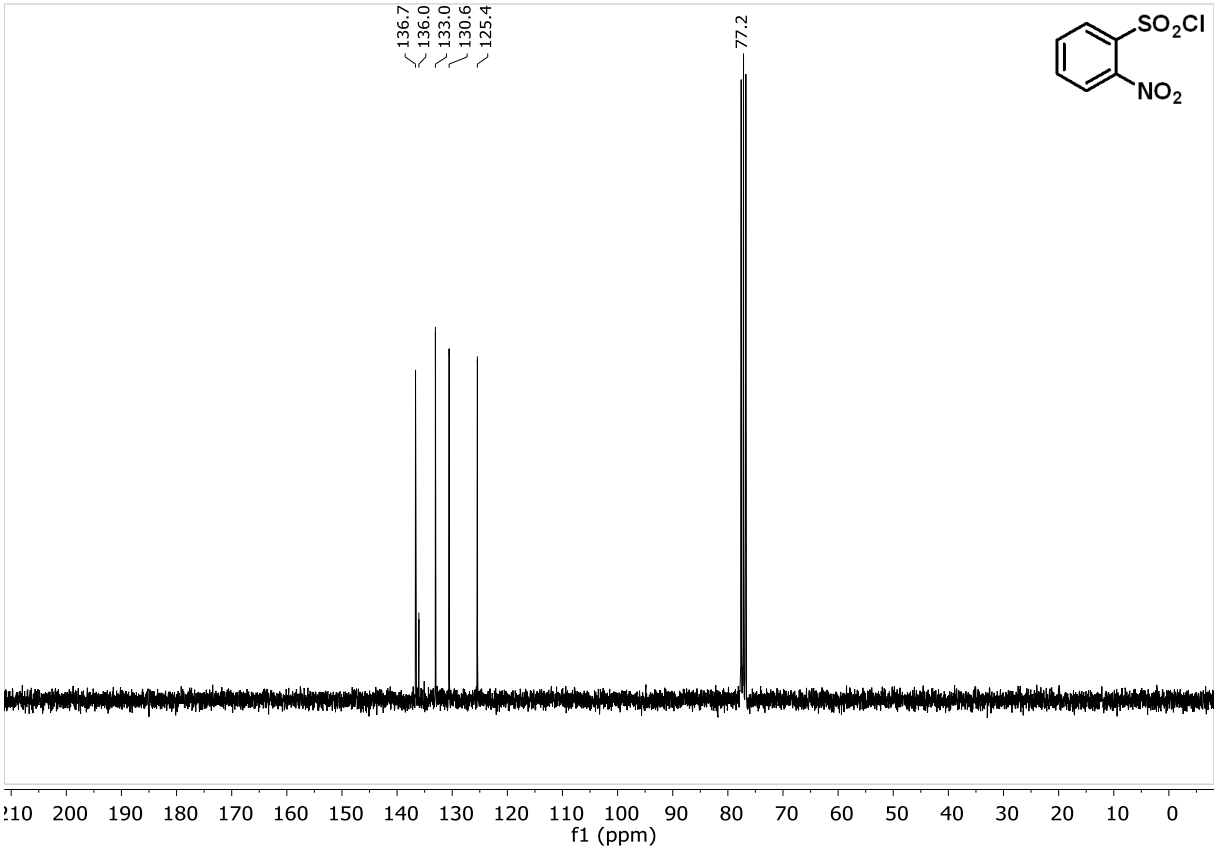
136.7
136.0
133.0
130.6
125.4
77.2
SO2Cl
NO2
210 200 190 180 170 160 150 140 130 120 110 100 90 80 70 60 50 40 30 20 10 0
f1 (ppm)

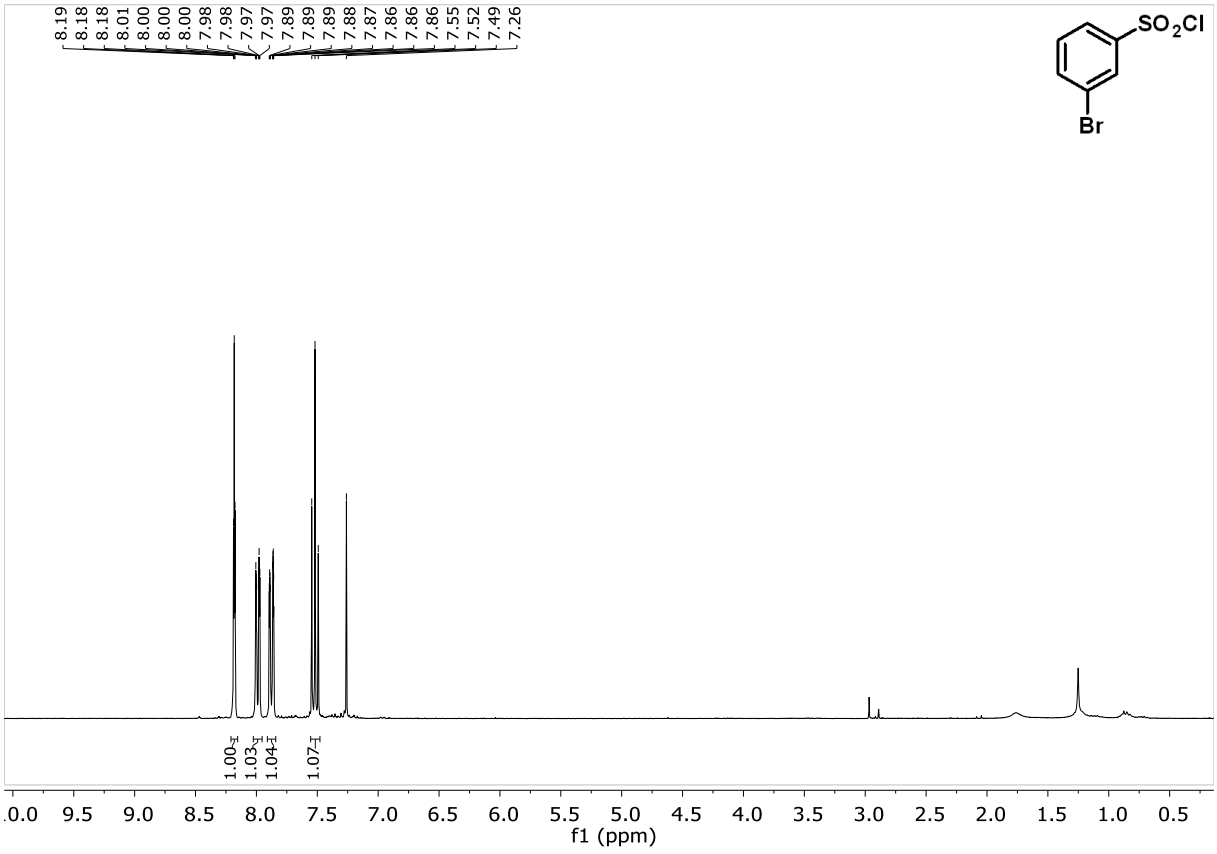
8.19
8.18
8.18
8.01
8.00
8.00
8.00
7.98
7.98
7.97
7.97
7.89
7.89
7.89
7.88
7.87
7.86
7.86
7.86
7.55
7.52
7.49
7.26
SO2Cl
Br
1.00
1.03
1.04
1.07
f1 (ppm)

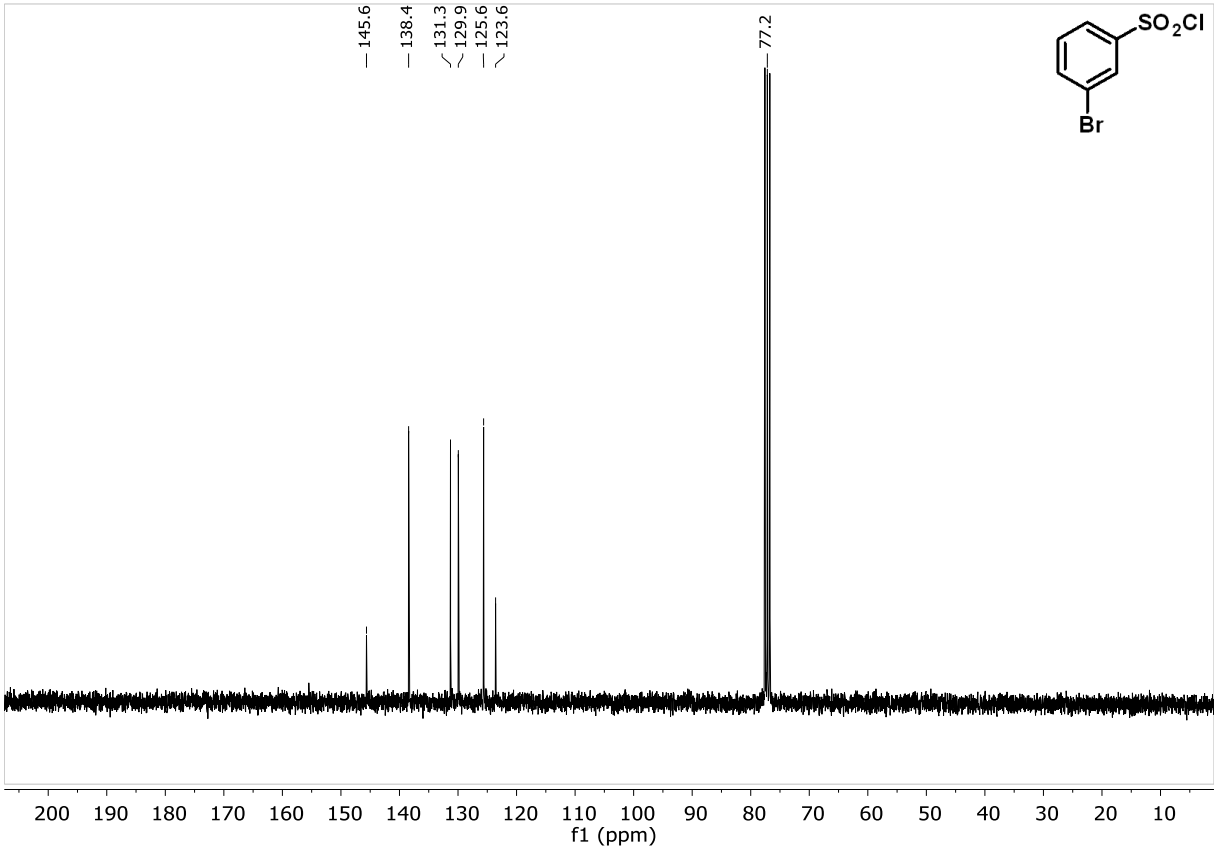
145.6
138.4
131.3
129.9
125.6
123.6
77.2
SO2Cl
Br
f1 (ppm)

3.5 References

[1] a) J. Hoyle, in: *The Chemistry of Sulfonic Acids, Esters and their Derivatives*, Eds.: S. Patai, Z. Rappoport, Wiley, New York, **1991**, pp. 351-399; b) K. Tanaka, in: *The Chemistry of Sulfonic Acids, Esters and their Derivatives*, Eds.: S. Patai, Z. Rappoport, Wiley, New York, **1991**, pp. 401-452; c) G. P. Dado, E. A. Knaggs, M. J. Nepras, in: *Kirk-Othmer Encyclopedia of Chemical Technology*, *5th ed., Vol. 23*, Wiley, New York, **2006**; d) O. Lindner, in: *Ullmann's Encyclopedia of Industrial Chemistry, 5th Ed., Vol. A3*, VCH, Weinheim **1985**, pp. 507-537.

[2] a) Compilation of the top 200 prescription drugs in the U.S. in 2012: C. W. Lindsley, *ACS Chem. Neurosci.* **2013**, *4*, 905−907; b) S. D. Roughley, A. M. Jordan, *J. Med. Chem.* **2011**, *54*, 3451-3479; c) J. S. Carey, D. Laffan, C. Thomson, M. T. Williams, *Org. Biomol. Chem.* **2006**, *4*, 2337-2347.

[3] a) T. W. Greene, P. G. M. Wuts, in: *Protective Groups in Organic Chemistry*, 3rd ed., Wiley, New York, **1999**; b) G. Theodoridis, *Tetrahedron* **2000**, *56*, 2339-2358.

[4] See for example the use of activated esters in cross-coupling reactions: a) D. G. Yu, B. J. Li, Z. J. Shi, *Acc. Chem. Res.* **2010**, *43*,1486-1495; b) B.-J. Li, D.-G. Yu, C.-L. Sun, Z.-J. Shi, *Chem. Eur. J.* **2011**, *17*, 1728-1759; c) J. Cornella, C. Zarate, R. Martin, *Chem. Soc. Rev.* **2014**, *43*, 8081-8097.

[5] Z. Wang, in: *Comprehensive Organic Name Reactions and Reagents*, Wiley, New York, **2010**, Ch. 316, 1418-1421.

[6] R. Adams, C. S. Marvel, H. T. Clarke, G. S. Babcock, T. F. Murray, *Org. Synth*. **1921**, *1*, 21-28.

[7] G. Blotny, *Tetrahedron Lett.* **2003**, *44*, 1499-1501.

[8] a) T. B. Johnson, J. M. Sprague, *J. Am. Chem. Soc.* **1936**, *58*, 1348-1352; b) Z. Yang, B. Zhou, J. Xu, *Synthesis* **2014**, *46*, 225-229; c) G. K. S. Prakash, T. Mathew, C. Panja, G. Olah, *J. Org. Chem.* **2007**, *72*, 5847-5850; d) K. Bahrami, M. M. Khodaei, M. Soheilizad, *J. Org. Chem.* **2009**, *74*, 9287-9291.

[9] a) M. B. Smith, J. March, *March's Advanced Organic Chemistry: Reactions, Mechanisms, and Structure*, *6th ed.*, Wiley, New York, **2006**, pp. 920; b) *ibid.* pp. 1850.

[10] H. Meerwein, G. Dittmar, R. Göllner, K. Hafner, F. Mensch, O. Steinfort, *Chem. Ber.* **1957**, *90*, 841-852.

[11] A. J. Prinsen, H. Cerfontain, *Recl. Trav. Chim. Pays-Bas* **1965**, *84*, 24-30.

[12] E. J. Emmett, M. C. Willis, *Asian J. Org. Chem.* **2015**, *4*, 602-611.

[13] P. J. Hogan, B. G. Cox, *Org. Process. Res. Dev.* **2009**, *13*, 875-879.

[14] a) J. J. Byerley, G. L. Rempel, V. Thang Le, *J. Chem. Eng. Data* **1980**, *25*, 55-56; b) L. Malet-Sanz, J. Madrzak, S. V. Ley, I. R. Baxendale, *Org. Biomol. Chem.* **2010**, *8*, 5324-5332.

[15] See experimental section 3.4 or the Supporting Information of the published manuscript.

[16] M. Májek, F. Filace, A. Jacobi von Wangelin, *Chem. Eur. J.* **2015**, *21,* 4518-4522.

[17] M. Majek, A. Jacobi von Wangelin, *Acc. Chem. Res.* **2016**, *49, 2316-2327.*

[18] M. Májek, F. Filace, A. Jacobi von Wangelin, *Beilstein J. Org. Chem.* **2014**, *10*, 981-989.

[19] A. R. Katritzky, in: *Handbook of Heterocyclic Chemistry*, Pergamon, Oxford, **1985**, pp. 219-220.

[20] L. Gu, C. Jin, J. Liu, H. Ding, B. Fan, *Chem. Commun.* **2014**, *50*, 4643-4945.

[21] J. D. Nguyen, E. M. D'Amato, J. M. R. Narayanam, C. R. J. Stephenson, *Nat. Chem.* **2012**, *4*, 854-859.

[22] L. He, G. Qiu, Y. Gao, J. Wu, *Org. Biomol. Chem.* **2014**, *12*, 6965-6971.

[23] D. J. Ager, D. P. Pantaleone, S. A. Henderson, A. R. Katritzky, I. Prakash, D. E. Walters, *Angew. Chem. Int. Ed.* **1998**, *37*, 1802-1823.

[24] a) M. Májek, A. Jacobi von Wangelin, *Chem. Commun*. **2013**, *49*, 5507-5509; b) M. Májek, A. Jacobi von Wangelin, *Angew. Chem. Int. Ed.* **2015**, *54*, 2270-2274.

[25] a) D. P. Hari, P. Schroll, B. König, *J. Am. Chem. Soc.* **2012**, *134*, 2958-2961; b) I. Ghosh, L. Marzo, A. Das, R. Shaikh, B. König, *Acc. Chem. Res.* **2016**, *49*, 1566-1577.

[26] A. U. Meyer, S. Jäger, D. P. Hari, B. König, *Adv. Synth. Catal.* **2015** 357, 2050-2054.

[27] B. L. Johansson, B. Persson, *Acta Chem. Scand. B* **1978**, *32*, 431-436.

[28] U. Megerle, R. Lechner, B. König, E. Riedle, *Photochem. Photobiol. Sci.* **2010**, *9*, 1400-1406.

[29] J. Schachtner, P. Bayer, A. Jacobi von Wangelin, *Beilstein J. Org. Chem.* **2016**, *12*, 1798-1811.

[30] U. Megerle, R. Lechner, B. König, E. Riedle, *Photochem Photobiol Sci.* **2010**, *9*, 1400-1406.

4 Dichromatic photocatalytic substitutions of aryl halides with a small organic dye[i,ii]

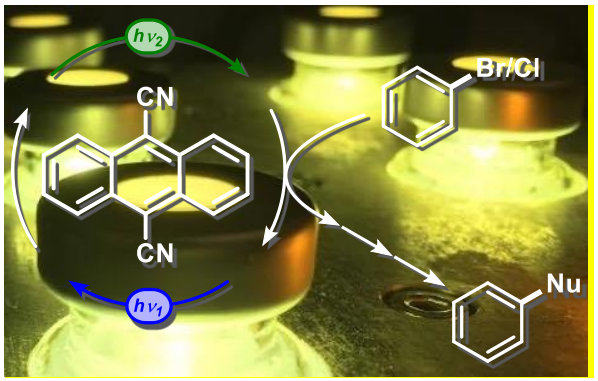

Abstract: Photocatalytic bond activations are generally limited by the photon energy and the efficiency of energy and electron transfer processes. Direct two-photon processes provide sufficient energy but the ultra-short lifetimes of the excited states prohibit chemical reactions. The commercial dye 9,10-dicyanoanthracene enabled photocatalytic aromatic substitutions of non-activated aryl halides. This reaction operates under VIS irradiation via sequential photonic, electronic, and photonic activation of the simple organic dye. The resultant highly reducing excited photocatalyst anion readily effected C-H, C-C, C-P, C-S, and C-B bond formations. Detailed synthetic, spectroscopic, and theoretical studies support a biphotonic catalytic mechanism.

[i] Reproduced from M. Neumeier, D. Sampedro, M. Májek, V. de la Peña O´Shea, A. Jacobi von Wangelin, R. Pérez-Ruiz, *Chem. Eur. J.* **2018**, *24*, 105-108 with permission of Wiley-VCH. Schemes, tables and text may differ from published version.

[ii] Author contributions: M.N. performed experimental and analytical work. D.S. performed theoretical calculations. M.M. contributed to the extension of standard protocol towards other heteroatoms. R.P-R. and V.P.O.performed and evaluated the spectroscopic experiments. A.J.v.W. and R.P-R. guided the project. All authors contributed to the writing of the manuscript.

4.1 Introduction

The efficient utilization of visible light for the activation of organic molecules has been developed to great maturity over the past decade.[1] However, many of the photocatalytic processes require activated substrates that facilitate the generation of radical intermediates in the vicinity of heteroatomic functional groups (amines, carbonyls)[2] or by irreversible reaction steps[3]. Consequently, photocatalytic activations of unbiased or non-activated substrates have received very little attention. Generally, the scope of photocatalytic bond activations is limited by the energy of the visible photon (which is sufficient for the cleavage of weak C-I, C_{sp3}-Br and π-bonds) and the energetic losses during the involved energy and electron transfers.[4] The reductive cleavage of non-activated aryl bromides/chlorides by photocatalytic energy transfer or single electron transfer (SET) is beyond the range of the visible spectrum which constitutes a severe limitation of arene functionalizations. Apart from direct UV processes,[5] recent examples of successful activations of non-activated aryl halides with visible light include the use of strongly reducing excited iridium photocatalysts (with transition metal co-catalysts)[6] and indirect two-photon processes (Scheme 1).[7] The latter approach holds great potential due to its high modularity by combining different photocatalysts with photonic activation, energy transfer, and electronic activation steps. While the physical properties of such biphotonic processes are fairly well understood with simple model systems,[8] their applications to more complex organic synthesis settings are scarce. Recent examples of biphotonic activations of aryl halides toward aromatic substitutions include consecutive photo-induced SET cascades[7a-d] and triplet-triplet annihilation[7e-f] (Scheme 4-1, bottom).

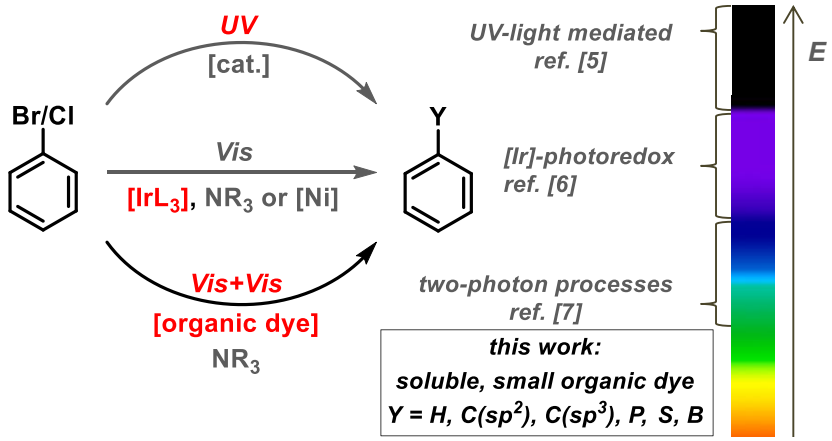

Scheme 4-1. Methods of photocatalytic aryl halide activation.

These approaches constitute new modes of reductive bond activation by the accumulation of two visible photons which significantly expand the “energy window” of photocatalytic aromatic substitutions. However, the overall photocatalytic efficiency is still rather low, the reaction scope barely explored, the reaction conditions mostly complex, and the mechanistic minutiae of the multicomponent reactions not fully understood. Therefore, we have initiated a program that aimed at the extension of the

concept of sequential photonic and electronic activations in order to populate a highly reducing excited radical anion state of the photocatalyst which engages in facile reductive bond activation of various aryl-Br/Cl electrophiles. We believed that a powerful photocatalyst would be a single small weight organic dye that combines the benefits of commercial availability, low price, high solubility, high absorbance of the ground state and the radical anion in the visible region, long lifetime of the excited states, and facile access to the radical anion.

With these framework conditions, we investigated 9,10-dicyanoanthracene (DCA), a simple molecule that fulfills all afore-mentioned criteria. The photophysical data of DCA and its radical anion were reported (Figure 4-1).[9] While DCA itself is a moderate photo-oxidant,[10] the oxidation potential (–2.5 eV)[11] and lifetime (~5 ns)[9a] of the excited radical anion DCA$^{\bullet-*}$ are prime qualifications for its use as a strongly reducing photocatalyst. Applications of DCA$^{\bullet-*}$ to reductive activations of non-activated aryl halides were so far not reported. Herein, we demonstrate the competence of DCA to act as a simple yet powerful photo-reductant in the presence of low-power visible light. This combination exhibits tangible advances over the current state of photocatalytic reductive activation of aryl halides in terms of catalyst and reagents loading, reaction conditions, and applicability to various aromatic functionalization reactions. Further, a detailed mechanistic picture of the underlying photophysical and chemical events was drawn from laser flash photolysis, steady-state fluorescence, and DFT calculations.

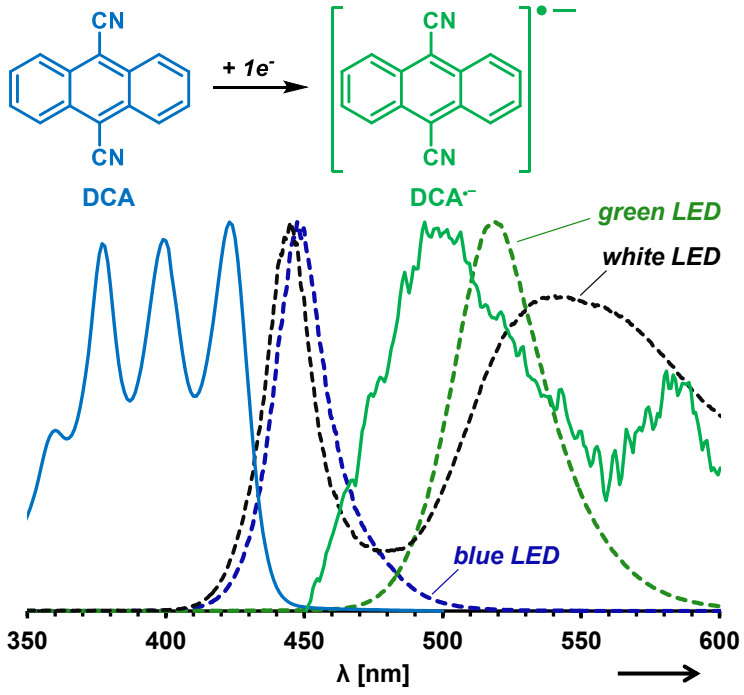

Figure 4-1. Normalized spectra of white, blue, green LED emission (dashed lines) and DCA (blue line), transient DCA$^{\bullet-}$ absorption (green line).

4.2 Results and discussion

The small organic dye DCA has three distinct absorption bands in the visible near-UV-to-blue region while the radical anion $DCA^{\bullet-}$ absorbs green light.[9] The need of simultaneous irradiation with green and blue light was circumvented by an operationally simpler setup with a single cold-white LED that exhibits very similar emission and no tailing into the UV (Figure 4-1).

We studied the reaction of 4-bromobenzonitrile (**1**) and the electron-rich *N*-methyl pyrrole (Table 4-1).[11] Initially, we adopted literature conditions[7a] in the presence of a high excess of *N*-methyl pyrrole and diisopropylethylamine (DIPEA) which afforded very good yields of **2a** (Entry 1, Table 4-1) with 10 mol% photocatalyst. The high catalytic efficiency of DCA even allowed a significant optimization of the reaction conditions under irradiation with a single cold-white LED for 5 h at 20 °C (higher substrate concentration, lower excess of *N*-methyl pyrrole, no excess of amine, Entry 2, Table 4-1). In the absence of either component (catalyst, pyrrole, base, light), no cross-coupling was observed (Entries 3-5, Table 4-1). The poor reactivity with either blue (455 nm) or green light (525 nm) irradiation supports the notion of a dual photoactivation by excitation of DCA and its radical anion (Entry 6, Table 4-1). It is important to note that the photocatalyst exhibited good solubility in acetonitrile and good stability toward bleaching and decomposition. Quantitative analysis of a standard reaction documented a loss of less than ¼ of the catalyst concentration at total conversion of **1**.[11]

Table 4-1. Selected results of optimization reactions.[a]

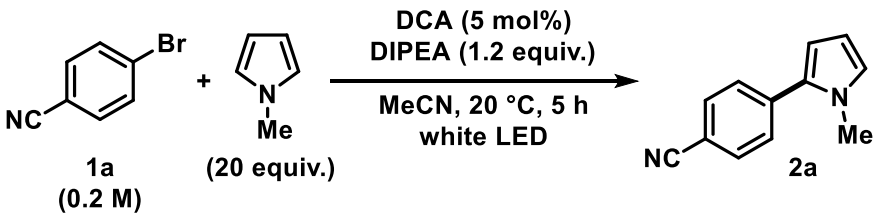

Entry	Deviations from conditions above	Yield in %[b]
1	0.04 M **1a**, 10 mol% DCA, 2 equiv. DIPEA, 40 equiv. *N*-methyl pyrrole, 2 h	87 [c]
2	**no**	**85**
3	as entry 1, w/out *N*-methyl pyrrole	0 (64) [d]
4	as entry 1, w/out photocatalyst or w/out base	0 (0)
5	as entry 1, in the dark	0 (0)
6	as entry 1, blue (455 nm) or green LED (525 nm)	<4 (<10)

[a] **1a** (0.2 M), DCA (5 mol%), DIPEA (1.2 equiv.), *N*-methyl pyrrole (20 equiv.) in MeCN (1 mL); irradiation (cold-white LED, >410 nm), 20 °C, 5 h. [b] GC yields of **2a**; conversion in parentheses if not >95%. [c] 82% isolated yield. [d] 45% benzonitrile as single product.

The optimized conditions (Entry 2, Table 4-1) were applied to various aryl bromides and chlorides (Scheme 4-2). Rapid conversions of challenging electrophiles with an oxidation potential of up to -2.5 V (vs. SCE in acetonitrile) were observed.[11] Aryl halides bearing electron-withdrawing substituents showed higher reactivity which is a direct consequence of the oxidation potentials and the activation barriers of the SET.[11] The same conditions could be applied to the alkylation of *N*-methyl pyrrole.[12]

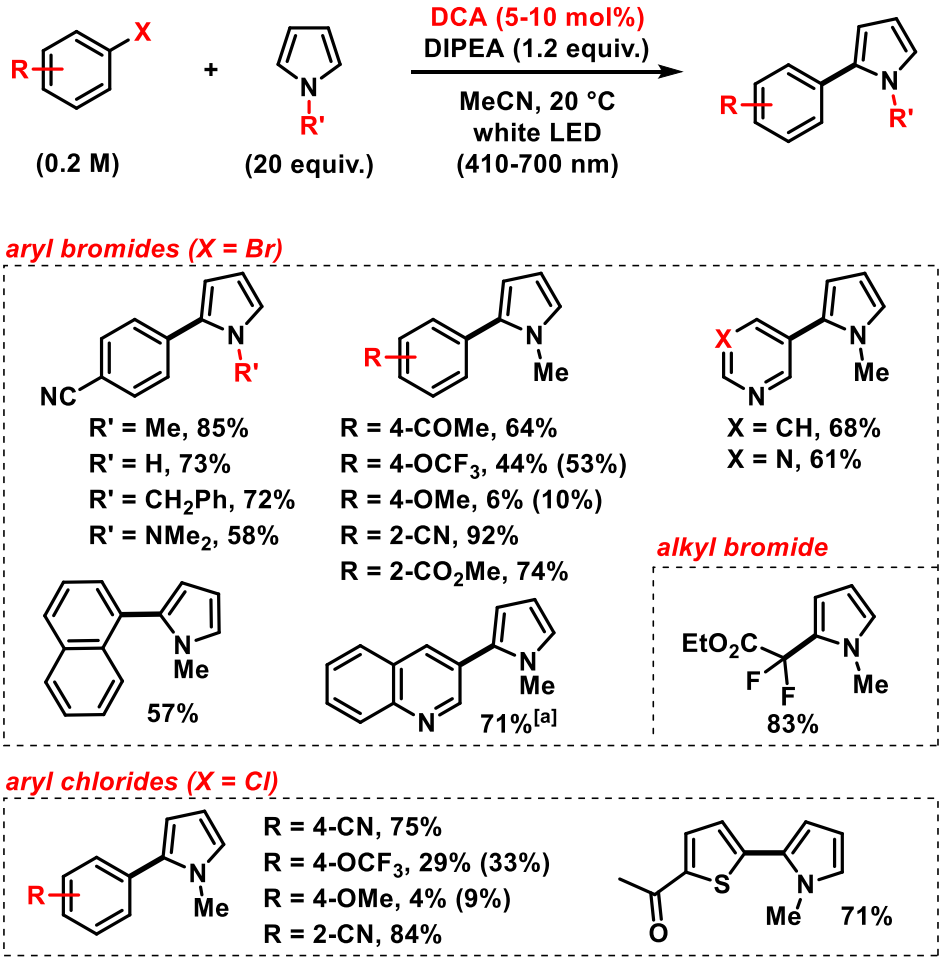

Scheme 4-2. Substrate scope of the 2-aryl pyrrole synthesis.[11] Conversions are given in parentheses if not >90%. [a] 40 equiv. *N*-methyl pyrrole.

We postulate a reaction mechanism that commences with the selective excitation of DCA with blue light to the excited singlet state ^{1}DCA* (Scheme 4-3). From fluorescence quenching studies in the presence of DIPEA (Figure 4-2, top), a quenching rate constant of $k_q(S_1) = 2.3 \cdot 10^{10} M^{-1}s^{-1}$ was calculated[11] which indicates that the radical ion pair formation (DIPEA$^{\bullet+}$ DCA$^{\bullet-}$) in the first catalytic turnover occurs at diffusion rates. Fluorescence studies documented that the quenching with DIPEA is the major deactivation pathway of ^{1}DCA* (99%) which proves the high efficiency of catalytic reaction initiation.[11] Excitation of DCA$^{\bullet-}$ with green light results in the formation of DCA$^{\bullet-*}$. This highly reducing species effects mesolysis of aryl bromides and chlorides to give Ar$^\bullet$ which was confirmed by TEMPO trapping.[11] Reaction of Ar$^\bullet$ with *N*-methyl

pyrrole gives a cyclic vinylogous amino radical which undergoes thermodynamically favoured oxidation by DCA* (ΔG = -2.7 eV). Experimental support for this process rather than the SET from DIPEA comes from the high synthetic efficiency of reactions in the presence of only 1.1 equiv. DIPEA despite the consumption of 1 equiv. base in the terminal acid-base reaction with HBr (Entry 2, Table 4-1 and Scheme 4-2). SET between the cyclic α-enamine radical intermediate with ground state DCA is 4.55 kcal mol^{-1} (0.2 eV) uphill. The quasi co-catalytic role of amine for the initiation of photocatalysis is also evident from the fact that little to no hydro-dehalogenation was observed under standard conditions as, unlike literature protocols,[7a] no excess of DIPEA was employed and the majority of amine resides as HBr salt. Reaction of **1a** in *d*$_3$-acetonitrile gave no *deutero*-benzonitrile.

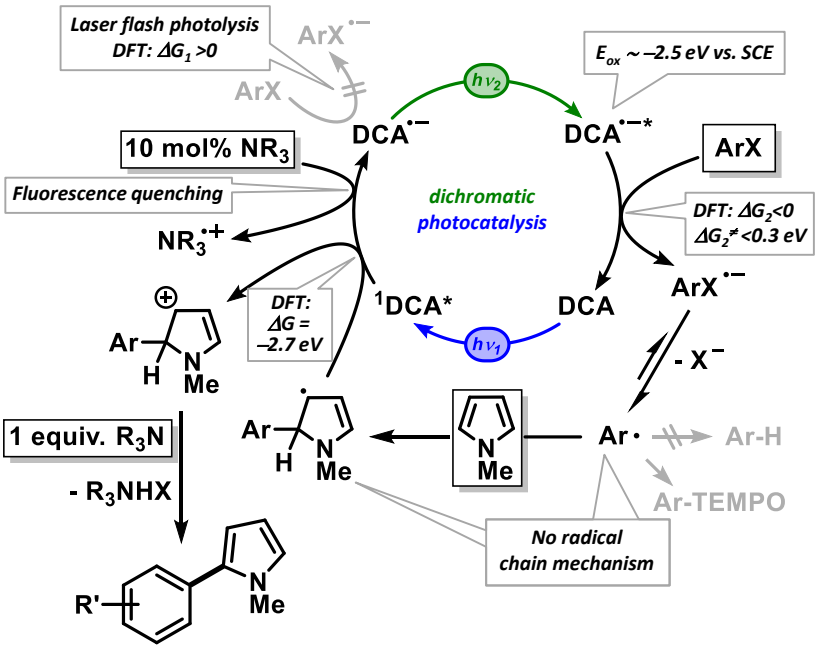

Scheme 4-3. Key experimental and theoretical data in support of a reaction mechanism that involves sequential photonic, electronic, and photonic activation of DCA.

An alternative radical chain mechanism via SET from the 2-aryl-2*H*-pyrrol-3-yl radical to ArX is thermodynamically prohibited (ΔG >30 kcal mol^{-1}).[11] Likewise, the halogen atom transfer from ArHal to the same intermediate is an uphill process. We believed that the SET from the excited radical anion DCA$^{\bullet-}$* (-2.5 eV vs. SCE) to the aryl halide would constitute the rate-limiting step in reactions with deactivated electrophiles. A detailed thermodynamic and kinetic analysis was derived from DFT calculations (CAM-B3LYP/6-31++G**).[11] The 1e-reductions of **1a** and the other reactive electrophiles by DCA$^{\bullet-}$* are thermodynamically feasible ($\Delta G_2 \leq 0$). The kinetic barriers toward the radical anion ArX$^{\bullet-}$ are generally small ($\Delta G_2^{\neq}$ = 0-0.3 eV). The trend of substrate reactivity is very accurately mirrored by the thermodynamic and kinetic data which predict unfavourable Gibbs energies and higher activation barriers only for the reactions of electron-rich aryl halides.[11] However, low reactivity can be a direct consequence of reversibility of the electron transfer and subsequent mesolysis. The

insufficient reducing power of ground-state-DCA$^{\bullet-}$ (-0.6 to -0.89 V vs. SCE) for the reductive activation of aryl bromides (DFT: ΔG_1 >0) was demonstrated by laser flash photolysis experiments which showed identical decay traces of DCA$^{\bullet-}$ in the absence and in the presence of **1a**, respectively (at 520 nm, see Figure 4-2, bottom). This observation is in full agreement with the thermodynamics of this hypothetical SET-event.[11]

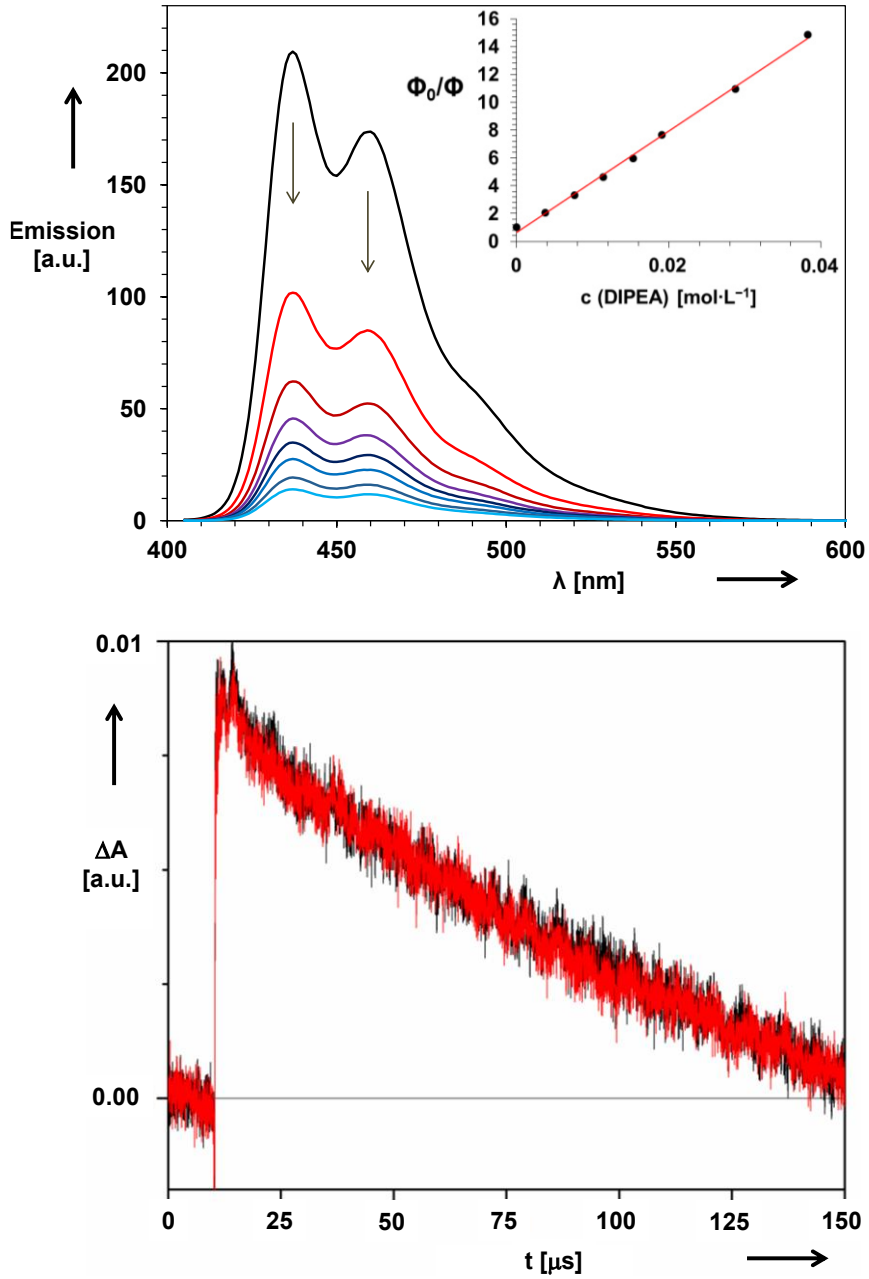

Figure 4-2. *Top:* Fluorescence quenching of DCA (0.01 mM) with DIPEA (0, 4, 8, 11, 15, 19, 28, 39 mM) in MeCN/air. DCA absorption: 0.5 (λ_{exc} 400 nm). *Inset:* Stern-Volmer plot for $k_q(S_1)$. *Bottom:* DCA$^{\bullet-}$ decay monitored at 520 nm after laser flash photolysis (355 nm; 10 mJ/pulse): DCA (10^{-4} M), Et_3N ($6 \cdot 10^{-2}$ M), MeCN, Ar: without **1a** (black), with 10^{-3} M **1a** (red).[11]

The scope of dichromatic photocatalytic aromatic substitutions could also be extended to other C-heteroatom functionalizations (Scheme 4-4). The DCA-catalyzed reaction enabled phosphorylation at low catalyst loading and catalytic (10 mol%!) amine concentration,[13] sulfide formation from disulfide,[14] and the metal-free borylation from diborane[15].

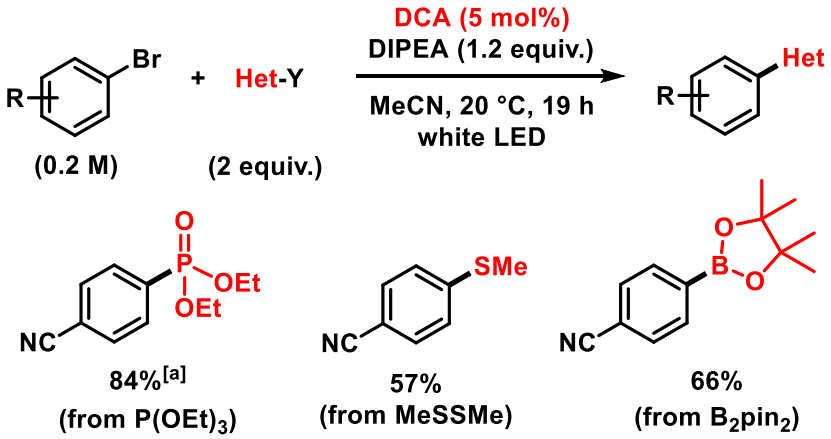

Scheme 4-4. Method extensions to C-Het couplings.[11] [a] 10 mol% DIPEA.

4.3 Conclusion

In conclusion, we have developed an operationally simple photocatalytic reductive activation of aryl halides under mild conditions. Synthetic, spectroscopic, and theoretical studies support the notion of a dichromatic/biphotonic photocatalysis mechanism which does not require a sacrificial reductant. Sequential photonic, electronic, and photonic activation of 9,10-dicyanoanthracene, a simple, low-molecular weight, soluble, and photostable organic dye, resulted in the formation of the strongly reducing excited radical anion $DCA^{\bullet -*}$ that is capable of cleaving unactivated C-halide bonds. Photocatalytic applications to aromatic C-H, C-C, C-S, C-P, and C-B bond formations were demonstrated. Further endeavours toward the development of effective biphotonic activations with simple organic dyes are currently being investigated.

4.4 Experimental section

4.4.1 Materials and methods

Chemicals and solvents: All reagents and solvents were purchased from commercial suppliers (Acros, Alfa Aesar, Fisher, Fluka, Merck, Sigma Aldrich and TCI) and used as received unless otherwise indicated. Pyrrole derivatives were distilled before use.

Reaction setup: The reactions were carried out in Rotilabo®-sample vials (6 mL, Ø 22 mm, Roth) sealed with Rotilabo®-aluminium caps with septum (Ø 20 mm, Roth). Irradiation was performed with a cold white LED (LED Cree MK-R, cold-white, 11.6 V, 700 mA, P = 8.5 W) through the plain bottom side of the reaction vials. The reaction setup was held at constant temperature throughout the reaction time with a cryostat.

Nuclear magnetic resonance (NMR) spectroscopy: ^{1}H NMR, ^{13}C NMR and ^{19}F NMR spectroscopy were used for purity and structure confirmation/determination of products. NMR spectral data were collected on a Bruker Avance 300 (300 MHz for ^{1}H; 75 MHz for ^{13}C, 282 MHz for ^{19}F, 162 MHz for ^{31}P) spectrometer or a Bruker Avance 400 (400 MHz for ^{1}H; 100 MHz for ^{13}C, 128 MHz for ^{11}B) spectrometer at 20 °C. Chemical shifts are reported in δ/ppm, coupling constants *J* are given in Hertz. Solvent residual peaks were used as internal standard for all NMR measurements. The quantification of ^{1}H cores was obtained from integrations of appropriate resonance signals. Abbreviations used in NMR spectra: s – singlet, d – doublet, t – triplet, q – quartet, m – multiplet, bs – broad singlet, dd – doublet of doublet, ddd – doublet of doublet of doublet.

Gas chromatography (GC-FID and GC-MS): GC-FID measurements on an Agilent 7820A GC-system with N_2 as carrier gas were used for quantification purposes in reaction optimization screenings, kinetic experiments and for selected substrates. 1-Dodecanenitrile was used as internal standard; the yield-% was calculated from a linear calibration curve that was set up from at least three data points of various concentrations of authentic product material. Low-resolution mass spectrometry (LRMS) was carried out on an Agilent 6890N GC-System coupled with a 5975 MS mass detector (EI ionization source) and H_2 as carrier gas. LRMS was used for reaction control purposes and structure determination of literature-known products

High resolution mass spectrometry (HRMS): HRMS was carried out by the Central Analytics at the department of chemistry, University of Regensburg. Abbreviations used in MS spectra: M – molar mass of target compound, EI – electron impact ionization, ESI – electrospray ionization.

Column (CC) and thin layer (TLC) chromatography: TLC was performed on commercial SiO_2-coated aluminium plates (DC60 F254, Merck). Visualization was done by UV-light (254 nm) or by staining with molybdophosphoric acid. Column chromatography was performed using silica gel (Acros Organics, mesh 35-70, 60 Å pore size) as the stationary phase.

Cyclic voltammetry: The redox potentials were measured by cyclic voltammetry with an Autolab PGSTAT302N Metrohm apparatus. All measurements were performed in deaerated MeCN containing tetrabutylammonium tetrafluoroborate (0.1 M) as supporting electrolyte, a glassy carbon as working electrode, a platinum wire as counter electrode, a silver wire as pseudo reference and ferrocene as internal standard. The scan rate was 0.05 V s^{-1}. Potentials are reported with respect to the saturated calomel electrode (SCE) as reference.

Fluorescence spectroscopy: The steady-state fluorescence spectra were obtained with a JASCO FP-8500 spectrofluorometer system. The samples were placed into a screw-cap quartz cuvette of 1 cm path length with a PTFE-coated silicon septum. The concentration of DCA was fixed adjusting the absorbance of the solution at an arbitrary value of 0.5 at λ_{exc} = 400 nm.

Laser flash photolysis: The measurements were performed with a Pump-Probe Setup LP980-K purchased by Edinburgh Co. The Pump source is an optical parametric oscillator (OPO) pumped by the third Harmonic of a Nd:YAG laser (EKSPLA). The wavelength can be set from 210 nm to about 2600 nm, with a pulse width of about 5 nm using an OPO mod. NT342A-10 with an UV extension NT242 with typical pulse duration of 5 ns. The repetition rate is 10 Hz. The white probe light is generated by a pulsed xenon flash lamp (150 W) and passes the sample orthogonal to the Pump beam. The duration of the probe pulse is 250 µs. This probe pulse is longer than the recorded time window of a measurement. A monochormator (TMS302-A, grating 150 lines/mm) disperses the probe light after it passed the sample. The probe light is then passed on to a PMT detector (Hamamatsu Photonics) to obtain the temporal resolved picture. The time resolution in each window is about 10 % of the temporal window width. All components are controlled by the software L900 provided by Edinburgh.

4.4.2 General procedures

General procedure A for photoreactions employing pyrrole derivatives:

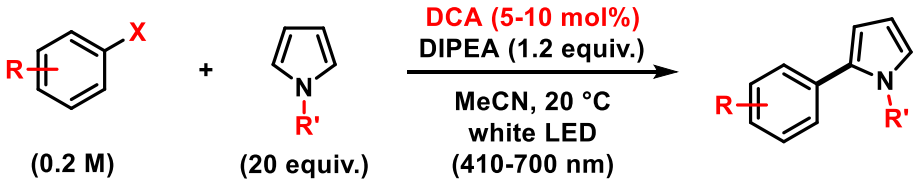

A vial (6 mL) was charged with a magnetic stirring bar, aryl halide (200 µmol, 1.0 equiv.) and 9,10-dicyanoanthracene (2.28 mg, 10.0 µmol, 0.05 equiv.). The vial was sealed with a septum. Acetonitrile (1.0 mL) and the pyrrole derivative (4.00 mmol, 20 eq.) were added to the mixture, before it was purged with an argon gas stream for 5 minutes. Then *N*,*N*-diisopropylethylamine (42 µL, 240 µmol, 1.2 eq.) and 1-dodecanenitrile (10 µL) were added under argon atmosphere. The reaction was irradiated with an external LED through the plain bottom side of the vial at 20 °C for the respective reaction time (to ensure full conversion for challenging reactions the vial was opened after some time under argon atmosphere and another portion of catalyst (5 mol%) was added to the mixture before it was resealed under argon and irradiated again). The reaction progress was monitored by GC-FID analysis. For isolation purposes, water (10 mL) was added and the aqueous phase was extracted with ethyl acetate (3 × 10 mL). The combined organic phases were washed with brine (10 mL), dried over magnesium sulfate, filtered from the drying agent and concentrated *in vacuo*. The crude product was purified *via* column chromatography on a silica gel column using a pentane/ethyl acetate mixture as the mobile phase.

General procedure B for the photocatalytic C-heteroatom couplings:

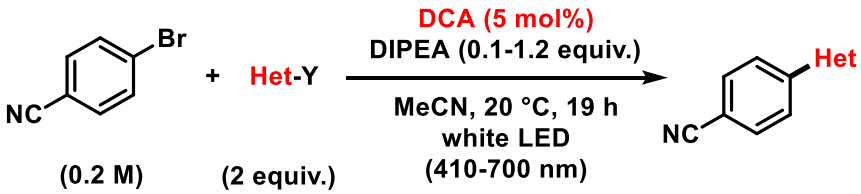

A vial (6 mL) was charged with a magnetic stirring bar, 4-bromobenzonitrile (36.4 mg, 200 µmol, 1.0 equiv.) and 9,10-dicyanoanthracene (2.28 mg, 10.0 µmol, 0.05 equiv.). The vial was sealed with a septum. Acetonitrile (1.0 mL) was added to the mixture, before it was purged with an argon gas stream for 5 minutes. Then *N*,*N*-diisopropylethylamine (0.1-1.2 eq.) and the trapping agent (400 µmol, 2.0 equiv.) were added under argon atmosphere. The reaction was irradiated with an external LED through the plain bottom side of the vial at 20 °C for 19 hours. Then water (10 mL) was added, and the mixture was extracted with ethyl acetate (3 × 10 mL). The combined organic phases were washed with brine (10 mL), dried over sodium sulfate, filtered from the drying agent and concentrated *in vacuo*. The crude product was purified *via* chromatography on a silica gel column using pentane/ethyl acetate mixture as the mobile phase.

4.4.3 Kinetic studies

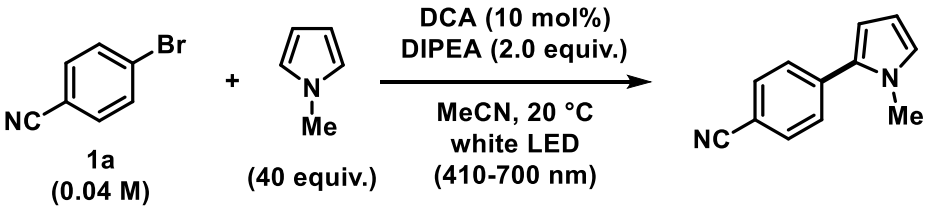

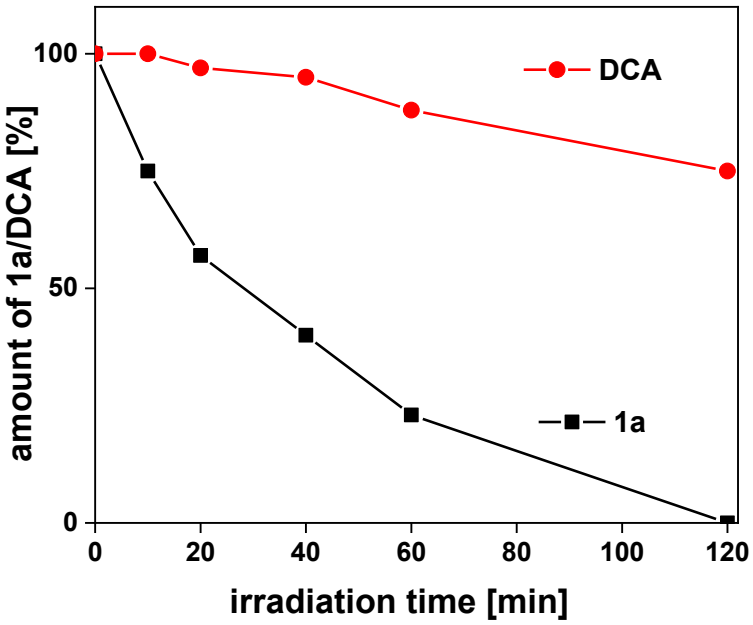

Figure 4-3. Plot comparing the conversion of **1a** vs. degradation of **DCA** during the course of the reaction. A solution of 1a (0.04 M), DCA (10 mol%), DIPEA (2.0 equiv.), and N-methylpyrrole (40 equiv.) in MeCN was irradiated with a cold-white LED (>410 nm) at 20 °C for 2 h. Datapoints were obtained from GC-FID measurements using 1-dodecanenitrile as an internal standard.

4.4.4 Detailed overview of optimization experiments

Table 4-2. Optimization reactions: Variations of solvent.[a]

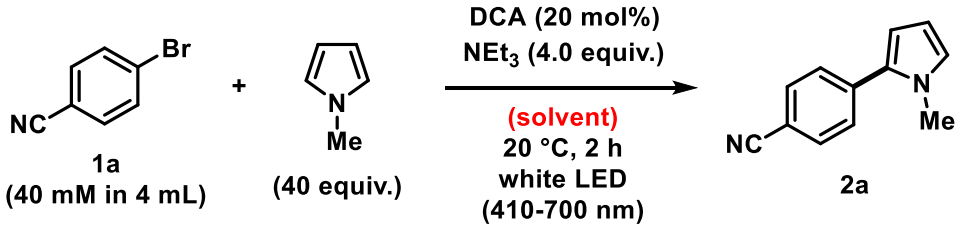

Entry	Solvent	Yield of 2a [%]	Red. Product yield [%]	Conversion [%]	Selectivity [a.u.]
1	CH_2Cl_2	4	2	12	33
2	DMF	14	24	62	23
3	DMSO	63	n.d.	94	67
4	MeOH	31	10	49	63
5	α-Trifluoro-toluene	3	0	15	20
6	MeCN	55	12	76	72

[a] Yields of **2a** were determined by GC-FID analysis using 1-dodecanenitrile as internal standard.

Table 4-3. Optimization experiments: Variations of bases.[a]

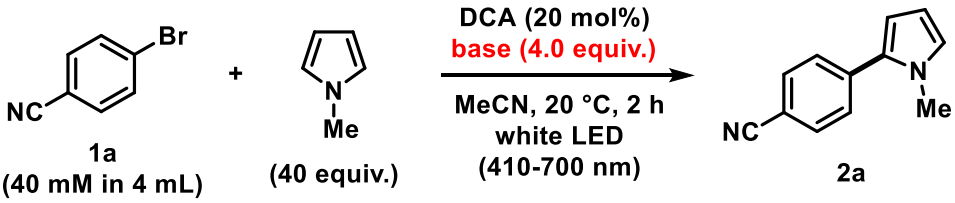

Entry	Base	Yield of 2a [%]	Red. Product yield [%]	Conversion [%]	Selectivity [a.u.]
1	Ph_3N	0	0	12	0
2	Ph_3P	0	0	10	0
3	DABCO	0	n.d.	9	0
4	DBU	53	n.d.	89	60
5	*N,N*-Dimethyl-aniline	0	n.d.	7	0
6	Isopropyl-amine	64	8	89	72
7	Diisopropyl-amine	65	8	89	73
8	DIPEA	62	11	83	74

[a] Yields of **2a** were determined by GC-FID analysis using 1-dodecanenitrile as internal standard.

Table 4-4. Optimization experiments: Further variations.[a]

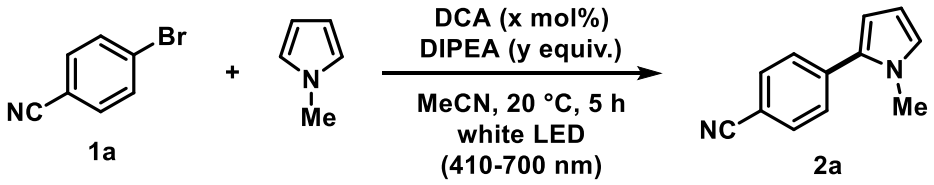

Entry	Conc. of 1a [M]	Pyrrole [equiv.]	DIPEA [equiv.]	DCA [mol%]	Yield of 2a [%]	Reduc. [%]	Conv. [%]
1[b]	0.04	40	2	10	87[c]	4	100
2[d]	0.04	40	1.1	10	85	4	100
3	0.1	20	1.2	5	68	6	81
4	0.2	20	1.2	5	85	6	100
5	0.1	20	1.2	10	85	6	100
6	0.4	10	2	10	64	24	100
7	0.4	5	4	10	35	49	92
8	0.4	2.5	1.5	5	33	29	74

[a] Yields of **2a** were determined by GC-FID analysis using 1-dodecanenitrile as internal standard. [b] 2 hours of reaction time; [c] 82% isolated yield; [d] 15 hours of reaction time.

Table 4-5. Control experiments.

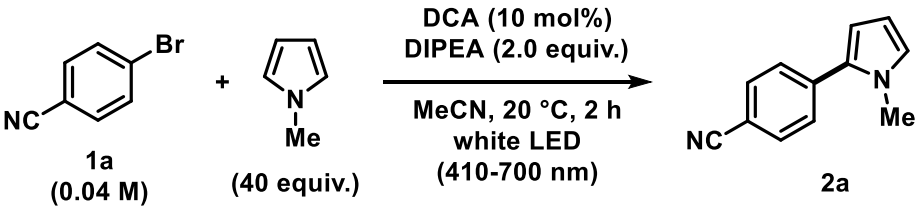

Entry	Deviations from conditions above	Yield of 2a [%]
1	no	87 [b]
2	1.1 equiv. DIPEA, 15 h	85
3	w/out *N*-methyl pyrrole	0 (64) [c]
4	w/out photocatalyst	0 (0)
5	w/out base	0 (0)
6	dark reaction	0 (0)
7	blue LED (455 nm)	4 (10)
8	green LED (525 nm)	0 (0)

[a] Yields of **2a** were determined by GC-FID using 1-dodecanenitrile as internal standard; conversion is given in parentheses if not >95%. [b] 82% isolated yield. [c] 45% benzonitrile as single product.

4.4.5 Cyclic voltammetry measurements

Table 4-6. Reduction potentials of employed substrates.

Substrate	E_{red} vs. SCE in MeCN	Substrate	E_{red} vs. SCE in MeCN
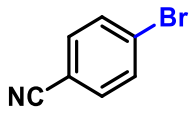	−1.95 V	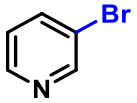	−2.32 V
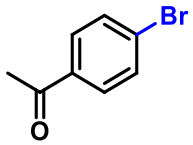	−1.81 V	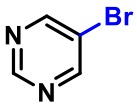	−1.91 V
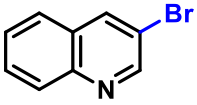	−1.82 V	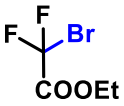	−1.60 V
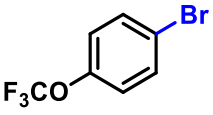	−2.59 V	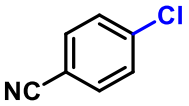	−2.06 V
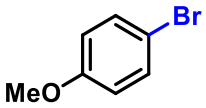	−2.75 V	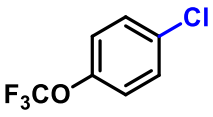	−2.64 V
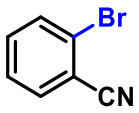	−1.90 V	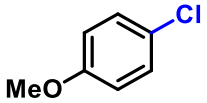	−2.88 V
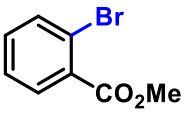	−1.98 V	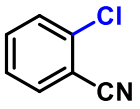	−2.01 V
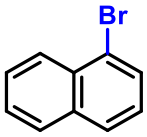	−2.14 V	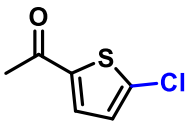	−1.69 V

4-Bromobenzonitrile

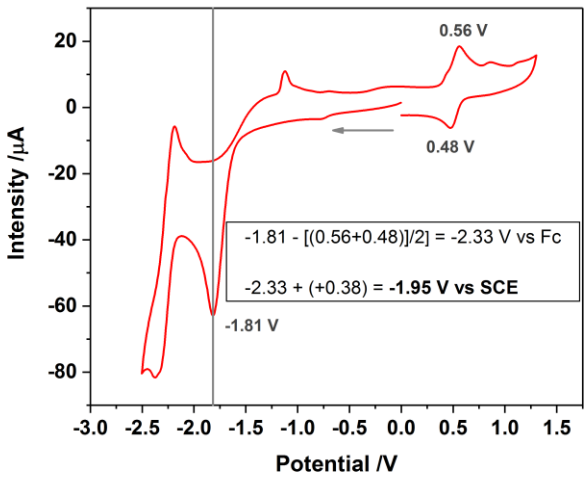

3-Bromopyridine

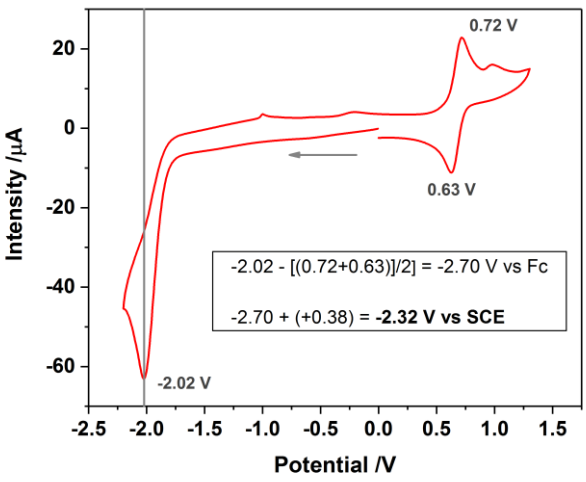

4'-Bromoacetophenone

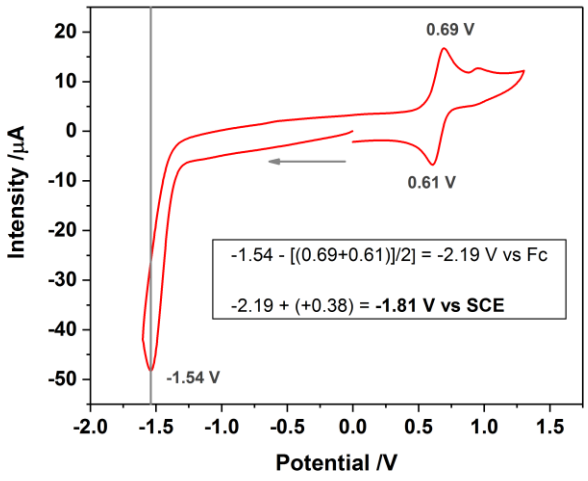

5-Bromopyrimidine

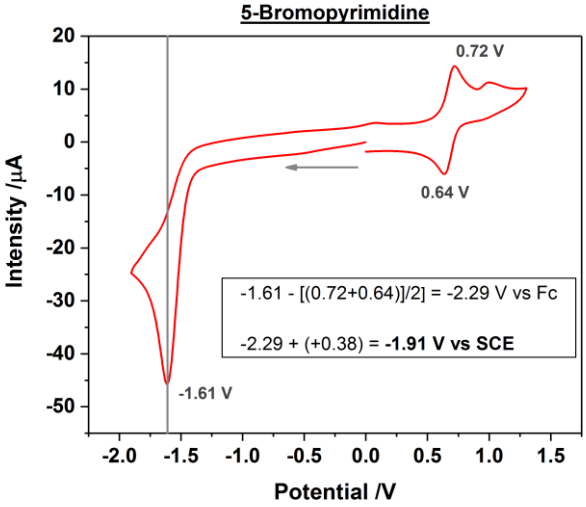

3-Bromoquinoline

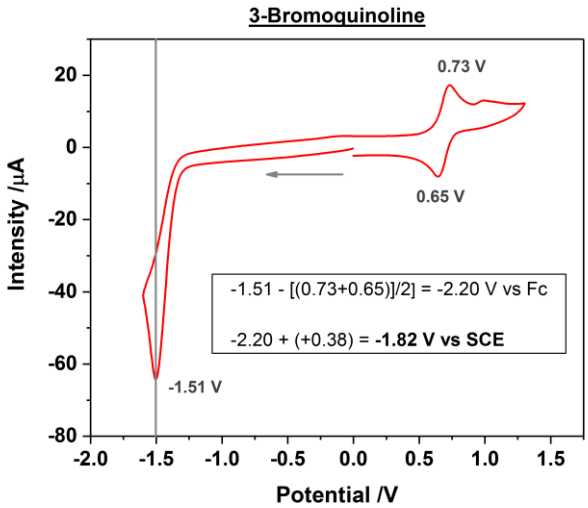

Ethyl 2-bromo-2,2-difluoroacetate

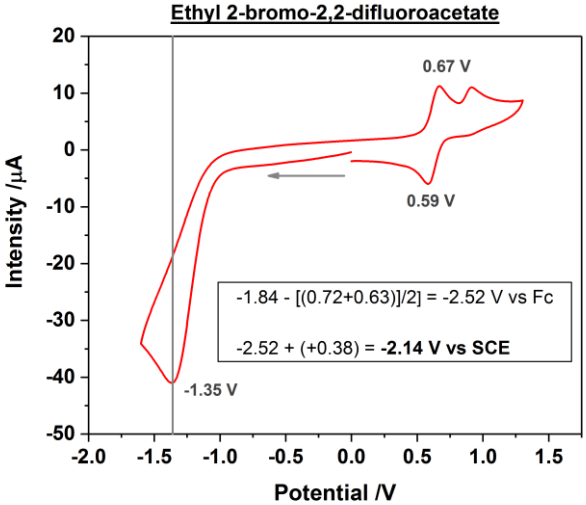

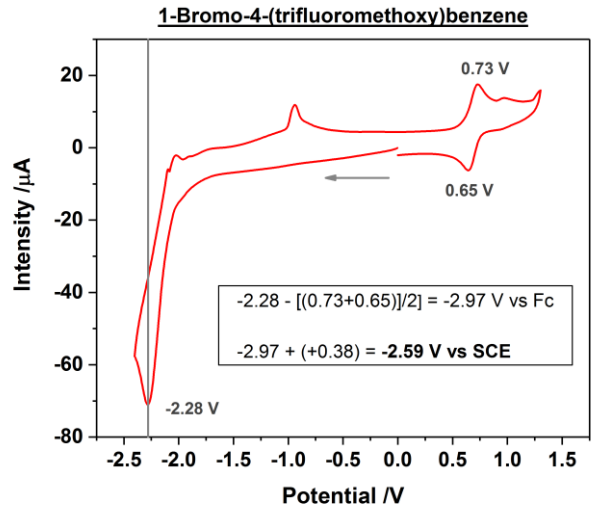
1-Bromo-4-(trifluoromethoxy)benzene
0.73 V
0.65 V
-2.28 V
-2.28 - [(0.73+0.65)]/2] = -2.97 V vs Fc
-2.97 + (+0.38) = -2.59 V vs SCE
Intensity /μA
Potential /V

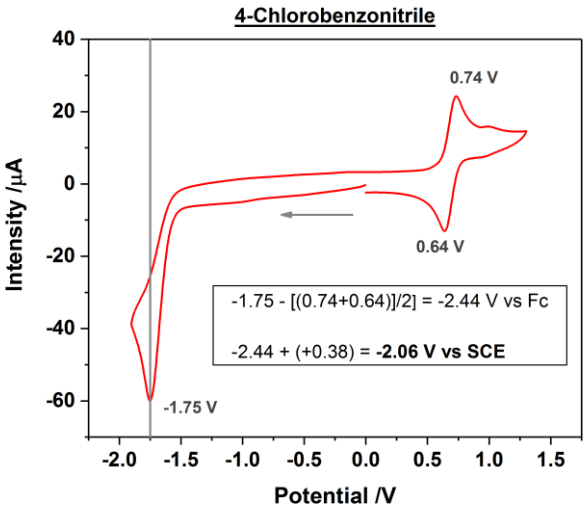
4-Chlorobenzonitrile
0.74 V
0.64 V
-1.75 V
-1.75 - [(0.74+0.64)]/2] = -2.44 V vs Fc
-2.44 + (+0.38) = -2.06 V vs SCE
Intensity /μA
Potential /V

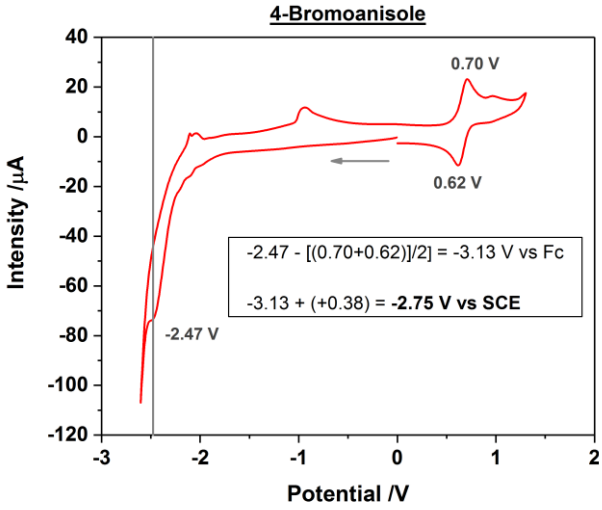
4-Bromoanisole
0.70 V
0.62 V
-2.47 V
-2.47 - [(0.70+0.62)]/2] = -3.13 V vs Fc
-3.13 + (+0.38) = -2.75 V vs SCE
Intensity /μA
Potential /V

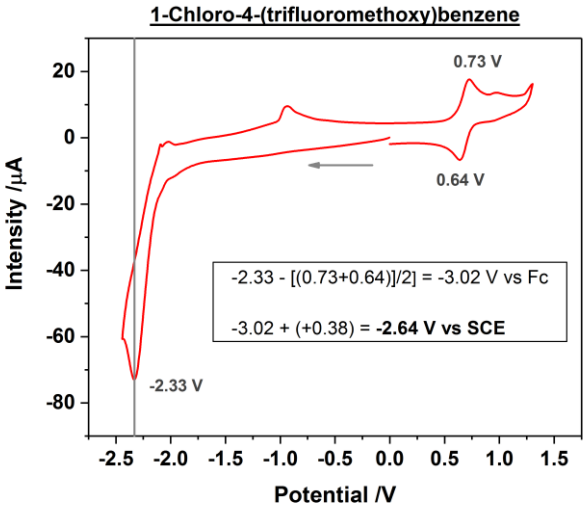
1-Chloro-4-(trifluoromethoxy)benzene
0.73 V
0.64 V
-2.33 V
-2.33 - [(0.73+0.64)]/2] = -3.02 V vs Fc
-3.02 + (+0.38) = -2.64 V vs SCE
Intensity /μA
Potential /V

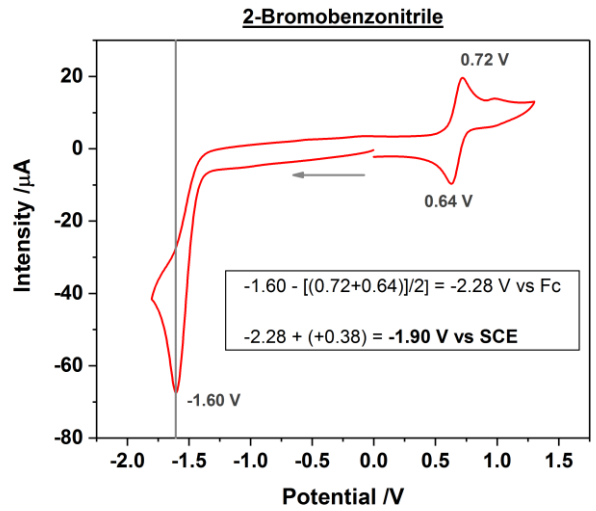
2-Bromobenzonitrile
0.72 V
0.64 V
-1.60 V
-1.60 - [(0.72+0.64)]/2] = -2.28 V vs Fc
-2.28 + (+0.38) = -1.90 V vs SCE
Intensity /μA
Potential /V

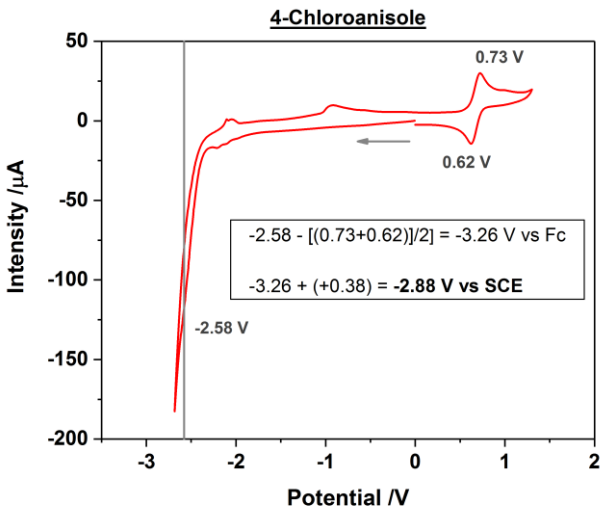
4-Chloroanisole
0.73 V
0.62 V
-2.58 V
-2.58 - [(0.73+0.62)]/2] = -3.26 V vs Fc
-3.26 + (+0.38) = -2.88 V vs SCE
Intensity /μA
Potential /V

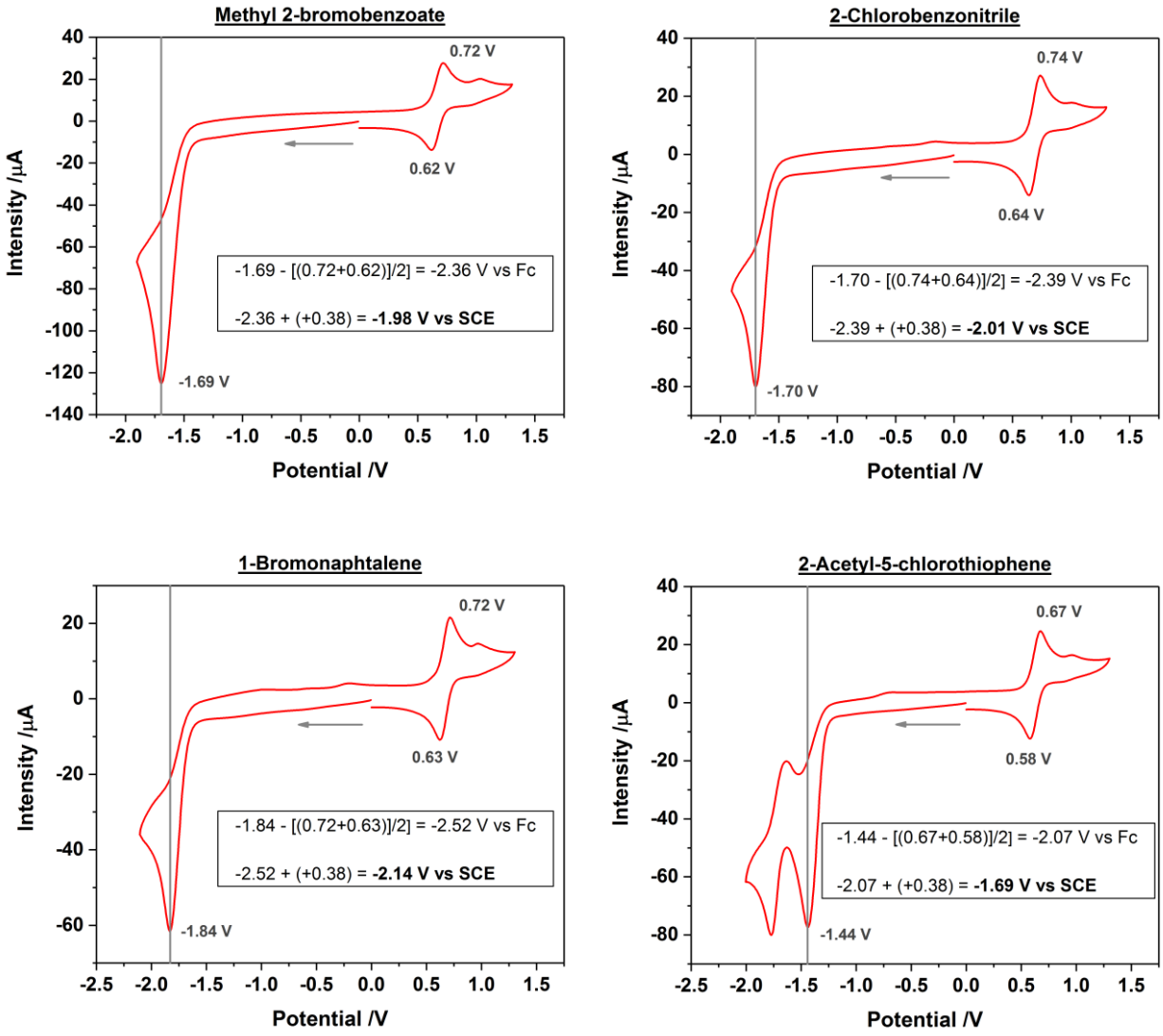

Figure 4-4. Cyclic voltammograms of employed substrates.

4.4.6 Stern-Volmer analysis

Equations for the Stern-Volmer analysis:

$\Phi_0/\ \Phi = 1 + K_{SV}[DIPEA]$ eq 4.1

$K_{SV} = \tau_S k_q(S_1)$ eq 4.2

The quenching rate constant $k_q(S_1) = 2.3 \cdot 10^{10} M^{-1}s^{-1}$ was obtained from Stern-Volmer analysis[16] (see eq. 4.1, 4.2 and the inset of Figure 4.2, top) with the **^{1}DCA*** singlet lifetime τ_S = 15.9 ns[17] and the Stern-Volmer constant K_{SV} = 364 M^{-1}.

Deactivation pathways of ^{1}DCA:*

Equations for calculating the contribution of the different deactivation pathways of the **^{1}DCA***

$k_D(S_1) = k_q(S_1)[DIPEA] + k_F + k_{ISC}$ eq 4.3

$\tau_S k_F = \Phi_F$ eq 4.4

$\tau_S k_{ISC} = \Phi_{ISC}$ eq 4.5

The deactivation of **^{1}DCA*** should be governed by the respective rate constants of fluorescence emission, fluorescence quenching, and intersystem crossing and by the quencher concentration ([DIPEA] = 0.24 M) (see eq. S3). The fluorescence (k_F) and intersystem crossing (k_{ISC}) rate constants were $k_F = 5.4 \cdot 10^7$ s^{-1} and $k_{ISC} = 2.5 \cdot 10^6$ s^{-1}, respectively (see eq. S4 and S5), considering quantum yields of fluorescence (Φ_F = 0.87)[17] and intersystem crossing (Φ_{ISC} = 0.04),[17] respectively.

4.4.7 Trapping and deuteration experiments

Trapping experiment:

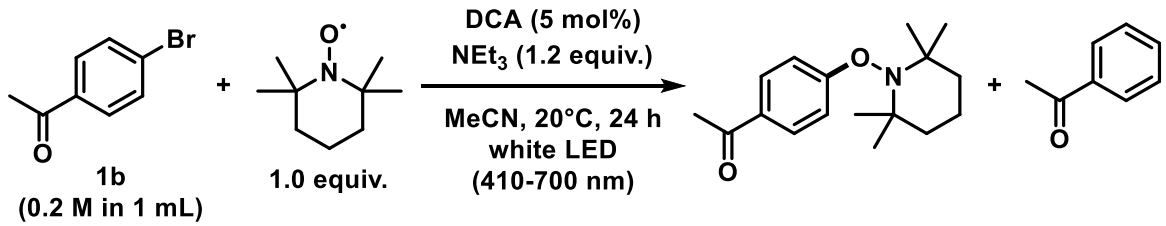

The reaction was performed according to the general procedure A using 4'-bromo-acetophenone (39.8 mg, 200 µmol, 1.0 equiv.) as aryl halide and TEMPO (31.2 mg, 200 µmol, 1.0 equiv.) as trapping agent. The mixture was irradiated for 24 hours and analyzed by HRMS. The HRMS analysis shows the exact molecular ion indicating the formation of the proposed TEMPO adduct of **1b**.

HRMS (ESI): *m/z* = calcd. for $(C_{17}H_{26}NO_2)^+$: 276.1964, found: 276.1958

Deuteration experiment:

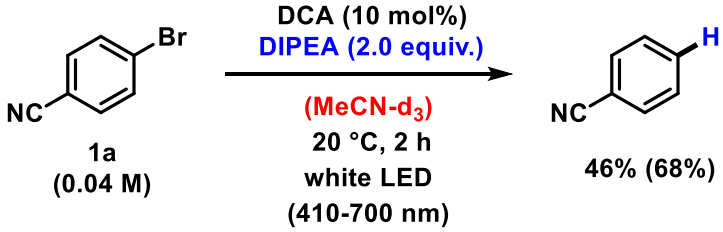

The irradiation of 4-bromobenzonitrile (7.28 mg, 40 µmol, 1.0 equiv.) in deuterated acetonitrile and without trapping agent afforded 46% of reduction product at 62% conversion according to GC-FID analysis. GC-MS analysis and NMR spectra of the crude mixture did not indicate incorporation of deuterium in the reduction product. A similar outcome was recorded for the standard reaction in the presence of *N*-methyl pyrrole and 1.2 equiv. DIPEA in d_3-acetonitrile. This experiment again suggests that the incorporated hydrogen atom in the hydrodebromination reaction is abstracted from DIPEA.

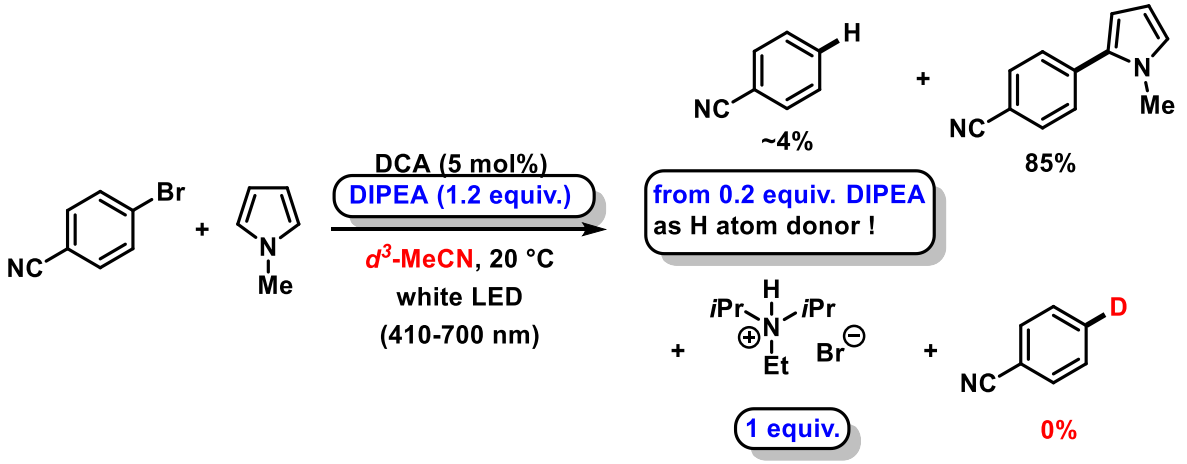

4.4.8 Analytical data of compounds

4-(1-Methyl-1*H*-pyrrol-2-yl)benzonitrile

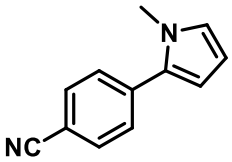

The compound was prepared according to the general procedure A using 4-bromobenzonitrile (36.4 mg, 200 µmol, 1.0 equiv.) as aryl halide and *N*-methylpyrrole (355 µL, 4.00 mmol, 20 equiv.) as trapping agent. The reaction mixture was irradiated for 5 hours. GC-FID analysis provided a yield of 85%. After subjecting the reaction mixture to the work-up and purification steps outlined in the general procedure, the title compound (29.8 mg, 82%) was obtained as a slightly yellow solid.

The compound was also prepared according to the general procedure A using 4-chloro-benzonitrile (27.5 mg, 200 µmol, 1.0 equiv.) as aryl halide and *N*-methylpyrrole (355 µL, 4.00 mmol, 20 equiv.) as trapping agent. The reaction mixture was irradiated for 24 hours before a second portion of 9,10-dicyanoanthracene (2.28 mg, 5 mol%) was added and the mixture was irradiated for further 24 hours. GC-FID analysis provided a yield of 75%.

^{1}H NMR (300 MHz, $CDCl_3$): δ = 7.70-7.63 (m, 2H), 7.53-7.46 (m, 2H), 6.81-6.77 (m, 1H), 6.35 (dd, *J* = 3.7 Hz, 1.8 Hz, 1H), 6.23 (dd, *J* = 3.7 Hz, 2.7 Hz, 1H), 3.72 (s, 3H).

^{13}C NMR (75 MHz, $CDCl_3$): δ= 137.8 (C), 132.7 (C), 132.4 (2CH), 128.4 (2CH), 126.0 (CH), 119.2 (C), 110.9 (CH), 109.8 (C), 108.7 (CH), 35.6 (CH_3).

GC-MS (EI): *m/z* (relative intensity) = 182 (100), 181 (49), 154 (8.3), 140 (22).

Spectral data were consistent with J. Roger, H. Doucet, *Adv. Synth. Catal.* **2009**, *351*, 1977-1990.

1-(4-(1-Methyl-1*H*-pyrrol-2-yl)phenyl)ethan-1-one

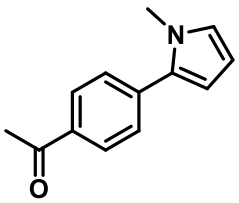

The compound was prepared according to the general procedure A using 4'-bromoacetophenone (39.8 mg, 200 µmol, 1.0 equiv.) as aryl halide and *N*-methylpyrrole (355 µL, 4.00 mmol, 20 equiv.) as trapping agent. The reaction mixture was irradiated for 24 hours. GC-FID analysis provided a yield of 64%.

^{1}H NMR (300 MHz, $CDCl_3$): δ= 8.03-7.95 (m, 2H), 7.54-7.46 (m, 2H), 6.80-6.75 (m, 1H), 6.35 (dd, *J* = 3.6 Hz, 1.7 Hz, 1H), 6.23 (dd, *J* = 3.6 Hz, 2.6 Hz, 1H), 3.73 (s, 3H), 2.63 (s, 3H).

^{13}C NMR (100 MHz, $CDCl_3$): δ = 197.7 (C), 138.0 (C), 135.0 (C), 133.5 (C), 128.7 (2CH), 128.1 (2CH), 125.5 (CH), 110.4 (CH), 108.5 (CH), 35.6 (CH_3), 26.7 (CH_3).

GC-MS (EI): *m/z* (relative intensity) = 199 (94), 184 (100), 156 (41), 128 (22).

Spectral data were consistent with S. Gowrisankar, J. Seayad, *Chem. Eur. J.* **2014**, *20*, 12754-12758.

3-(1-Methyl-1*H*-pyrrol-2-yl)quinoline

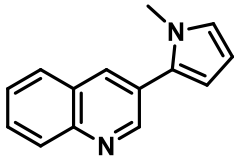

The compound was prepared according to the general procedure A using 3-bromoquinoline (41.6 mg, 200 µmol, 1.0 equiv.) as aryl halide and *N*-methylpyrrole (355 µL, 4.00 mmol, 20 equiv.) as trapping agent. The reaction mixture was irradiated for 15 hours. GC-FID analysis provided a yield of 71%.

^{1}H NMR (300 MHz, $CDCl_3$): δ = 9.03 (d, *J* = 2.2 Hz, 1H), 8.19-8.11 (m, 2H), 7.88-7.81 (m, 1H), 7.73 (ddd, *J* = 8.5 Hz, 7.5 Hz, 1.3 Hz, 1H), 7.63-7.54 (m, 1H), 6.86-6.79 (m, 1H), 6.43 (dd, *J* = 3.6 Hz, 1.8 Hz, 1H), 6.32-6.28 (m, 1H), 3.76 (s, 3H).

^{13}C NMR (75 MHz, $CDCl_3$): δ= 151.1 (CH), 146.8 (C), 133.9 (CH), 131.1 (C), 129.4 (CH), 129.3 (CH), 127.9 (CH), 127.9 (C), 127.2 (CH), 126.6 (C) 125.1 (CH), 110.4 (CH), 108.6 (CH), 35.4 (CH_3).

HRMS (EI): *m/z* = calcd. for $C_{14}H_{12}N_2^{+\bullet}$: 208.0995, found: 208.0990.

Spectral data were consistent with I. Gosh, R. S. Shaikh, B. König*, Angew. Chem. Int. Ed.* **2017**, *56*, 8544-8549.

1-Methyl-2-(4-(trifluoromethoxy)phenyl)-1*H*-pyrrole

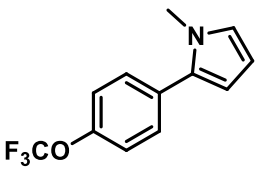

The compound was prepared according to the general procedure A using 1-bromo-4-(trifluoromethoxy)benzene (48.2 mg, 200µmol, 1.0 equiv.) as aryl halide and *N*-methylpyrrole (355 µL, 4.00 mmol, 20 equiv.) as trapping agent. The reaction

mixture was irradiated for 8 hours before a second portion of 9,10-dicyanoanthracene (2.28 mg, 5 mol%) was added and the mixture was irradiated for further 16 hours. GC-FID analysis provided a yield of 44% at 53% conversion.

The compound was also prepared according to the general procedure A using 1-chloro-4-(trifluoromethoxy)benzene (39.3 mg, 200 µmol, 1.0 equiv.) as aryl halide and *N*-methylpyrrole (355 µL, 4.00 mmol, 20 equiv.) as trapping agent. The reaction mixture was irradiated for 24 hours before a second portion of 9,10-dicyanoanthracene (2.28 mg, 5 mol%) was added and the mixture was irradiated for further 24 hours. GC-FID analysis provided a yield of 29% at 33% conversion.

^{1}H NMR (300 MHz, $CDCl_3$): δ = 7.45-7.38 (m, 2H), 7.28-7.20 (m, 2H), 6.76-6.70 (m, 1H), 6.25-6.18 (m, 2H), 3.66 (s, 3H).

^{13}C NMR (75 MHz, $CDCl_3$): δ = 148.2 (C), 132.2 (C), 131.6 (q, J = 246.8 Hz, CF_3) 130.0 (2CH), 124.2 (CH), 121.1 (2CH), 119.0 (C), 109.3 (CH), 108.1 (CH), 35.2 (CH_3).

^{19}F NMR (282 MHz, $CDCl_3$): δ = −58.3 (s).

HRMS (EI): *m/z* = calcd. for $C_{12}H_{10}F_3NO^{+\bullet}$: 241.0709, found: 241.0707.

2-(4-Methoxyphenyl)-1-methyl-1*H*-pyrrole

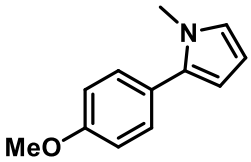

The compound was prepared according to the general procedure A using 4-bromoanisole (37.4 mg, 200 µmol, 1.0 equiv.) as aryl halide and *N*-methylpyrrole (355 µL, 4.00 mmol, 20 equiv.) as trapping agent. The reaction mixture was irradiated for 15 hours. GC-FID analysis provided a yield of 6% at 10% conversion.

The compound was also prepared according to the general procedure A using 4-chloro-anisole (28.5 mg, 200 µmol, 1.0 equiv.) as aryl halide and *N*-methylpyrrole (355 µL, 4.00 mmol, 20 equiv.) as trapping agent. The reaction mixture was irradiated for 24 hours before a second portion of 9,10-dicyanoanthracene (2.28 mg, 5 mol%) was added and the mixture was irradiated for further 24 hours. GC-FID analysis provided a yield of 4% at 9% conversion.

^{1}H NMR (400 MHz, benzene-d_6): δ = 7.24-7.19 (m, 2H), 6.81-6.75 (m, 2H), 6.48-6.44 (m, 1H), 6.42 (dd, J = 3.6 Hz, 1.9 Hz, 1H), 6.40-6.37 (m, 1H), 3.31 (s, 3H), 3.03 (s, 3H).

^{13}C NMR (100 MHz, benzene-d_6): δ = 159.2 (C), 134.5 (C), 130.4 (2CH), 126.8 (C), 123.1 (CH), 114.2 (2CH) 108.9 (CH), 108.4 (CH), 54.8 (CH_3), 34.4 (CH_3).

GC-MS (EI): *m/z* (relative intensity) = 187 (89), 172 (100), 144 (26), 128 (10).

Spectral data were consistent with J. Roger, H. Doucet, *Adv. Synth. Catal.* **2009**, *351*, 1977-1990.

2-(1-Methyl-1*H*-pyrrol-2-yl)benzonitrile

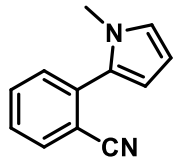

The compound was prepared according to the general procedure A using 2-bromobenzonitrlie (36.4 mg, 200 µmol, 1.0 equiv.) as aryl halide and *N*-methylpyrrole (355 µL, 4.00 mmol, 20 equiv.) as trapping agent. The reaction mixture was irradiated for 6 hours. GC-FID analysis provided a yield of 92%.

The compound was also prepared according to the general procedure A using 2-chloro-benzonitrile (27.5 mg, 200 µmol, 1.0 equiv.) as aryl halide and *N*-methylpyrrole (355 µL, 4.00 mmol, 20 equiv.) as trapping agent. The reaction mixture was irradiated for 24 hours before a second portion of 9,10-dicyanoanthracene (2.28 mg, 5 mol%) was added and the mixture was irradiated for further 24 hours. GC-FID analysis provided a yield of 84%.

^{1}H NMR (300 MHz, $CDCl_3$): δ = 7.78-7.70 (m, 1H), 7.66-7.56 (m, 1H), 7.47-7.35 (m, 2H), 6.80 (dd, *J* = 2.6 Hz, 1.8 Hz, 1H), 6.41 (dd, *J* = 3.7 Hz, 1.8 Hz, 1H), 6.25 (dd, *J* = 3.7, 2.6 Hz, 1H), 3.62 (s, 3H).

^{13}C NMR (75 MHz, $CDCl_3$): δ = 137.0 (C), 133.7 (CH), 132.5 (CH), 131.0 (CH), 130.0 (C), 127.5 (CH), 125.0 (CH), 118.8 (C), 113.0 (C), 111.6 (CH), 108.4 (CH), 35.0 (CH_3).

GC-MS (EI): *m/z* (relative intensity) = 182 (100), 181 (86), 154 (21), 140 (14).

Spectral data were consistent with D. T. Gryko, O. Vakuliuk, D. Gryko, B. Koszarna, *J. Org. Chem.* **2009**, *74*, 9517-9520.

Methyl 2-(1-methyl-1*H*-pyrrol-2-yl)benzoate

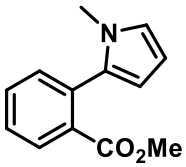

The compound was prepared according to the general procedure A using methyl 2-bromobenzoate (43.0 mg, 200 µmol, 1.0 equiv.) as aryl halide and *N*-methylpyrrole (355 µL, 4.00 mmol, 20 equiv.) as trapping agent. The reaction mixture was irradiated for 24 hours before a second portion of 9,10-dicyanoanthracene (2.28 mg, 5 mol%) was added and the mixture was irradiated for further 24 hours. After subjecting the

reaction mixture to the work-up and purification steps outlined in the general procedure the title compound (31.6 mg, 74%) was obtained as a slightly yellow oil.

^{1}H NMR (400 MHz, $CDCl_3$): δ = 7.93-7.86 (m, 1H), 7.58-7.48 (m, 1H), 7.47-7.36 (m, 2H), 6.73-6.67 (m, 1H), 6.22-6.16 (m, 1H), 6.06 (dd, *J* = 3.5, 1.8 Hz, 1H), 3.73 (s, 3H), 3.40 (s, 3H).

^{13}C NMR (100 MHz, $CDCl_3$): δ = 168.2 (C=O), 134.0 (C), 132.8 (C), 132.5 (CH), 132.1 (C), 131.5 (CH), 129.9 (CH), 127.9 (CH), 122.4 (CH), 108.6 (CH), 107.6 (CH), 52.4 (CH_3), 34.3 (CH_3).

GC-MS (EI): *m/z* (relative intensity) = 215 (100), 182 (27), 156 (61), 128 (15).

Spectral data were consistent with I. Gosh, R. S. Shaikh, B. König*, Angew. Chem. Int. Ed.* **2017**, *56*, 8544-8549.

1-Methyl-2-(naphthalen-1-yl)-1*H*-pyrrole

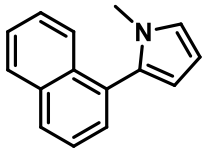

The compound was prepared according to the general procedure A using 1-bromonaphtalene (41.4 mg, 200 µmol, 1.0 equiv.) as aryl halide and *N*-methylpyrrole* (710 µL, 8.00 mmol, 40 equiv.) as trapping agent. The reaction mixture was irradiated for 24 hours before a second portion of 9,10-dicyanoanthracene (2.28 mg, 5 mol%) was added and the mixture was irradiated for further 24 hours. After subjecting the reaction mixture to the work-up and purification steps outlined in the general procedure, the title compound (23.7 mg, 57%) was obtained as a yellow oil.

(* deviation from the general procedure A: use 40 equivalents of trapping agent).

^{1}H NMR (400 MHz, $CDCl_3$): δ = 7.93-7.85 (m, 2H), 7.76-7.70 (m, 1H), 7.55-7-42 (m, 4H), 6.86-6.80 (m, 1H), 6.34-6.30 (m, 1H), 6.27 (dd, *J* = 3.5, 1.8 Hz, 1H), 3.40 (s, 3H).

^{13}C NMR (100 MHz, $CDCl_3$): δ= 133.8 (C), 133.5 (C), 132.3 (C), 131.4 (C), 128.9 (CH), 128.3 (CH), 128.3 (CH), 126.4 (CH), 126.4 (CH), 126.0 (CH), 125.3 (CH), 122.6 (CH), 110.1 (CH), 107.7 (CH), 34.7 (CH_3).

GC-MS (EI): *m/z* (relative intensity) = 207 (100), 206 (70), 191 (15), 165 (20).

Spectral data were consistent with Y.-X. Liu, D. Xue, J.-D. Wang, C.-J. Zhao, Q.-Z. Zou, C. Wang, J. Xiao, *Synlett* **2013**, *24*, 507-513.

3-(1-Methyl-1*H*-pyrrol-2-yl)pyridine

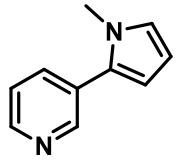

The compound was prepared according to the general procedure A using 3-bromopyridine (31.6 mg, 200 µmol, 1.0 equiv.) as aryl halide and *N*-methylpyrrole (355 µL, 4.00 mmol, 20 equiv.) as trapping agent. The reaction mixture was irradiated for 24 hours before a second portion of 9,10-dicyanoanthracene (2.28 mg, 5 mol%) was added and the mixture was irradiated for further 24 hours. After subjecting the reaction mixture to the work-up and purification steps outlined in the general procedure, the title compound (21.5 mg, 68%) was obtained as a colourless oil.

^{1}H NMR (300 MHz, $CDCl_3$): δ= 8.69 (d, *J* = 1.8 Hz, 1H), 8.53 (dd, *J* = 4.8 Hz, 1.5 Hz, 1H), 7.74-7.66 (m, 1H), 7.36-7.28 (m, 1H), 6.81-6.72 (m, 1H), 6.30 (dd, *J* = 3.6, 1.8 Hz, 1H), 6.25-6.18 (m, 1H), 3.68 (s, 3H).

^{13}C NMR (75 MHz, $CDCl_3$): δ = 149.4 (CH), 147.9 (CH), 135.6 (CH), 131.0 (C), 129.4 (C), 124.8 (CH), 123.3 (CH), 109.9 (CH), 108.4 (CH), 35.2 (CH_3).

GC-MS (EI): *m/z* (relative intensity) = 158 (100), 157 (50), 130 (18).

Spectral data were consistent with I. Ghosh, B. König, *Angew. Chem. Int. Ed.* **2016**, *55*, 7676-7679.

5-(1-Methyl-1*H*-pyrrol-2-yl)pyrimidine

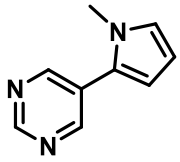

The compound was prepared according to the general procedure A using 5-bromopyrimidine (31.2 mg, 200 µmol, 1.0 equiv.) as aryl halide and *N*-methylpyrrole (355 µL, 4.00 mmol, 20 equiv.) as trapping agent. The reaction mixture was irradiated for 24 hours before a second portion of 9,10-dicyanoanthracene (2.28 mg, 5 mol%) was added and the mixture was irradiated for further 24 hours. After subjecting the reaction mixture to the work-up and purification steps outlined in the general procedure, the title compound (19.2 mg, 61%) was obtained as a slightly yellow oil.

^{1}H NMR (300 MHz, $CDCl_3$): δ = 9.12 (s, 1H), 8.79 (s, 2H), 6.85-6.79 (m, 1H), 6.37 (dd, *J* = 3.7, 1.8 Hz, 1H), 6.25 (dd, *J* = 3.7 Hz, 2.7 Hz, 1H), 3.71 (s, 3H).

^{13}C NMR (75 MHz, $CDCl_3$): δ = 156.6 (CH), 155.5 (2 CH), 127.7 (C), 127.1(C), 126.1 (CH), 111.0 (CH), 108.9 (CH), 35.4 (CH_3).

GC-MS (EI): *m/z* (relative intensity) = 159 (100), 158 (17), 131 (19), 105 (23).

Spectral data were consistent with I. Gosh, R. S. Shaikh, B. König*, Angew. Chem. Int. Ed.* **2017**, *56*, 8544-8549.

1-(5-(1-Methyl-1*H*-pyrrol-2-yl)thiophen-2-yl)ethan-1-one

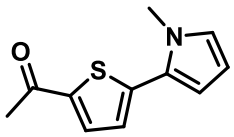

The compound was prepared according to the general procedure A using 2-acetyl-5-chlorothiophene (32.1 mg, 200 µmol, 1.0 equiv.) as aryl halide and *N*-methylpyrrole (355 µL, 4.00 mmol, 20 equiv.) as trapping agent. The reaction mixture was irradiated for 18 hours. After subjecting the reaction mixture to the work-up and purification steps outlined in the general procedure, the title compound (29.0 mg, 71%) was obtained as a slightly yellow solid.

^{1}H NMR (300 MHz, $CDCl_3$): δ = 7.62 (d, *J* = 4.0 Hz, 1H), 7.06 (d, *J* = 4.0 Hz, 1H), 6.77-6.72 (m, 1H), 6.51 (dd, *J* = 3.8, 1.8 Hz, 1H), 6.18 (dd, *J* = 3.8 Hz, 2.7 Hz, 1H), 3.81 (s, 3H), 2.55 (s, 3H).

^{13}C NMR (75 MHz, $CDCl_3$): δ = 190.6 (C=O), 144.0 (C), 141.9 (C), 133.3 (CH), 126.9 (C), 126.3 (CH), 124.4 (CH), 111.7 (CH), 108.7 (CH), 36.0 (CH_3), 26.7 (CH_3).

GC-MS (EI): *m/z* (relative intensity) = 205 (100), 190 (88), 162 (17), 118 (32).

Spectral data were consistent with L. Marzo, I. Ghosh, F. Esteban, B. König, *ACS Catal.* **2016**, *6*, 6780-6784.

Ethyl 2,2-difluoro-2-(1-methyl-1*H*-pyrrol-2-yl)acetate

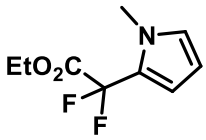

The compound was prepared according to the general procedure A using ethyl 2-bromo-2,2-difluoroacetate (40.6 mg, 200 µmol, 1.0 equiv.) as aryl halide and *N*-methylpyrrole (355 µL, 4.00 mmol, 20 equiv.) as trapping agent. The reaction mixture was irradiated for 19 hours. After subjecting the reaction mixture to the work-up and purification steps outlined in the general procedure, the title compound (33.8 mg, 83%) was obtained as a yellow oil.

^{1}H NMR (300 MHz, $CDCl_3$): δ = 6.73-6.67 (m, 1H), 6.38 (dd, *J* = 3.8 Hz, 1.8 Hz, 1H), 6.11-6.03 (m, 1H), 4.38 (q, *J* = 7.1 Hz, 2H), 3.77 (s, 3H), 1.38 (t, *J* = 7.1 Hz, 3H).

^{13}C NMR (100 MHz, $CDCl_3$): δ = 163.6 (t, *J* = 34.5 Hz, C=O), 127.2 (t, *J* = 1.8 Hz, CH), 122.8 (t, *J* = 29.0 Hz, C) 112.5 (t, *J* = 5.7 Hz, CH), 111.4 (t, *J* = 246.4 Hz, CF_2), 107.5 (CH), 63.4 (CH_2), 35.6 (t, *J* = 3.1 Hz, CH_3), 14.1 (CH_3).

^{19}F NMR (282 MHz, $CDCl_3$): δ = −96.7 (s).

GC-MS (EI): *m/z* (relative intensity) = 203 (19), 156 (2), 130 (100), 89 (4).

Spectral data were consistent with J. Jung, E. Kim, Y. You, E. J. Cho, *Adv. Synth. Catal.* **2014**, *356*, 2741-2748.

4-(1*H*-Pyrrol-2-yl)benzonitrile

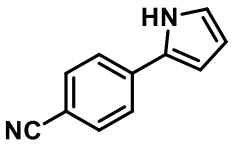

The compound was prepared according to the general procedure A using 4-bromobenzonitrile (36.4 mg, 200 µmol, 1.0 equiv.) as the halide and pyrrole (280 µL, 4.00 mmol, 20 equiv.) as trapping agent. The reaction mixture was irradiated for 20 hours. After subjecting the reaction mixture to the work-up and purification steps outlined in the general procedure, the title compound (24.4 mg, 73%) was obtained as a slightly yellow solid.

^{1}H NMR (400 MHz, $CDCl_3$): δ = 8.58 (bs, 1H), 7.66-7.60 (m, 2H), 7.58-7.50 (m, 2H), 6.98-6.93 (m, 1H), 6.70-6.64 (m, 1H), 6.37-6.32 (m, 1H).

^{13}C NMR (100 MHz, $CDCl_3$): δ = 136.9 (C), 132.9 (2CH), 130.2 (C), 123.8 (2CH), 121.1 (CH), 119.3 (C), 111.2 (CH), 109.0 (C), 108.9 (CH).

GC-MS (EI): *m/z* (relative intensity) = 168 (100), 141 (13), 140 (27), 114 (12).

Spectral data were consistent with S. O. Poelma, G. L. Burnett, E. H. Discekici, K. M. Mattson, N. J. Treat, Y. Luo, Z. M. Hudson, S. L. Shankel, P. G. Clark, J. W. Kramer, C. J. Hawker, J. Read de Alaniz, *J. Org. Chem.* **2016**, *81*, 7155-7160.

4-(1-(Dimethylamino)-1*H*-pyrrol-2-yl)benzonitrile

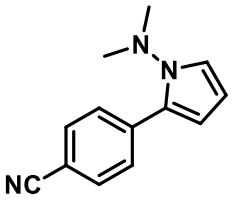

The compound was prepared according to the general procedure A using 4-bromobenzonitrile (36.4 mg, 200 µmol, 1.0 equiv.) as aryl halide and 1-(dimethylamino)pyrrole (480 µL, 4.00 mmol, 20 equiv.) as trapping agent. The

reaction mixture was irradiated for 5 hours before a second portion of 9,10-dicyanoanthracene (2.28 mg, 5 mol%) was added and the mixture was irradiated for further 19 hours. After subjecting the reaction mixture to the work-up and purification steps outlined in the general procedure, the title compound (24.5 mg, 58%) was obtained as a colourless solid.

^{1}H NMR (400 MHz, $CDCl_3$): δ = 7.84-7.77 (m, 2H), 7.64-7.58 (m, 2H), 7.15 (dd, *J* = 3.0 Hz, 1.8 Hz, 1H), 6.33 (dd, *J* = 4.0 Hz, 1.8 Hz, 1H), 6.25 (dd, *J* = 4.0 Hz, 3.0 Hz, 1H), 2.83 (s, 6H).

^{13}C NMR (100 MHz, $CDCl_3$): δ = 137.0 (C), 132.0 (2CH), 130.1 (C), 127.6 (2CH), 119.6 (C), 116.5 (CH), 109.1 (C), 108.3 (CH), 107.4 (CH), 47.8 ($2CH_3$).

HRMS (ESI): *m/z* = calcd. for $(C_{13}H_{14}N_3+H)^+$: 212.1182, found: 212.1184.

4-(1-Benzyl-1*H*-pyrrol-2-yl)benzonitrile

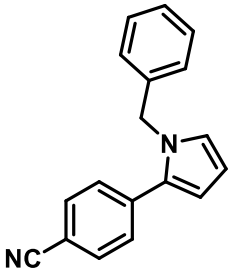

The compound was prepared according to the general procedure A using 4-bromobenzonitrile (36.4 mg, 200 µmol, 1.0 equiv.) as aryl halide and *N*-benzylpyrrole (620 µL, 4.00 mmol, 20 equiv.) as trapping agent. The reaction mixture was irradiated for 5 hours before a second portion of 9,10-dicyanoanthracene (2.28 mg, 5 mol%) was added and the mixture was irradiated for further 19 hours. After subjecting the reaction mixture to the work-up and purification steps outlined in the general procedure, the title compound (37.1 mg, 72%) was obtained as a yellow oil.

^{1}H NMR (300 MHz, $CDCl_3$): δ = 7.62-7.55 (m, 2H), 7.43-7.36 (m, 2H), 7.35-7.20 (m, 3H), 7.02-6.96 (m, 2H), 6.84 (dd, *J* = 2.7 Hz, 1.8 Hz, 1H), 6.39 (dd, *J* = 3.7 Hz, 1.8 Hz, 1H), 6.32 (dd, *J* = 3.7 Hz, 2.7 Hz, 1H), 5.18 (s, 2H).

^{13}C NMR (75 MHz, $CDCl_3$): δ = 138.2 (C), 137.8 (C), 133.0 (C), 132.4 (2CH), 129.0 (2CH), 128.7 (2CH), 127.8 (CH), 126.3 (2CH), 125.4 (CH), 119.1 (C), 111.1 (CH), 110.1 (C), 109.4 (CH), 51.1 (CH_2).

GC-MS (EI): *m/z* (relative intensity) = 258 (40), 140 (4), 91 (100).

Spectral data were consistent with R. Jin, K. Yuan, E. Chatelain, J.-F. Soulé, H. Doucet, *Adv. Synth. Catal.* **2014**, *356*, 3831-3841.

Diethyl (4-cyanophenyl)phosphonate

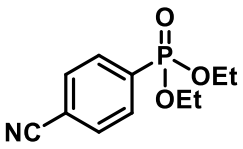

The compound was prepared according to the general procedure B using triethylphosphite (70 µL, 400 µmol, 2.0 equiv.) as trapping agent and 0.1 equivalents of *N*,*N*-diisopropylethylamine (3.5 µL, 20 µmol). After subjecting the reaction mixture to the work-up and purification steps outlined in the general procedure, the title compound (40.1 mg, 84%) was obtained as a yellow oil.

^{1}H NMR (300 MHz, $CDCl_3$): δ = 7.92 (dd, *J* = 13.1 Hz, 8.4 Hz, 2H), 7.76 (dd, *J* = 8.4 Hz, 3.6 Hz, 2H), 4.25-3.97 (m, 4H), 1.31 (t, *J* = 7.1 Hz, 6H).

^{13}C NMR (75 MHz, $CDCl_3$): δ = 134.1 (d, *J* = 187.6 Hz, C), 132.4 (d, *J* = 9.8 Hz, CH), 132.1 (d, *J* = 15.0 Hz, CH), 118.0 (d, *J* = 1.4 Hz, C), 116.1 (d, *J* = 3.6 Hz, C), 62.8 (d, *J* = 5.6 Hz, CH_2), 16.5 (d, *J* = 6.4 Hz, CH_3).

^{31}P NMR (162 MHz, $CDCl_3$): δ = 16.1 (s).

GC-MS (EI): *m/z* (relative intensity) = 239 (6.7), 212 (17), 184 (100), 166 (97).

Spectral data were consistent with R. Zhuang, J. Xu, Z. Cai, G. Tang, M. Fang, Y. Zhao, *Org. Lett.* **2011**, *13*, 2110-2113.

4-(Methylthio)benzonitrile

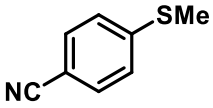

The compound was prepared according to the general procedure B using dimethyl disulfide (36 µL, 400 µmol, 2.0 equiv.) as trapping agent and 1.2 equivalents of *N*,*N*-diisopropylethylamine (42 µL, 240 µmol). After subjecting the reaction mixture to the work-up and purification steps outlined in the general procedure, the title compound (16.9 mg, 57%) was obtained as a slight yellow solid.

^{1}H NMR (300 MHz, $CDCl_3$): δ = 7.53 (d, *J* = 8.4 Hz, 2H), 7.30-7.20 (m, 2H), 2.51 (s, 3H).

^{13}C NMR (75 MHz, $CDCl_3$): δ = 146.2 (C), 132.3 (2CH), 125.6 (2CH), 119.1 (C), 107.8 (C), 14.8 (CH_3).

GC-MS (EI): *m/z* (relative intensity) = 149 (100), 134 (44), 116 (50), 104 (20).

Spectral data were consistent with C. Fang, M. Li, X. Hu, W. Mo, B. Hu, N. Sun, L. Jin, Z. Shen, *Adv.Synth. Catal.* **2016**, *358*, 1157-1163.

4-(4,4,5,5-Tetramethyl-1,3,2-dioxaborolan-2-yl)benzonitrile

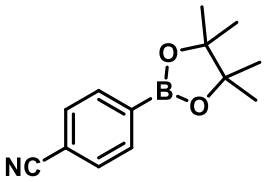

The compound was prepared according to the general procedure B using bis(pinacolato)diboron* (102 mg, 400 µmol, 2.0 equiv.) as trapping agent and 1.2 equivalents of *N*,*N*-diisopropylethylamine (42 µL, 240 µmol). After subjecting the reaction mixture to an aqueous work-up and removing the volatile compounds *in vacuo*, the yield (66%) was calculated from the crude product using 1,3,5-trimethoxybenzene (33.7 mg, 240 µmol) as an internal standard since purification *via* column chromatography was not possible.

(* deviation from the general procedure B: add the trapping agent from the very beginning because it is a solid).

^{1}H NMR (400 MHz, $CDCl_3$): δ = 7.88 (d, *J* = 8.2 Hz, 2H), 7.63 (d, *J* = 8.2 Hz, 2H), 1.35 (s, 12H).

^{13}C NMR (101 MHz, $CDCl_3$): δ= 135.2 (2CH), 131.3 (2CH), 119.0 (C), 114.7 (C), 84.6 (C), 25.0 (CH_3). Carbon bearing boron was not observed.

^{11}B NMR (128 MHz, $CDCl_3$): δ = 30.4 (s).

GC-MS (EI): *m/z* (relative intensity) = 229 (6.9), 214 (96), 186 (11), 143 (100).

Spectral data were consistent with K. Chen, S. Zhang, P. He, P. Li, *Chem. Sci.* **2016**, *7*, 3676-3680.

4.4.9 Selected NMR spectra

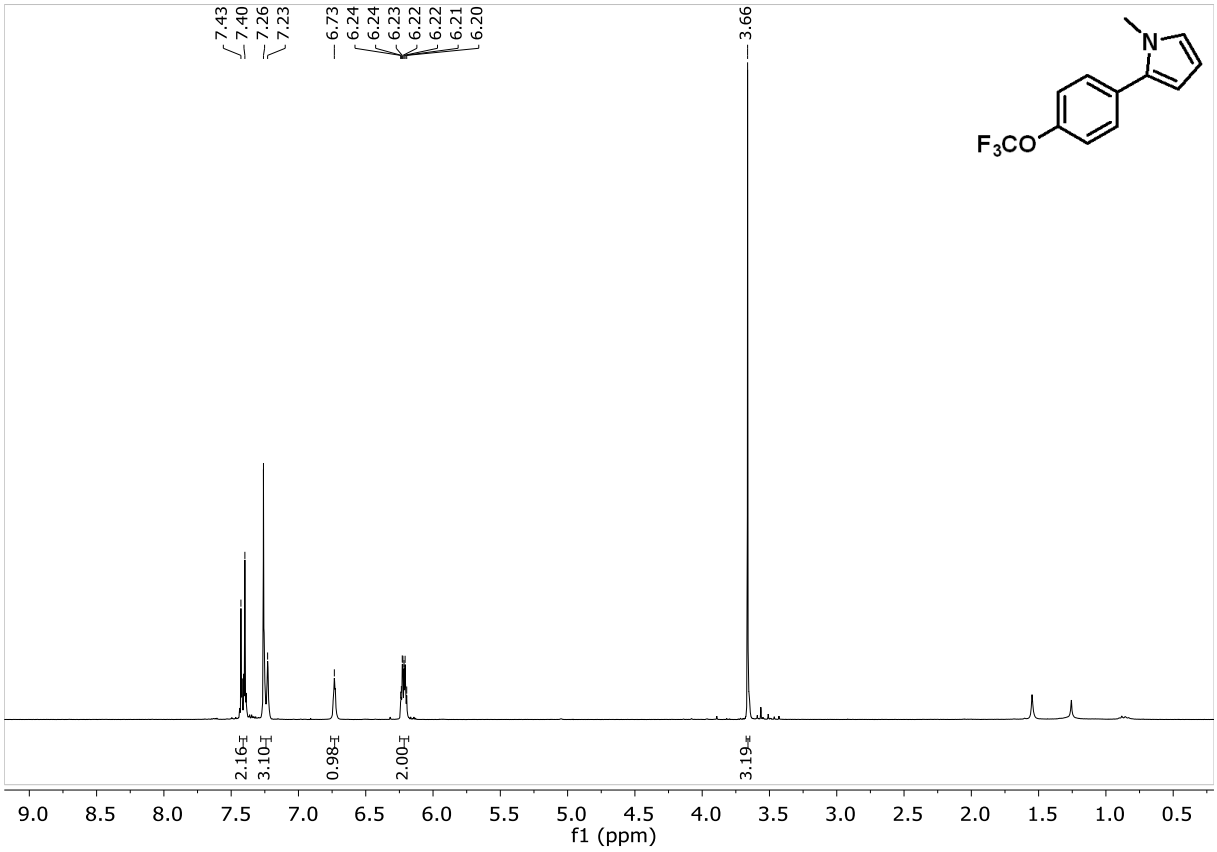

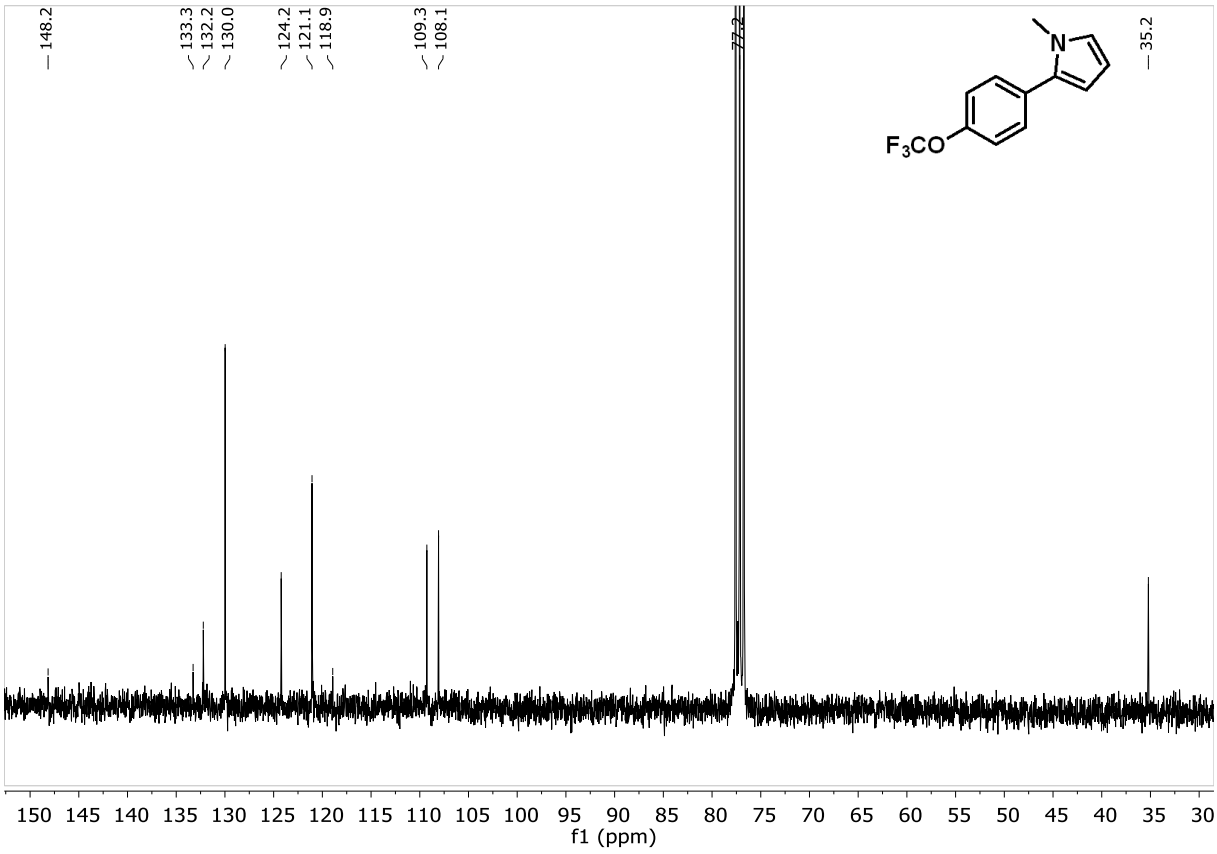

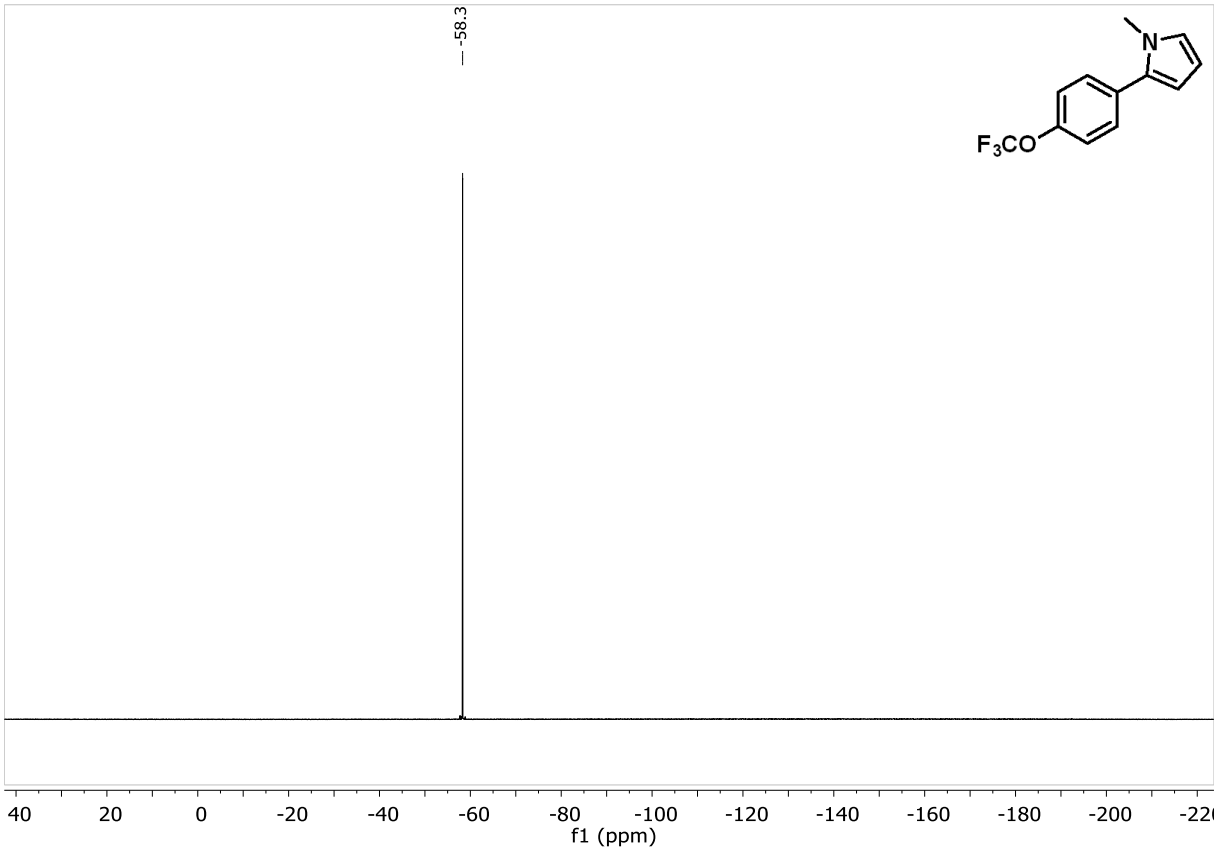
-58.3
N
F3CO
40
20
0
-20
-40
-60
-80
-100
-120
-140
-160
-180
-200
f1 (ppm)

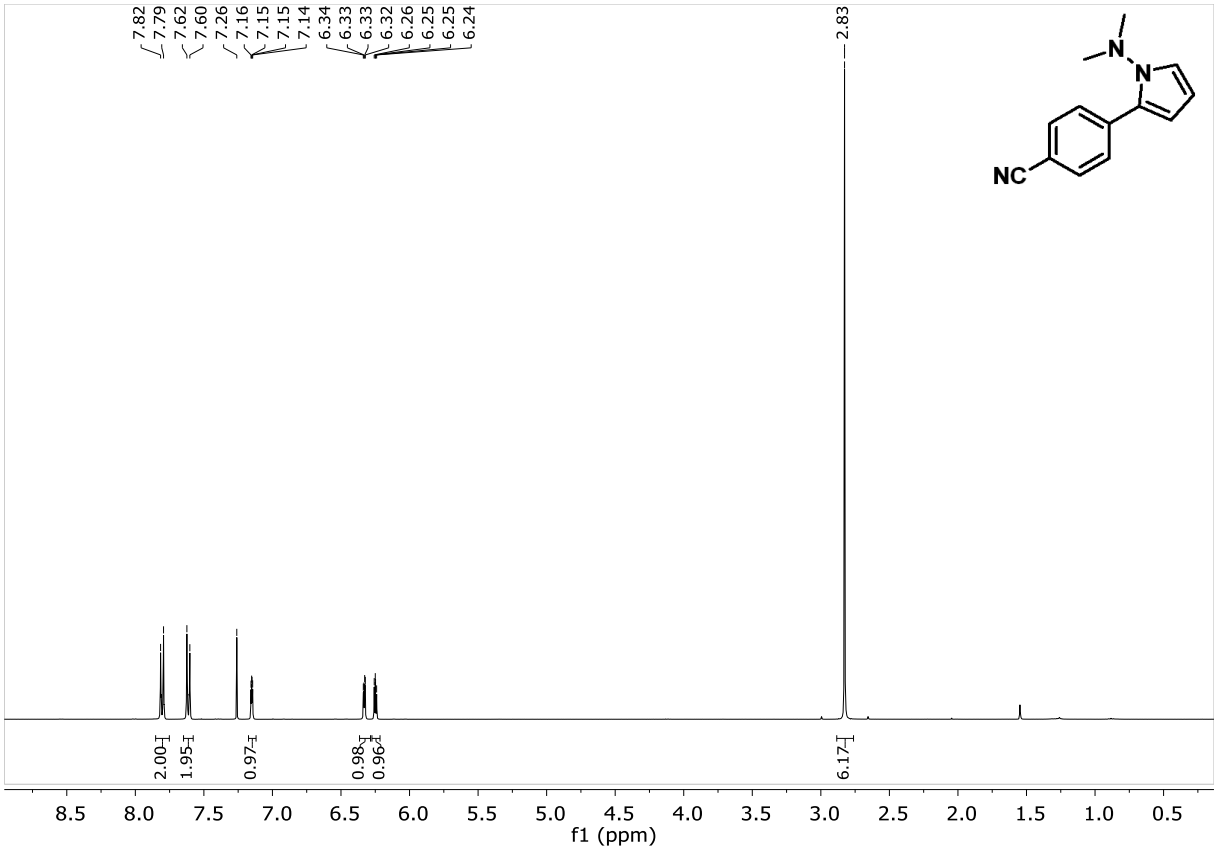
7.82
7.79
7.62
7.60
7.26
7.16
7.15
7.15
7.14
6.34
6.33
6.33
6.32
6.26
6.25
6.25
6.24
2.83
N
N
NC
2.00
1.95
0.97
0.98
0.96
6.17
8.5
8.0
7.5
7.0
6.5
6.0
5.5
5.0
4.5
4.0
3.5
3.0
2.5
2.0
1.5
1.0
0.5
f1 (ppm)

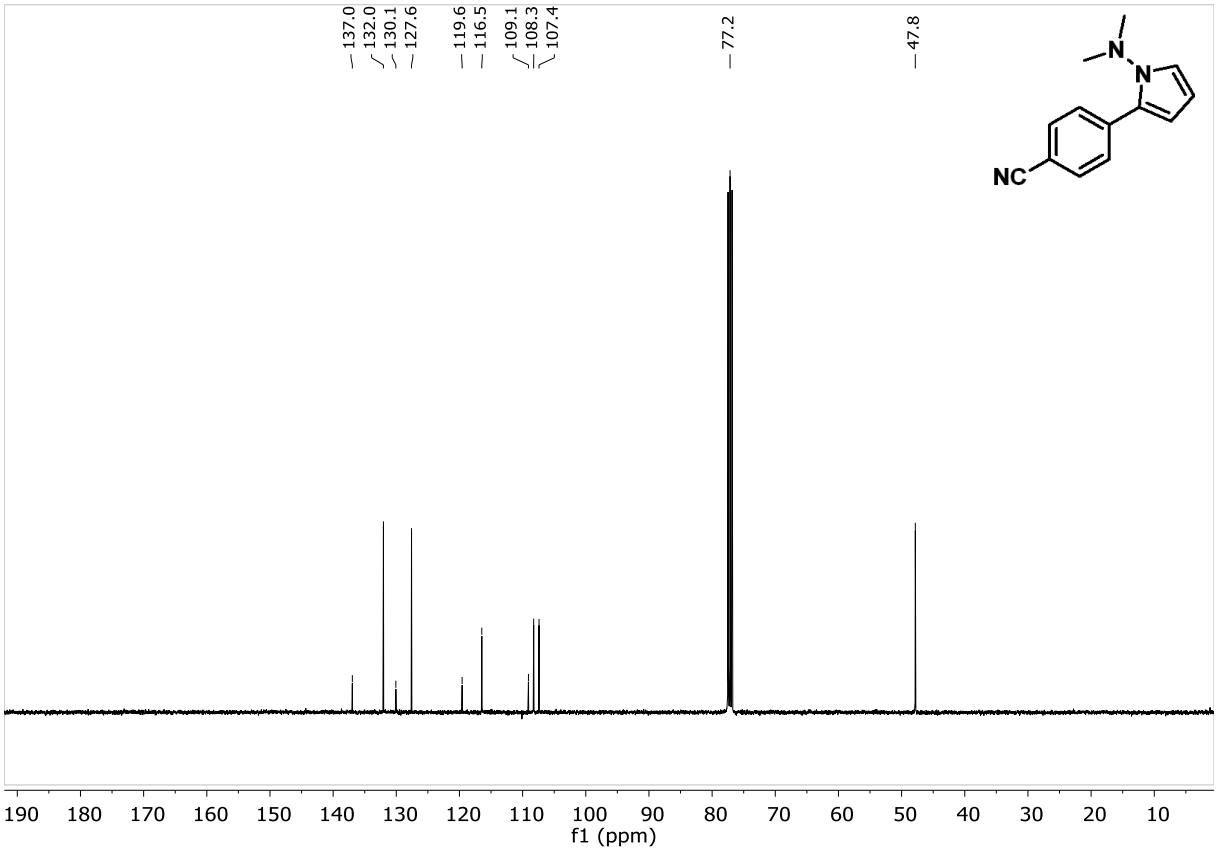
137.0
132.0
130.1
127.6
119.6
116.5
109.1
108.3
107.4
77.2
47.8
N
N
NC
190 180 170 160 150 140 130 120 110 100 90 80 70 60 50 40 30 20 10
f1 (ppm)

4.10 Thermodynamic and kinetic DFT calculations

For computational details: see the Supporting Information of the published manuscript.

Table 4-7. Thermodynamic (ΔG) and kinetic ($\Delta G^{\neq}$) data of the SET processes from $DCA^{\bullet -*}$ and $DCA^{\bullet -}$ to ArX (CAM-B3LYP/6-31++G**).

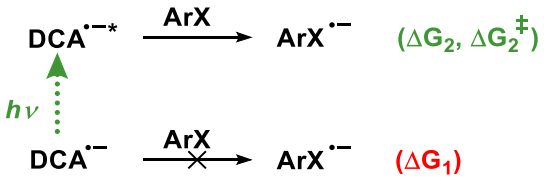

Substrate	ΔG_1 [eV]	ΔG_2 [eV]	$\Delta G_2^{\neq}$ [eV]	Substrate	ΔG_1 [eV]	ΔG_2 [eV]	$\Delta G_2^{\neq}$ [eV]
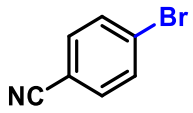	+ 1.3	− 0.6	+ 0.08	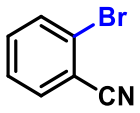	+ 1.3	− 0.6	+ 0.10
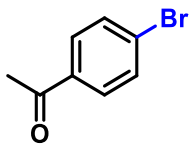	+ 1.1	− 0.8	+ 0.24	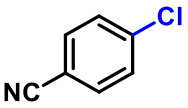	+ 2.0	+ 0.1	+ 0.15
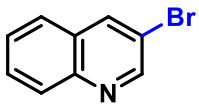	+ 1.1	− 0.7	+ 0.15	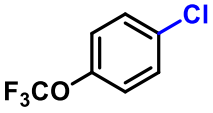	+ 2.2	+ 0.3	+ 0.29
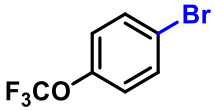	+ 2.2	+ 0.3	+ 0.32	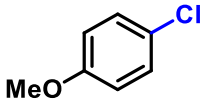	+ 2.2	+ 0.3	+ 0.31
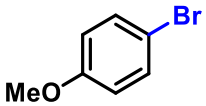	+ 2.2	+ 0.3	+ 0.32	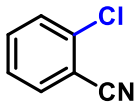	+ 1.3	− 0.6	+ 0.11

Thermodynamic energies ΔG of SET between 2-aryl-2H-pyrrol-3-yl radical and ArBr:

4-Bromobenzonitrile: +34.7 kcal/mol

4'-Bromoacetophenone: +29.4 kcal/mol

4-Bromoanisole: +56.0 kcal/mol

4-Chlorobenzonitrile: +51.2 kcal/mol

4-Chloroacetophenone: +29.3 kcal/mol

4-Chloroanisole: +55.5 kcal/mol

4.5 References

[1] a) A. G. Griesbeck, M. Oelgemoeller, F. Ghetti, *CRC Handbook of Organic Photochemistry and Photobiology*, 3rd ed., CRC Press, Boca Raton, **2012**; b) V. Balzani, P. Ceroni, A. Juris, *Photochemistry and Photophysics: Concepts, Research, Applications*, Wiley-VCH, Weinheim, **2014**.

[2] a) J. W. Beatty, C. R. J. Stephenson, *Acc. Chem. Res.* **2015**, *48*, 1474-1484; b) K. Nakajima, Y. Miyake, Y. Nishibayashi, *Acc. Chem. Res.* **2016**, *49*, 1946-1956; c) N. A. Romero, D. A. Nicewicz, *Chem. Rev.* **2016**, *116*, 10075-10166; d) C. K. Prier, D. A. Rankic, D. W. C. MacMillan, *Chem. Rev.* **2013**, *113*, 5322-5363.

[3] a) M. Májek, A. Jacobi von Wangelin, *Acc. Chem. Res*. **2016**, *49*, 2316-2327; b) I. Ghosh, L. Marzo, A. Das, R. Shaikh, B. König, *Acc. Chem. Res*. **2016**, *49*, 1566-1577; c) Y. Jin, H. Fu, *Asian J. Org. Chem.* **2017**, *6*, 368-385; d) J. Xuan, Z.-G. Zhang, W.-J. Xiao, *Angew. Chem. Int. Ed.* **2015**, *54*, 15632-15641.

[4] a) D. M. Schultz, T. P. Yoon, *Science* **2014**, *343*, 1239176; b) D. Ravelli, S. Protti, M. Fagnoni, A. Albini, *Curr. Org. Chem.* **2013**, *17*, 2366-2373; c) M. Reckenthaler, A. G. Griesbeck, *Adv. Synth. Catal.* **2013**, *355*, 2727-2744.

[5] a) S. Lazzaroni, D. Ravelli, S. Protti, M. Fagnoni, A. Albini, *C. R. Chimie* **2017**, *20*, 261-271. Selected examples: b) G. Revol, T. McCallum, M. Morin, F. Gagosz, L. Barriault, *Angew. Chem. Int. Ed.* **2013**, *52*, 13342-13345; c) H. Yin, Y. Jin, J. E. Hertzog, K. C. Mullane, P. J. Carroll, B. C. Manor, J. M. Anna, E. J. Schelter, *J. Am. Chem. Soc.* **2016**, *138*, 16266-16273; d) E. H. Discekici, N. J. Treat, S. O. Poelma, K. M. Mattson, Z. M. Hudson, Y. Luo, C. J. Hawker, J. Read de Alaniz, *Chem. Commun.* **2015**, *51*, 11705-11708.

[6] a) K. L. Skubi, T. R. Blum, T. P. Yoon, *Chem. Rev.* **2016**, *116*, 10035-10074; b) J. C. Tellis, C. B. Kelly, D. N. Primer, M. Jouffroy, N. R. Patel, G. A. Molander, *Acc. Chem. Res.* **2016**, *49*, 1429-1439. Selected examples: c) B. J. Shields, A. G. Doyle, *J. Am. Chem. Soc.* **2016**, *138*, 12719-12722; d) E. R. Welin, C. Le, D. M. Arias-Rotondo, J. K. McCusker, D. W. C. MacMillan, *Science* **2017**, *355*, 380-385; e) J. J. Devery, III, J. D. Nguyen, C. Dai, C. R. J. Stephenson, *ACS Catal.* **2016**, *6*, 5962-5967.

[7] a) I. Ghosh, T. Ghosh, J. I. Bardagi, B. König, *Science* **2014**, *346*, 725-728; b) I. Ghosh, B. König, *Angew. Chem. Int. Ed.* **2016**, *55*, 7676-7679; c) L. Zeng, T. Liu, C. He, D. Shi, F. Zhang, C. Duan, *J. Am. Chem. Soc.* **2016**, *138*, 3958-3964; d) W. Wei, D. Liu, Z. Wei, Y. Zhu, *ACS Catal*. **2017**, *7*, 652-656; e) M. Májek, U. Faltermeier, B. Dick, R. Perez-Ruiz, A. Jacobi von Wangelin, *Chem. Eur. J.* **2015**, *21*, 15496-15501; f) M. Häring, R. Perez-Ruiz, A. Jacobi von Wangelin, D. Diaz Diaz, *Chem. Commun.* **2015**, *51*, 16848-16851.

[8] a) C. Ye, L. Zhou, X. Wang, Z. Liang, *Phys. Chem. Chem. Phys.* **2016**, *18*, 10818-10835; b) J. Zhou, Q. Liu, W. Feng, Y. Sun, F. Li, *Chem. Rev.* **2015**, *115*, 395-465; Photophysical data: c) S. van de Linde, I. Krstic, T. Prisner, S. Doose, M. Heilemann, M. Sauer, *Photochem. Photobiol. Sci.* **2011**, *10*, 499-506; d) D. Gosztola, M. P. Niemczyk, W. Svec, A. S. Lukas, M. R. Wasielewski, *J. Phys. Chem. A* **2000**, *104*, 6545-6551.

[9] a) M. Fujita, A. Ishida, T. Majima, S. Takamuku, *J. Phys. Chem.* **1996**, *100*, 5382-5387; b) J.-C. Gumy, E. Vauthey, *J. Phys. Chem. A* **1997**, *101*, 8575-8580. c) T. Shida, *Electronic Absorption Spectra of Radical Ions*, Elsevier, Amsterdam, **1988**, pp. 246.

[10] a) S. M. Bonesi, M. Fagnoni, A. Albini, *Eur. J. Org. Chem.* **2008**, *15*, 2612-2620; b) H. Ikeda, T. Nomura, K. Akiyama, M. Oshima, H. D. Roth, S. Tero-Kubota, T. Miyashi, *J. Am. Chem. Soc.* **2005**, *127*, 14497-14504; c) M. Nakamura, R. Dohno, T. Majima, *J. Org. Chem.* **1998**, *63*, 6258-6265; d) K. Shima, A. Sazaki, K. Nakabayashi, M. Yasuda, *Bull. Chem. Soc. Jpn.* **1992**, *65*, 1472-1474.

[11] See experimental section 4.4 or the ESI of the published manuscript.

[12] a) J. Jung, E. Kim, Y. You, E. J. Cho, *Adv. Synth. Catal.* **2014**, *356*, 2741-2748; b) T. Chatterjee, N. Iqbal, Y. You, E. J. Cho, *Acc. Chem. Res.* **2016**, *49*, 2284-2294.

[13] R. S. Shaikh, S. J. S. Düsel, B. König, *ACS Catal.* **2016**, *6*, 8410-8414.

[14] With arenediazonium salts: M. Májek, A. Jacobi von Wangelin, *Chem. Commun.* **2013**, *49*, 5507-5509.

[15] With arenediazonium salts: M. Jiang, H. Yang, H. Fu, *Org. Lett.* **2016**, *18*, 5248-5251.

[16] A. D. McNaught, A. Wilkinson, Eds.; *IUPAC Compendium of Chemical Terminology*, 2nd ed., RSC: Cambridge, **1997**.

[17] A. F. Olea, D. R. Worrall, F. Wilkinson, S. L. Williams, A. A. Abdel-Shafi, *Phys. Chem. Chem. Phys.* **2002**, *4*, 161.

5 Visible light-driven iron-catalyzed cyclotrimerization[i,ii]

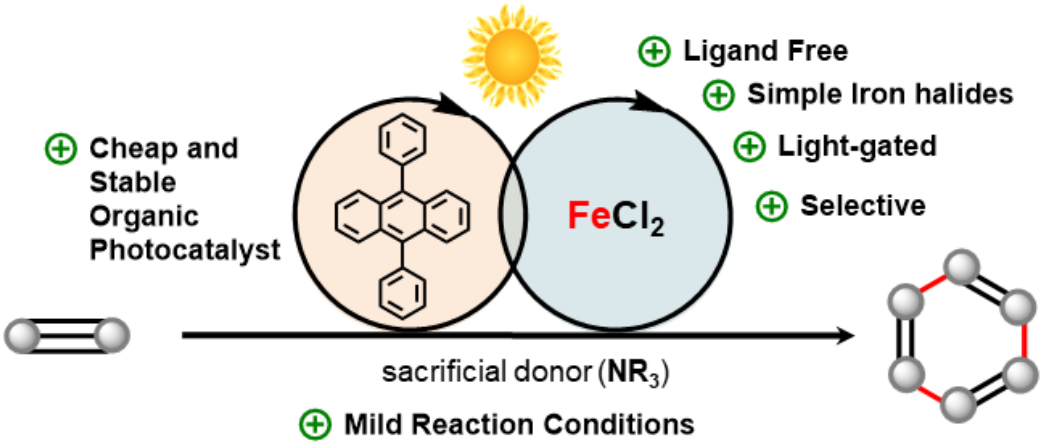

Merging transition metal catalysis and photocatalysis has emerged as a powerful strategy for the development of new synthetic methodologies. The dual catalytic protocol enables highly selective cyclotrimerizations of terminal alkynes via visible light irradiation. The presented ligand-free and light-gated arene-assembly involves the photoreduction of a simple ferrous salt and operates under mild reaction conditions and low catalyst loadings. Spectroscopic studies support a dual role of the photocatalyst (9,10-diphenylanthracene).

[i] Reproduced from M. Neumeier, U. Chakraborty, D. Schaarschmidt, V. de la Peña O´Shea, R. Pérez-Ruíz, A. Jacobi von Wangelin, *manuscript to be submitted to Angewandte Chemie*.

[ii] Author contributions: M.N., U.C. and A.J.v.W designed, performed and analyzed the catalytic experiments, scope and mechanistic studies. M.N., R.P.-R. and V.d.O. designed, performed and analyzed the photophysical experiments. M.N. and D.S. designed, performed and analyzed the cyclic voltammetry measurements. U.C. and A.J.v.W. directed the study. All authors contributed to the preparation of the manuscript.

5.1 Introduction

The merging of visible light photocatalysis with earth-abundant metal catalysis constitutes a highly sustainable and versatile approach to organic transformations. Such approaches benefit from the manifold of bond activation and formation events in the coordination sphere of the metal catalyst and the distinct reactivity patterns of photoactivated species and open-shell intermediates.[1,2] While several protocols involve the direct irradiation of metal complexes by UV-Vis light, the spatial separation of photocatalyst and metal-catalyst centers may enable much more diverse mechanistic scenarios, and the modular bi-catalytic setup may facilitate manipulation and selectivity control. The various modes of photo-activation of metal complexes involve ligand dissociation, M-X homolysis (mostly by UV irradiation),[3-5] electronic excitation of metal-to-ligand or ligand-to-metal charge transfer bands (MLCT, LMCT),[5-9] and single-electron transfer (SET) reactions in the presence of suitable 1e-redox partners (Figure 5-1, top).[1] Most of the transition metal complexes especially those of 3d metals do not favor the photo-physical behavior for direct visible light driven catalytic reactions.[7,10] Application of high-energy UV light often leads to decomposition of the organometallic photocatalyst as well as limited scope and poor selectivity of the catalytic reactions; more often, the pre-catalyst highly depends on the complex ligand design.[3,11] Thus, the successful merging of visible light excitation and one-electron redox processes with conventional organo-metallic reaction mechanisms has enabled the development of hitherto unknown chemical transformations.[1] However, this newly emerging field of metallaphotoredox catalysis has so far mostly relied on expensive (phenylpyridine)iridium(III) and (bipyridine)ruthenium(II) complexes as photoredox catalysts and coordination complexes of late transition metals (Co, Ni, Pd, Cu, Au) with phosphine, bipyridine derivatives, N-heterocyclic carbene, or multidentate amine ligands (e.g Ni^{II}(dtbbpy)Cl_2,[12] Ni^0(dtbbpy)$(COD)_2$[13], $Co(PR_3)_2X_2$,[14]) (Figure 5-1).[1,15] We wished to challenge this established paradigm and surmised that a more sustainable yet effective catalytic system would be composed of *i)* an inexpensive, easily available metal-free photoredox catalyst, *ii)* an inexpensive and non-toxic earth-abundant metal catalyst that operates *iii)* in the absence of complex ligands. There are very few examples of reductive photo-activations of ligand-free transition metal catalysts.[15,16] The application of iron complexes in metallaphotoredox catalysis is still in its infancy; a prominent example includes the reduction of CO_2 to methane mediated by Fe(0) species that were generated from Fe(III)-porphyrins by photoredox catalysis.[17] Here, we report the first combination of a visible light-driven photoredox-activation of a simple ferrous salt with an iron-catalyzed cyclotrimerization.

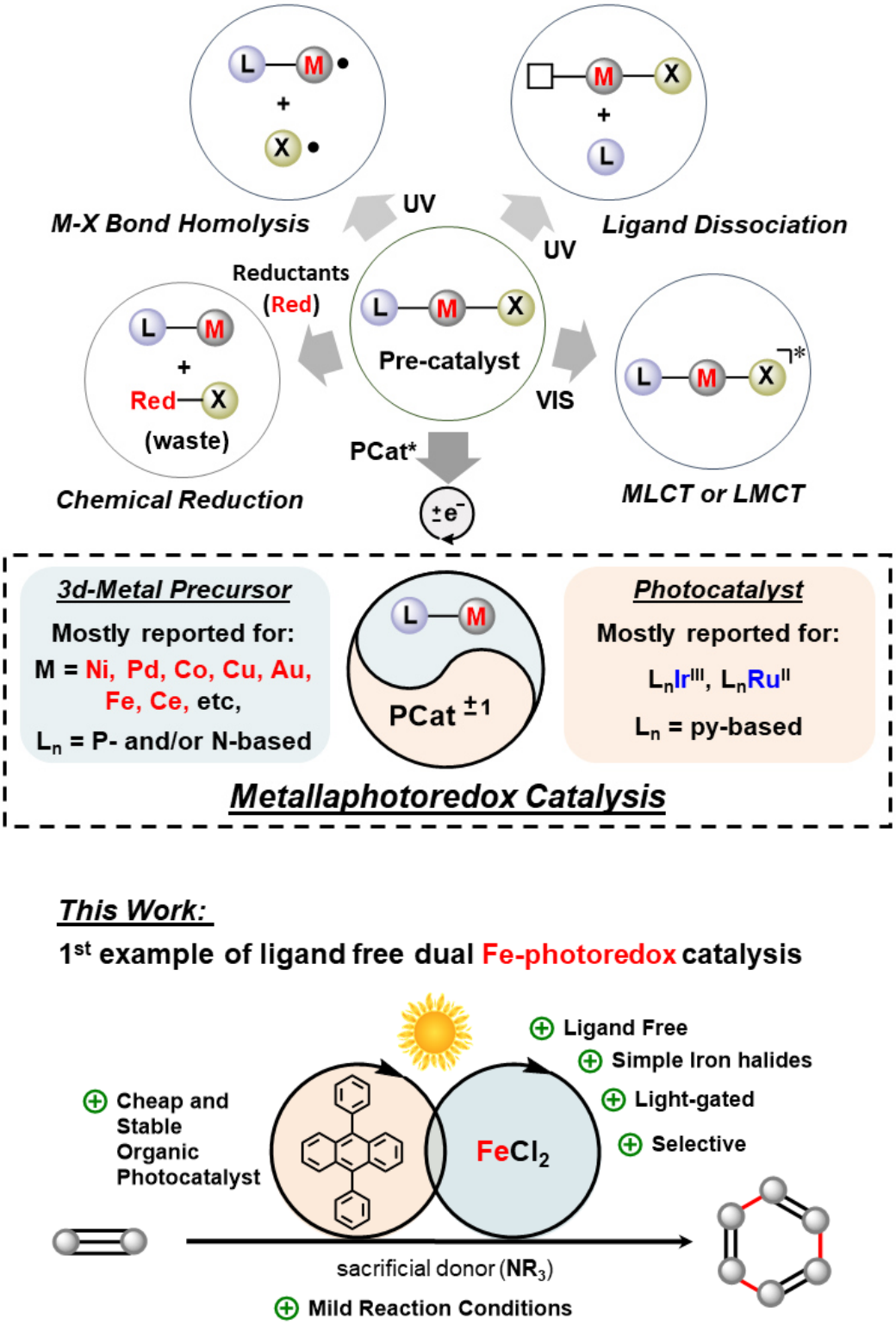

Figure 5-1. General strategies for photo/chemical activations of metal pre-catalysts (top); concept and features of the presented work (bottom).

5.2 Results and discussion

Although iron-catalyzed cyclotrimerizations of alkynes are well explored, they often require preparation and handling of highly reactive iron complexes in the presence of suitable ligands and reductants.[18-23] Thus, we considered the photoredox-generation of a low-valent iron species as the crucial challenge in our goal of combining the numerous advantages of iron and photoredox catalysis with respect to sustainability in [2+2+2] alkyne cycloaddition reactions. This thesis was corroborated by the work of *Jutand et al.* who investigated the electrochemical reduction (at high potentials. −1.6 V to −1.9 V) of simple Fe(III) salts in presence of *N,N*-ligands (dmeda or phen).[24] Our initial studies started with 9,10-diphenylanthracene (DPA), a well-known but to our sensation very under-estimated commercial organodye. Conceptually, we believed that its high oxidation potentials ($E_{1/2}$ ($DPA^{\bullet+}$/DPA* = -1.77 V); $E_{1/2}$ (DPA/$DPA^{\bullet-}$ = -1.94 V)) as well as it being a hydrocarbon only compound would give us an edge over traditional Iridium catalysts (Figure 5-2b).[25] Indeed, an early system consisting of phenylacetylene as the model substrate, a soluble irondichloride species, Huenig's base (DIPEA) and tricyclohexyl phosphine as the ligand led to 1,2,4-triphenylbenzene as the major product in 43% yield and a high regioselectivity (97:3) under UV-A irradiation in acetonitrile (Table 5-1, Entry 2). Major achievements during the reaction optimization process were the omission of a ligand as well as a shift of the irradiation wavelength into the visible light. Drastic reduction of catalyst loadings culminated in trace amounts of DPA, making the photocatalytic system catalytic towards the metal cycle.

The optimized set of reaction conditions involved a 0.5 M solution of phenylacetylene in acetonitrile with 1.0 mol% $FeCl_2$, 2.0 mol% DIPEA and 0.4 mol% DPA under 395-410 nm irradiation at 22 °C for 30 minutes (Table 5-1, Entry 1).[26] In the absence of either catalytic component (iron salt, amine, photocatalyst, light), no cyclotrimerization occurred (Table 5-1, Entries 7-10). Other solvents like toluene, DMF, etc. did not show any reactivity at all.[26] Employment of a 14 W CFL lamp or other LED's (410-700 nm) did not prosper in success as indicated by the UV-VIS spectrum of the diluted reaction mixture.[26] Changing the photocatalyst and adjusting the light-source to its λ_{max} did neither exhibit any reactivity, except for anthracene at 365 nm irradiation (Table 5-1, Entries 5-6). We attribute this to either insufficient reduction potentials of the other photocatalysts or non-beneficial interactions of their functional groups with the transition metal system. $FeBr_2$ and $FeCl_2(thf)_{1.5}$ produced similar results like $FeCl_2$, whereas $Fe(OAc)_2$, $Fe(acac)_2$ and $FeCl_3$ were inactive precursors.[26] Other metal salts derived from cobalt or manganese showed reasonable reactivity as well. Details for these systems are currently being under further investigation.[26]

Table 5-1. Selected optimization experiments.

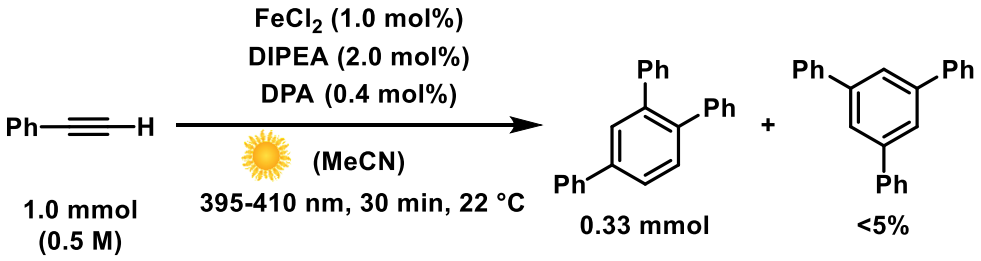

Entry	Deviations from conditions above	Conv. in %[a]	Yield in %[a]
1	none	100	100[b]
2	5 mol% [$FeCl_2(thf)_{1.5}$/2PCy_3], 5 mol % DPA, 50 mol% DIPEA, 2.5 h, 365 nm, 0.2 mmol PhCCH	82	43
3	2.5 mol% $FeCl_3$, 7.5 mol% DIPEA	0	0
4	2.5 mol% $FeCl_2$, 7.5 mol% diiso-propylamine (DIPA)	39	39
5	2.5 mol% $FeCl_2$, 5.0 mol% DIPEA, 0.04 mol% Anthracene (365 nm irradiation)	17	13
6[c]	other photocatalysts (EoY-Na_2, Rh6G, Fluorescein, DCA, $[Ru(bpy)_3]^{2+}$, $[Ir(ppy)_3]^{+}$)	<5	<5
7	no $FeCl_2$	9	0
8	no DPA	2	0
9	no DIPEA	0	0
10	no light, 18 h	0	0

[a] Determined by GC-FID analysis with pentadecane as internal standard. Yield based on max. 0.33 mmol of triphenylbenzene. Trace metal pure $FeCl_2$ (>99.99%) was used as precatalyst. [b] 95% isolated yield. [c] 5 mol% $FeCl_2$, 10 mol% DIPEA, 5 mol% photocat., 0.2 mmol phenylacetylene, 15 hours, light source adjusted to the absorption of the photocat..

With the optimized reaction conditions in hand, we investigated a range of terminal alkynes that were amendable to this photo-catalyzed cyclotrimerization (Figure 5-2a). In order to preserve activity, catalyst loadings were increased for several challenging functional groups.[26] Generally, the developed protocol provided good to excellent yields and regioselectivities in favor of mostly the 1,2,4-substituted benzene. Statistical as well as sterical arguments support the formation of this unsymmetrically substituted products.[27] A functional group screening disclosed the tolerance of halogen- keto-, ether-, and boron-groups in case of aromatic alkynes (Figure 5-2c). Notably, 3-ethynyl-thiophene was converted to 56% and provided a regio-isomeric ratio of 94:6. Unfortunately, amine-, aldehyde-, amide, ester or pyridine groups were not tolerated.

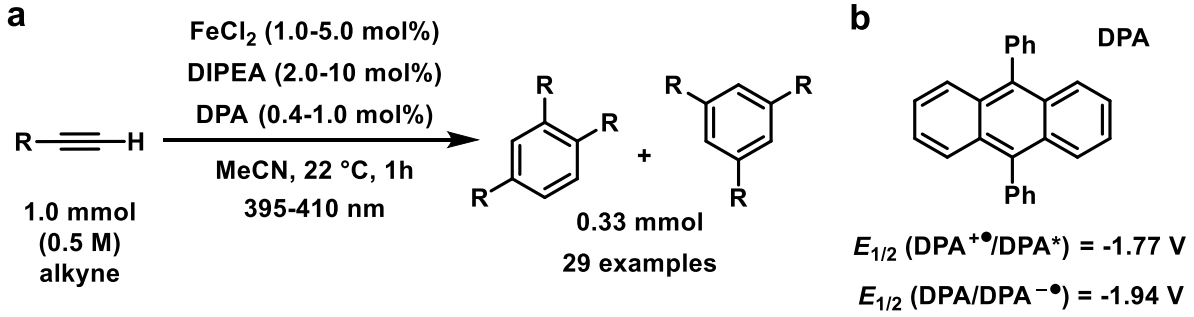
a
FeCl2 (1.0-5.0 mol%)
DIPEA (2.0-10 mol%)
DPA (0.4-1.0 mol%)
MeCN, 22 °C, 1h
395-410 nm
1.0 mmol
(0.5 M)
alkyne
0.33 mmol
29 examples
b
DPA
E1/2 (DPA+•/DPA*) = -1.77 V
E1/2 (DPA/DPA−•) = -1.94 V

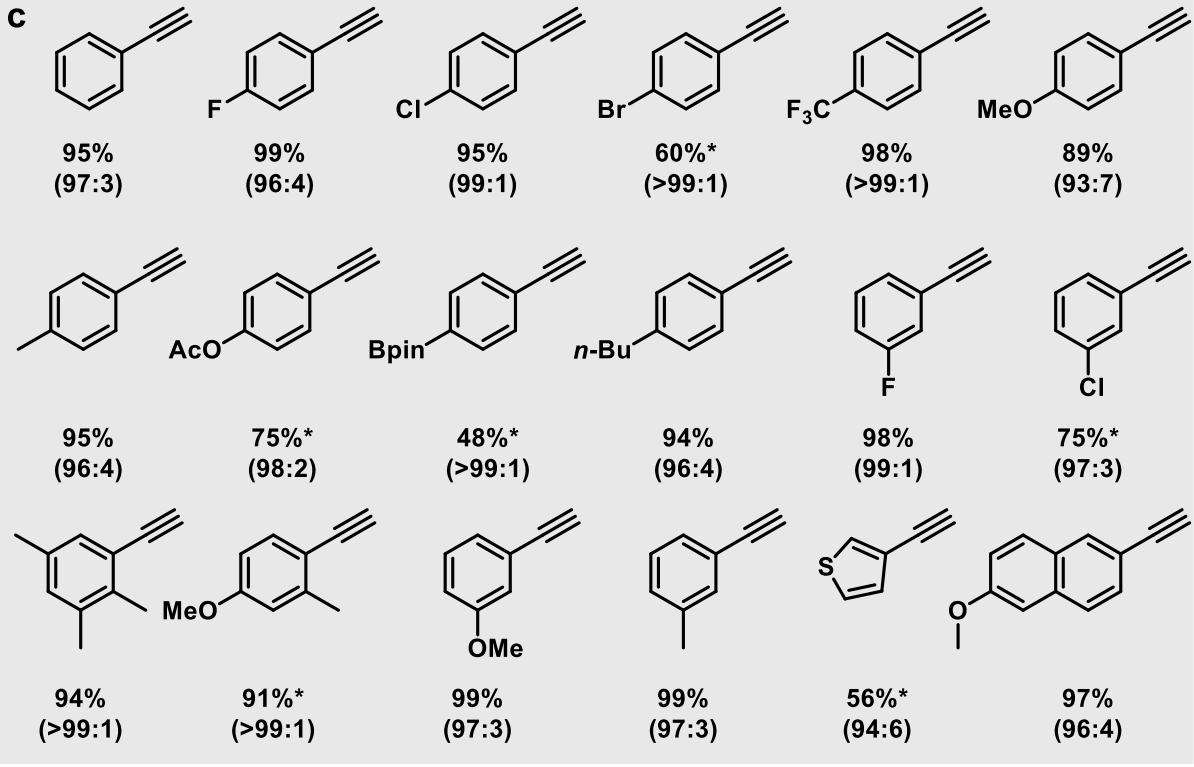
c
95% (97:3)
99% (96:4)
95% (99:1)
60%* (>99:1)
98% (>99:1)
89% (93:7)
95% (96:4)
75%* (98:2)
48%* (>99:1)
94% (96:4)
98% (99:1)
75%* (97:3)
94% (>99:1)
91%* (>99:1)
99% (97:3)
99% (97:3)
56%* (94:6)
97% (96:4)

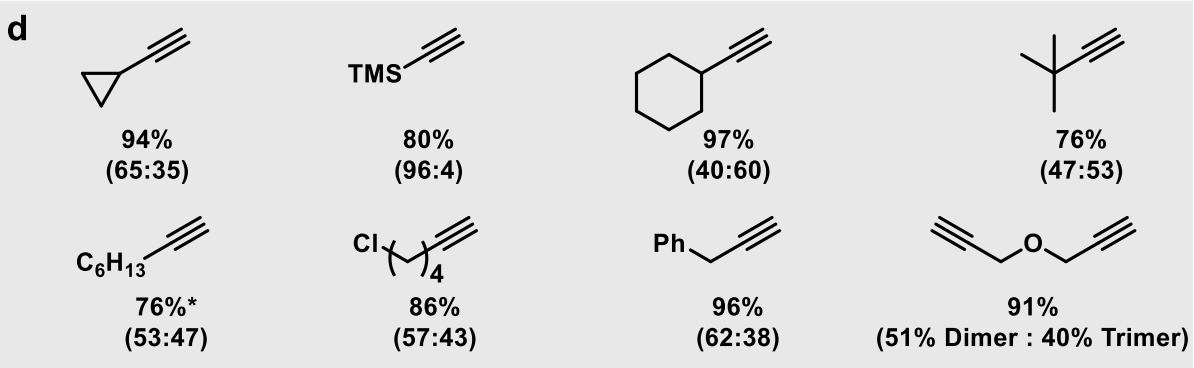
d
94% (65:35)
80% (96:4)
97% (40:60)
76% (47:53)
76%* (53:47)
86% (57:43)
96% (62:38)
91% (51% Dimer : 40% Trimer)

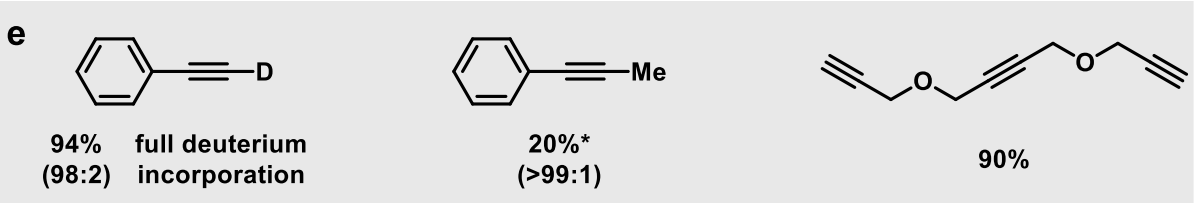
e
94% (98:2) full deuterium incorporation
20%* (>99:1)
90%

Figure 5-2. Scope of alkynes. **a**, General conditions used for the scope preparation; for details see experimental section 5.4. **b**, Structure of the organic photocatalyst and its reduction potentials in Volts versus SCE in acetonitrile. **c**, scope of tolerated functional groups on aromatic acetylene derivatives. **d**, scope of alkyl substituted acetylenes. **e**, further acetylene derivatives. Yields are given as isolated yields based on 0.33 mmol of total trimerization product; regioisomeric ratio of the formed 1,2,4- vs. 1,3,5-substituted products is depicted in brackets; * incomplete conversion, NMR yields given.

As some of these functional groups are key parts in the scaffold of most commercial photocatalysts, the exclusiveness of DPA as a functioning photocatalyst during the optimization process of the presented system may be explained. Sterically highly demanding substrates such as diortho-substituted mesitylacetylene showed no conversion (contrary to 1,2,4-trimethylbenzene). Alkylic alkynes also displayed promising reactivity with a higher tendency to generate 1,3,5-substituted products (Figure 5-2d). Further experiments revealed the complete conservation of deuterium content in the product of [D]phenylacetylene (Figure 5-2e). The reactivity of internal alkynes like 1-phenyl-1-propyne was rather limited, whereas a designed molecule containing two terminal and one internal triple bond afforded the aromatic product in high yield (Figure 5-2e).

A substantial requirement for most of the following experiments towards the elucidation of the reaction mechanism (Scheme 5-1) was the substitution of $FeCl_2$ with a highly soluble derivative. $FeCl_2(MeCN)_{1.4}$ turned out to be the most promising choice, while also providing a similar reactivity in terms of catalyst loading and reaction velocity.[26,28] Monitoring of the reaction mixture by IR spectroscopy showed no changes in $\nu_{C\equiv N}$ neither in presence of DIPEA nor phenylacetylene. Complete consumption of the starting $FeCl_2(MeCN)_{1.4}$ was observed in presence of DIPEA (2 equiv.) and phenylacetylene (2 equiv.). The IR spectrum of the light brown reaction mixture showed two bands at 2250 and 2290 cm^{-1} which are close to those of free MeCN, however no $\nu_{C\equiv C}$ bands were observed in the range 1700-2200 cm^{-1}. This indicates an absence of Fe^{II}-alkynyl species, which usually appears at ca. 2000-2100 cm^{-1},[29,30] whereas the pi-alkyne-iron complexes display $\nu_{C\equiv C}$ bands in the range 1700 to 1800 cm^{-1}.[30-32] However, strong back bonding from iron to alkyne in pi-alkyne complexes or polymetallic alkyne bridged complex may lead to a decrease in $\nu_{C\equiv C}$ band frequency well below 1600 cm^{-1} as well as a decrease in intensity.[33,34] Thus, we postulate the formation of a mono- or polynuclear iron-alkyne pi-complex species $[FeCl_2L_x(PhCCH)_y]_n$ in the reaction mixture (L = ligand).[35] In accordance with the Fe-alkyne interaction, a slight shift of the ^1H NMR signals for PhC≡CH was observed upon addition of DIPEA to $FeCl_2(MeCN)_{1.4}$ and phenylacetylene. DIPEA may have an assisting effect to replace the strongly coordinating MeCN with phenylacetylene from the iron center. UV-VIS-studies suggest that in the absence of the photocatalyst there is no catalytically (photo)active species forming before or after irradiation. Unlike in well-investigated copper-systems, we were unable to detect hints for a defined iron acetylide complex.[26,36] The cyclic voltammetry measurements of the reaction mixture containing $FeCl_2(MeCN)_{1.4}$ in presence of DIPEA (2.0 equiv.) and phenylacetylene (20 equiv.) showed reduction corresponding to the metal center at ca. −1.2 V (vs SCE),

whereas $FeCl_2(MeCN)_{1.4}$ displayed reduction at ca. −1.3 V. This slight shift may hint to the electron poor nature of the iron alkyne species $[FeCl_2L_x(PhCCH)_y]_n$. The CV-data also clearly indicate that a reduction of this iron-species by the photocatalyst would be thermodynamically favoured.[26]

To disclose the first steps of the photocatalytic side of the reaction mechanism, quenching studies of ^{1}DPA* by time-resolved fluorescence were performed. The lifetime of ^{1}DPA* gradually decreased with by the addition of increasing amounts of DIPEA (Figure 5-3a), indicating the formation of the radical ion pair of DIPEA$^{\bullet+}$ and DPA$^{\bullet-}$ by single electron transfer (SET). Stern-Volmer analysis (Figure 5-3b) revealed a quenching rate constant of $k_q(S1) = 8.8 \times 10^9$ $M^{-1}s^{-1}$ on the edges of diffusion limitation.[26] Moreover, phenylacetylene and $FeCl_2(MeCN)_{1.4}$ do not interact with the excited photocatalyst and neither have an influence on the quenching with DIPEA. Transient absorption spectroscopy (Figure 5-3c) confirmed the existence of DPA$^{\bullet-}$ (distinct absorption bands at 565 nm, 610 nm and 670 nm) in presence of DIPEA and light.[26,37] According to laser flash photolysis data (Figure 5-3d), this highly reducing species is exclusively quenched by $FeCl_2(MeCN)_{1.4}$ and thus regenerates DPA in the groundstate to close a photocatalytic cycle. However, the photocatalytic reduction of the iron salt itself in presence of the alkyne does not yet generate a fully active catalyst for cyclotrimerization reactions.

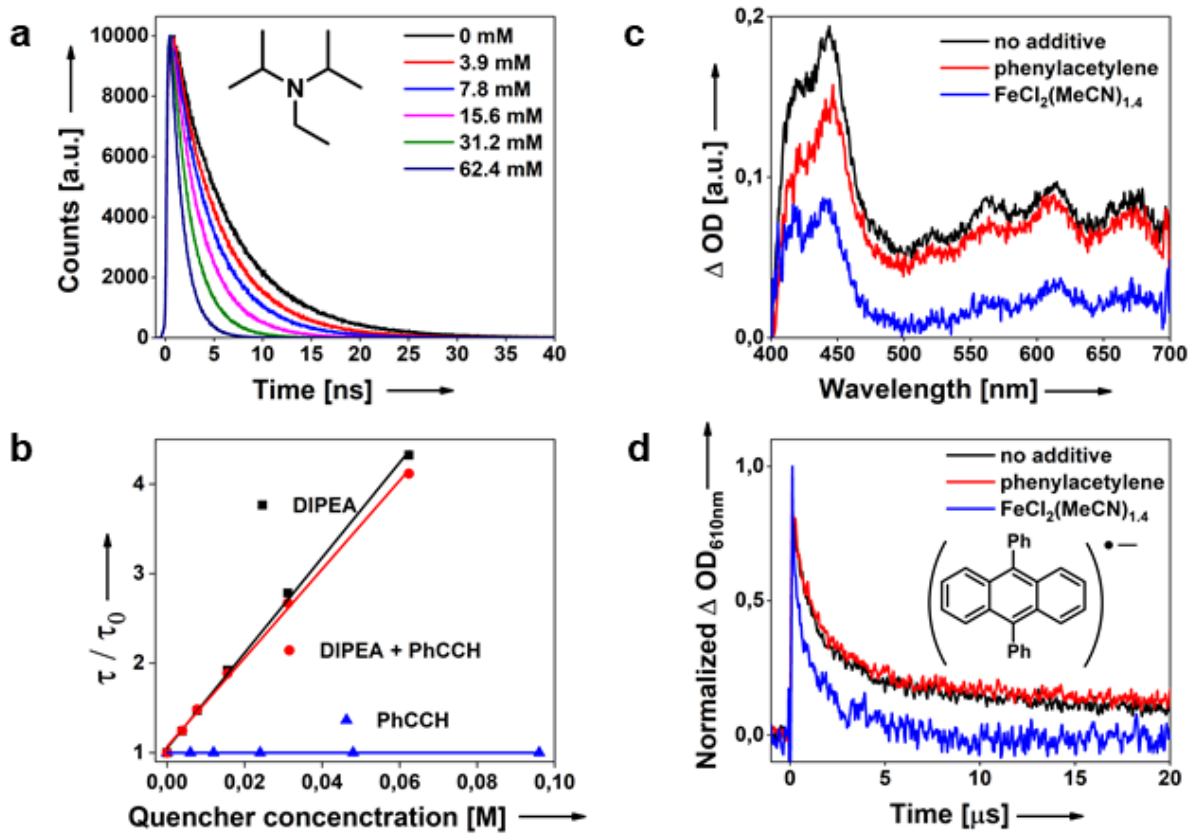

Figure 5-3. Spectroscopic studies.[26] **a**, fluorescence quenching of DPA* by DIPEA; **b**, Stern-Volmer plots for several quenchers; **c**, transient absorption spectrum of DPA$^{\bullet-}$ in absence and presence of quenchers; **d**, decay of DPA$^{\bullet-}$ at 610 nm monitored by laser flash photolysis.

Monitoring of the conversion during light on and off phases (Figure 5-4, right) suggests another involvement of light in the metal cycle and therefore makes the presented system susceptible to the unique opportunities presented by a visible light-gated reaction. This feature is reported for a cobalt-based system and was recently attributed to a ligand-to-metal-charge-transfer (LMCT) for the Co-alkynyl species which was identified via fluorescence spectroscopy in the excited state of the metal complex.[8] However, a correlation of Hammett constants with the reaction kinetics for a small number of different substrates was not observed for our system.[26] In combination with the IR and NMR studies as well as the fact, that the light-gated feature is also present for alkyl substrates, we assume that the presented system does not operate via a LMCT process or the like involving an Fe-alkynyl species.[26] Heating in the dark phase of the light on/off experiments showed that elevated temperature (80°C) is neither sufficient for the reaction to proceed without irradiation.

Steady-state fluorescence quenching of DPA with an *in situ* generated Fe system from $FeCl_2$/DibalH/phenylacetylene (1:2:40) suggests a possible energy/electron transfer (rate constant of $k_q(S1) = 4.8 \times 10^{10}$ $M^{-1}s^{-1}$) from the excited DPA* (triplet energy = 1.77 eV)[25b] to the low valent Fe-organometallic species,[26] which we attribute to a Fe^0-arene species generated as an intermediate by cyclotrimerization at the naked iron center.[20-22] The activated [Fe^0-arene]* species undergoes arene dissociation and generates back the naked iron species. Monitoring of the reaction mixture by UV-Vis spectroscopy after irradiation showed two new weak bands at 305 and 325 nm, which were also observed in the $FeCl_2$/DibalH/phenylacetylene (1:2:40) system and appear in the similar position for a LMCT band in a $[Fe(\eta^6\text{-mesitylene})_2]^{2+}$ complex.[38] Deligation of an arene compound generated by the cyclotrimerization of alkynes on a Ru(II)-center has been reported to be facilitated by UV irradiation,[39] while photodissociation of arene ligands from iron centers has also been well investigated, especially for the Fe(II) complexes $CpFe(arene)^+$ or $[Fe(arene)_2]^{2+}$ which originates from the visible light excited electronic states of the arene complexes weakening the Fe-arene bond and thereby deligating the arene in presence of donor solvents or ligands.[38, 40-44] Similar photodissociation ($\lambda \geq 270$ nm) of arene ligand also was observed for Fe(0) complex {(η-Ph)PhEtP}(η-2,3-dimethylbutadiene)Fe(0)] in presence of 2,3-dimethylbutadiene.[45] The known deligation of the arene ligands from Fe(arene) complexes are always facilitated by ligands or donor solvent such as MeCN. This fact also supports our assumption for the catalytic mechanism as the yield of the cyclotrimerization reaction drastically drops in solvents other than MeCN. However, direct activation of the Fe^0-arene species can not be absolutely ruled out as light seems to enhance the reactivity of insitu generated iron(0)-catalyzed cyclo-trimerizations even without photocatalyst DPA ($FeCl_2$/DibalH system).[26]

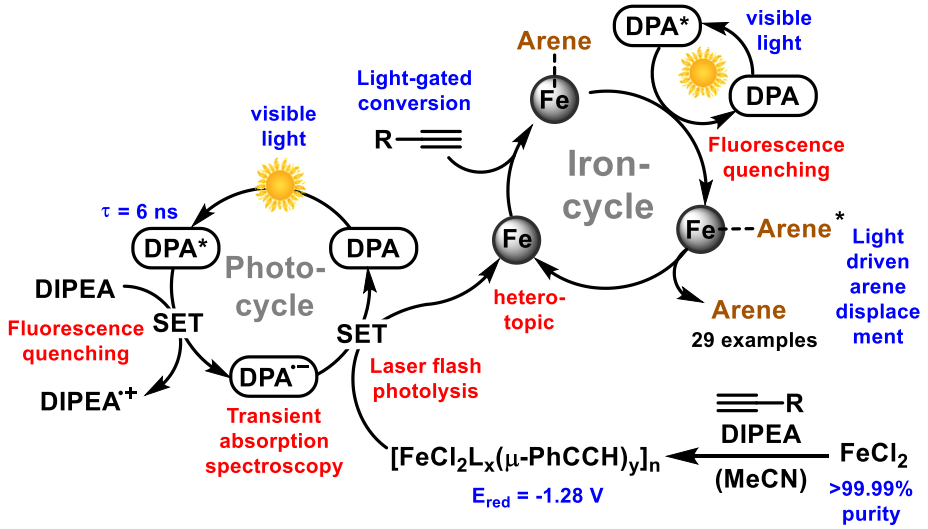

Scheme 5-1. Postulated reaction mechanism of the visible light-driven iron-catalyzed cyclotrimerization.

Kinetic poisoning studies (Figure 5-4, left) clearly disclose the presented reaction as a heterotopic system. Addition of substoichiometric trimethylphosphite (0.1 equiv. per Fe) unambiguously resulted in inhibition of catalysis.[46] Addition of the selective homotopic poison dibenzo[*a,e*]cyclooctatetraene (DCT), had no impact on the reaction kinetics.[47]

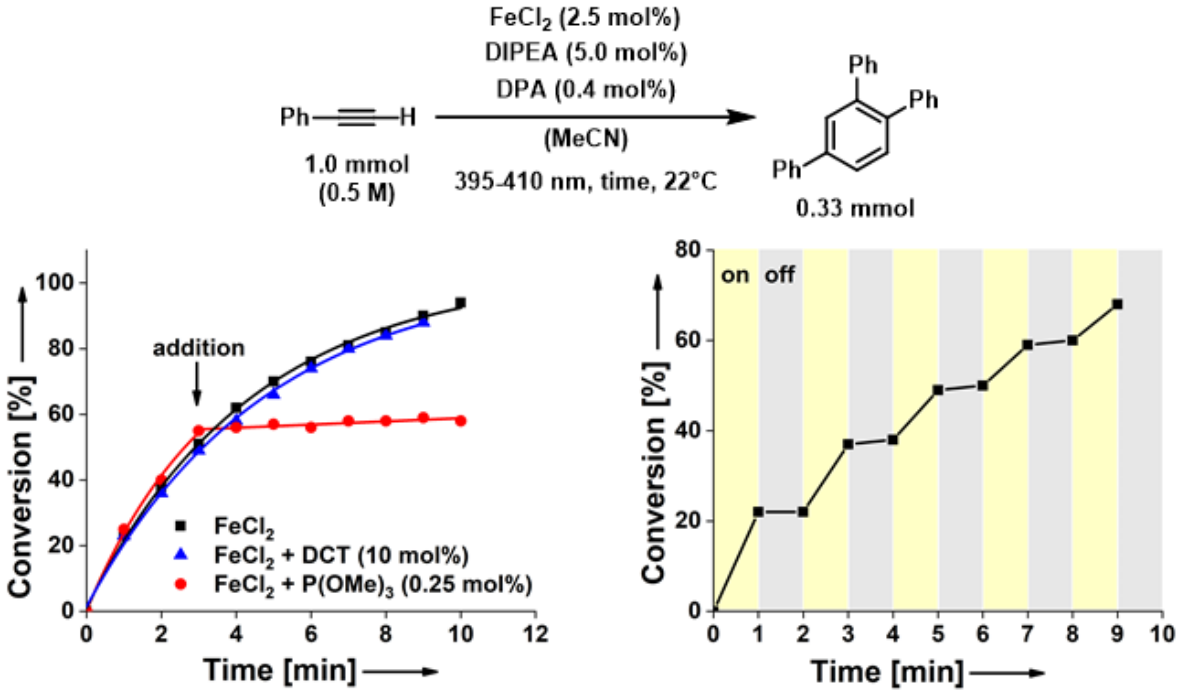

Figure 5-4. Poisoning studies (left) and kinetic reaction monitoring including alternation of light on and off phases (right) of the model reaction.[26]

According to our studies on reaction orders for each component, the photocatalytic steps are not rate-limiting at all. The presented protocol seems to proceed at 0^{th} order in DIPEA as well as DPA under the optimized conditions, which is also supported by the two quenching constants obtained from Stern-Volmer studies. In iron dichloride a reaction order of three, and in phenylacetylene an order of ca. 0.5 was observed.

5.3 Conclusion

In conclusion, we have developed the first dual catalytic protocol combining photoredox- and iron catalysis for synthetic applications. A small, cheap and highly photostable, organic dye enabled the photoreduction of simple $FeCl_2$ under visible light irradiation. In our ligand-free and light-gated arene assembly, cyclotrimerization reactions of terminal alkynes into the corresponding 1,2,4-trisubstituted benzenes were achieved under very mild conditions. With no need for ligands, external reductants, expensive or toxic transition metals (Ir, Ni, etc.) the presented procedure is not only most user-friendly, but also highly sustainable compared to other protocols in this field. Additionally, we provide detailed insights into the reaction mechanism via spectroscopy, kinetic monitoring and poisoning studies.

5.4 Experimental section

5.4.1 Materials and methods

Chemicals and solvents: All reagents (≥96% purity) and solvents (≥99% purity) were purchased from commercial suppliers (Acros, Alfa Aesar, Fisher, Fluka, Merck, Sigma Aldrich, TCI, Th. Geyer) and used as received unless otherwise indicated. Liquid acetylene derivatives as well as Hünig's base were distilled under vacuum prior to use. Dry solvents were obtained by either common drying techniques or directly purchased in extra dry (>99.9%+, over molecular sieves) form. $FeCl_2$ (99.99%, trace metal pure) beads were ground with mortar and pestle to obtain a homogeneous powder. All reagents and dried solvents were stored in an argon-filled glovebox.

Reaction setup: All reactions were carried out in Rotilabo®-sample vials (6 mL, Ø 22 mm, Roth) sealed with Rotilabo®-aluminium caps with septum (Ø 20 mm, Roth). Weighing-in and charging of the reaction vials was performed under inert conditions inside an argon-filled glovebox. Irradiation was performed outside of the glovebox with commercial LED's (for the scope: Edison Edixeon 3 W, 395-410 nm, U = 3.5 V, I = 700 mA, P = 2.45 W per LED; for the optimizations: various Cree 3 W LED's with wavelengths λ_{max} = 365 nm, 452 nm, 525 nm and 400-700 nm) - in a six LED array equipped with a cooling block - through the plain bottom side of the reaction vials.

Nuclear magnetic resonance (NMR) spectroscopy: ^{1}H NMR, ^{13}C NMR and ^{19}F NMR were used for purity and structure determination of products. NMR spectral data were collected on a Bruker Avance 300 (300 MHz for ^{1}H; 75 MHz for ^{13}C, 282 MHz for ^{19}F) spectrometer, a Bruker Avance 400 (400 MHz for ^{1}H; 100 MHz for ^{13}C) spectrometer or a Bruker Avance III 600 (600 MHz for ^{1}H; 585 MHz for ^{19}F) spectrometer at 20 °C. Chemical shifts are reported in δ/ppm, coupling constants *J* are given in Hertz. Solvent residual peaks were used as internal standard for all NMR measurements. The quantification of ^{1}H cores was obtained from integrations of appropriate resonance signals. Abbreviations used in NMR spectra: s – singlet, d – doublet, t – triplet, q – quartet, m – multiplet, bs – broad singlet, dd – doublet of doublet.

Gas chromatography (GC-FID and GC-MS): GC-FID measurements on an Agilent 7820A GC-system with N_2 as carrier gas were used for quantification purposes in reaction optimization screenings and kinetic experiments. Mesitylene or pentadecane were used as an internal standard; the conversion-% and yield-% were calculated from a linear calibration curve that was set up from at least three data points of various concentrations of the respective analytically pure material. GC-MS measurements on an Agilent 7820A GC-system coupled with a 5977B MSD detector (EI ionization source) and H_2 as carrier gas were used for reaction control purposes and structure determination of literature-known products (LMRS).

High resolution mass spectrometry (HRMS): HRMS was carried out by the Central Analytics at the department of chemistry, University of Regensburg. Abbreviations used in MS spectra: M – molar mass of target compound, EI – electron impact ionization, ESI – electrospray ionization.

Column chromatography: Column chromatography was performed using silica gel (Acros Organics, mesh 35-70, 60 Å pore size) as the stationary phase.

UV/VIS absorption spectroscopy: UV-Vis absorption spectroscopy was performed at room temperature on an Agilent Cary 5000 UV/VIS NIR double beam spectrometer with a 10 mm quartz cuvette.

Infrared (IR) spectroscopy: IR spectroscopy was performed at room temperature on an Agilent Cary 630 FTIR spectrometer with an ATR unit under inert conditions inside an argon-filled glovebox.

Cyclic voltammetry: CV measurements were performed with a potentiostat galvanostat PGSTAT101 from Metrohm Autolab using a glassy carbon working electrode, a platinum wire counter electrode, a silver/silver(I)chloride reference electrode and $N(n\text{-}Bu)_4PF_6$ (0.1 M) as supporting electrolyte. The potentials were achieved relative to the Fc/Fc^+ redox couple with ferrocene as external standard.

Steady-state fluorescence spectroscopy: The steady-state fluorescence spectra were recorded on an Agilent Cary Eclipse spectrofluorimeter system. The samples were placed into screw-cap quartz cuvettes of 1 cm path length with PTFE-coated silicon septum. The excitation wavelength was set at 372 nm.

Time-resolved fluorescence spectroscopy: Lifetime measurements were carried out at room temperature using a Mini-τ equipment from Edinburgh Instruments. As excitation source a laser diode (model EPL375) at 372 nm with a pulse width of 61.2 ps and repetition rate of 1 MHz was employed.

Laser flash photolysis: The measurements were performed with a Pump-Probe Setup LP980-K purchased by Edinburgh Co. The Pump source is an optical parametric oscillator (OPO) pumped by the third Harmonic of a Nd:YAG laser (EKSPLA). The wavelength can be set from 210 nm to about 2600 nm, with a pulse width of about 5 nm using an OPO mod. NT342A-10 with an UV extension NT242 with typical pulse duration of 5 ns. The repetition rate is 10 Hz. The white probe light is generated by a pulsed xenon flash lamp (150 W) and passes the sample orthogonal to the Pump beam. The duration of the probe pulse is 250 µs. This probe pulse is longer than the recorded time window of a measurement. A monochormator (TMS302-A, grating 150 lines/mm) disperses the probe light after it passed the sample. The probe light is then passed on to a PMT detector (Hamamatsu Photonics) to obtain the temporal resolved picture. The time resolution in each window is about 10 % of the temporal window width. All components are controlled by the software L900 provided by Edinburgh.

Determination of regioisomeric ratios: The ratios of regioisomers were determined by integration of either GC-FID or ^{1}H-NMR signals. In case of GC-FID evaluation an equal response factor of both regioisomers was assumed. For regioisomeric ratios greater than 90:10 only the main isomer is depicted in the following NMR characterizations.

5.4.2 General procedures

General method A for the optimization of reaction conditions:

A simple iron(II)salt (**a** mmol, **a** equiv.) and the photocatalyst (**b** mmol, **b** equiv.) were dissolved in the solvent (2.0 mL). Hünig's base (**c** mmol, **c** equiv.), phenylacetylene (**d** mmol, **d** equiv.) and pentadecane (50 µl) were added consecutively. The reaction mixture was irradiated at 22 °C with an adequate (with respect to the absorption of the photocatalyst) LED for the respective time. After switching off the light, the reaction was immediately quenched by addition of aqueous hydrochloric acid (3 mL, 1 M) and extracted with ethyl acetate (3 mL). The organic phase was filtered through a small plug of silica in a pasteur pipette with additional ethyl acetate to remove inorganic impurities. The filtrate was analyzed by GC-FID measurement.

General method B for the scope of the [2+2+2] cyclotrimerizations:

$FeCl_2$ (0.025 mmol or 0.050 mmol, 0.025 equiv. or 0.050 equiv.) and 9,10-diphenyl-anthracene (0.004 mmol or 0.010 mmol, 0.004 equiv. or 0.010 equiv.) were dissolved in acetonitrile (2.0 mL). Hünig's base (0.050 mmol or 0.100 mmol, 0.050 equiv. or 0.100 equiv.) and the respective acetylene derivative (1.0 mmol, 1.0 equiv.) were added consecutively. The reaction mixture was irradiated at 22 °C with a 395-410 nm LED for one hour. After switching off the light, the reaction was immediately quenched by addition of aqueous hydrochloric acid (3 mL, 1 M) and extracted with ethyl acetate (3×10 mL). The combined organic layers were washed with brine (10 mL), dried over sodium sulfate and filtered from the drying agent. After removing the volatiles in vacuum, the residue was filtered through a plug of silica in a pasteur pipette with an appropriate solvent mixture of pentane and ethyl acetate. Evaporation of the solvents afforded a product mixture that was sufficiently pure. The isolated yields were given as combined yields of both regioisomers.

Efforts to separate the 1,2,4-regioisomer from 1,3,5-regioisomer (and/or residual starting material) failed due to lacking differences in polarity. 9,10-Diphenylanthracene was also inseparable from the product mixture, but was only present in trace amounts (< 2 mg).

5.4.3 Detailed overview of optimization experiments

Table 5-2. Optimization of reaction conditions: Variation of λ_{max} and control reactions.

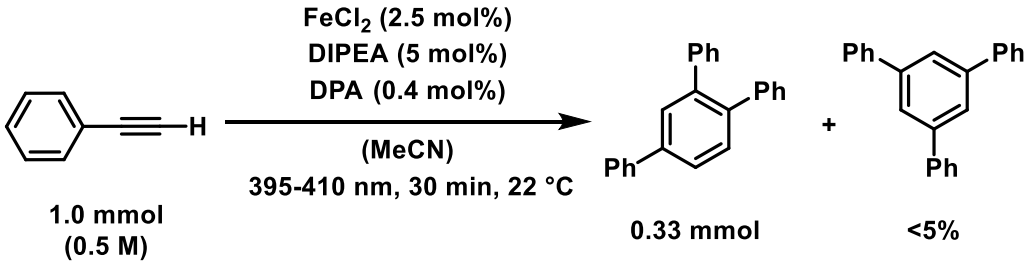

Entry	Deviations from condition above	Conversion[(a)] [%]	Yield[(a)] [%]
1	None	100	100
2	365 nm irradiation	100	100
3	410-700 nm irradiation	0	0
4	14 W CFL lamp	0	0
5	1.0 mol% $FeCl_2$, 2.0 mol% DIPEA	100	100
6	2.5 mol% $FeCl_2(MeCN)_{1.4}$	98	98
7	2.5 mol% $FeCl_3$, 7.5 mol% DIPEA	0	0
8	5.0 mol% Diisopropylamin (DIPA)	39	39
9	5.0 mol% DIPA, no light	0	0
10	0.04 mol% Anthracene (λ_{irr} = 365 nm)	17	13
11	no $FeCl_2$	9	0
12	no 9,10-Diphenylanthracene (DPA)	2	2
13	no DIPEA	0	0
14	no light, 18 hours reaction time	0	0

[(a)] Determined by GC-FID analysis with pentadecane as internal standard. Yields are given as combined yields of 1,2,4- and 1,3,5-regioisomers. Reaction setup according to general method A.

Table 5-3. Optimization of reaction conditions: Variation of solvents.

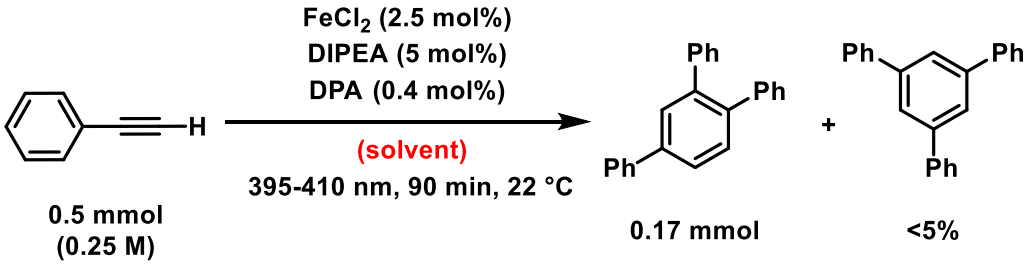

Entry	Solvent	Conversion[a] [%]	Yield[a] [%]
1	Tetrahydrofuran	0	0
2	*N*,*N*-Dimethylformamide	2	0
3	Toluene	0	0
4	Hexane	0	0
5	1,1-Dichloroethane	0	0
6	*N*-Methylpyrrolidone	12	2
7	Dimethylsulfoxide	0	0

[a] Determined by GC-FID analysis with pentadecane as internal standard. Yields are given as combined yields of 1,2,4- and 1,3,5-regioisomers. Reaction setup according to general method A.

Table 5-4. Optimization of reaction conditions: screening of different transition metal salts.

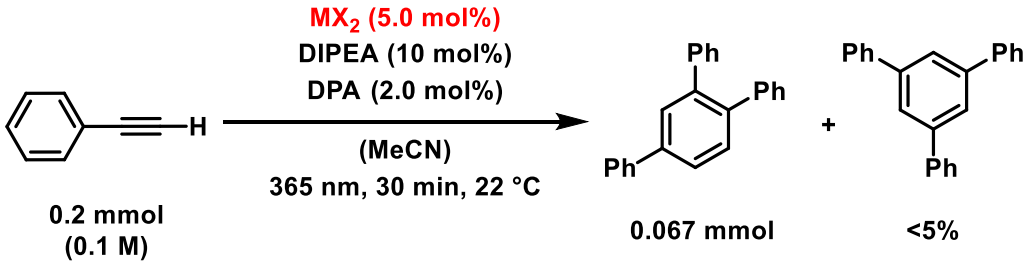

Entry	MX_2	Conversion[a] [%]	Yield[a] [%]
1	$FeCl_2(thf)_{1.5}$	100	92
2	$FeCl_2$ (>99.99% purity)	100	100
3	$FeBr_2$	100	92
4	$Fe(OAc)_2$	11	1
5	$Fe(acac)_2$	1	1
6	$CoBr_2$	93	71
7	$MnBr_2$	42	23

[a] Determined by GC-FID analysis with pentadecane as internal standard. Yields are given as combined yields of 1,2,4- and 1,3,5-regioisomers. Reaction setup according to general method A.

Table 5-5. Optimization of reaction conditions: screening of different photocatalysts.

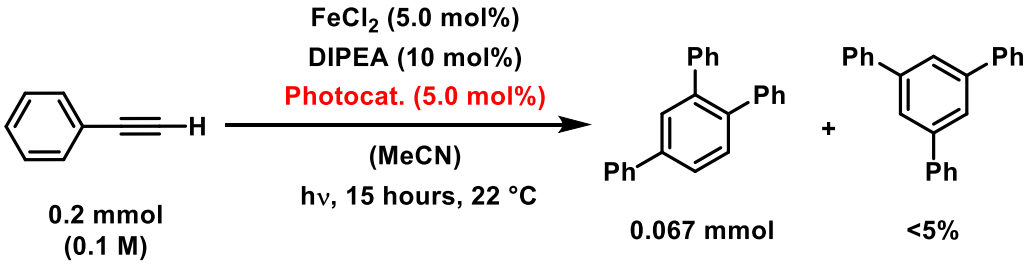

0.2 mmol (0.1 M) | 0.067 mmol | <5%

Entry	Photocat. (λ_{irr})	Conversion[(a)] [%]	Yield[(a)] [%]
1	Eosin Y Na_2-salt (525 nm)	5	0
2	Fluorescein (525 nm)	0	0
3	Rhodamin 6G (525 nm)	0	0
4	Rhodamin 6G (410-700 nm)	0	0
5	Dicyanoanthracene (452 nm)	0	0
6	Dicyanoanthracene (410-700 nm)	1	0
7	$Ru(bpy)_3$ (452 nm)	0	0
8	$Ru(bpy)_3$ + pyrene (452 nm)	0	0
9	*fac*-$Ir(ppy)_3$ (365 nm)	4	0

[(a)] Determined by GC-FID analysis with pentadecane as internal standard. Yields are given as combined yields of 1,2,4- and 1,3,5-regioisomers. Reaction setup according to general method A.

5.4.4 Kinetic experiments

Procedure for determining the reaction kinetics (conversion vs. time diagram) of the model reaction:

$FeCl_2$ (0.025 mmol, 0.025 equiv.) or $FeCl_2(MeCN)_{1.4}$ (0.025 mmol, 0.025 equiv.) and 9,10-diphenylanthracene (0.004 mmol, 0.004 equiv.) were dissolved in acetonitrile (2.0 mL). Hünig's base (0.050 mmol, 0.050 equiv.), phenylacetylene (1.0 mmol, 1.0 equiv.) and mesitylene (50 µL) were added consecutively. The reaction mixture was irradiated directly in the glovebox at ambient temperature with a 395-410 nm LED for the respective time. Aliquots of 50 µL were taken during irradiation within the given time intervals. These aliquots were directly quenched with *p*-toluenesulfonic acid (ca. 5 mg) inside the glovebox. After the irradiation, workup and GC-FID analysis was performed according to General Method A.

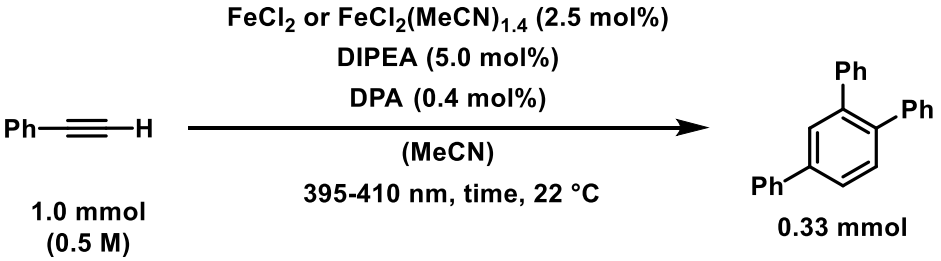

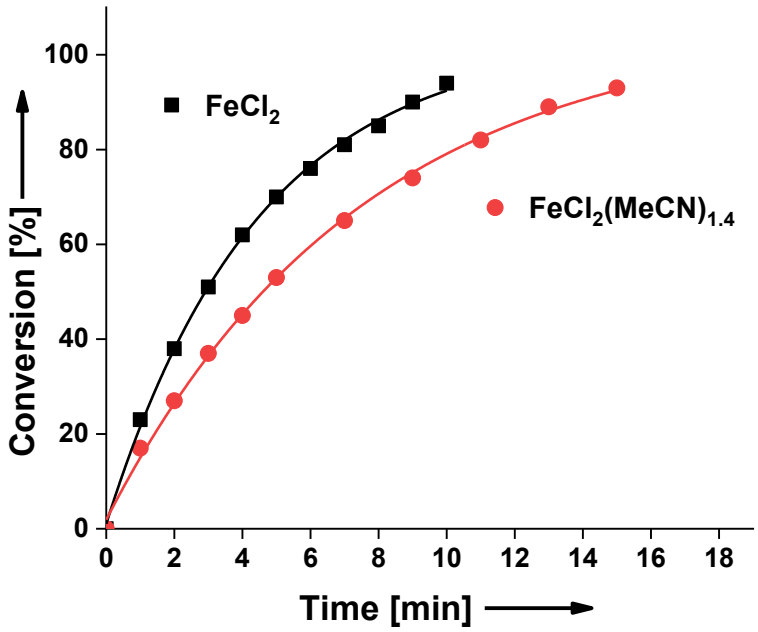

Figure 5-5. Conversion vs. time diagram of the model reaction with different iron dichloride sources. Conversion was determined by GC-FID analysis with mesitylene as internal standard.

Procedure for the kinetic poisoning experiments of the model reaction:

$FeCl_2$ (0.025 mmol, 0.025 equiv.) or $FeCl_2(MeCN)_{1.4}$ (0.025 mmol, 0.025 equiv.) and 9,10-diphenylanthracene (0.004 mmol, 0.004 equiv.) were dissolved in acetonitrile (2.0 mL). Hünig's base (0.050 mmol, 0.050 equiv.), phenylacetylene (1.0 mmol, 1.0 equiv.) and mesitylene (50 µL) were added consecutively. The reaction mixture was irradiated directly in the glovebox at ambient temperature with a 395-410 nm LED for the respective time. Aliquots of 50 µL were taken during irradiation within the given time intervals. These aliquots were directly quenched with *p*-toluenesulfonic acid (ca. 5 mg) inside the glovebox. After three minutes of irradiation a stock solution of DCT (100 µmol in 100 µL, 0.1 equiv.) or respectively $P(OMe)_3$ (2.5 µmol in 100 µL, 0.0025 equiv.) was added to the reaction mixture. For the rest of the reaction time aliquots were taken as described before. After the irradiation, workup and GC-FID analysis was performed according to General Method A.

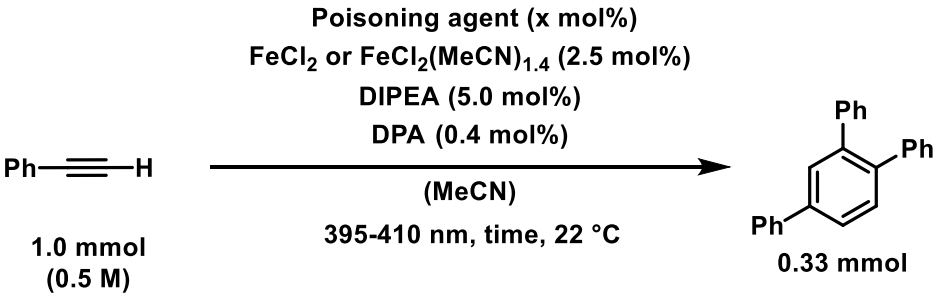

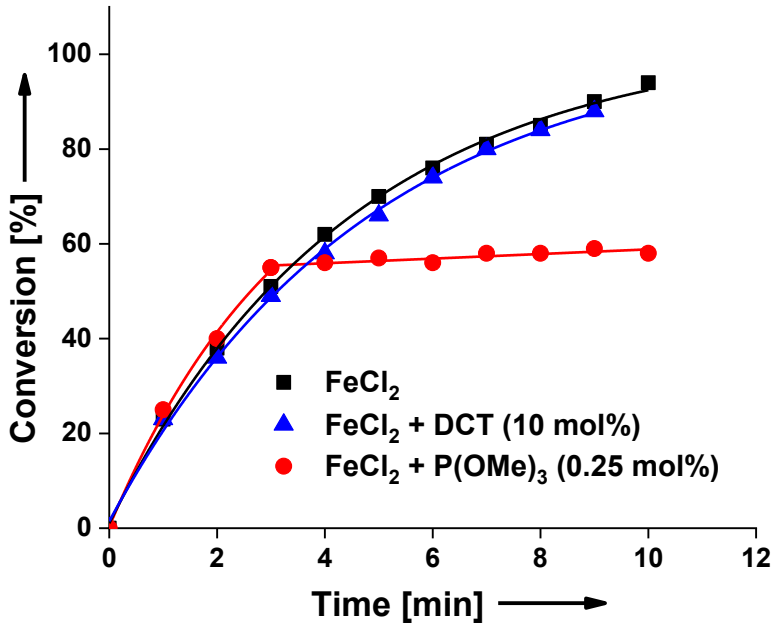

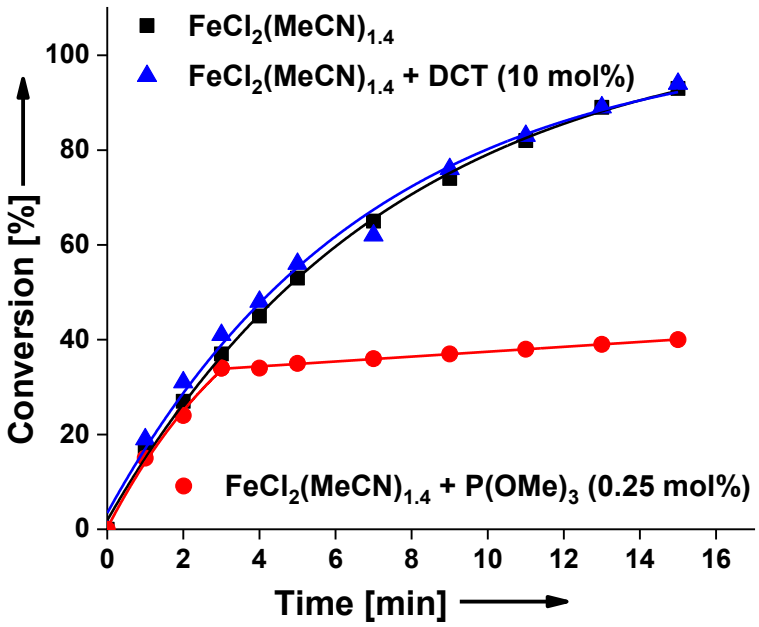

Figure 5-6. Conversion vs. time diagram of the model reaction with addition of different poisoning agents. Conversion was determined by GC-FID analysis with mesitylene as internal standard.

Procedure for the kinetic lights on/off experiments of the model reaction:

$FeCl_2$ (0.025 mmol, 0.025 equiv.) or $FeCl_2(MeCN)_{1.4}$ (0.025 mmol, 0.025 equiv.) and 9,10-diphenylanthracene (0.004 mmol, 0.004 equiv.) were dissolved in acetonitrile (2.0 mL). Hünig's base (0.050 mmol, 0.050 equiv.), phenylacetylene (1.0 mmol, 1.0 equiv.) or cyclohexylacetylene (1.0 mmol, 1.0 equiv.), and mesitylene (50 µL) were added consecutively. The reaction mixture was irradiated directly in the glovebox at ambient temperature with a 395-410 nm LED for the respective time interval before an aliquot (50 µL) was taken. After that, the light was switched off and the mixture was stirred for the same time intervall in the dark before another aliquot was taken. Aliquots were directly quenched with *p*-toluenesulfonic acid (ca. 5 mg) inside the glovebox. Workup and GC-FID analysis was performed according to General Method A.

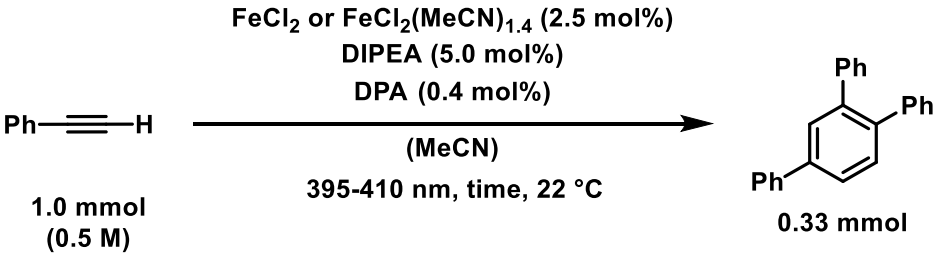

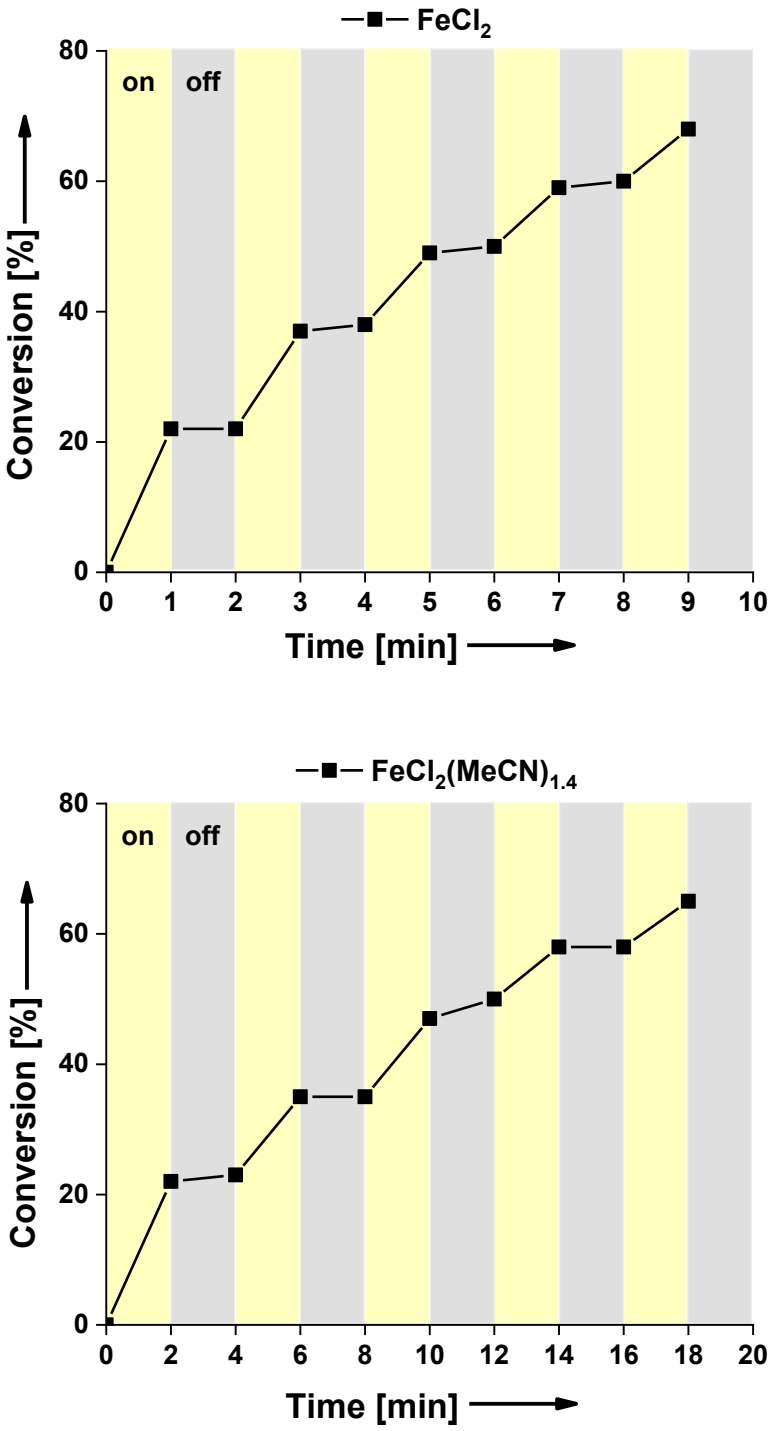

Figure 5-7. Conversion vs. time diagram of the model reaction with **$FeCl_2$** (top) and **$FeCl_2(MeCN)_{1.4}$** (bottom) during switching on (●) and off (●) the light. Conversion was determined by GC-FID analysis with mesitylene as internal standard.

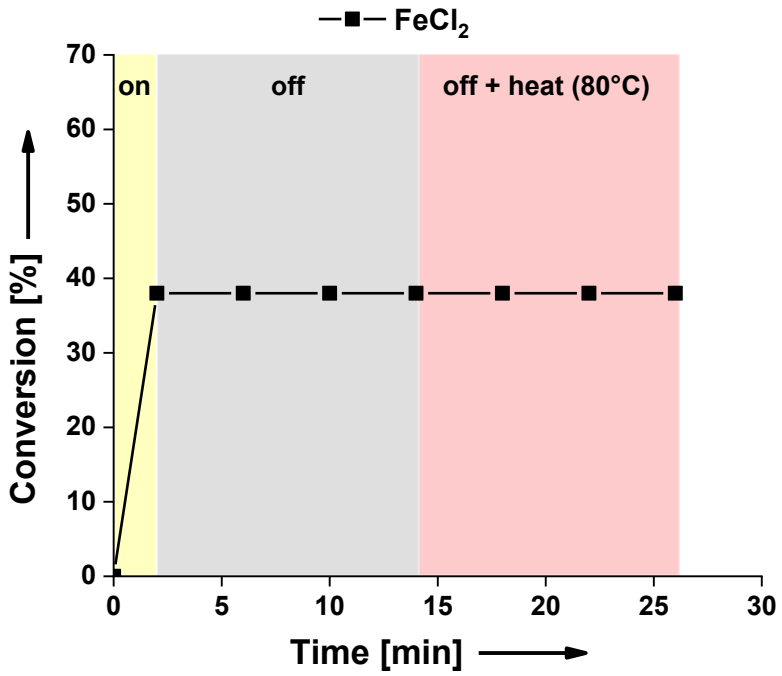

Figure 5-8. Conversion vs. time diagram of the model reaction with **$FeCl_2$** during switching on (●) and off (●) the light and heating to 80 °C after switching the lights off (●). Conversion was determined by GC-FID analysis with mesitylene as internal standard.

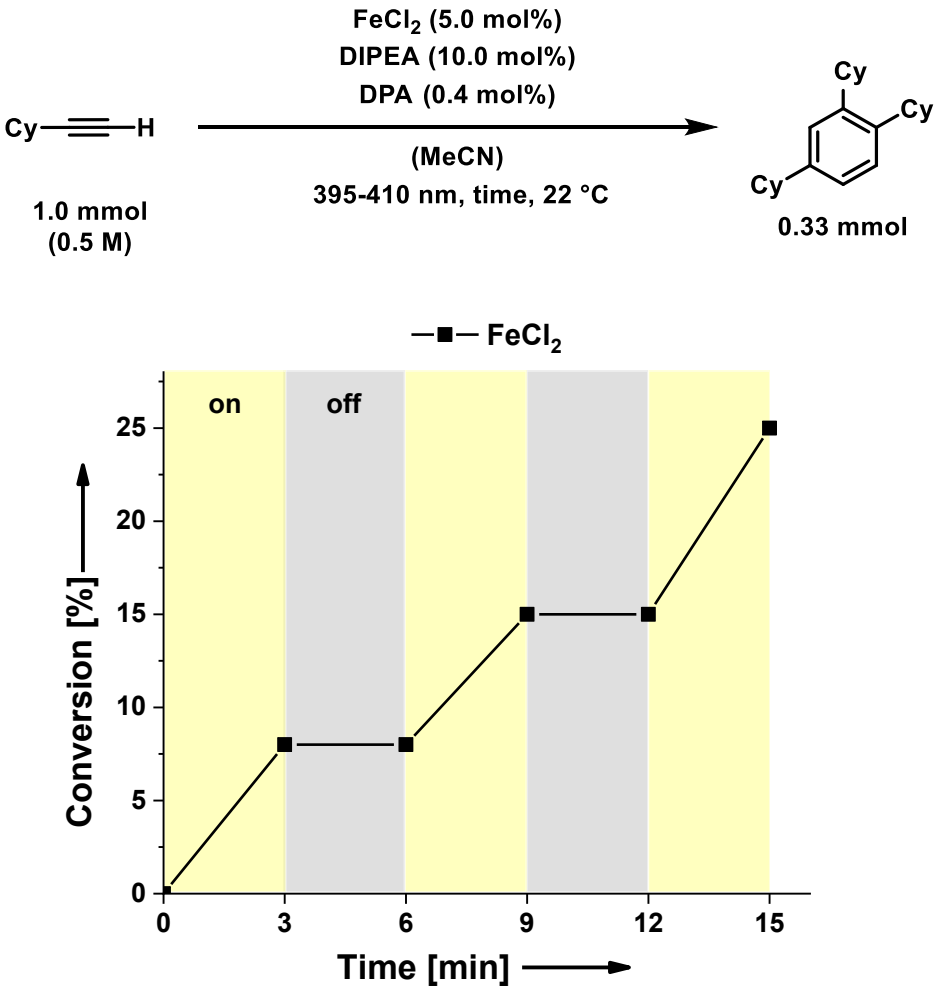

Figure 5-9. Conversion vs. time diagram of the model reaction (using cyclohexylacetylene as substrate) with **$FeCl_2$** during switching on (●) and off (●) the light. Conversion was determined by GC-FID analysis with mesitylene as internal standard.

5.4.5 Fluorescence quenching experiments

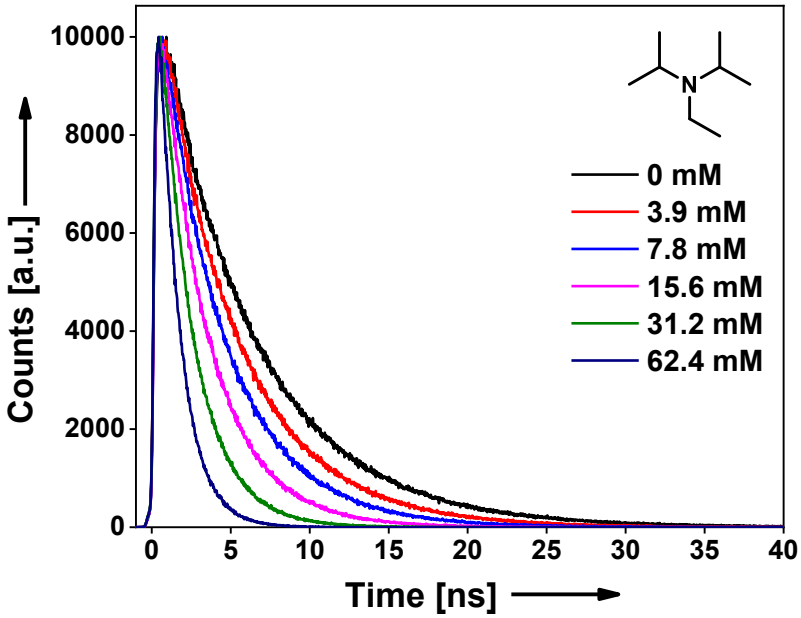

Figure 5-10. Time-resolved fluorescence (λ_{exc} = 372 nm) of 9,10-diphenylanthracene (0.1 mM) in the presence of increasing amounts of DIPEA in acetonitrile under aerobic conditions.

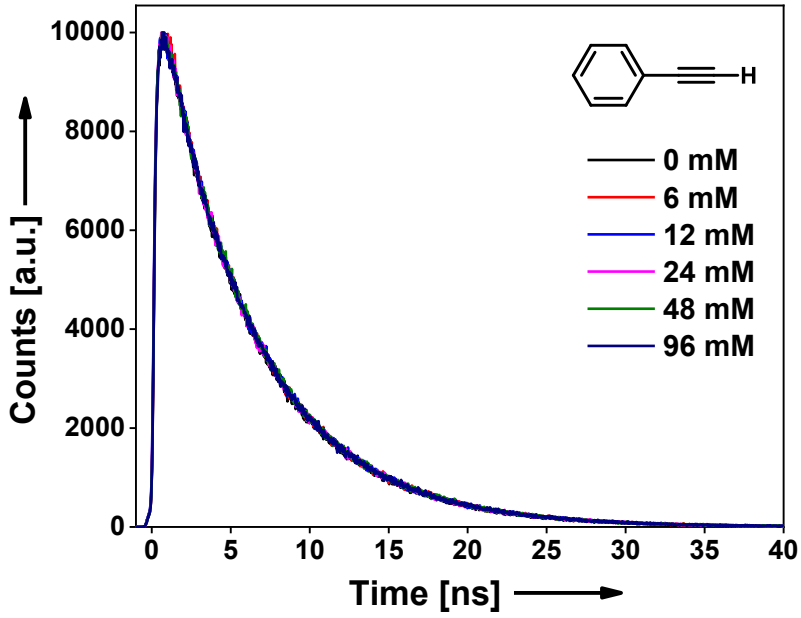

Figure 5-11. Time-resolved fluorescence (λ_{exc} = 372 nm) of 9,10-diphenylanthracene (0.1 mM) in the presence of increasing amounts of phenylacetylene in acetonitrile under aerobic conditions.

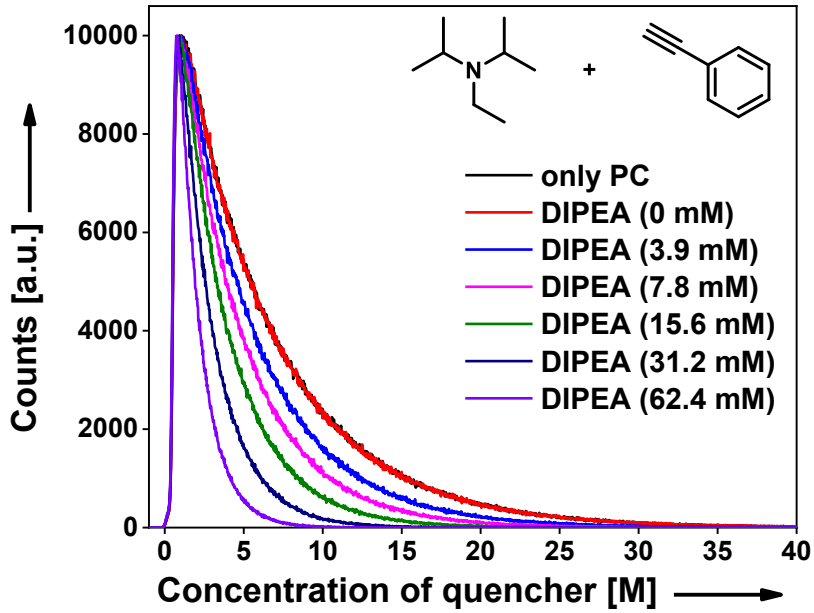

Figure 5-12. Time-resolved fluorescence (λ_{exc} = 372 nm) of 9,10-diphenylanthracene (0.1 mM) in the presence of phenylacetylene (96 mM) and increasing amounts of DIPEA in acetonitrile under aerobic conditions.

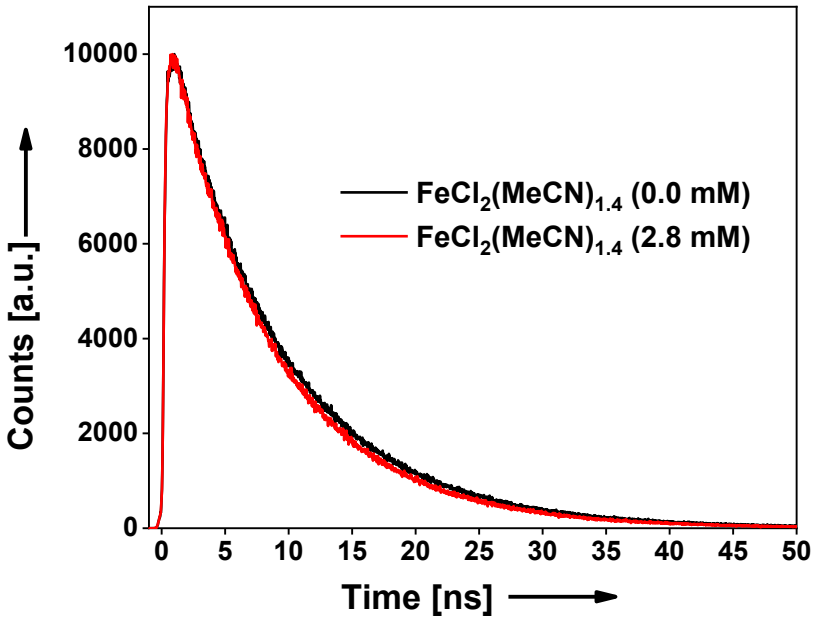

Figure 5-13. Time-resolved fluorescence (λ_{exc} = 372 nm) of 9,10-diphenylanthracene (0.1 mM) in the presence (●) and absence (●) of $FeCl_2(MeCN)_{1.4}$ (2.8 mM) in acetonitrile under anaerobic conditions.

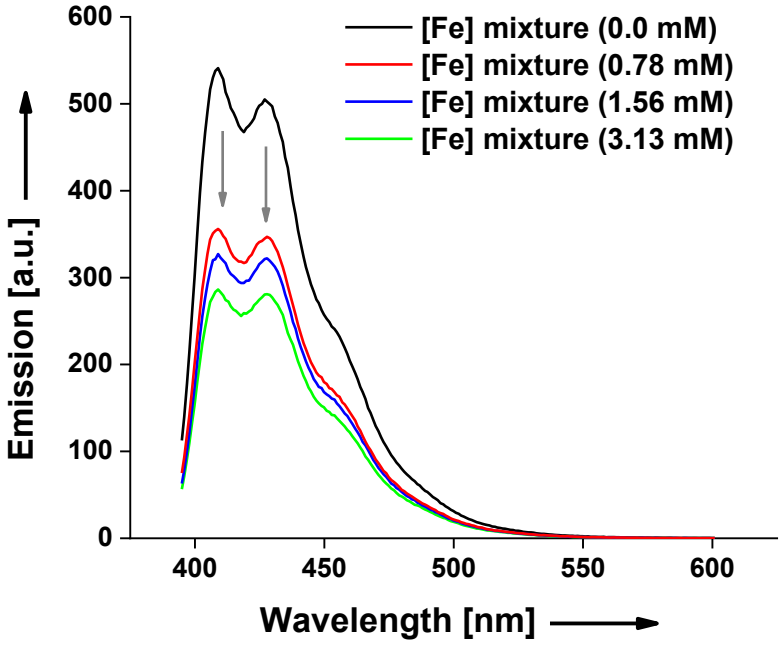

Figure 5-14. Steady-state fluorescence (λ_{exc} = 372 nm) of 9,10-diphenylanthracene (0.01 mM) in the presence of different concenctrations of a mixture consisting of $FeCl_2$ (1.0 eq.), DIBAL-H (2.0 eq.) and phenylacetylene (40 eq.) in acetonitrile under anaerobic conditions.

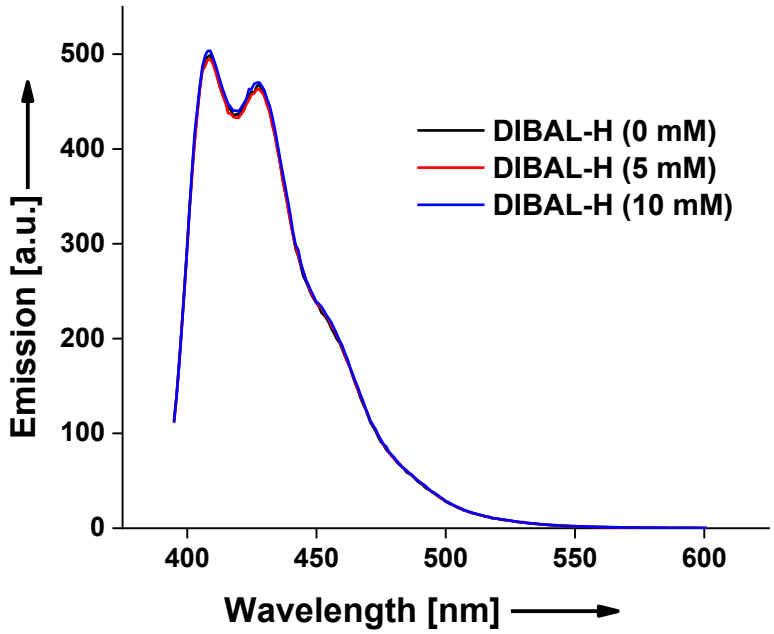

Figure 5-15. Steady-state fluorescence (λ_{exc} = 372 nm) of 9,10-diphenylanthracene (0.01 mM) in the presence of different concenctrations of DIBAL-H.

5.4.6 Stern-Volmer analysis

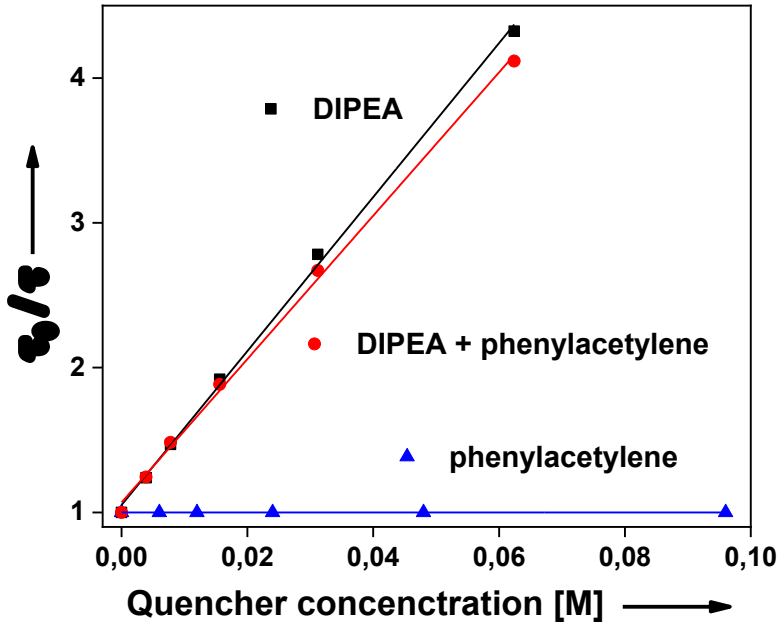

Figure 5-16. Stern-Volmer plots to obtain k_q(S1) for the DPA* quenching with DIPEA and phenylacetylene. Experimental errors were lower than 5% of the obtained values.

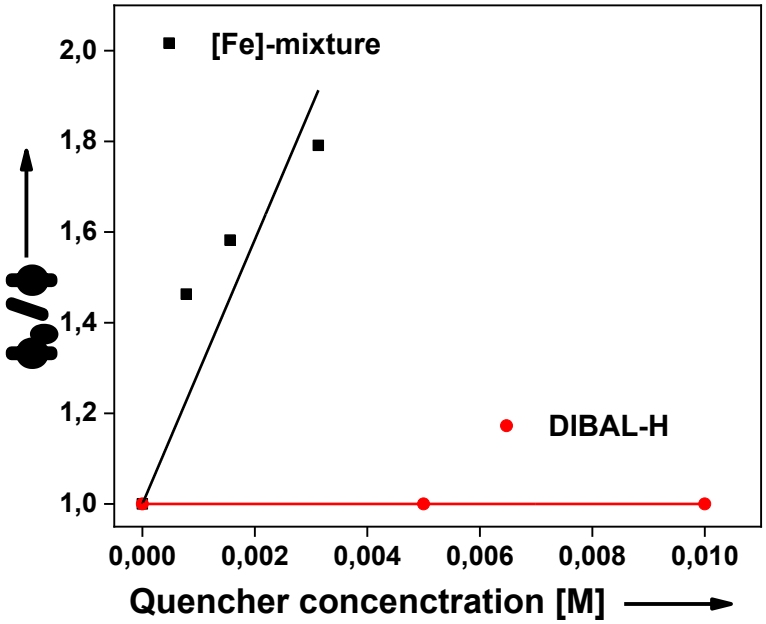

Figure 5-17. Stern-Volmer plots to obtain k_q(S1) for the DPA* quenching with a mixture consisting of $FeCl_2$ (1.0 eq.), DIBAL-H (2.0 eq.) and phenylacetylene (40 eq.) and DIBAL-H itself.

Equations for the Stern-Volmer analysis:

$\tau_0/\tau = 1 + K_{SV} \cdot [Quencher]$ eq 5.1

$K_{SV} = \tau_F \cdot k_q(S1)$ eq 5.2

For DIPEA quenching:

$K_{SV} = 53.17\ M^{-1}$

$\tau_F = 6.01$ ns (measured lifetime)

$\boldsymbol{k_q(S1) = 8.8 \times 10^9\ M^{-1}s^{-1}}$

For DIPEA quenching in presence of phenylacetylene:

$K_{SV} = 49.5\ M^{-1}$

$\tau_F = 6.01$ ns (measured lifetime)

$\boldsymbol{k_q(S1) = 8.2 \times 10^9\ M^{-1}s^{-1}}$

For [Fe]-mixture quenching:

$K_{SV} = 291.6\ M^{-1}$

$\tau_F = 6.01$ ns (measured lifetime)

$\boldsymbol{k_q(S1) = 4.8 \times 10^{10}\ M^{-1}s^{-1}}$

The fluorescence quenching experiments clearly indicate:

- no quenching of the excited photocatalyst lifetime with phenylacetylene,
- quenching of the excited photocatalyst lifetime with increasing amounts of DIPEA, which is attributed to a single electron transfer from DIPEA to the excited photocatalyst
- no influence of phenylacetylene towards the quenching of the excited photocatalyst with DIPEA
- no quenching of the excited photocatalyst with $FeCl_2(MeCN)_{1.4}$
- no quenching of the excited photocatalyst with DIBAL-H
- quenching of the photocatalyst emission by a chemically reduced iron species, which we attribute to either another single electron or energy transfer from the excited photocatalyst to this species

5.4.7 Laser flash photolysis

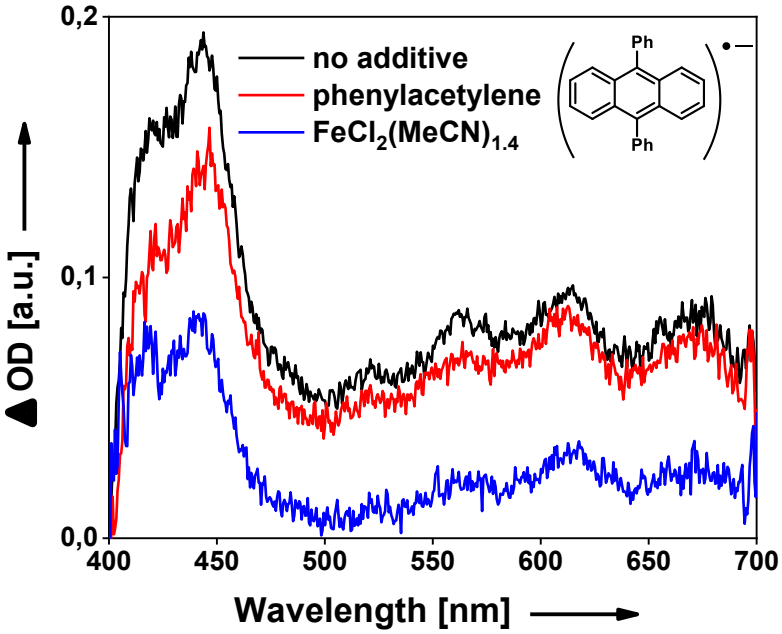

Figure 5-18. Transient absorption spectra (λ_{exc} = 355 nm, ~300 µJ/pulse) of 9,10-diphenylanthracene (0.1 mM) and DIPEA (20 mM) (●) with additional phenylacetylene (30 mM) (●) or with additional $FeCl_2(MeCN)_{1.4}$ (2.8 mM) (●) recorded at 1 µs after the laser pulse in dry acetonitrile under anaerobic conditions.

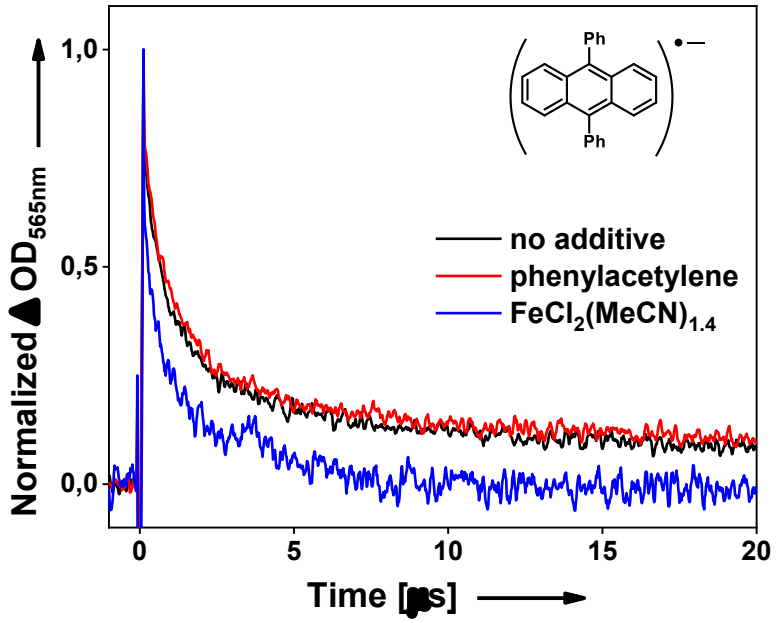

Figure 5-19. Temporal profile monitored at 565 nm after laser flash photolysis (λ_{exc} = 355 nm, ~300 µJ/pulse) for 9,10-diphenylanthracene (0.1 mM) and DIPEA (20 mM) (●) with additional phenylacetylene (30 mM) (●) or with additional $FeCl_2(MeCN)_{1.4}$ (2.8 mM) (●) in dry acetonitrile under anaerobic conditions.

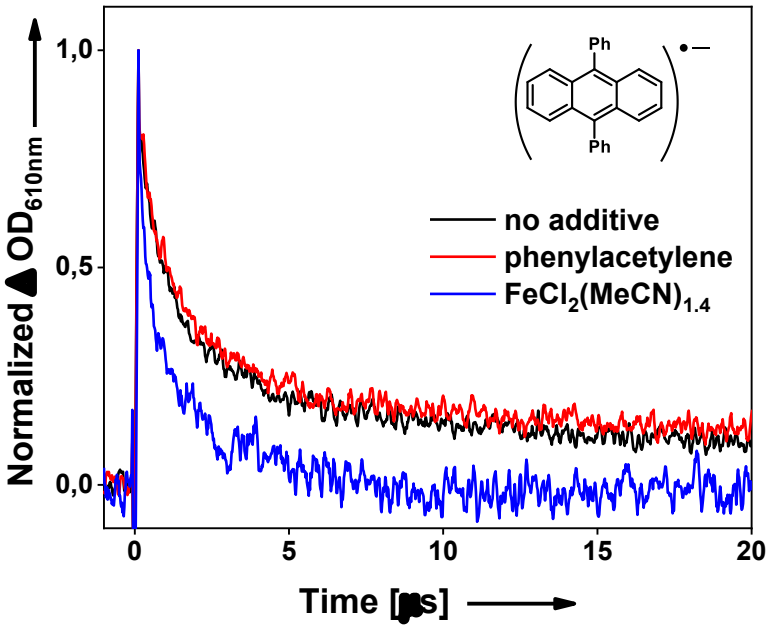

Figure 5-20. Temporal profile monitored at 610 nm after laser flash photolysis (λ_{exc} = 355 nm, ~300 µJ/pulse) for 9,10-diphenylanthracene (0.1 mM) and DIPEA (20 mM) (●) with additional phenylacetylene (30 mM) (●) or with additional $FeCl_2(MeCN)_{1.4}$ (2.8 mM) (●) in dry acetonitrile under anaerobic conditions.

5.4.8 Cyclic voltammetry

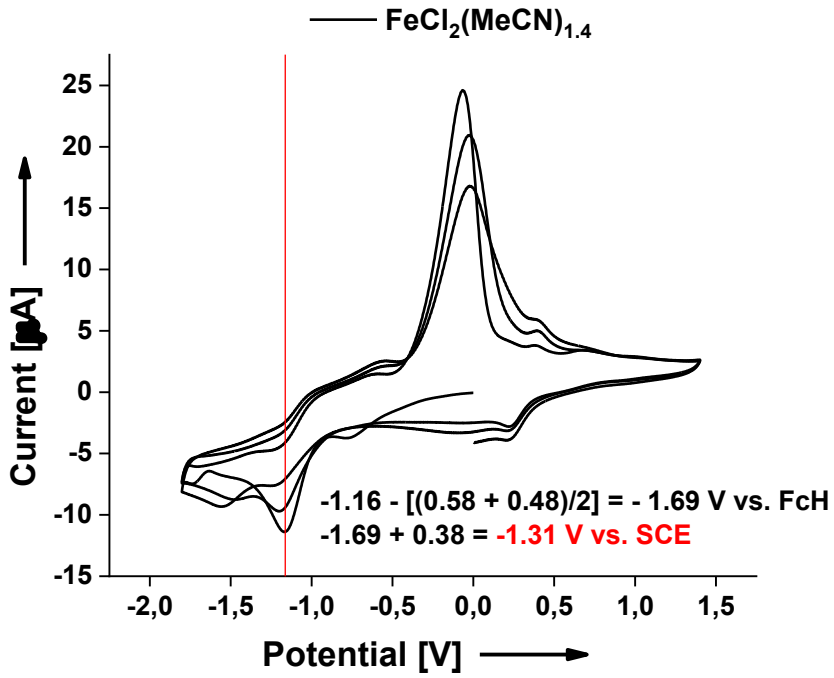

Figure 5-21. Cyclic voltammogram of a $FeCl_2(MeCN)_{1.4}$ (0.5 mM) solution including three cycles ranging from -1.8 V to +1.4 V with a scan rate of 100 mV s^{-1}.

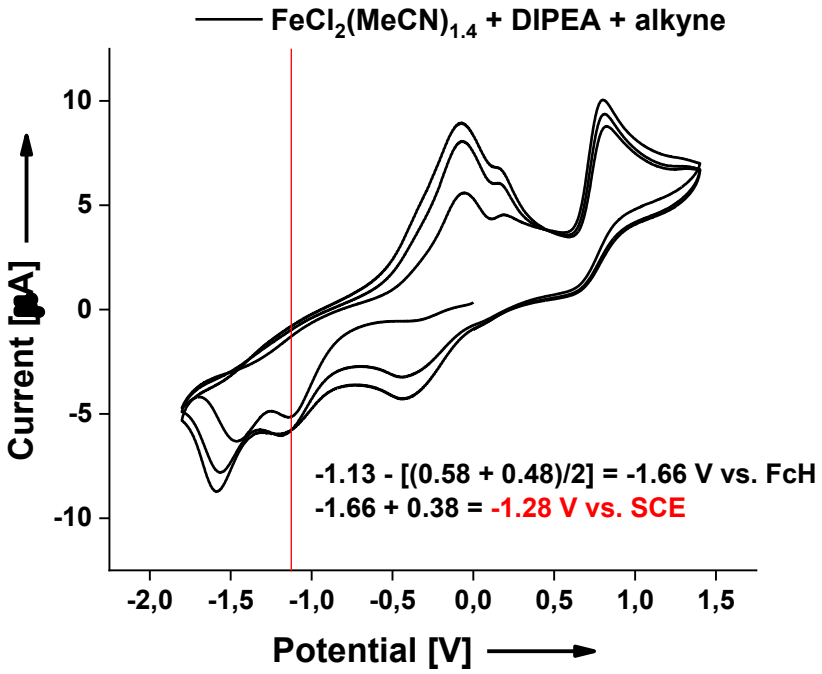

Figure 5-22. Cyclic voltammogram of a solution of $FeCl_2(MeCN)_{1.4}$ (0.5 mM), DIPEA (1 mM) and phenylacetylene (10 mM) including three cycles ranging from -1.8 V to +1.4 V with a scan rate of 100 mV s^{-1}.

5.4.9 UV/VIS absorption spectroscopy

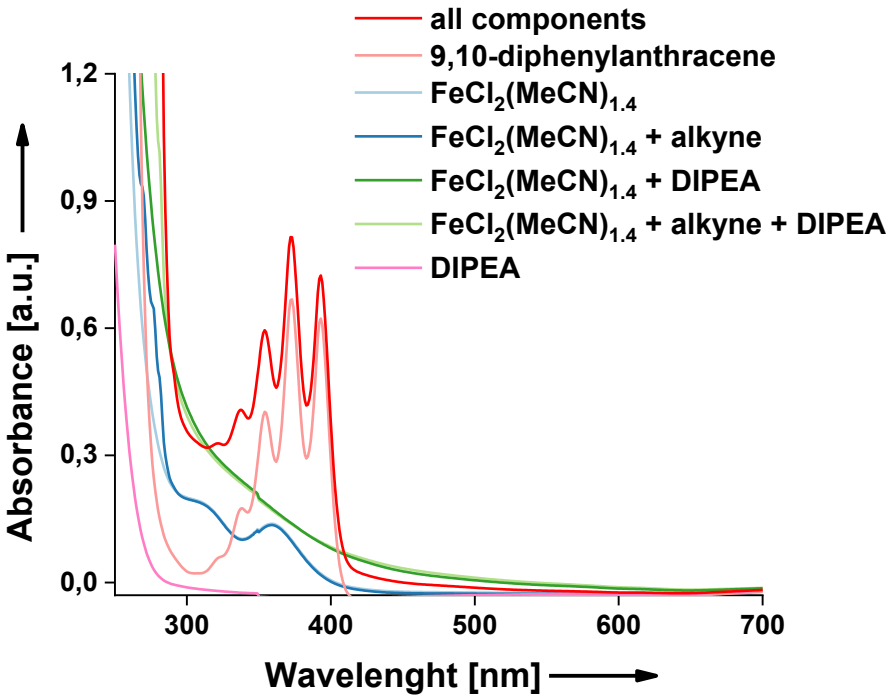

Figure 5-23. UV/VIS absorption spectra of mixture of several components of the standard reaction without irradiation. Measured compononents: 9,10-diphenylanthracene (4.0×10^{-5} M), $FeCl_2(MeCN)_{1.4}$ (2.5×10^{-4} M), DIPEA (5.0×10^{-4} M), phenylacetylene (1.0×10^{-2} M). The stoichiometry of the optimized conditions was conserved during the UV/VIS measurements.

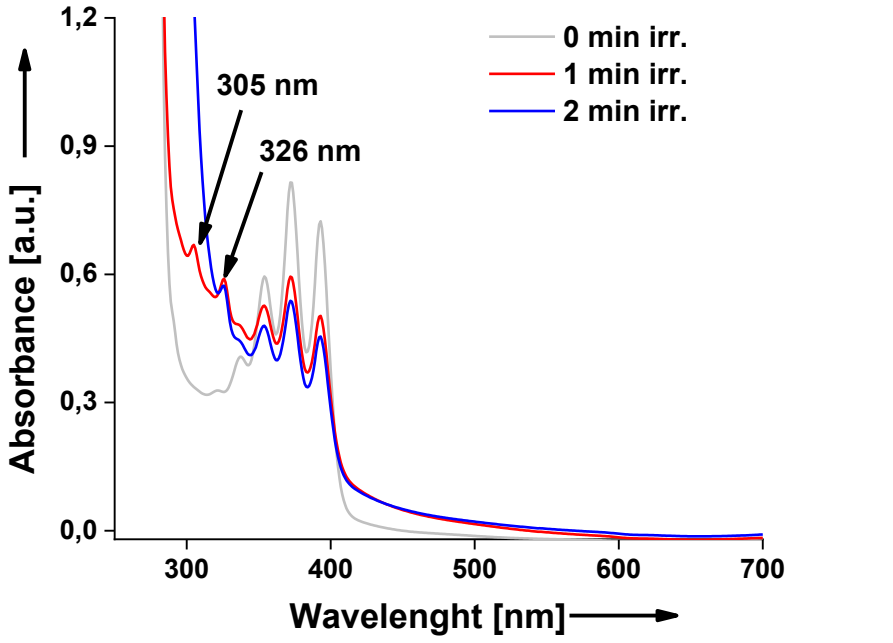

Figure 5-24. UV/VIS absorption spectra of the reaction mixture before and after irradiation.

5.4.10 Infrared spectroscopy

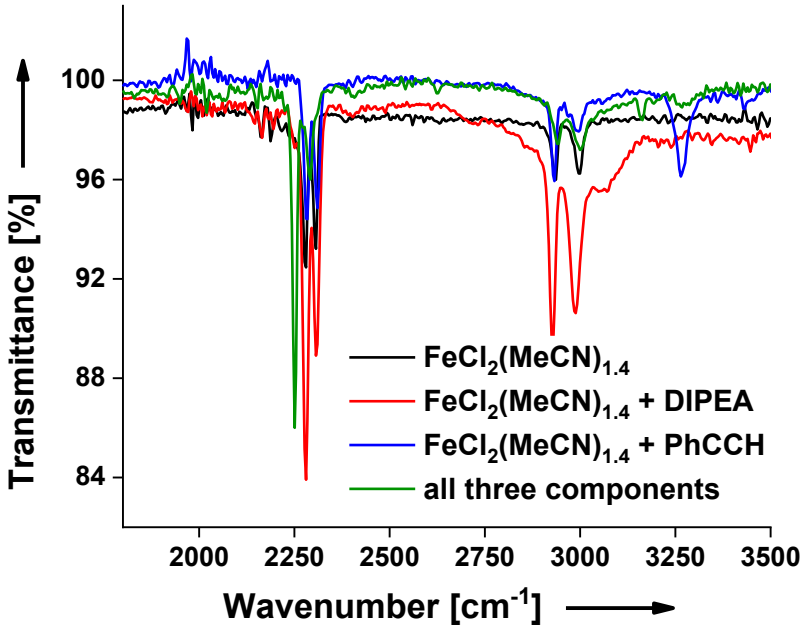

Figure 5-25. IR spectrum of a solution of $FeCl_2(MeCN)_{1.4}$ (25 mM) (●), additional DIPEA (50 mM) (●), additional phenylacetylene (50 mM) (●), all three components (●).

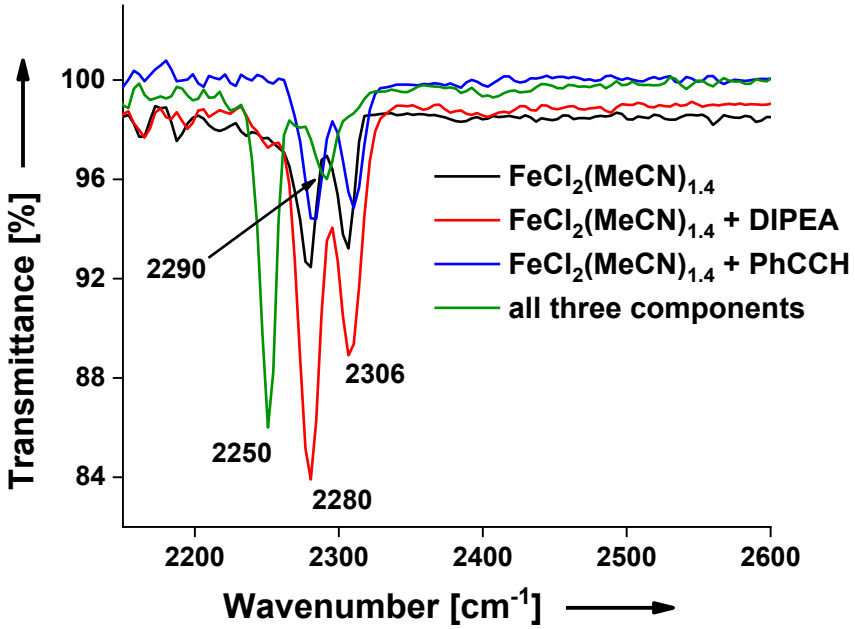

Figure 5-26. Extract of the IR analysis in the area of 2200 to 2500 cm^{-1}.

5.4.11 NMR studies towards the reaction mechanism

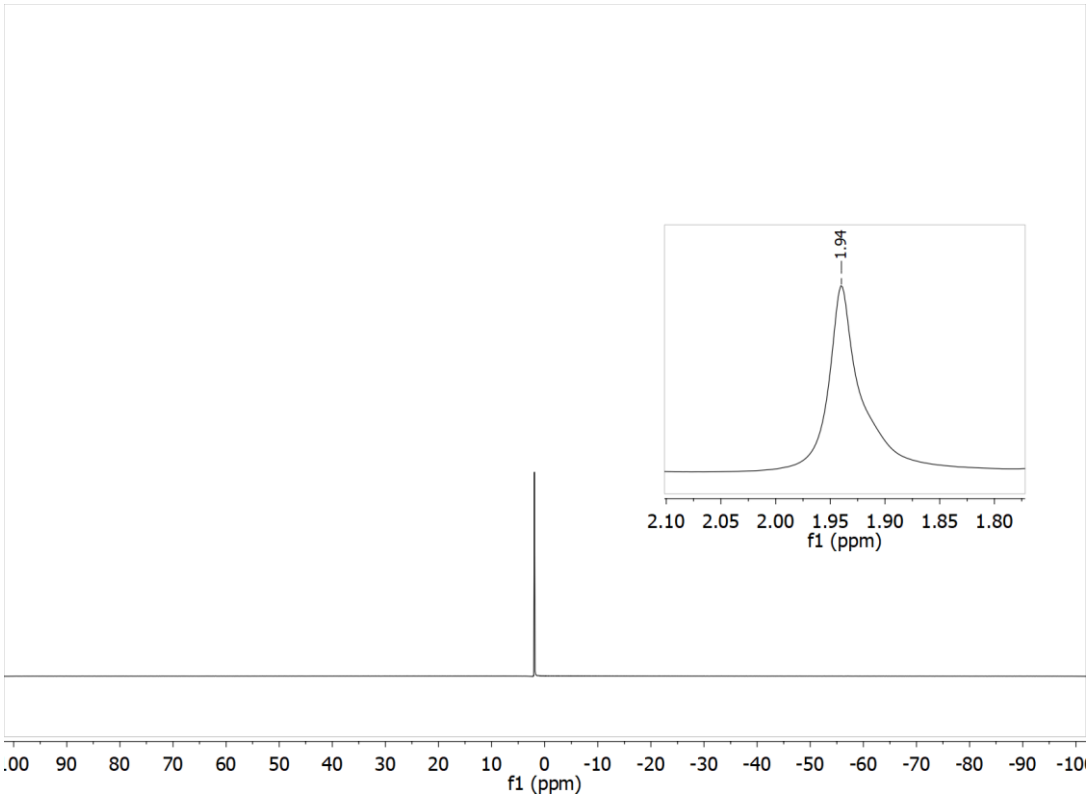

Figure 5-27. ^{1}H NMR of $FeCl_2(MeCN)_{1.4}$ (25.0 µmol) in dry CD_3CN.

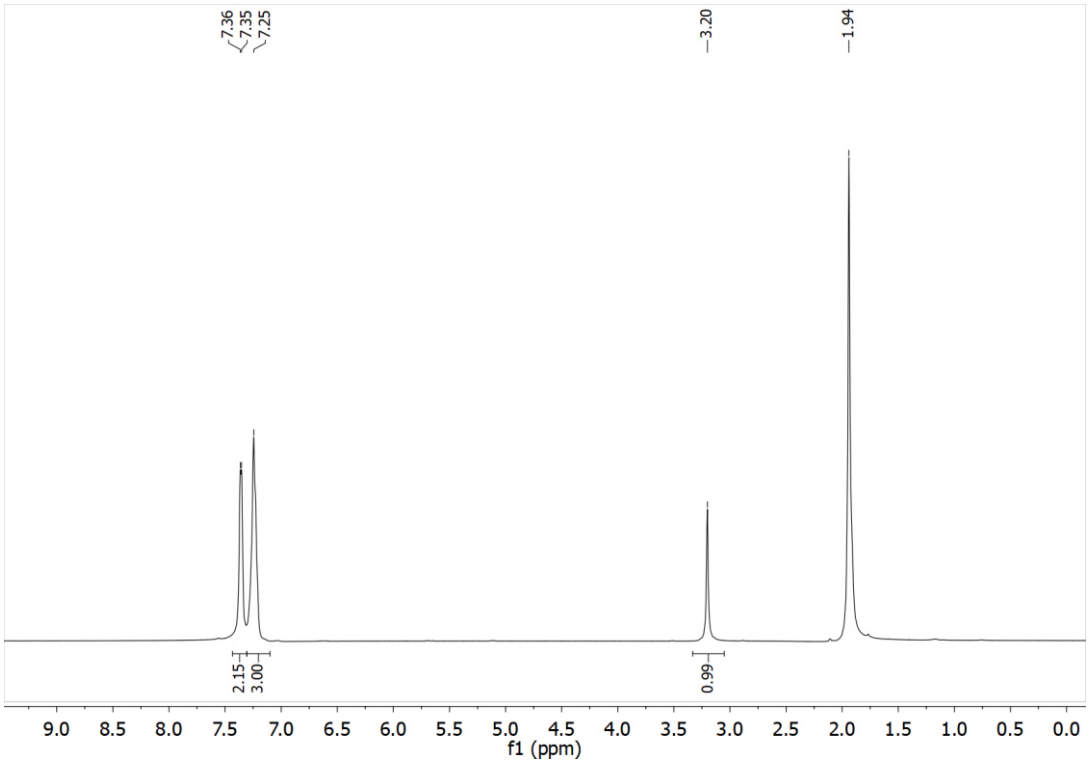

Figure 5-28. ^{1}H NMR of $FeCl_2(MeCN)_{1.4}$ (25.0 µmol) and phenylacetylene (50.0 µmol) in dry CD_3CN.

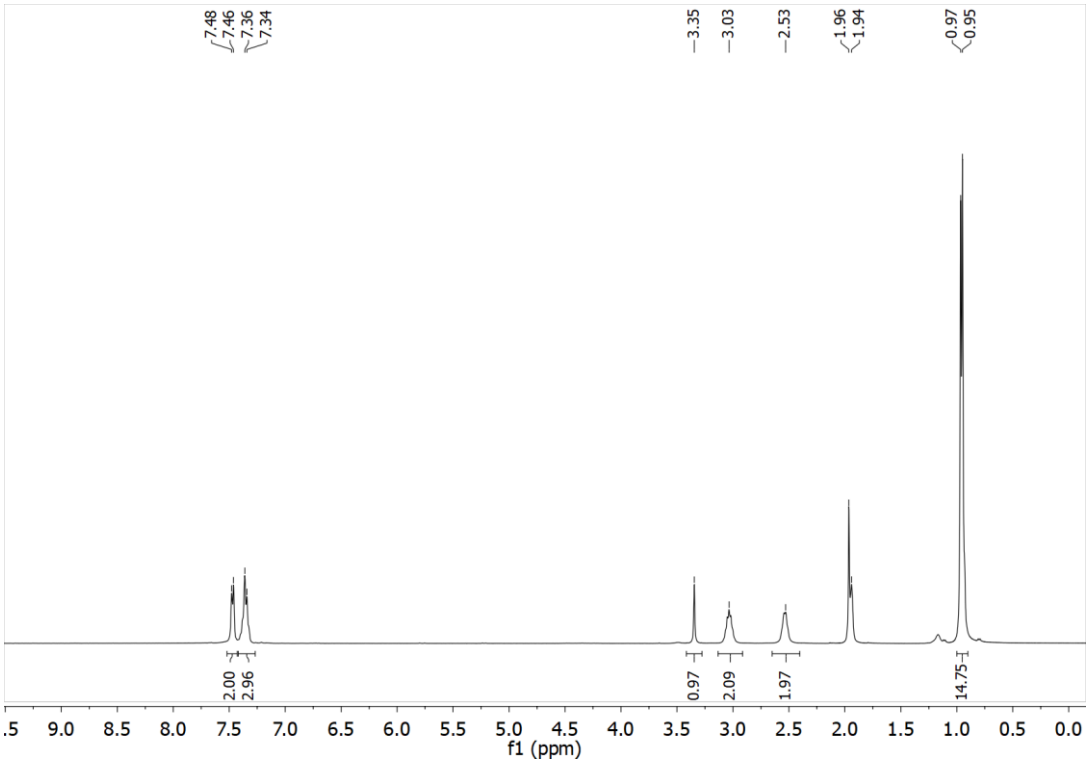

Figure 5-29. ^{1}H NMR of $FeCl_2(MeCN)_{1.4}$ (25.0 µmol), phenylacetylene (50.0 µmol) and Hünig's base (50.0 µmol) in dry CD_3CN.

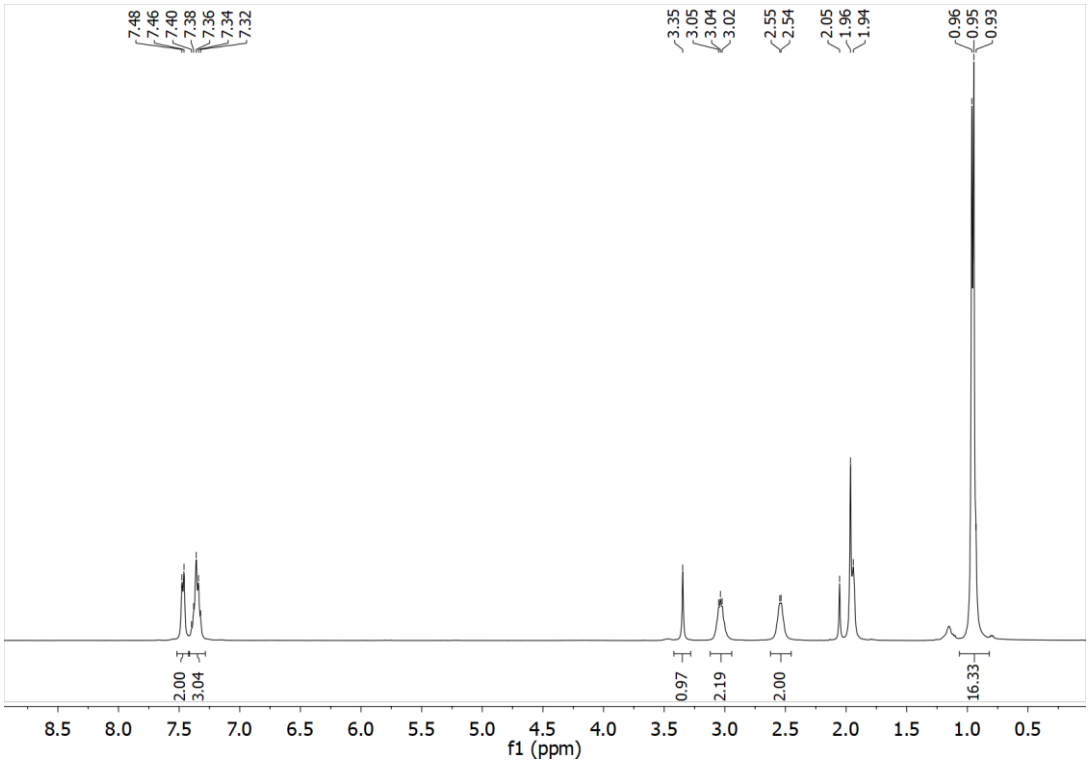

Figure 5-30. ^{1}H NMR of $FeCl_2(MeCN)_{1.4}$ (25.0 µmol), phenylacetylene (50.0 µmol) and Hünig's base (50.0 µmol) in CD_3CN after 30 min of irradiation at 395-410 nm.

5.4.12 Investigations towards reaction orders

General procedure for the experimental setup in this investigations:

$FeCl_2$ (0.025 mmol, 0.025 equiv.) and 9,10-diphenylanthracene (0.004 mmol, 0.004 equiv.) were dissolved in acetonitrile (2.0 mL). Hünig's base (0.050 mmol, 0.050 equiv.), phenylacetylene (1.0 mmol, 1.0 equiv.) and mesitylene (50 µl) were added consecutively. The reaction mixture was irradiated at 22 °C with a 395-410 nm LED for 1 min. After switching off the light, the reaction was immediately quenched by addition of aqueous hydrochloric acid (3 mL, 1 M) and extracted with ethyl acetate (3 mL). The organic phase was filtered through a small plug of silica in a pasteur pipette with additional ethyl acetate to remove inorganic impurities. The filtrate was analyzed by GC-FID measurement.

Table 5-6. Determination of reaction orders – varying amount of DIPEA.

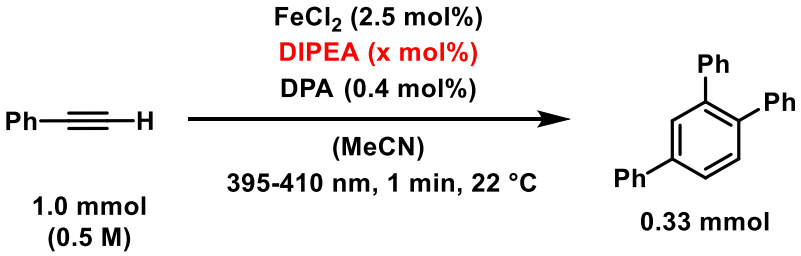

Amount of DIPEA	c (DIPEA) [mol/l]	log c	v[(a)] [mmol/s]	log v
5.0 mol%	0,025	-1,602	0,00433	-2,364
10 mol%	0,05	-1,301	0,00483	-2,316
20 mol%	0,1	-1	0,00483	-2,316
100 mol%	0,5	-0,3010	0,003	-2,523
400 mol%	2	0,3010	0,002	-2,690

[(a)] Determined by GC-FID analysis with mesitylene as internal standard. The reaction velocity v was determined at small conversions as the consumption of phenylacetylene per time period in mmol per second.

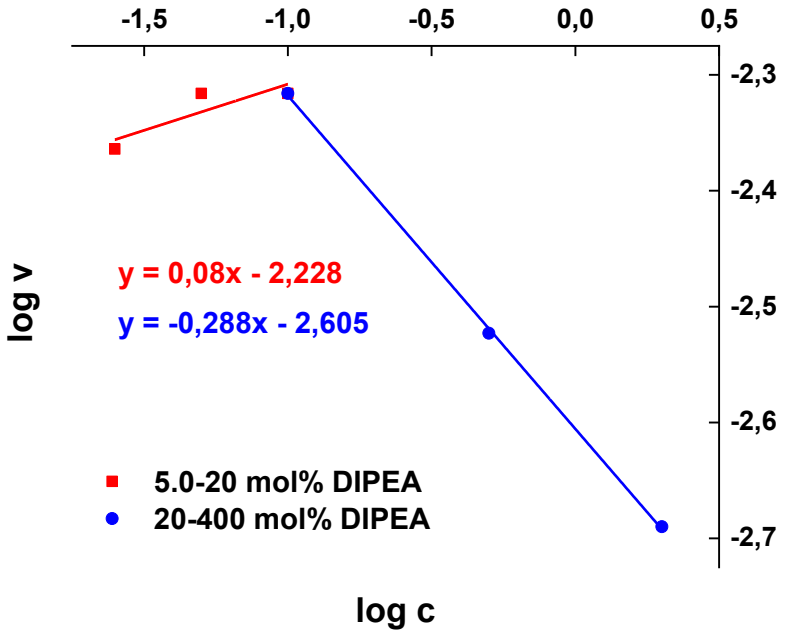

Figure 5-31. Determination of reaction orders under varying amounts of DIPEA.

For very high excess of DIPEA, DPA* concentration should be low as it is quenched by DIPEA (see fluorescence quenchings) whereas c ($DPA^{\bullet -}$) should be high.

⇒ reaction order at 20-400 mol% DIPEA becomes negative

Table 5-7. Determination of reaction orders – varying amount of photocatalyst.

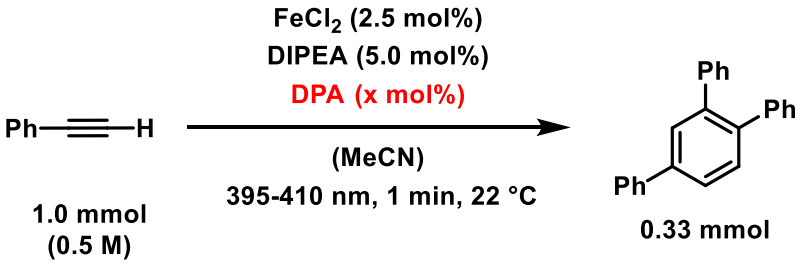

Amount of DPA	c (DPA) [mol/l]	log c	v[(a)] [mmol/s]	log v
0,002 mol%	0.00001	-5	0	-
0,01 mol%	0.00005	-4,301	0,0025	-2,602
0,02 mol%	0,0001	-4	0,0027	-2,569
0,04 mol%	0,0002	-3,7	0,003	-2,523
0,4 mol%	0,002	-2,7	0,003	-2,523

[(a)] Determined by GC-FID analysis with mesitylene as internal standard. The reaction velocity v was determined at small conversions as the consumption of phenylacetylene per time period in mmol per second.

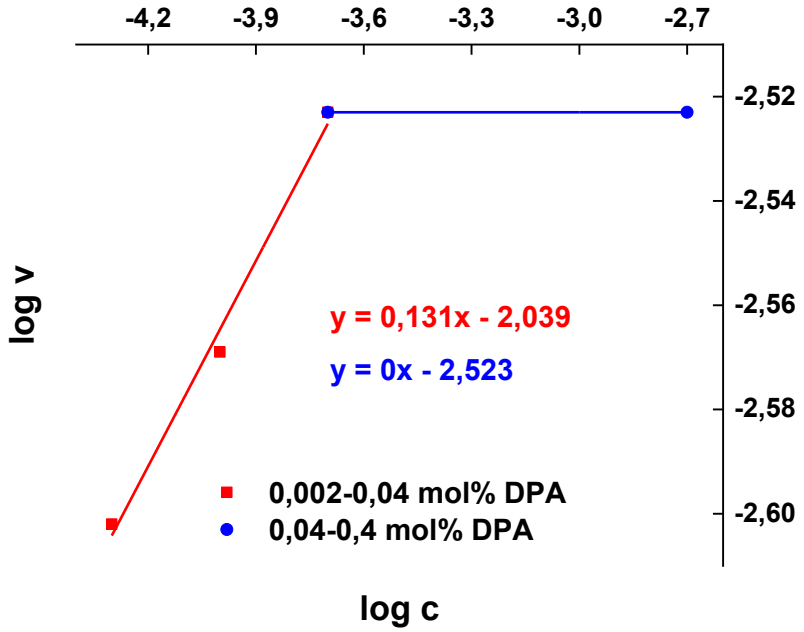

Figure 5-32. Determination of reaction orders under varying amounts of DPA.

At concentrations higher than 0.2 mM the solubility of DPA in MeCN reaches its maximum. ⇒ reaction order at c (DPA) > 0.04-0.4 mol% is automatically 0

Table 5-8. Determination of reaction orders – varying amount of $FeCl_2$.

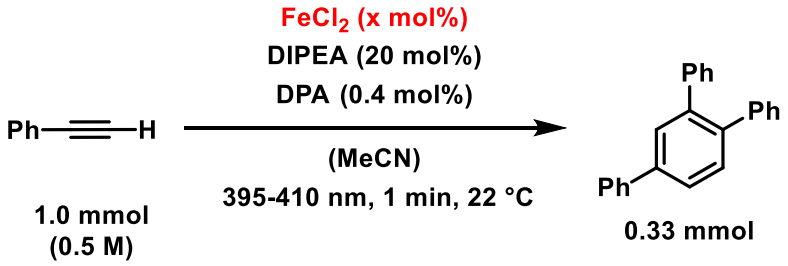

Amount of $FeCl_2$	c ($FeCl_2$) [mol/l]	log c	v[(a)] [mmol/s]	log v
1.5 mol%	0,0075	-2,125	0,00117	-2,932
2.5 mol%	0,0125	-1,903	0,00583	-2,234
5.0 mol%	0,025	-1,602	0,00417	-2,38
7.5 mol%	0,0375	-1,426	0,00233	-2,633
10 mol%	0,05	-1,301	0,001	-3

[(a)] Determined by GC-FID analysis with mesitylene as internal standard. The reaction velocity v was determined at small conversions as the consumption of phenylacetylene per time period in mmol per second.

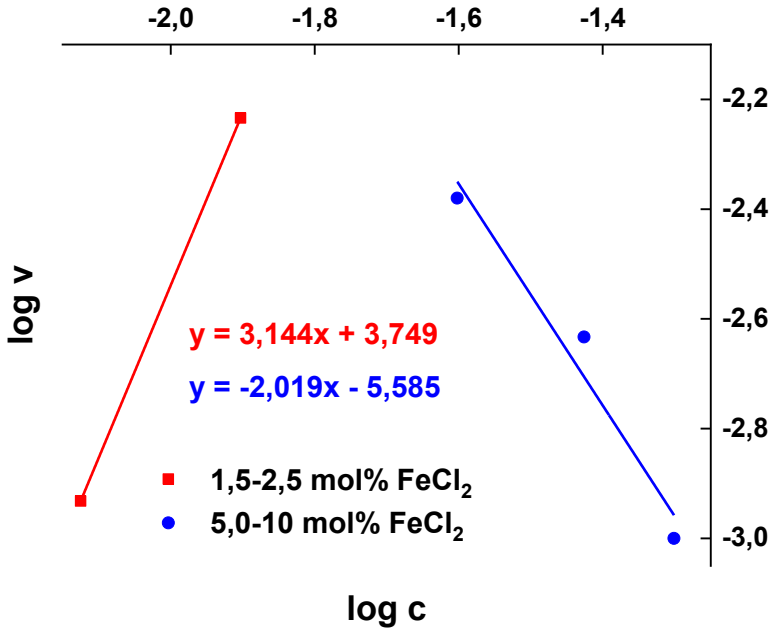

Figure 5-33. Determination of reaction orders under varying amounts of $FeCl_2$.

For high loadings of $FeCl_2$ the reaction mixture becomes very dark. Thus, we postulate an intrinsic reaction inhibition as no light could be absorbed by DPA anymore.

⇒ reaction order at 5.0-10 mol% $FeCl_2$ becomes negative

Table 5-9. Determination of reaction orders – varying amount of phenylacetylene.

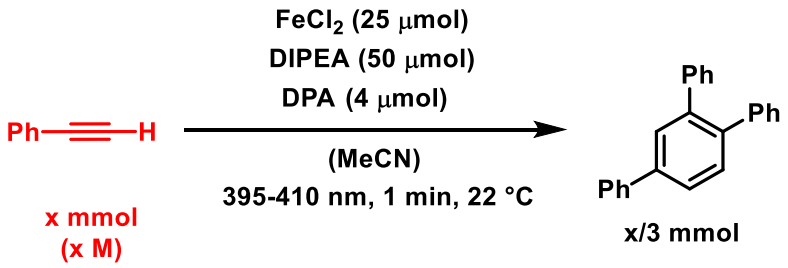

Amount of PhCCH	c (PhCCH) [mol/l]	log c	v[(a)] [mmol/s]	log v
0.25 mmol	0,125	-0,903	0,00242	-2,616
0.5 mmol	0,25	-0,602	0,00317	-2,499
1 mmol	0,5	-0,301	0,00467	-2,331
2 mmol	1	0	0,00267	-2,573
4 mmol	2	0,301	0	-

[(a)] Determined by GC-FID analysis with mesitylene as internal standard. The reaction velocity v was determined at small conversions as the consumption of phenylacetylene per time period in mmol per second.

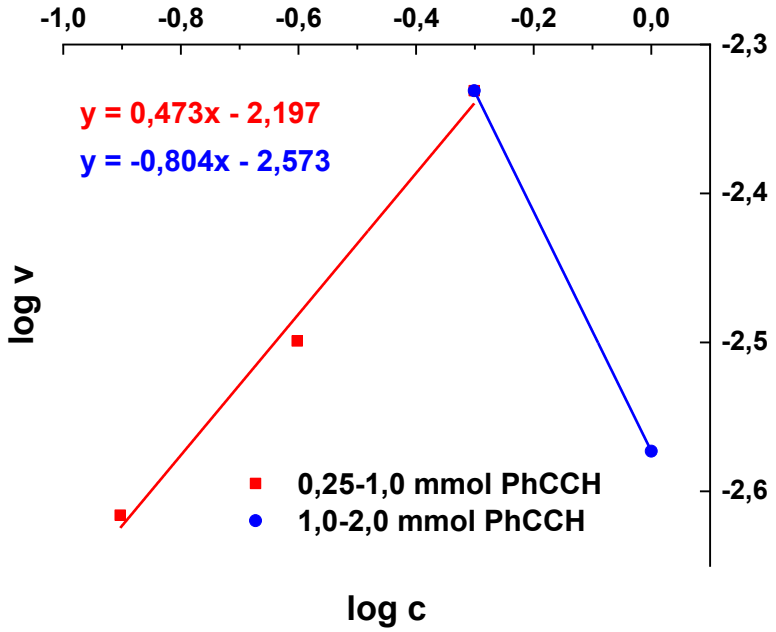

Figure 5-34. Determination of reaction orders under varying amounts of phenylacetylene.

For high amounts of Phenylacetylene, the relative catalyst loading gets to borderline of no reactivity at all (see last entry).

5.4.13 Further mechanistic investigations

In situ formation of active catalyst particles before addition of the substrate:

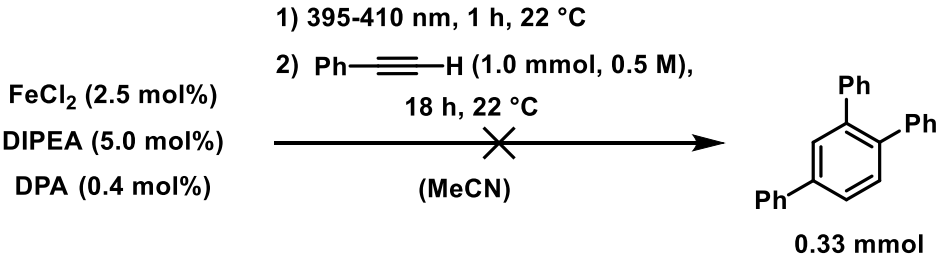

$FeCl_2$ (0.025 mmol, 0.025 equiv.) 9,10-diphenylanthracene (0.004 mmol, 0.004 equiv.) and Hünig's base (0.050 mmol, 0.050 equiv.) were dissolved in acetonitrile (2.0 mL). The reaction mixture was irradiated at 22 °C with a 395-410 nm LED for 1 hour. After switching off the light, the reaction mixture was transferred into the glovebox without quenching and phenylacetylene (1.00 mmol, 1.0 equiv.) was added. The mixture was then stirred in the glovebox without further irradiation overnight. After quenching with aqueous hydrochloric acid (3 mL, 1 M) and extraction with ethyl acetate (3 mL), the organic phase was filtered through a small plug of silica in a pasteur pipette with additional ethyl acetate to remove inorganic impurities. The filtrate was analyzed by GC-MS measurement. No trimerization product was observed (only phenylacetylene).

➔ **No formation of active catalyst in the absence of substrate and/or light**

➔ **Not happening:**

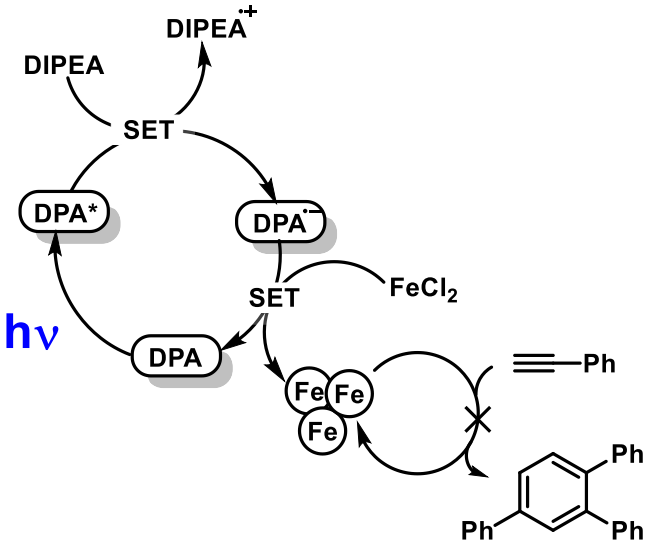

Scheme 5-2. Alternative mechanism.

Investigations on the effect of light on heterogeneous iron-catalyzed cyclotrimerizations:

$FeCl_2$ (0.013 mmol, 0.025 equiv.) and phenylacetylene (0.5 mmol, 1.0 equiv.) were dissolved in acetonitrile (2.0 mL) before DIBAL-H (0.025 mmol, 1 M in toluene, 0.05 equiv.) was added to the mixture. The reaction mixture was (not) irradiated at 22 °C with a 395-410 nm LED for 15 hours. After switching off the light, the reaction mixture was quenched with aqueous hydrochloric acid (3 mL, 1 M) and extracted with ethyl acetate (3 mL). The organic phase was filtered through a small plug of silica in a pasteur pipette with additional ethyl acetate to remove inorganic impurities. The filtrate was analyzed by GC-FID measurements.

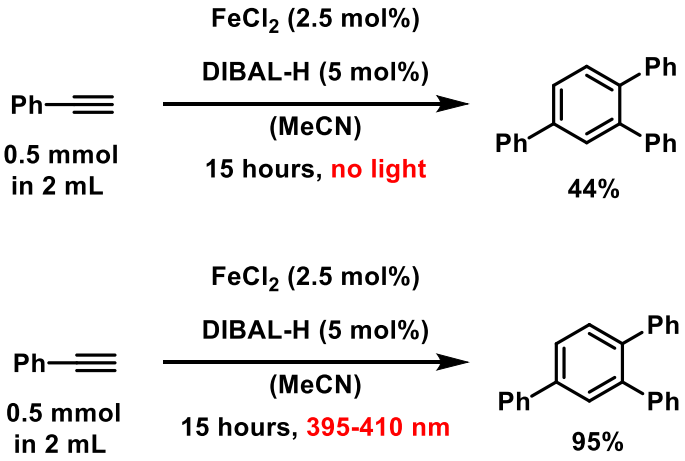

Scheme 5-3. The influence of light in iron-catalyzed cyclotrimerizations. Yields are determined by GC-FID analysis with mesitylene as external standard.

Small Hammett study for determining a charge transfer complex intermediate:

$FeCl_2$ (0.025 mmol, 0.025 equiv.) and 9,10-diphenylanthracene (0.004 mmol, 0.004 equiv.) were dissolved in acetonitrile (2.0 mL). Hünig's base (0.050 mmol, 0.050 equiv.) and alkyne (1.0 mmol, 1.0 equiv.) were added consecutively. The reaction mixture was irradiated at 22 °C with a 395-410 nm LED for 2 min. After switching off the light and addition of mesitylene (50 µl), the reaction was immediately quenched by addition of aqueous hydrochloric acid (3 mL, 1 M) and extracted with ethyl acetate (3 mL). The organic phase was filtered through a small plug of silica in a pasteur pipette with additional ethyl acetate to remove inorganic impurities. The filtrate was analyzed by GC-FID measurement.

Table 5-10. Hammet study.

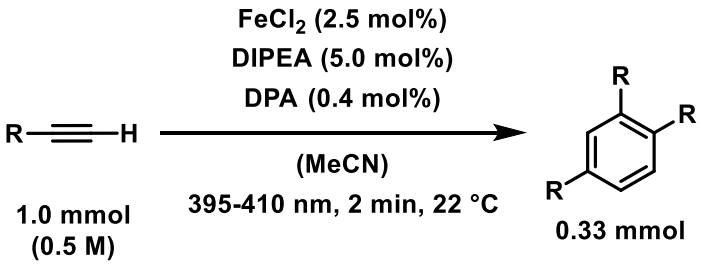

Entry	R =	Hammet constant σ	Conversion[a] [%]	Yield[a] [%]
1	4-F-C_6H_5	0.06	23	23
2	3-F-C_6H_5	0.34	36	36
3	4-Me-C_6H_5	-0.17	26	25
4	3-Me-C_6H_5	-0.07	37	36
5	4-OMe-C_6H_5	-0.27	19	19
6	3-OMe-C_6H_5	0.12	29	29

[a] Determined by GC-FID analysis with mesitylene as external standard. Yields are given as combined yields of 1,2,4- and 1,3,5-regioisomers. Reaction setup according to general method A.

5.4.14 Details on the substrate scope

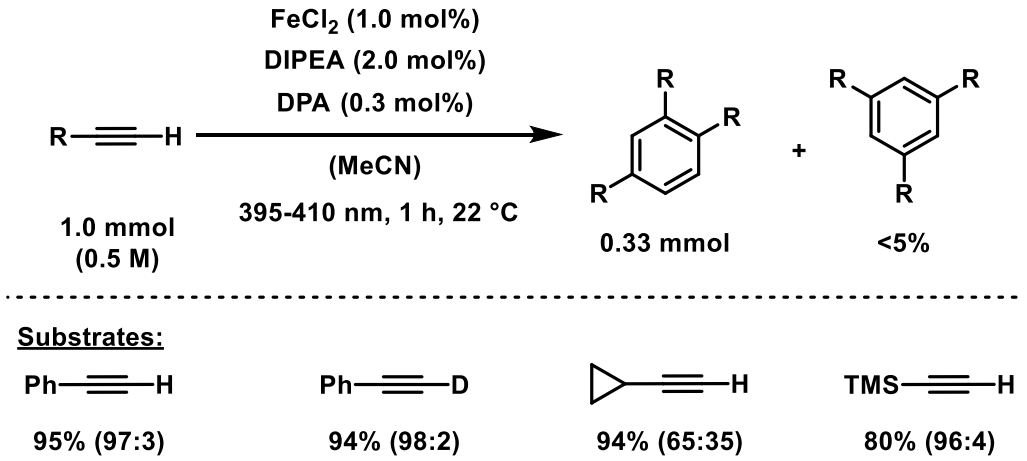

Figure 5-35. Substrate scope with 1.0 mol% $FeCl_2$; yields are given as isolated yields.

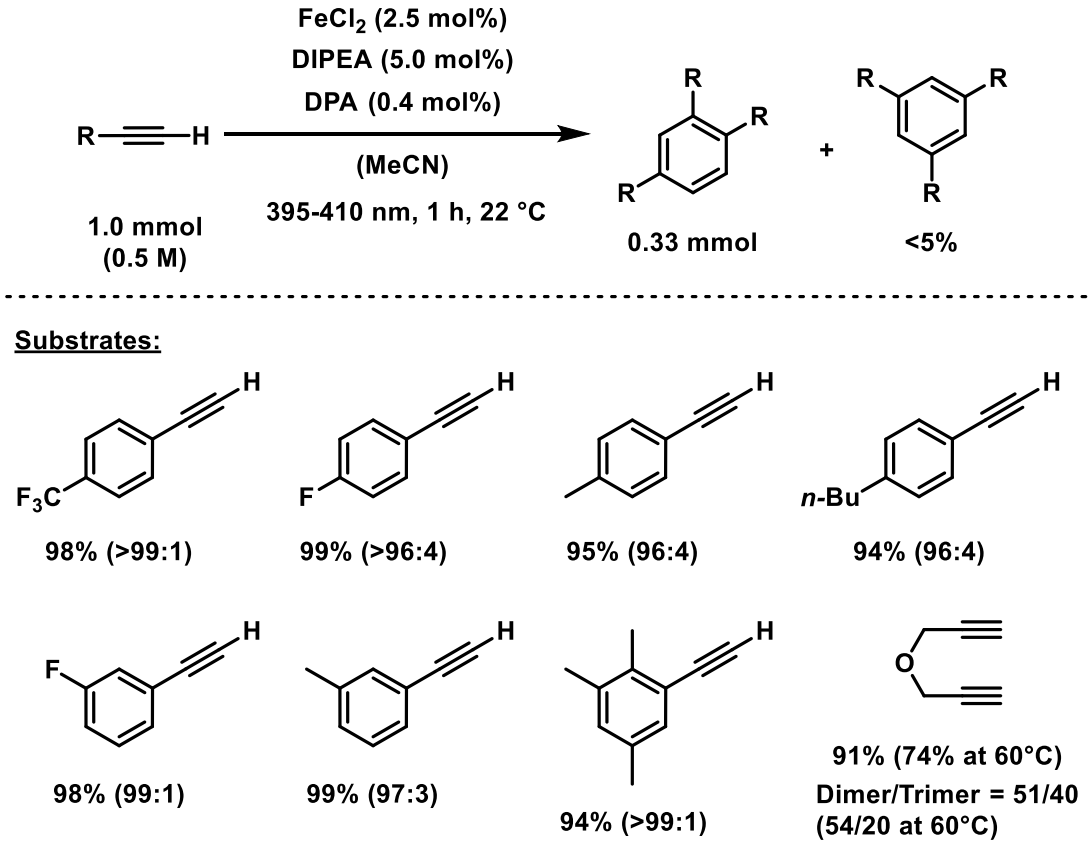

Figure 5-36. Substrate scope with 2.5 mol% $FeCl_2$; yields are given as isolated yields.

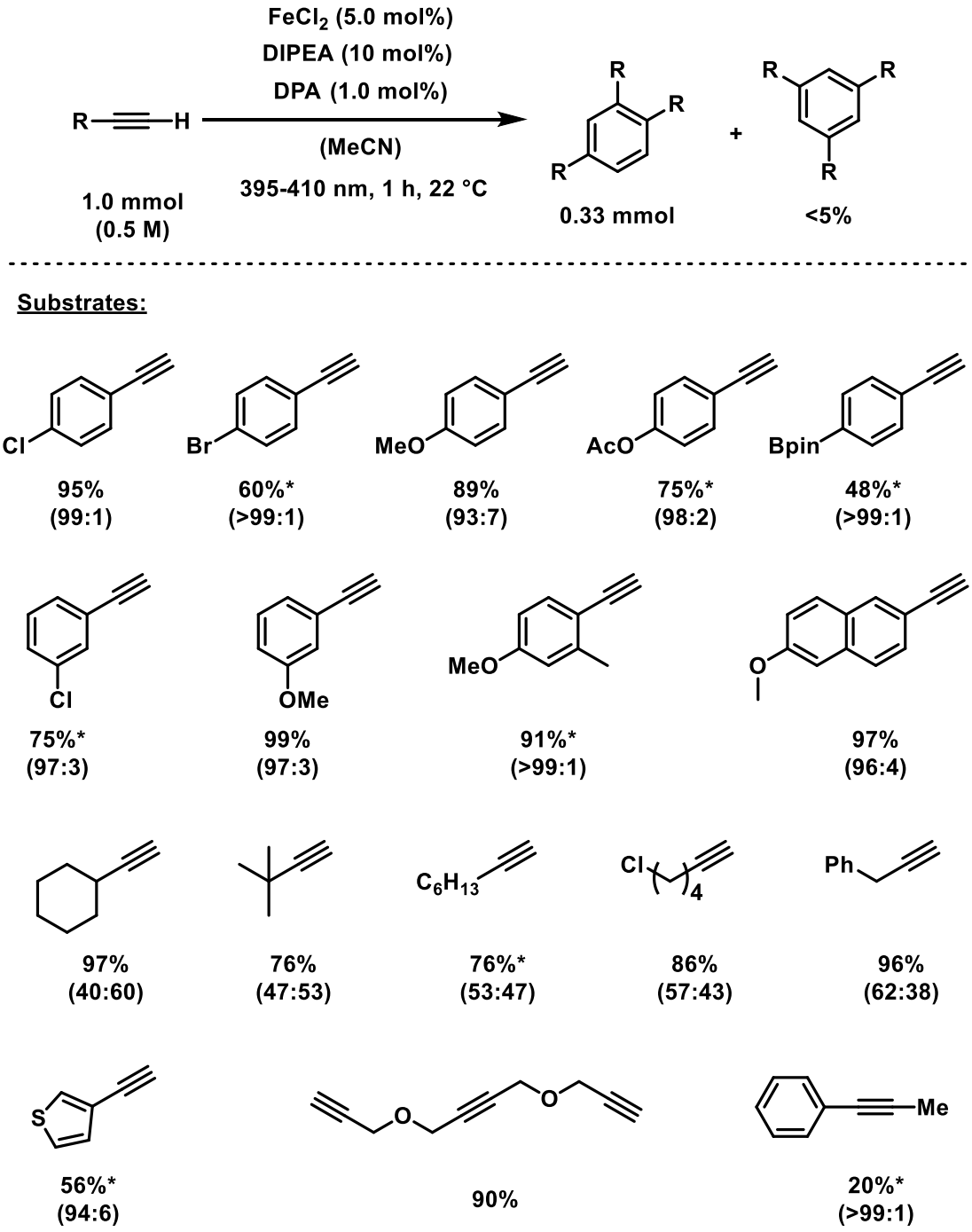

Figure 5-37. Substrate scope with 5.0 mol% $FeCl_2$; yields are given as isolated yields unless otherwise noted; star indicates incomplete conversion of the substrate.

5.4.15 Analytical data of compounds

1,2,4-Triphenylbenzene

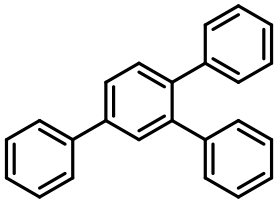

^{1}H NMR (300 MHz, $CDCl_3$): δ= 7.73-7.64 (m, 4H), 7.57-7.44 (m, 3H), 7.42-7.34 (m, 1H), 7.30-7.15 (m, 10H).

^{13}C NMR (101 MHz, $CDCl_3$): δ = 141.6, 141.3, 141.1, 140.7, 140.5, 139.7, 131.2, 130.1 (2C), 130.0 (2C), 129.6, 129.0 (2C), 128.1 (2C), 128.0 (2C), 127.6, 127.3 (2C), 126.7, 126.7, 126.3.

GC-MS (EI): *m/z* (relative intensity) = 306 (100), 289 (26), 228 (20).

Amount of the 1,3,5-regioisomer (characteristic NMR signal at δ= 7.81 ppm) according to ^{1}H NMR: (0.09/3)/[(4.00/4)+(0.09/3)] = 3%

The analytical data were in agreement with D. Brenna, M. Villa, T. N. Gieshoff, F. Fischer, M. Hapke, A. Jacobi von Wangelin, *Angew. Chem. Int. Ed.* **2017**, *56*, 8451-8454.

1,2,4-Triphenyl-3,5,6-trideuterobenzene

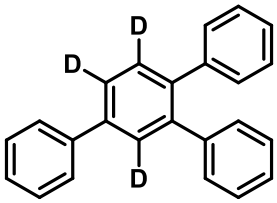

^{1}H NMR (300 MHz, $CDCl_3$): δ = 7.73-7.64 (m, 2H), 7.53-7.43 (m, 2H), 7.42-7.34 (m, 1H), 7.30-7.15 (m, 10H).

^{13}C NMR (75 MHz, $CDCl_3$): δ = 141.6, 141.2, 141.0, 140.7, 140.3, 139.6, 130.0 (2C), 130.0 (2C), 129.0 (2C), 128.1 (2C), 128.0 (2C), 127.6, 127.3 (2C), 126.7, 126.7. The signals for deuterium bearing carbon atoms were not detected.

GC-MS (EI): *m/z* (relative intensity) = 309 (100), 292 (17), 231 (10).

Amount of the 1,3,5-regioisomer according to GC-FID analysis: 16/856 = 2%

The analytical data were in agreement with G. Kalikhman, *Bull. Acad. Sciences of the USSR*, *Div. Chem. Sci. (Engl. Transl.)* **1969**, 1714.

1,2,4-Tris(4-fluorophenyl)benzene

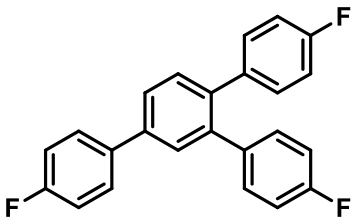

^{1}H NMR (300 MHz, $CDCl_3$): δ = 7.67-7.56 (m, 4H), 7.49-7.45 (m, 1H), 7.21-7.08 (m, 6H), 7.01-6.90 (m, 4H).

^{13}C NMR (75 MHz, $CDCl_3$): δ = 162.8 (d, *J* = 246.4 Hz, C-F), 162.0 (d, *J* = 246.4 Hz, C-F), 162.0 (d, *J* = 246.4 Hz, C-F), 140.2, 139.8, 138.7, 137.3 (d, *J* = 3.4 Hz), 136.9 (d, *J* = 3.4 Hz), 136.6 (d, *J* = 3.4 Hz), 131.5 (d, *J* = 8.1 Hz, 2C), 131.5 (d, *J* = 8.1 Hz, 2C), 131.2, 129.3, 128.8 (d, *J* = 8.1 Hz, 2C), 126.3, 115.9 (d, *J* = 21.4 Hz, 2C), 115.2 (d, *J* = 21.4 Hz, 2C), 115.2 (d, *J* = 21.4 Hz, 2C).

^{19}F NMR (565 MHz, $CDCl_3$): δ = −115.16 (m, 1F), −115.63 (m, 1F), −115.75 (m, 1F).

GC-MS (EI): *m/z* (relative intensity) = 360 (100), 338 (18), 262 (14).

Amount of the 1,3,5-regioisomer (characteristic NMR signal at δ = 7.68 ppm) according to ^{1}H NMR: (0.13/3)/[(4.00/4)+(0.13/3)] = 4%

The analytical data were in agreement with Z. Zhu, J. Wang, Z. Zhang, X. Xiang, X. Zhou, *Organometallics* **2007***, 26,* 2499–2500.

1,2,4-Tris(3-fluorophenyl)benzene

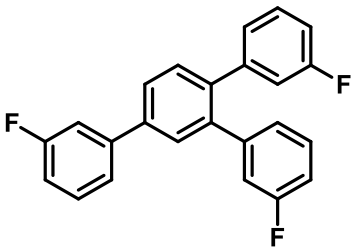

^{1}H NMR (300 MHz, $CDCl_3$): δ = 7.69-7.60 (m, 2H), 7.54-7.32 (m, 4H), 7.26-7.16 (m, 2H), 7.13-7.03 (m, 1H), 7.01-6.86 (m, 6H).

^{13}C NMR (75 MHz, $CDCl_3$): δ = 163.4 (d, *J* = 246.0 Hz, C-F), 162.6 (d, *J* = 245.8 Hz, 2C-F), 143.2 (d, *J* = 7.7 Hz), 142.9 (d, *J* = 7.8 Hz), 142.6 (d, *J* = 7.7 Hz), 140.0 (d, *J* = 2.0 Hz), 139.8 (d, *J* = 2.2 Hz), 139.0 (d, *J* = 2.0 Hz), 131.3, 130.5 (d, *J* = 8.4 Hz), 129.7 (d, *J* = 8.4 Hz), 129.7 (d, *J* = 8.4 Hz), 129.4, 126.7, 125.7 (d, *J* = 2.7 Hz), 125.7 (d, *J* = 2.7 Hz), 122.9 (d, *J* = 2.8 Hz), 116.8 (d, *J* = 21.9 Hz), 116.7 (d, *J* = 21.9 Hz), 114.6 (d, *J* = 21.2 Hz), 114.1 (d, *J* = 22.1 Hz), 114.0 (d, *J* = 21.0 Hz), 114.0 (d, *J* = 21.0 Hz).

^{19}F NMR (565 MHz, $CDCl_3$): δ = −112.72 (m), −113.26 (m), −113.34 (m).

HRMS (EI): *m/z* = calcd. for $(C_{24}H_{15}F_3)^{\bullet+}$: 360.1120, found: 360.1120

Amount of the 1,3,5-regioisomer (characteristic NMR signal at δ = 7.76 ppm) according to ^{1}H NMR: (0.04/3)/[(6.00/6)+(0.04/3)] = 1%

1,2,4-Tris(4-chlorophenyl)benzene

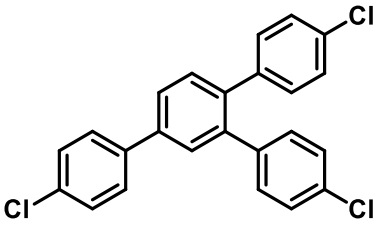

^{1}H NMR (300 MHz, $CDCl_3$): δ = 7.67-7.57 (m, 4H), 7.52-7.41 (m, 3H), 7.30-7.22 (m, 4H), 7.17-7.07 (m, 4H).

^{13}C NMR (75 MHz, $CDCl_3$): δ = 140.0, 139.8, 139.6, 139.2, 138.8, 138.7, 134.0, 133.2, 133.1, 131.3, 131.2 (2C), 131.2 (2C), 129.2, 129.2 (2C), 128.5 (2C), 128.5 (2C), 128.5 (2C), 126.5.

GC-MS (EI): *m/z* (relative intensity) = 410 (98), 408 (100), 338 (77), 302 (59), 150 (91).

Amount of the 1,3,5-regioisomer (characteristic NMR signal at δ = 7.71 ppm) according to ^{1}H NMR: (0.04/3)/[(4.00/4)+(0.04/3)] = 1%

The analytical data were in agreement with X. Bu, Z. Zhang, X. Zhou, *Organometallics* **2010**, *29*, 3530-3534.

1,2,4-Tris(3-chlorophenyl)benzene

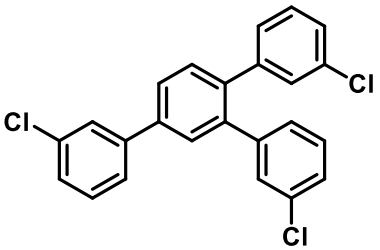

^{1}H NMR (300 MHz, $CDCl_3$): δ = 7.59-7.48 (m, 3H), 7.47-7.35 (m, 2H), 7.35-7.20 (m, 2H), 7.19-7.10 (m, 4H), 7.10-7.01 (m, 2H) 6.93-6.84 (m, 2H).

^{13}C NMR (75 MHz, $CDCl_3$): δ = 142.7, 142.4, 142.1, 139.9, 139.7, 138.8, 135.0, 134.2, 134.2, 131.3, 130.3, 129.8, 129.7, 129.4, 129.4, 129.3, 128.3, 128.3, 127.8, 127.4, 127.3, 127.2, 126.8, 125.4.

HRMS (EI): *m/z* = calcd. for $(C_{24}H_{15}Cl_3)^{\bullet+}$: 408.0234, found: 408.0231.

Amount of the 1,3,5-regioisomer (characteristic NMR signal at δ = 7.63 ppm) according to ^{1}H NMR: (0.09/3)/[(2.00/2)+(0.09/3)] = 3%

Incomplete conversion according to GC-MS and crude NMR data analysis. The starting material could not be removed from the mixture. Yield was calculated according to NMR integration based on the weight of the isolated mixture.

1,2,4-Tris(4-bromophenyl)benzene

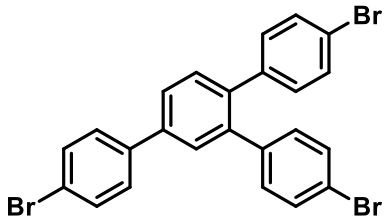

^{1}H NMR (300 MHz, $CDCl_3$): δ = 7.62-7.54 (m, 4H), 7.52-7.44 (m, 3H), 7.43-7.34 (m, 4H), 7.07-7.00 (m, 4H).

^{13}C NMR (75 MHz, $CDCl_3$): δ = 140.0, 140.0, 139.8, 139.7, 139.3, 138.7, 132.2 (2C), 131.6 (2C), 131.5 (2C), 131.5 (4C), 131.3, 129.2, 128.8 (2C), 126.5, 122.1, 121.4, 121.4.

Amount of the 1,3,5-regioisomer (characteristic NMR signal at δ = 7.65 ppm) according to ^{1}H NMR: no significant signal detected, therefore <1% assumed

Incomplete conversion according to GC-MS and crude NMR data analysis. The starting material could not be removed from the mixture. Yield was calculated according to NMR integration based on the weight of the isolated mixture.

The analytical data were in agreement with V. Cadierno, S. E. Garcia-Garrido, J. Gimeno, *J. Am. Chem. Soc.* **2006**, *128*, 15094-15095.

1,2,4-Tris(4-methoxyphenyl)benzene

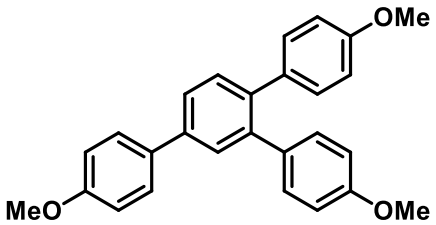

^{1}H NMR (300 MHz, $CDCl_3$): δ = 7.63-7.54 (m, 4H), 7.47-7.42 (m, 1H), 7.17-7.07 (m, 4H), 7.02-6.96 (m, 2H), 6.84-6.76 (m, 4H), 3.87 (s, 3H), 3.80 (2 s, 6H).

^{13}C NMR (75 MHz, $CDCl_3$): δ = 159.4, 158.5, 158.4, 140.5, 139.7, 138.6, 134.3, 133.9, 133.4, 131.1, 131.1 (2C), 131.0 (2C), 129.1, 128.2 (2C), 125.5, 114.4 (2C), 113.6 (2C), 113.6 (2C), 55.5, 55.3 (2C).

Amount of the 1,3,5-regioisomer (characteristic NMR signal at δ = 3.88 ppm) according to ^{1}H NMR: (0.66/9)/[(6.12/6)+(0.66/9)] = 7%

The analytical data were in agreement X. Bu, Z. Zhang, X. Zhou, *Organometallics* **2010**, *29*, 3530-3534.

1,2,4-Tris(3-methoxyphenyl)benzene

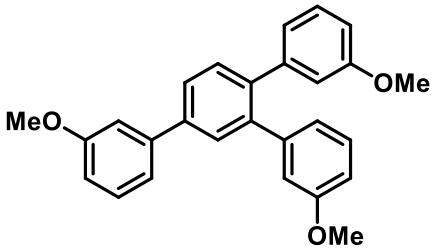

^{1}H NMR (300 MHz, $CDCl_3$): δ = 7.77-7.66 (m, 2H), 7.61-7.53 (m, 1H), 7.46-7.37 (m, 1H), 7.34-7.15 (m, 4H), 7.00-6.93 (m, 1H), 6.92-6.74 (m, 6H), 3.91 (s, 3H), 3.68 (2 s, 6H).

^{13}C NMR (75 MHz, $CDCl_3$): δ = 160.1, 159.3, 159.2, 142.9, 142.6, 142.2, 140.9, 140.4, 139.7, 131.0, 130.0, 129.3, 129.1, 129.0, 126.3, 122.4, 122.3, 119.8, 115.3, 115.2, 113.1, 112.9, 112.9, 112.9, 55.4, 55.2, 55.2.

Amount of the 1,3,5-regioisomer (characteristic NMR signal at δ = 7.84 ppm) according to ^{1}H NMR: (0.09/3)/[(6.00/6)+(0.09/3)] = 3%

The analytical data were in agreement with P. Tagliatesta, B. Floris, P. Galloni, A. Leoni, G. D'Arcangelo, *Inorg. Chem.* **2003**, *42*, 7701-7703.

1,2,4-Tris(4-methylphenyl)benzene

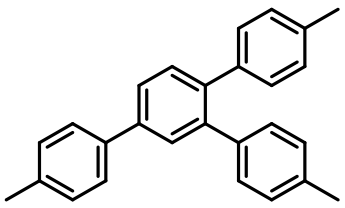

^{1}H NMR (300 MHz, $CDCl_3$): δ = 7.68-7.57 (m, 4H), 7.52-7.47 (m, 1H), 7.34-7.27 (m, 2H), 7.18-7.03 (m, 8H), 2.43 (s, 3H), 2.36 (s, 6H).

^{13}C NMR (75 MHz, $CDCl_3$): δ = 140.9, 140.2, 139.3, 138.9, 138.5, 138.0, 137.3, 136.2, 136.1, 131.2, 129.9 (2C), 129.8 (2C), 129.7 (2C), 129.4, 128.8 (2C), 128.8 (2C), 127.1 (2C), 125.8, 21.3 (3C).

GC-MS (EI): *m/z* (relative intensity) = 348 (100), 318 (15), 151 (13).

Amount of the 1,3,5-regioisomer (characteristic NMR signal at δ = 7.77 ppm) according to ^{1}H NMR: (0.14/3)/[(1.00/1)+(0.14/3)] = 4%

The analytical data were in agreement with X. Bu, Z. Zhang, X. Zhou, *Organometallics* **2010**, *29*, 3530-3534.

1,2,4-Tris(3-methylphenyl)benzene

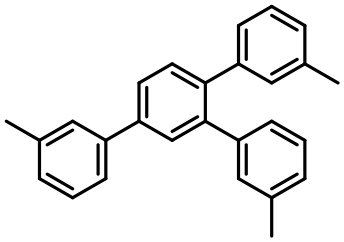

^{1}H NMR (300 MHz, $CDCl_3$): δ = 7.73-7.63 (m, 2H), 7.59-7.49 (m, 3H), 7.43-7.35 (m, 1H), 7.25-7.19 (m, 1H), 7.19-7.03 (m, 6H), 7.03-6.94 (m, 2H), 2.48 (s, 3H), 2.32 (s, 6H).

^{13}C NMR (75 MHz, $CDCl_3$): δ = 141.7, 141.3, 141.2, 140.8, 140.4, 139.7, 138.5, 137.5, 137.5, 131.1, 130.7, 130.7, 129.5, 128.9, 128.3, 128.1, 127.8, 127.7, 127.4, 127.3, 127.2, 127.2, 126.1, 124.4, 21.7, 21.5 (2C).

HRMS (EI): *m/z* = calcd. for $(C_{36}H_{42})^{\bullet+}$: 348.1872, found: 348.1864.

Amount of the 1,3,5-regioisomer (characteristic NMR signal at δ = 7.82 ppm) according to ^{1}H NMR: (0.09/3)/[(2.00/2)+(0.09/3)] = 3%

1,2,4-Tris(4-*n*-butylphenyl)benzene

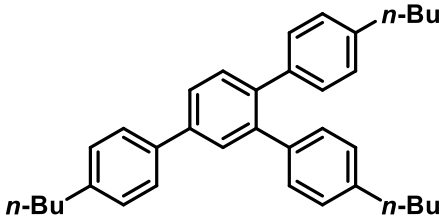

^{1}H NMR (300 MHz, $CDCl_3$): δ = 7.67-7.56 (m, 4H), 7.52-7.45 (m, 1H), 7.30-7.23 (m, 2H), 7.16-6.96 (m, 8H), 2.73-2.63 (m, 2H), 2.63-2.52 (m, 4H), 1.73-1.50 (m, 6H), 1.50-1.24 (m, 6H), 1.02-0.88 (m, 9H).

^{13}C NMR (75 MHz, $CDCl_3$): δ = 142.3, 141.2, 141.1, 141.0, 140.2, 139.4, 139.1, 138.7, 138.2, 131.1, 129.9 (2C), 129.8 (2C), 129.3, 129.0 (2C), 128.0 (2C), 128.0 (2C), 127.1 (2C), 125.8, 35.5, 35.4 (2C), 33.8, 33.6 (2C), 22.6, 22.5, 22.5, 14.1 (3C).

HRMS (EI): *m/z* = calcd. for $(C_{36}H_{42})^{\bullet+}$: 474.3281, found: 474.3275.

Amount of the 1,3,5-regioisomer (characteristic NMR signal at δ = 7.75 ppm) according to ^{1}H NMR: (0.12/3)/[(8.00/8)+(0.12/3)] = 4%

1,2,4-Tris(4-trifluoromethylphenyl)benzene

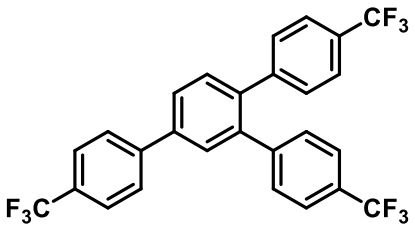

^{1}H NMR (300 MHz, $CDCl_3$): δ = 7.82-7.71 (m, 5H), 7.69-7.67 (m, 1H), 7.60-7.49 (m, 5H), 7.35-7.27 (m, 4H).

^{19}F NMR (565 MHz, $CDCl_3$): δ = −62.48 (s, 3F), −62.49 (s, 3F), −62.49 (s, 3F).

GC-MS (EI): *m/z* (relative intensity) = 510 (100), 372 (31), 211 (28).

Amount of the 1,3,5-regioisomer (characteristic NMR signal at δ = 7.83 ppm) according to ^{1}H NMR: no significant signal detected, therefore <1% assumed.

The analytical data were in agreement with D. Brenna, M. Villa, T. N. Gieshoff, F. Fischer, M. Hapke, A. Jacobi von Wangelin, *Angew. Chem. Int. Ed.* **2017**, *56*, 8451-8454, therefore the evaluation of **^{13}C NMR** was omitted.

1,2,4-Tris(4-acetylphenyl)benzene

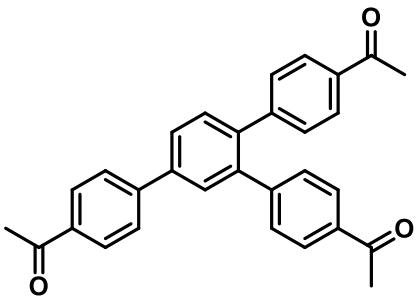

^{1}H NMR (600 MHz, $CDCl_3$): δ = 8.10-8.05 (m, 2H), 8.00-7.90 (m, 3H), 7.87 (d, *J* = 8.1 Hz, 2H), 7.86 (d, *J* = 8.1 Hz, 2H), 7.81 (d, *J* = 1.5 Hz, 1H), 7.62 (d, *J* = 8.1 Hz, 1H), 7.39 (d, *J* = 8.1 Hz, 2H), 7.32 (d, *J* = 8.1 Hz, 2H), 2.63 (s, 3H), 2.56 (s, 3H), 2.55 (s, 3H).

^{13}C NMR (151 MHz, $CDCl_3$): δ = 197.5, 197.5, 197.5, 145.2, 144.9, 143.5, 139.7, 138.9, 138.9, 136.0, 135.3, 135.2, 131.4, 130.0 (2C), 129.8 (2C), 129.1, 128.9 (2C), 128.1 (2C), 128.1 (2C), 127.1 (2C), 126.9, 26.8, 26.8, 26.7.

Amount of the 1,3,5-regioisomer (characteristic NMR signal at δ = 8.11 ppm) according to ^{1}H NMR: (0.07/3)/[(2.00/2)+(0.07/3)] = 2%

Incomplete conversion according to GC-MS and crude NMR data analysis. The starting material could not be removed from the mixture. Yield was calculated according to NMR integration based on the weight of the isolated mixture.

The analytical data were in agreement with Y. Liu, X. Yan, N. Yang, C. Xi, *Catalysis Communications* **2011**, *12*, 489-492.

1,2,4-Tris(4-(pinacolato)boronylphenyl)benzene

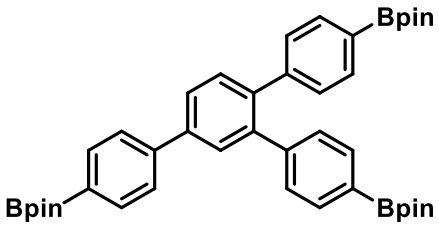

^{1}H NMR (300 MHz, $CDCl_3$): δ = 8.03-7.91 (m, 2H), 7.76-7.66 (m, 8H), 7.58-7.48 (m, 1H), 7.32-7.18 (m, 4H), 1.41 (s, 12H), 1.38 (s, 24H).

^{13}C NMR (75 MHz, $CDCl_3$): δ = 144.3, 143.9, 143.2, 141.0, 140.3, 139.8, 135.4, 134.6, 134.6, 134.5, 131.3 131.2, 129.5, 129.3, 129.2, 126.5, 126.4, 124.8, 84.0, 83.9, 83.8, 78.5, 24.9. (all signals from the crude product are shown except from residual pentane signals)

HRMS (EI): *m/z* = calcd. for $(C_{42}H_{51}B_3O_6)^{\bullet+}$: 684.3959, found: 684.4020.

Amount of the 1,3,5-regioisomer according to ^{1}H NMR: no significant signal detected, therefore <1% assumed.

Incomplete conversion according to GC-MS and crude NMR data analysis. The starting material could not be removed from the mixture. Yield was calculated according to NMR integration based on the weight of the isolated mixture.

1,2,4-Tris-(2',4',5'-trimethylphenyl)benzene

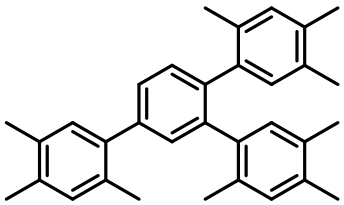

^{1}H NMR (300 MHz, $CDCl_3$): δ = 7.34-7.27 (m, 2H), 7.25-7.21 (m, 1H), 7.13 (s, 1H), 7.07 (s, 1H), 6.93-6.75 (m, 4H), 2.32 (s, 3H), 2.29 (s, 3H), 2.27 (s, 3H), 2.18 (s, 3H), 2.16 (s, 3H), 2.11 (s, 3H), 2.09 (s, 3H), 2.03 (s, 6H).

^{13}C NMR (75 MHz, $CDCl_3$): δ = 140.1, 139.2 (2C), 135.5, (2C), 134.7, 133.9 (2C), 132.9, 132.8, 132.7, 132.6 (2C), 131.9 (3C), 131.7, 131.4 (2C), 131.1, 130.5, 127.5 (2C), 20.2 (2C), 19.5 (4C), 19.3 (2C), 19.2, 19.1.

Amount of the 1,3,5-regioisomer according to ^{1}H NMR: no significant signal detected, therefore <1% assumed.

The analytical data were in agreement with D. Brenna, M. Villa, T. N. Gieshoff, F. Fischer, M. Hapke, A. Jacobi von Wangelin, *Angew. Chem. Int. Ed.* **2017**, *56*, 8451-8454.

1,2,4-Tris-(2'-methyl-4'-methoxyphenyl)benzene

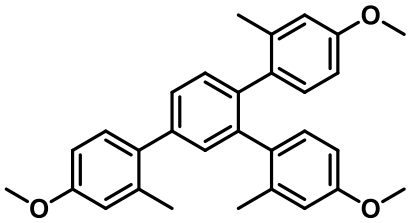

^{1}H NMR (300 MHz, $CDCl_3$): δ = 7.36-7.23 (m, 4H), 7.07-6.81 (m, 4H), 6.80-6.53 (m, 4H), 3.87 (s, 3H), 3.79 (s, 3H), 3.77 (s, 3H), 2.41 (s, 3H), 2.15 (s, 6H).

^{13}C NMR (75 MHz, $CDCl_3$): δ = 158.8, 158.3 (2C), 139.9, 137.2, 137.0, 136.9 (2C), 134.4, 132.1, 131.1 (2C), 130.8, 127.7 (2C), 115.9 (2C), 115.2, 115.1 (2C), 111.3 (2C), 110.6 (2C), 55.4, 55.1 (2C), 22.5, 21.1(2C).

Amount of the 1,3,5-regioisomer according to ^{1}H NMR: no significant signal detected, therefore <1% assumed.

Incomplete conversion according to GC-MS and crude NMR data analysis. The starting material could not be removed from the mixture. Yield was calculated according to NMR integration based on the weight of the isolated mixture.

The analytical data were in agreement with D. Brenna, M. Villa, T. N. Gieshoff, F. Fischer, M. Hapke, A. Jacobi von Wangelin, *Angew. Chem. Int. Ed.* **2017**, *56*, 8451-8454

1,2,4-Tris-(6-methoxy-2-naphthyl)benzene

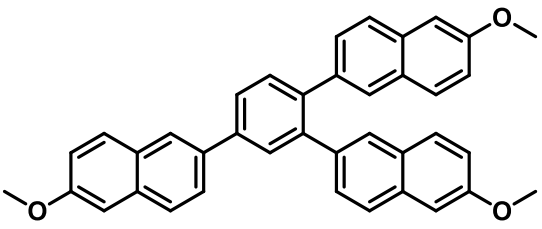

^{1}H NMR (300 MHz, $CDCl_3$): δ = 8.12 (s, 1H), 8.00-7.74 (m, 7H), 7.73-7.62 (m, 3H), 7.53-7.42 (m, 2H), 7.25-6.93 (m, 8H), 3.96 (s, 3H), 3.91 (s, 6H).

^{13}C NMR (75 MHz, $CDCl_3$): δ = 157.9, 157.7, 157.7, 141.1, 140.4, 139.4, 137.2, 136.8, 135.8, 134.0, 133.3, 133.3, 131.7, 129.9, 129.8, 129.6 (2C), 129.6 129.3, 129.0, 129.0 (2C), 128.3, 128.3, 127.5, 126.3, 126.2, 126.2, 126.0, 125.7, 119.3, 118.8, 118.8, 105.7, 105.7 (2C), 55.5, 55.4 (2C).

Amount of the 1,3,5-regioisomer (characteristic NMR signal at δ = 8.16 ppm) according to ^{1}H NMR: (0.12/3)/[(2.01/2)+(0.12/3)] = 4%

The analytical data were in agreement with D. Brenna, M. Villa, T. N. Gieshoff, F. Fischer, M. Hapke, A. Jacobi von Wangelin, *Angew. Chem. Int. Ed.* **2017**, *56*, 8451-8454.

1,2,4-Tris(3-thienyl)benzene

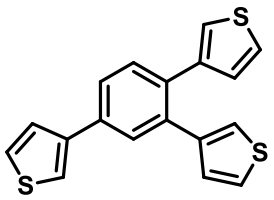

^{1}H NMR (400 MHz, $CDCl_3$): δ = 7.70 (d, *J* = 1.7 Hz, 1H), 7.60 (dd, *J* = 7.9 Hz, 1.7 Hz, 1H), 7.52-7.48 (m, 2H), 7.43-7.39 (m, 2H), 7.25-7.18 (m, 2H), 7.17-7.13 (m, 1H), 7.12-7.07 (m, 1H), 6.89-6.81 (m, 2H).

^{13}C NMR (101 MHz, $CDCl_3$): δ = 142.1, 141.8, 141.7, 135.9, 135.2, 134.3, 130.8, 129.1, 129.0, 128.4, 126.5, 126.4, 125.6, 125.0, 124.9, 123.1, 123.0, 120.6.

GC-MS (EI): *m/z* (relative intensity) = 324 (100), 290 (28), 279 (18).

Amount of the 1,3,5-regioisomer (characteristic NMR signal at δ = 7.75 ppm) according to ^{1}H NMR: (0.20/3)/[(2.00/2)+(0.20/3)] = 6%

Incomplete conversion according to GC-MS analysis. The starting material could partly be removed from the crude product by evaporation on high vacuum. Yield was calculated according to NMR integration based on the weight of the isolated mixture.

The analytical data were in agreement with C. Xi, Z. Sun, Y. Liu, *Dalton Trans.* **2013**, *42*, 13327-13330.

1,2,4-Tris(trimethylsilyl)benzene

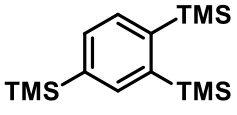

^{1}H NMR (400 MHz, $CDCl_3$): δ = 7.84 (s, 1H), 7.66 (d, *J* = 7.4 Hz, 1H), 7.50 (d, *J* = 7.4 Hz, 1H), 0.38 (s, 9H), 0.37 (s, 9H), 0.28 (s, 9H).

^{13}C NMR (101 MHz, $CDCl_3$): δ = 146.7, 145.0, 140.1, 139.5, 134.5, 132.9, 2.1 (3C), 2.0 (3C), -1.1 (3C).

GC-MS (EI): *m/z* (relative intensity) = 294 (20), 279 (100), 263 (79), 191 (39), 73 (51).

Amount of the 1,3,5-regioisomer (characteristic NMR signal at δ= 7.69 ppm) according to ^{1}H NMR: (0.11/3)/[(1.00/1)+(0.11/3)] = 4%

The analytical data were in agreement with K. Geetharani, S. Tussupbayev, J. Borowka, M. C: Holthausen, S. Gosh, *Chem. Eur. J.* **2012**, *18*, 8482-8489

1,2,4-Tricyclopropylbenzene and 1,3,5-tricyclopropylbenzene

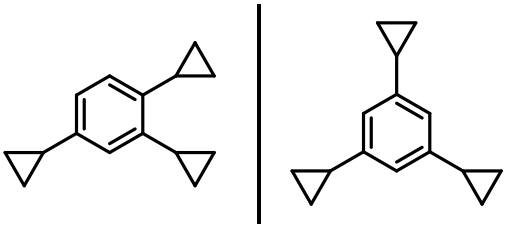

1,2,4: ^{1}H NMR (400 MHz, $CDCl_3$): δ = 6.87 (d, *J* = 7.9 Hz, 1H), 6.80 (dd, *J* = 7.9 Hz, 1.8 Hz, 1H), 6.71 (d, *J* = 1.8 Hz, 1H), 2.24-2.08 (m, 2H), 1.88-1.77 (m, 1H), 0.98-0.85 (m, 6H), 0.72-0.60 (m, 6H).

1,2,4: ^{13}C NMR (101 MHz, $CDCl_3$): δ = 142.4, 141.3, 139.8, 125.4, 122.9, 122.7, 15.2, 13.2, 12.9, 9.0 (2C), 7.3 (2C), 7.2 (2C).

1,2,4: GC-MS (EI): *m/z* (relative intensity) = 198 (73), 155 (65), 141 (100), 129 (88), 115 (63).

1,3,5: ^{1}H NMR (400 MHz, $CDCl_3$): δ = 6.58 (s, 3H), 1.88-1.77 (m, 3H), 0.98-0.85 (m, 6H), 0.72-0.60 (m, 6H).

1,3,5: ^{13}C NMR (101 MHz, $CDCl_3$): δ = 144.0 (3C), 120.4 (3C), 15.5 (3C), 9.1 (6C).

1,3,5: GC-MS (EI): *m/z* (relative intensity) = 198 (62), 157 (53), 141 (52), 129 (100), 115 (61).

Amount of the 1,3,5-regioisomer (characteristic NMR signal at δ = 6.58 ppm) according to ^{1}H NMR: (1.60/3)/[(1.00/1)+(1.53/3)] = 35%

The analytical data were in agreement with the S. K. Rodrigo, I. V. Powell, M. G: Coleman, J. A. Krause, H. Guan, *Org. Biomol. Chem.* **2013**, *11*, 7653–7657.

1,2,4-Tricyclohexylbenzene and 1,3,5-tricyclohexylbenzene

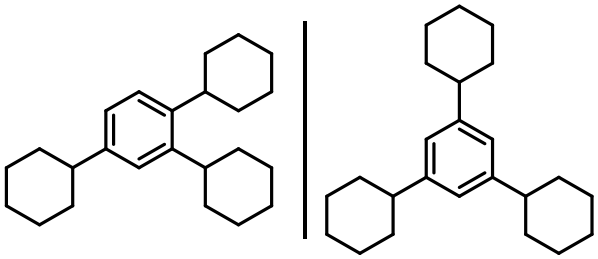

1,2,4: ^{1}H NMR (300 MHz, $CDCl_3$): δ = 7.16 (d, *J* = 8.0 Hz, 1H), 7.08 (dd, *J* = 1.7 Hz, 1H), 7.00 (dd, *J* = 8.0 Hz, *J* = 1.8 Hz, 1H), 2.85-2.67 (m, 2H), 2.56-2.36 (m, 1H), 2.00-1.65 (m, 15H), 1.55-1.15 (m, 15H).

1,2,4: ^{13}C NMR (75 MHz, $CDCl_3$): δ = 145.1, 144.6, 142.2, 125.7, 124.6, 124.0, 44.4, 39.4, 39.1, 34.9 (3C), 34.8 (3C), 34.6 (3C), 27.4 (3C), 26.5 (3C).

1,2,4: GC-MS (EI): *m/z* (relative intensity) = 324 (100), 129 (26), 83 (61).

1,3,5: ^{1}H NMR (300 MHz, $CDCl_3$): δ = 6.89 (s, 3H), 2.56-2.36 (m, 3H), 2.00-1.65 (m, 15H), 1.55-1.15 (m, 15H)

1,3,5: ^{13}C NMR (75 MHz, $CDCl_3$): δ = 147.9 (3C), 123.0 (3C), 44.9 (3C), 34.7 (6C), 27.2 (6C), 26.4 (3C).

1,3,5: GC-MS (EI): *m/z* (relative intensity) = 324 (81), 159 (39), 117 (48), 83 (100).

Amount of the 1,3,5-regioisomer (characteristic NMR signal at δ = 6.89 ppm) according to ^{1}H NMR: (3.00/3)/[(3.00/3)+(0.67/1)] = 60%

The analytical data were in agreement with X. Bu, Z. Zhang, X. Zhou, *Organometallics* **2010**, *29*, 3530-3534.

1,2,4-Tri-t*ert*-butylbenzene and 1,3,5-tri-*tert*-butylbenzene

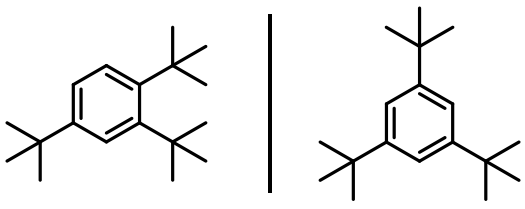

1,2,4: ^{1}H NMR (300 MHz, $CDCl_3$): δ = 7.66 (d, *J* = 2.2 Hz, 1H), 7.54 (d, *J* = 8.4 Hz, 1H), 7.15 (dd, *J* = 8.4Hz, 2.2Hz, 1H), 1.59 (s, 9H), 1.57 (s, 9H), 1.34 (s, 9H).

1,2,4: ^{13}C NMR (75 MHz, $CDCl_3$): δ = 148.3, 147.5, 145.7 129.3, 126.9, 122.4, 38.1, 37.4, 35.0 (3C), 35.0 (3C), 34.5, 31.5 (3C).

1,2,4: GC-MS (EI): *m/z* (relative intensity) = 246 (17), 231 (50), 175 (23), 57 (100).

1,3,5: ^{1}H NMR (300 MHz, $CDCl_3$): δ = 7.29 (s, 3H), 1.37 (s, 27H).

1,3,5: ^{13}C NMR (75 MHz, $CDCl_3$): δ = 150.1 (3C), 119.6 (3C), 35.2 (3C), 31.8 (9C).

1,3,5: GC-MS (EI): *m/z* (relative intensity) = 246 (11), 231 (100), 57 (57).

Amount of the 1,3,5-regioisomer (characteristic NMR signal at δ = 7.29 ppm) according to ^{1}H NMR: (3.00/3)/[(0.90/1)+(3.00/3)] = 53%

The analytical data were in agreement with H. Künzer, S. Berger, *J. Org. Chem.* **1985**, *50*, 3222-3223 and J. A. Murphy, J. Garnier, S. R. Park, F. Schönebeck, S. Zhou, A. T. Turner, *Org. Lett.* **2008**, *10*, 1227-1230.

1,2,4-Tri-*n*-hexylbenzene and 1,3,5-tri-*n*-hexylbenzene

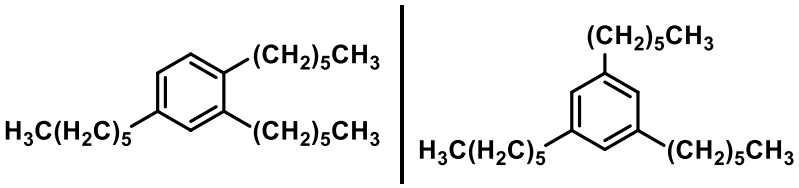

1,2,4: ^{1}H NMR (300 MHz, $CDCl_3$): δ = 7.08-7.01 (m, 1H), 6.98-6.89 (m, 2H), 2.63-2.47 (m, 6H), 1.68-1.48 (m, 6H), 1.44-1.18 (m, 18H), 0.98-0.80 (m, 9H).

1,2,4: ^{13}C NMR (75 MHz, $CDCl_3$): δ = 140.5, 140.3, 137.8, 129.4, 129.1, 125.8, 35.8, 32.9, 32.5, 31.9 (3C), 31.7, 31.5 (2C), 29.7 (2C), 29.3, 22.8 (3C), 14.3 (3C).

1,2,4: GC-MS (EI): *m/z* (relative intensity) = 330 (35), 259 (24), 189 (100).

1,3,5: ^{1}H NMR (300 MHz, $CDCl_3$): δ = 6.81 (s, 3H), 2.63-2.47 (m, 6H), 1.68-1.48 (m, 6H), 1.44-1.18 (m, 18H), 0.98-0.80 (m, 9H).

1,3,5: ^{13}C NMR (75 MHz, $CDCl_3$): δ = 142.8 (3C), 126.0 (3C), 36.1 (3C), 31.9 (3C), 31.7 (3C), 29.3 (3C), 22.8 (3C), 14.3 (3C).

1,3,5: GC-MS (EI): *m/z* (relative intensity) = 330 (42), 260 (100), 105 (77).

Amount of the 1,3,5-regioisomer (characteristic NMR signal at δ = 6.83 ppm) according to ^{1}H NMR: (2.61/3)/[(1.00/1)+(2.61/3)] = 47%

The analytical data were in agreement with the K. Tanaka, K. Toyoda, A. Wada, K. Shirasaka, M. Hirano, *Chem. Eur. J.* **2005**, *11*, 1145-1156.

1,2,4-Tris(4-chlorobutyl)benzene and 1,3,5-tris(4-chlorobutyl)benzene

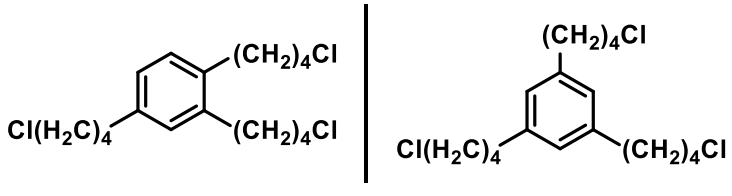

1,2,4: ^{1}H NMR (300 MHz, $CDCl_3$): δ = 7.09-7.05 (m, 1H), 6.99-6.93 (m, 2H), 3.63-3.51 (m, 6H), 2.68-2.55 (m, 6H), 1.93-1.69 (m, 12H).

1,2,4: ^{13}C NMR (75 MHz, $CDCl_3$): δ = 139.7, 139.6, 137.2, 129.4, 129.4, 126.3, 45.1, 45.0 (2C), 34.8, 32.6, 32.6, 32.3, 32.0, 31.6, 28.7, 28.6 (2C).

1,2,4: GC-MS (EI): *m/z* (relative intensity) = 350 (21), 348 (21), 271 (86), 195 (100).

1,3,5: ^{1}H NMR (300 MHz, $CDCl_3$): δ = 6.83 (s, 3H), 3.63-3.51 (m, 6H), 2.68-2.55 (m, 6H), 1.93-1.69 (m, 12H).

1,3,5: ^{13}C NMR (75 MHz, $CDCl_3$): δ = 142.1 (3C), 126.2 (3C), 45.1 (3C), 35.2 (3C), 32.3 (3C), 28.7 (3C).

1,3,5: GC-MS (EI): *m/z* (relative intensity) = 350 (22), 348 (23), 271 (86), 91 (100).

Amount of the 1,3,5-regioisomer (characteristic NMR signal at δ = 6.83 ppm) according to ^{1}H NMR: (2.27/3)/[(1.00/1)+(2.27/3)] = 43%

The analytical data were in agreement with C. C. Eichman, J. P. Bragdon, J. P. Stambuli, *Synlett* **2011**, *8*, 1109-1112.

1,2,4-Tri-benzylbenzene and 1,3,5-tri-benzylbenzene

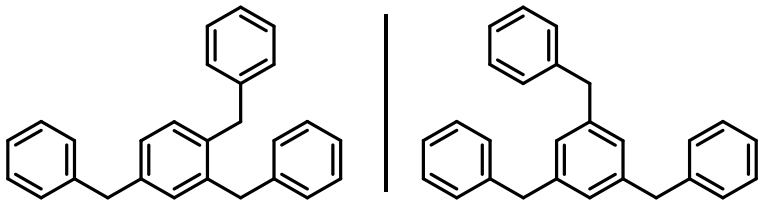

1,2,4: ^{1}H NMR (300 MHz, $CDCl_3$): δ = 7.34-6.95 (m, 18H), 3.93, (s, 2H), 3.91 (s, 2H), 3.89 (s, 2H).

1,3,5: ^{1}H NMR (300 MHz, $CDCl_3$): δ = 7.34-6.95 (m, 15H), 6.87 (s, 3H), 3.89 (s, 6H).

Mixture of 1,2,4- and 1,3,5-^{13}C NMR (75 MHz, $CDCl_3$): δ = 141.4, 141.4, 141.3, 140.8, 140.7, 139.4, 139.0, 137.0, 131.5, 130.8, 129.0, 129.0, 128.9, 128.8, 128.6, 128.5, 128.5, 127.7, 127.3, 126.1, 126.1, 126.1, 42.0, 41.7, 39.2, 38.7.

1,2,4: GC-MS (EI): *m/z* (relative intensity) = 348 (35), 257 (30), 179 (100), 91 (65).

1,3,5: GC-MS (EI): *m/z* (relative intensity) = 348 (68), 257 (86), 179 (43), 91 (100).

Amount of the 1,3,5-regioisomer (characteristic NMR signal at δ = 6.87 ppm) according to ^{1}H NMR: (1.81/3)/[(2.00/2)+(1.81/3)] = 38%

The analytical data were in agreement with K. Tanaka, K. Toyoda, A. Wada, K. Shirasaka, M. Hirano, *Chem. Eur. J.* **2005**, *11*, 1145-1156.

5-((Prop-2-ynyloxy)methyl)-1,3-dihydroisobenzofuran

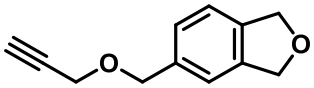

^{1}H NMR (300 MHz, $CDCl_3$): δ = 7.28-7.19 (m, 3H), 5.11 (s, 4H), 4.62 (s, 2H), 4.18 (d, J = 2.4 Hz, 2H), 2.48 (t, *J* = 2.4 Hz, 1H).

^{13}C NMR (75 MHz, $CDCl_3$): δ = 139.7, 138.8, 136.8, 127.2, 121.0, 120.6, 79.7, 74.8, 73.6 (2C), 71.5, 57.3.

GC-MS (EI): *m/z* (relative intensity) = 188 (11), 158 (16), 134 (30), 105 (79), 91 (100).

5,5'-Oxybis(methylene)bis(1,3-dihydroisobenzofuran)

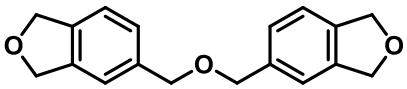

^{1}H NMR (300 MHz, $CDCl_3$): δ = 7.28-7.19 (m, 6H), 5.11 (s, 8H), 4.57 (s, 4H).

^{13}C NMR (75 MHz, $CDCl_3$): δ = 139.7 (2C), 139.1 (2C), 137.7 (2C), 127.5 (2C), 121.1 (2C), 120.9 (2C), 73.6 (4C), 72.2 (2C).

GC-MS (EI): *m/z* (relative intensity) = 282 (8), 149 (9), 134 (38), 132 (51), 105 (100), 91 (70).

Amount of di- vs. trimerized product was calculated (characteristic NMR signal at δ = 4.62 ppm vs δ = 4.57 ppm) according to ^{1}H NMR.

The analytical data were in agreement with A. Mallagaray, S. Medina, G. Dominguez, J. Perez-Castells, *Synlett* **2010**, *14*, 2114-2118.

1,3,6,8-Tetrahydro-2,7-dioxa-*as*-indacene

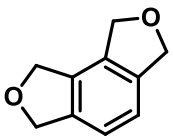

^{1}H NMR (300 MHz, $CDCl_3$): δ = 7.14 (s, 2H), 5.12 (s, 4H), 5.02 (s, 4H).

^{13}C NMR (75 MHz, $CDCl_3$): δ = 138.8 (2C), 132.5 (2C), 120.0 (2C), 73.5 (2C), 72.3 (2C).

GC-MS (EI): *m/z* (relative intensity) = 162 (57), 133 (25), 104 (100), 77 (37).

The analytical data were in agreement with A. Geny, N. Agenet, L. Iannazzo, M. Malacria, C. Aubert, V. Gandon, *Angew. Chem. Int. Ed.* **2009**, *48*, 1810-1813.

1,2,4-Trimethyl-3,5,6-triphenylbenzene

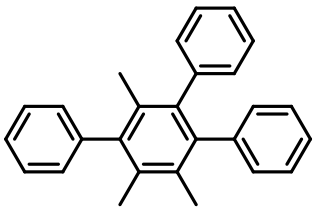

^{1}H NMR (300 MHz, $CDCl_3$): δ = 7.49-7.41 (m, 2H), 7.41-7.31 (m, 2H), 7.29-7.23 (m, 2H), 7.17-7.07 (m, 4H), 7.07-6.94 (m, 5H), 2.05 (s, 6H), 1.72 (s, 3H).

^{13}C NMR (75 MHz, $CDCl_3$): δ = 142.6, 141.8, 141.8, 141.6, 140.8, 139.4, 134.1, 132.0, 131.4, 130.5 (4C), 129.5 (2C), 128.6 (2C), 127.5 (2C), 127.4 (2C), 126.6, 125.9, 125.8, 19.6, 18.4, 18.2.

GC-MS (EI): *m/z* (relative intensity) = 348 (100), 333 (14), 239 (10).

Amount of the 1,3,5-regioisomer according to ^{1}H NMR: no significant signal detected, therefore <1% assumed.

Incomplete conversion according to GC-MS and crude NMR data analysis. The starting material was removed from the mixture by evaporation on high vacuum.

The analytical data were in agreement with J.-S. Yang, H.-H. Huang, S.-H. Lin, *J. Org. Chem.* **2009**, *74*, 3974-3977.

5.4.16 Selected NMR spectra

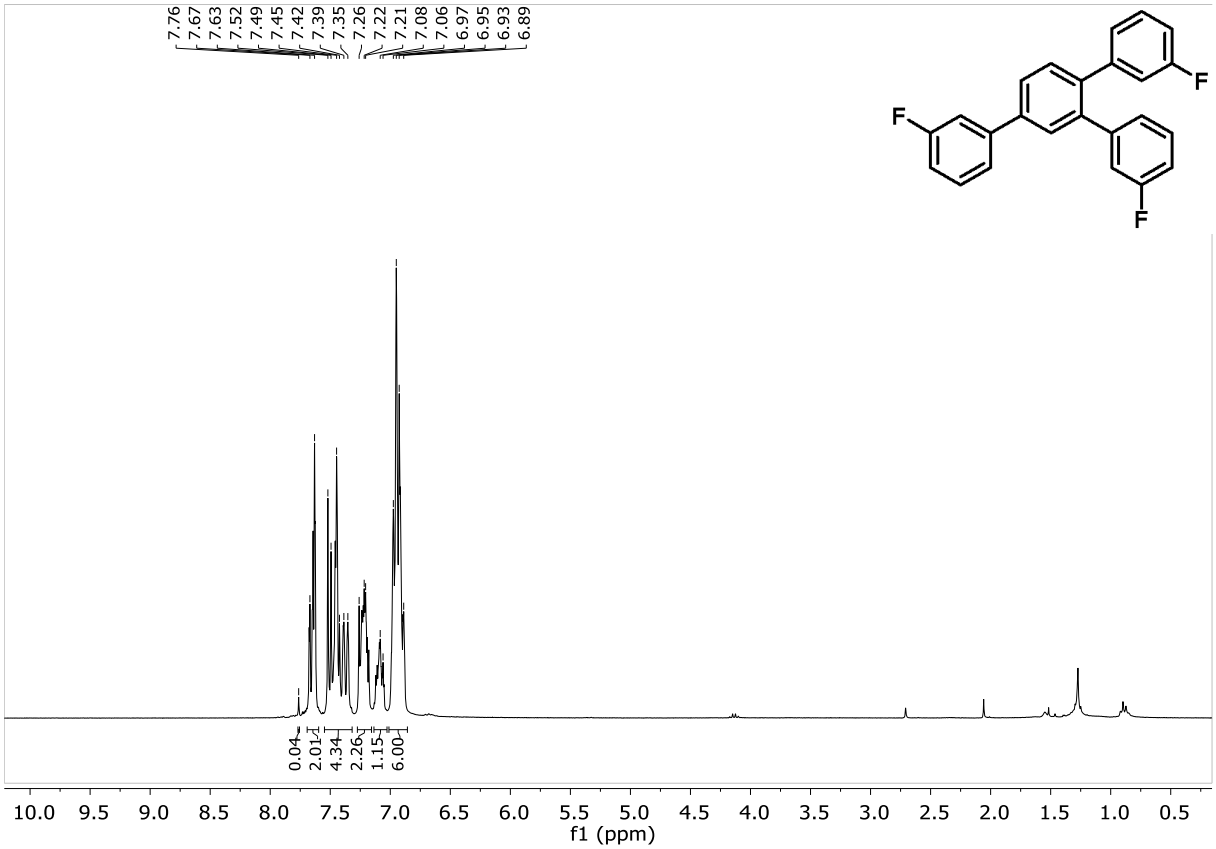

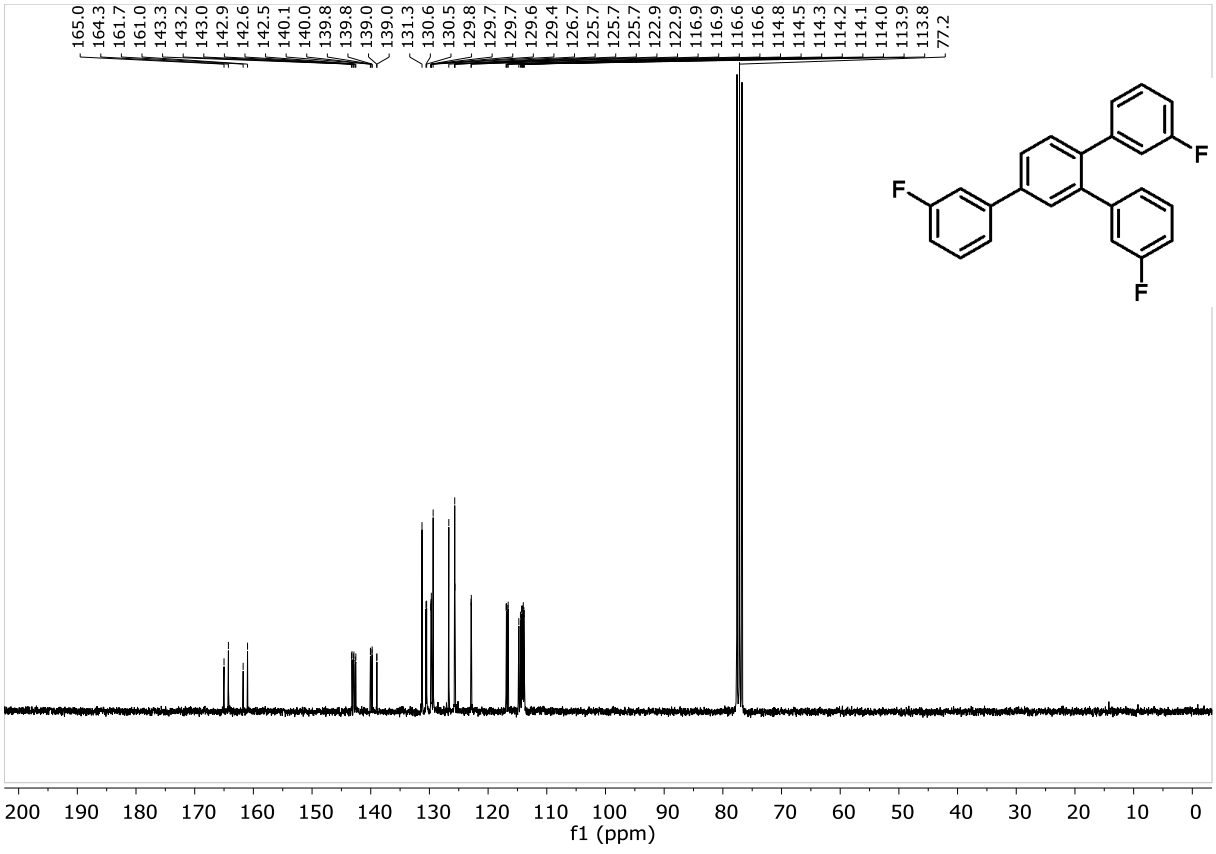

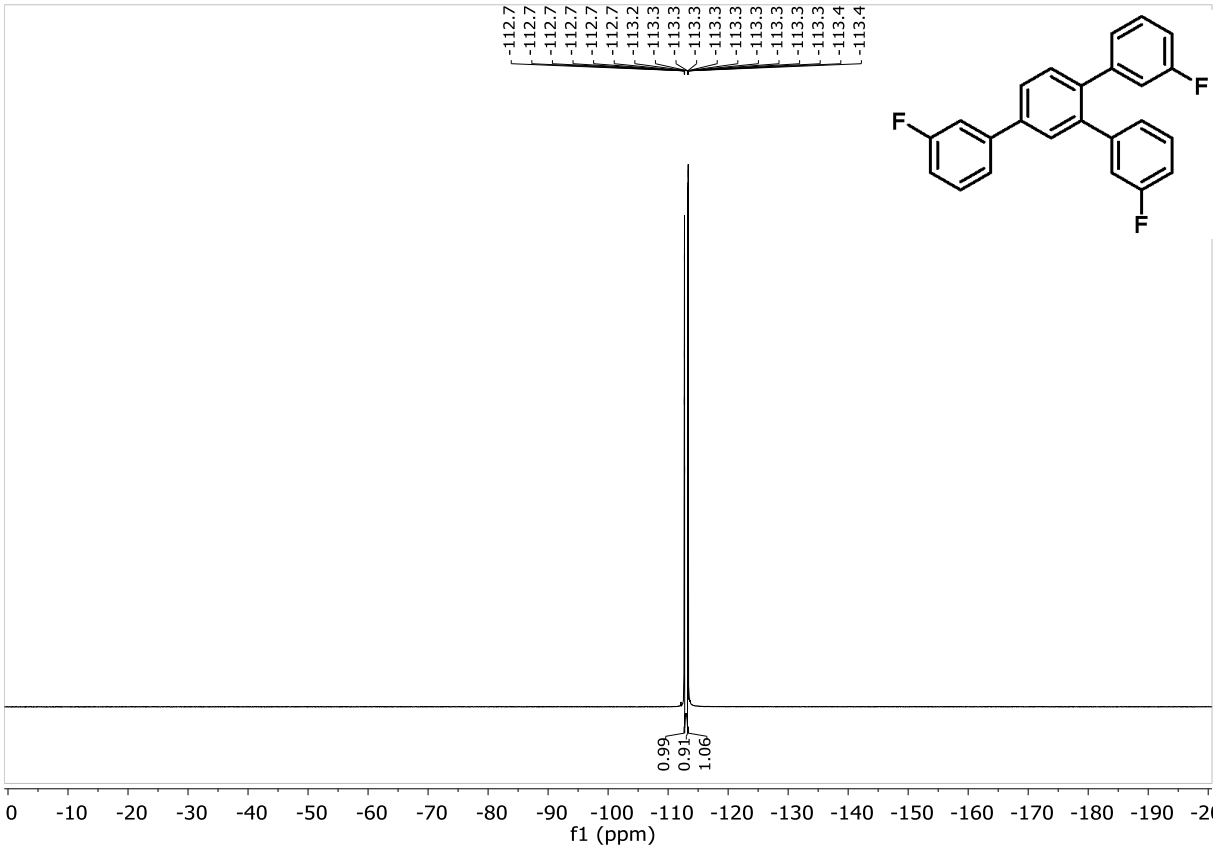
-112.7
-112.7
-112.7
-112.7
-112.7
-112.7
-113.2
-113.3
-113.3
-113.3
-113.3
-113.3
-113.3
-113.3
-113.3
-113.3
-113.4
-113.4
F
F
F
0.99
0.91
1.06
0 -10 -20 -30 -40 -50 -60 -70 -80 -90 -100 -110 -120 -130 -140 -150 -160 -170 -180 -190
f1 (ppm)

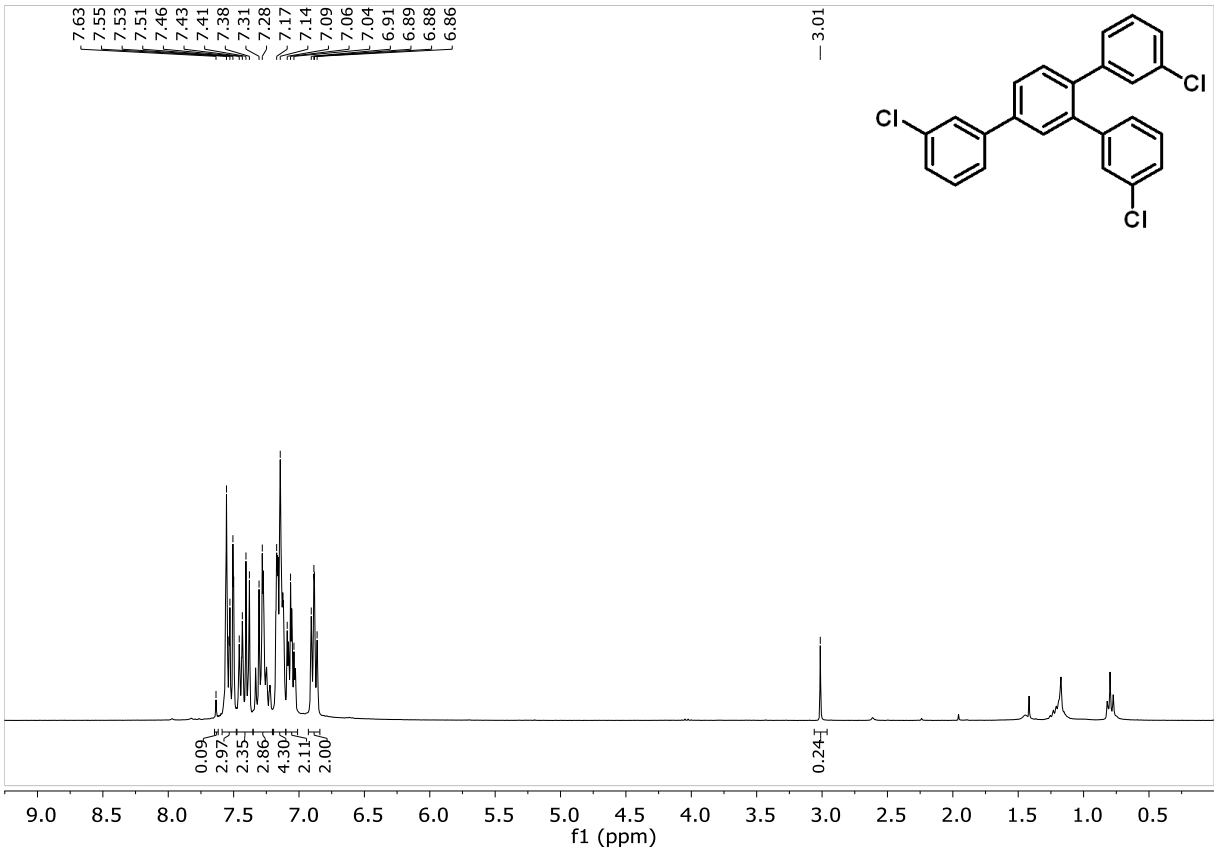
7.63
7.55
7.53
7.51
7.46
7.43
7.41
7.38
7.31
7.28
7.17
7.14
7.09
7.06
7.04
6.91
6.89
6.88
6.86
3.01
Cl
Cl
Cl
0.09
2.97
2.35
2.86
4.30
2.11
2.00
0.24
9.0 8.5 8.0 7.5 7.0 6.5 6.0 5.5 5.0 4.5 4.0 3.5 3.0 2.5 2.0 1.5 1.0 0.5
f1 (ppm)

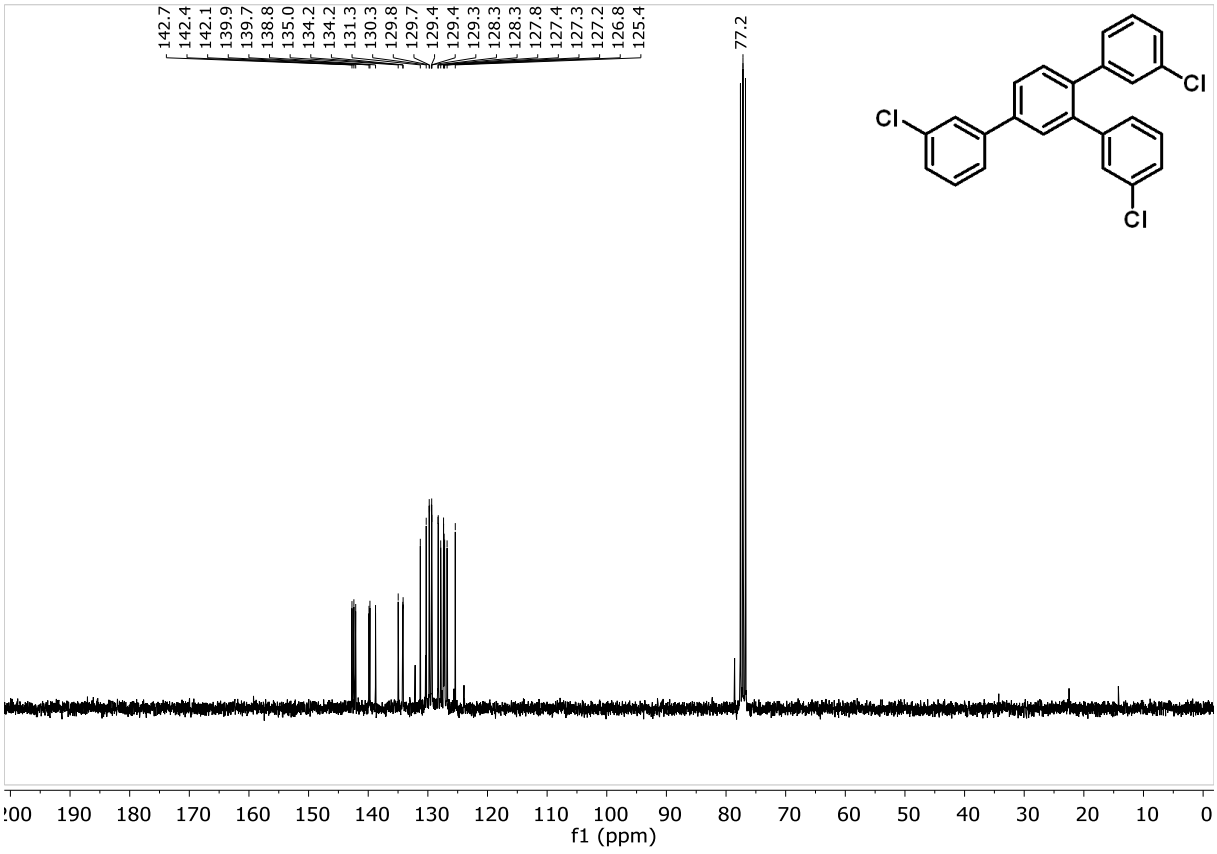
142.7
142.4
142.1
139.9
139.7
138.8
135.0
134.2
134.2
131.3
130.3
129.8
129.7
129.4
129.4
129.3
128.3
128.3
127.8
127.4
127.3
127.2
126.8
125.4
77.2
Cl
Cl
Cl
f1 (ppm)

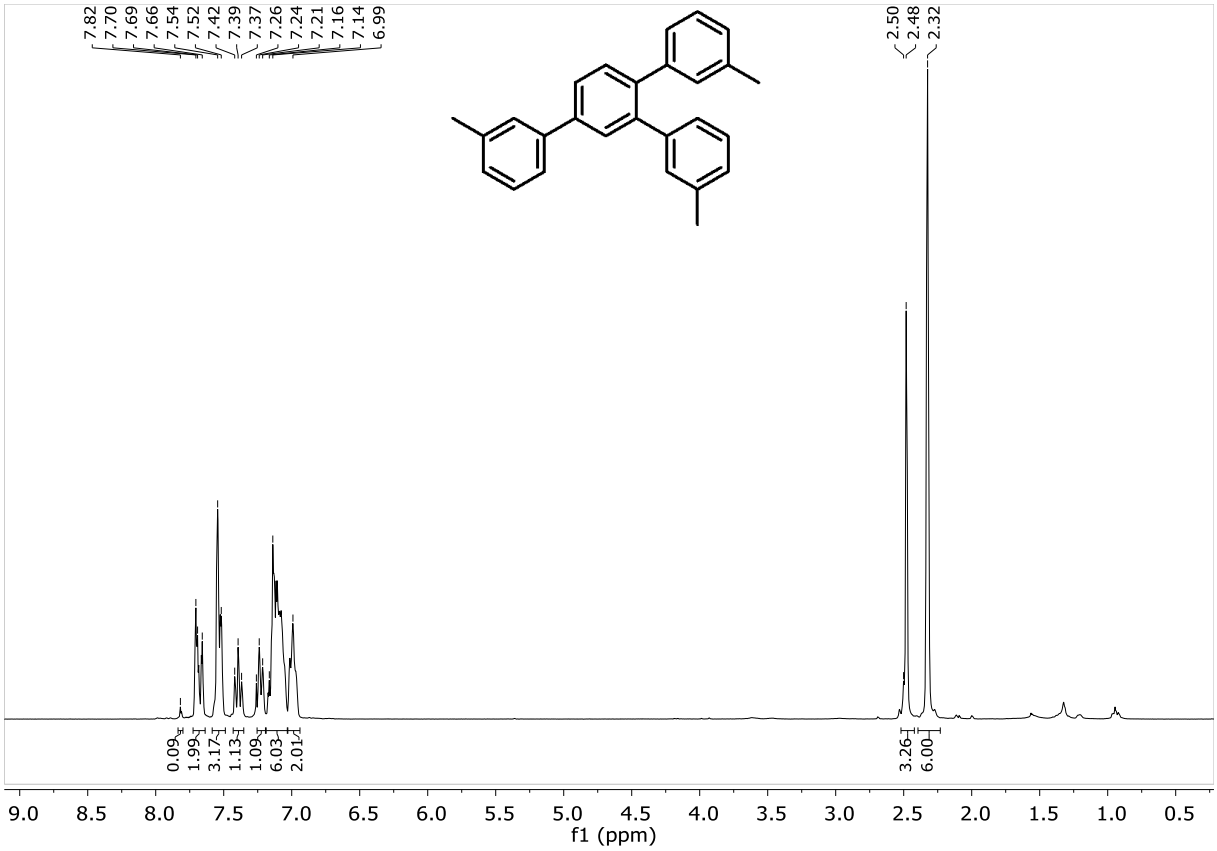
7.82
7.70
7.69
7.66
7.54
7.52
7.42
7.39
7.37
7.26
7.24
7.21
7.16
7.14
6.99
2.50
2.48
2.32
0.09
1.99
3.17
1.13
1.09
6.03
2.01
3.26
6.00
f1 (ppm)

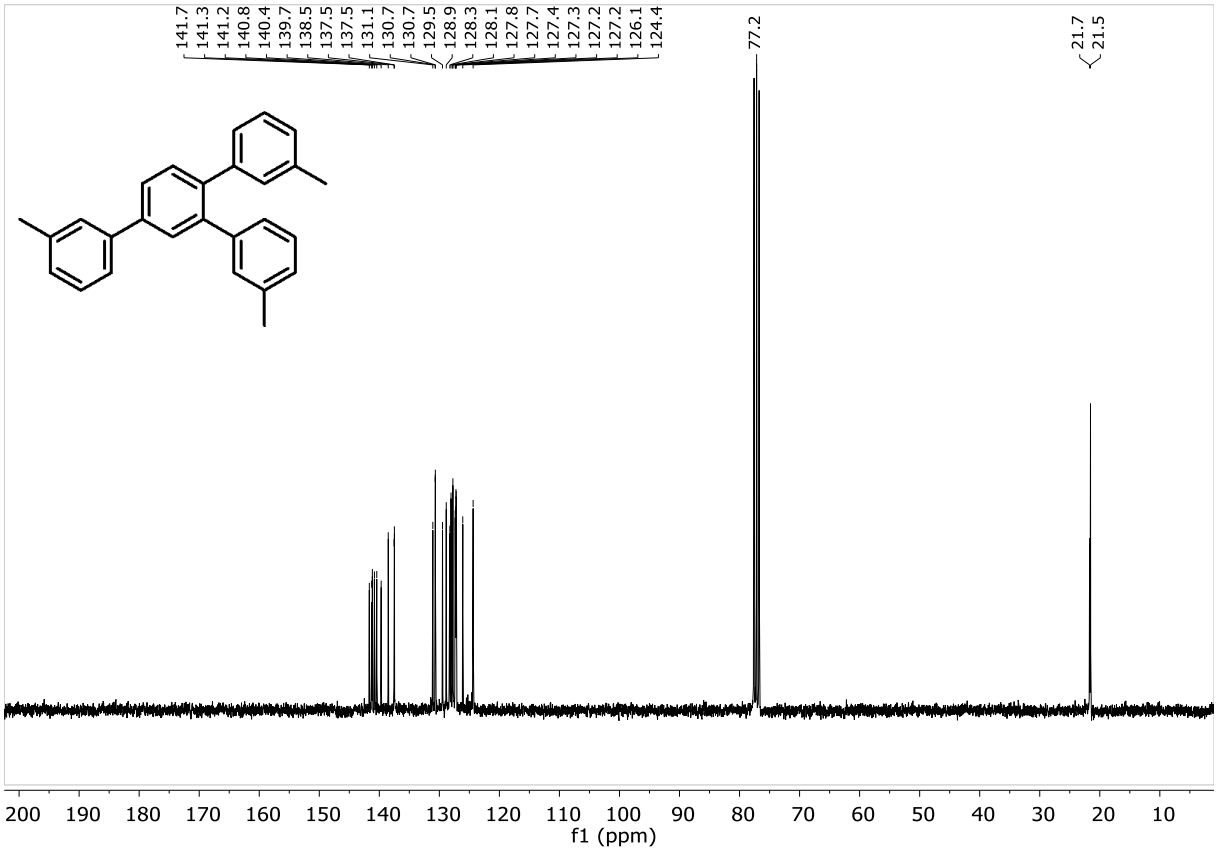
141.7
141.3
141.2
140.8
140.4
139.7
138.5
137.5
137.5
131.1
130.7
130.7
129.5
128.9
128.3
128.1
127.8
127.7
127.4
127.3
127.2
127.2
126.1
124.4
77.2
21.7
21.5
200 190 180 170 160 150 140 130 120 110 100 90 80 70 60 50 40 30 20 10
f1 (ppm)

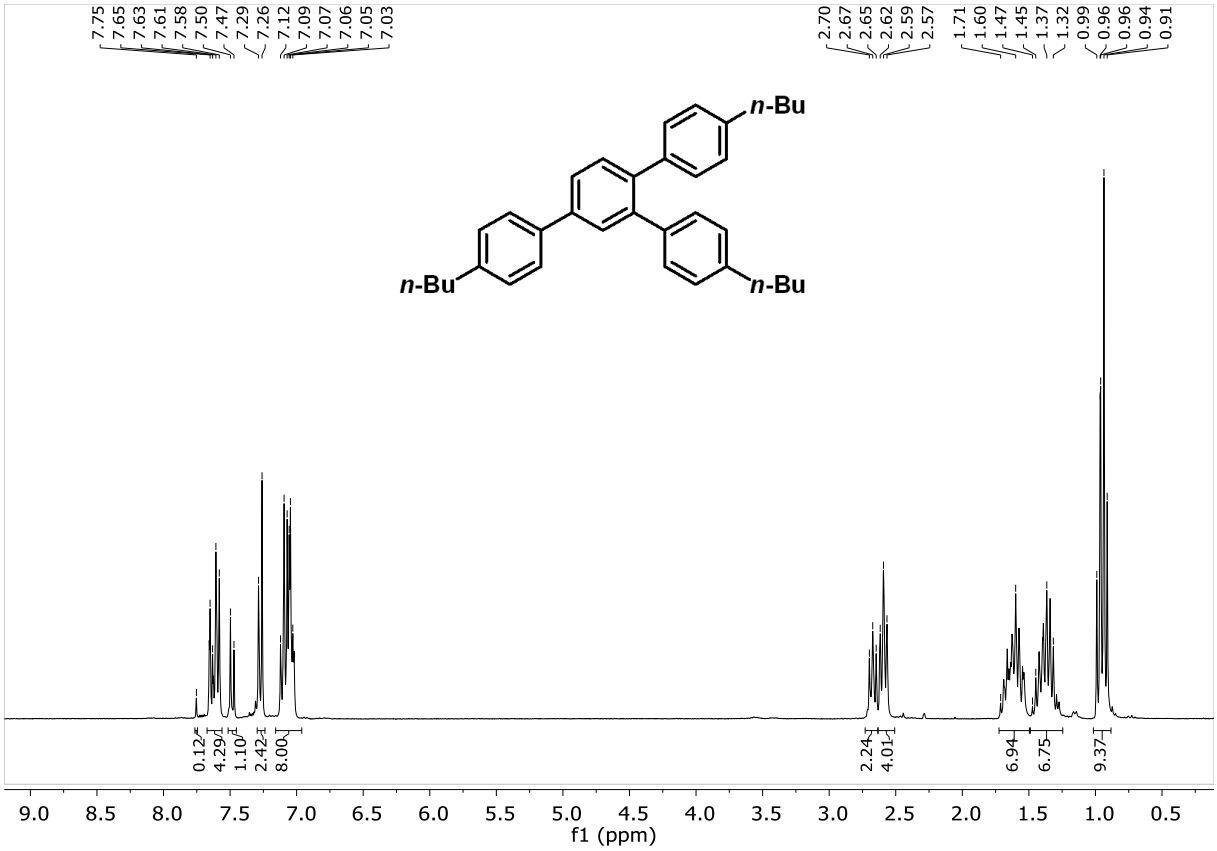
7.75
7.65
7.63
7.61
7.58
7.50
7.47
7.29
7.26
7.12
7.09
7.07
7.06
7.05
7.03
2.70
2.67
2.65
2.62
2.59
2.57
1.71
1.60
1.47
1.45
1.37
1.32
0.99
0.96
0.96
0.94
0.91
n-Bu
n-Bu
n-Bu
0.12
4.29
1.10
2.42
8.00
2.24
4.01
6.94
6.75
9.37
9.0 8.5 8.0 7.5 7.0 6.5 6.0 5.5 5.0 4.5 4.0 3.5 3.0 2.5 2.0 1.5 1.0 0.5
f1 (ppm)

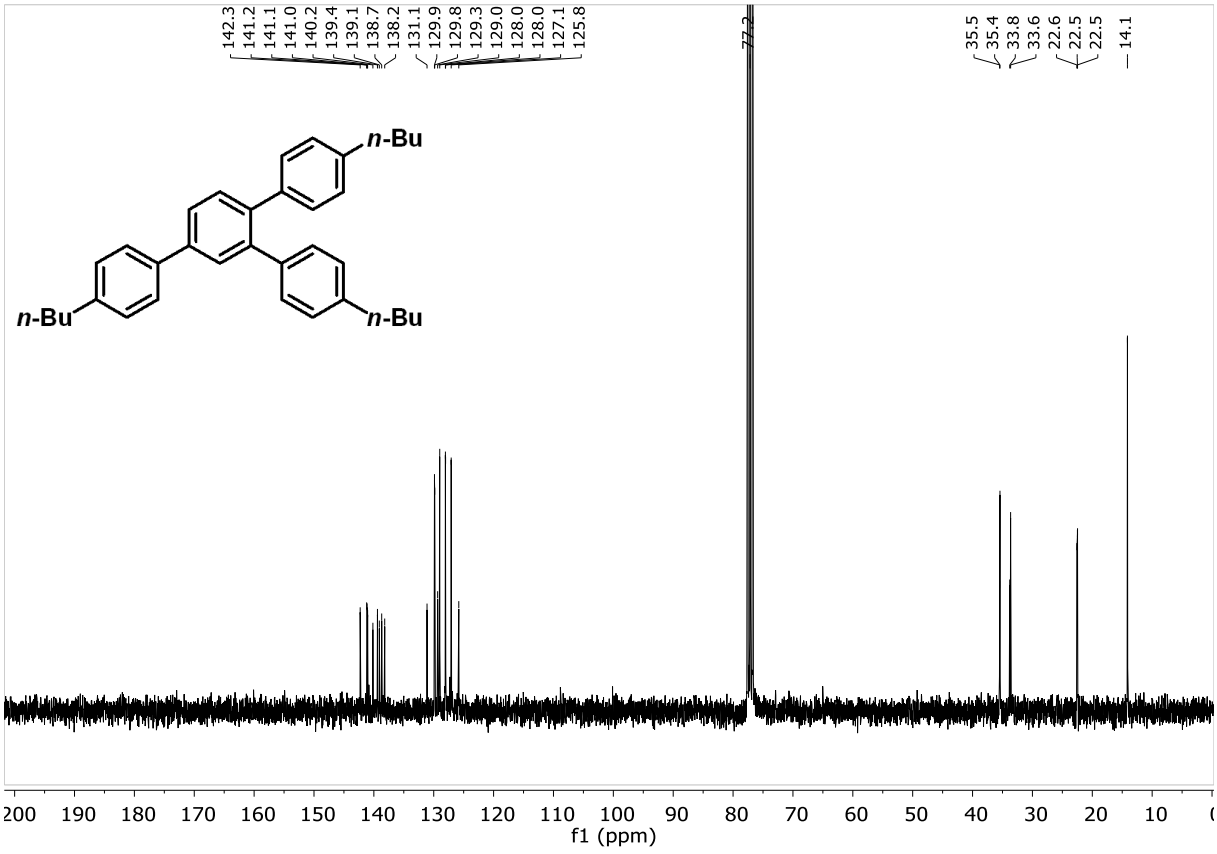
142.3
141.2
141.1
141.0
140.2
139.4
139.1
138.7
138.2
131.1
129.9
129.8
129.3
129.0
128.0
128.0
127.1
125.8
77.2
35.5
35.4
33.8
33.6
22.6
22.5
22.5
14.1
n-Bu
n-Bu
n-Bu
200 190 180 170 160 150 140 130 120 110 100 90 80 70 60 50 40 30 20 10
f1 (ppm)

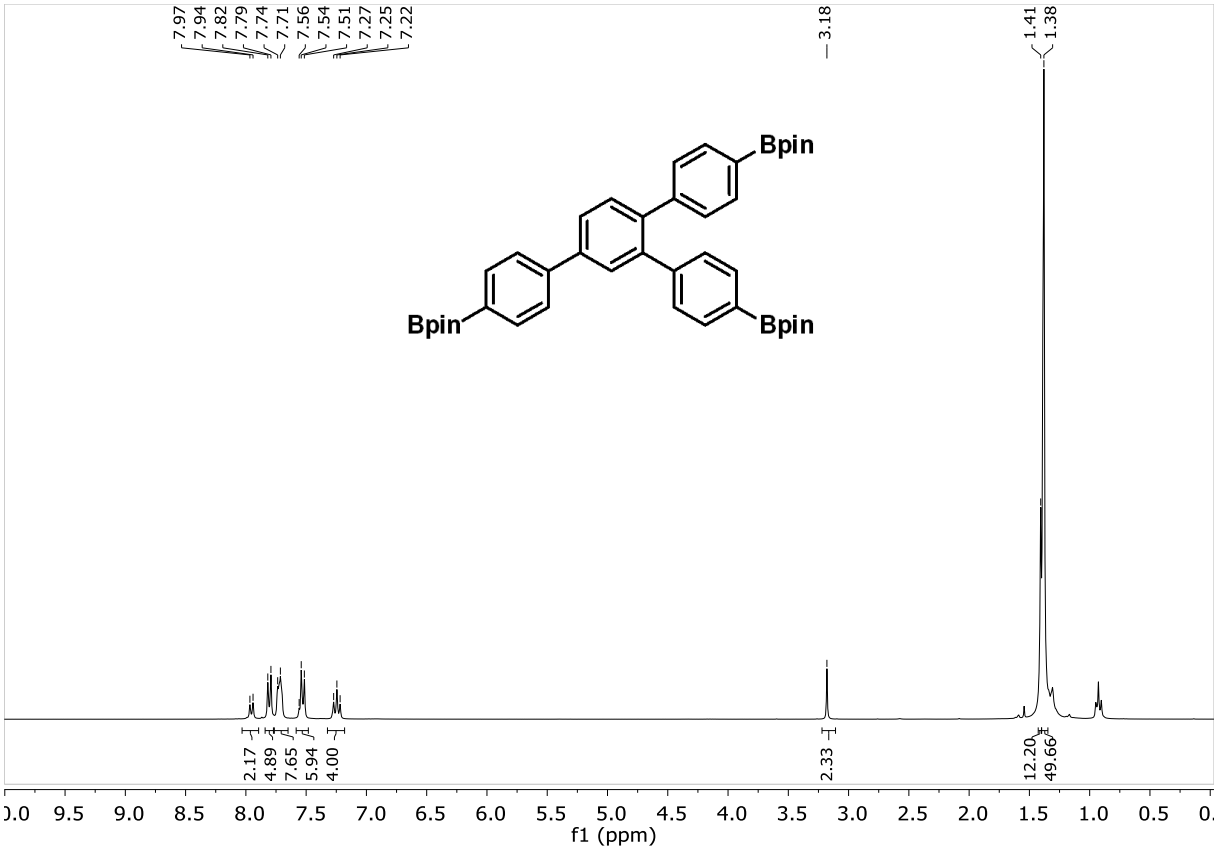
7.97
7.94
7.82
7.79
7.74
7.71
7.56
7.54
7.51
7.27
7.25
7.22
3.18
1.41
1.38
Bpin
Bpin
Bpin
2.17
4.89
7.65
5.94
4.00
2.33
12.20
49.66
0.0 9.5 9.0 8.5 8.0 7.5 7.0 6.5 6.0 5.5 5.0 4.5 4.0 3.5 3.0 2.5 2.0 1.5 1.0 0.5
f1 (ppm)

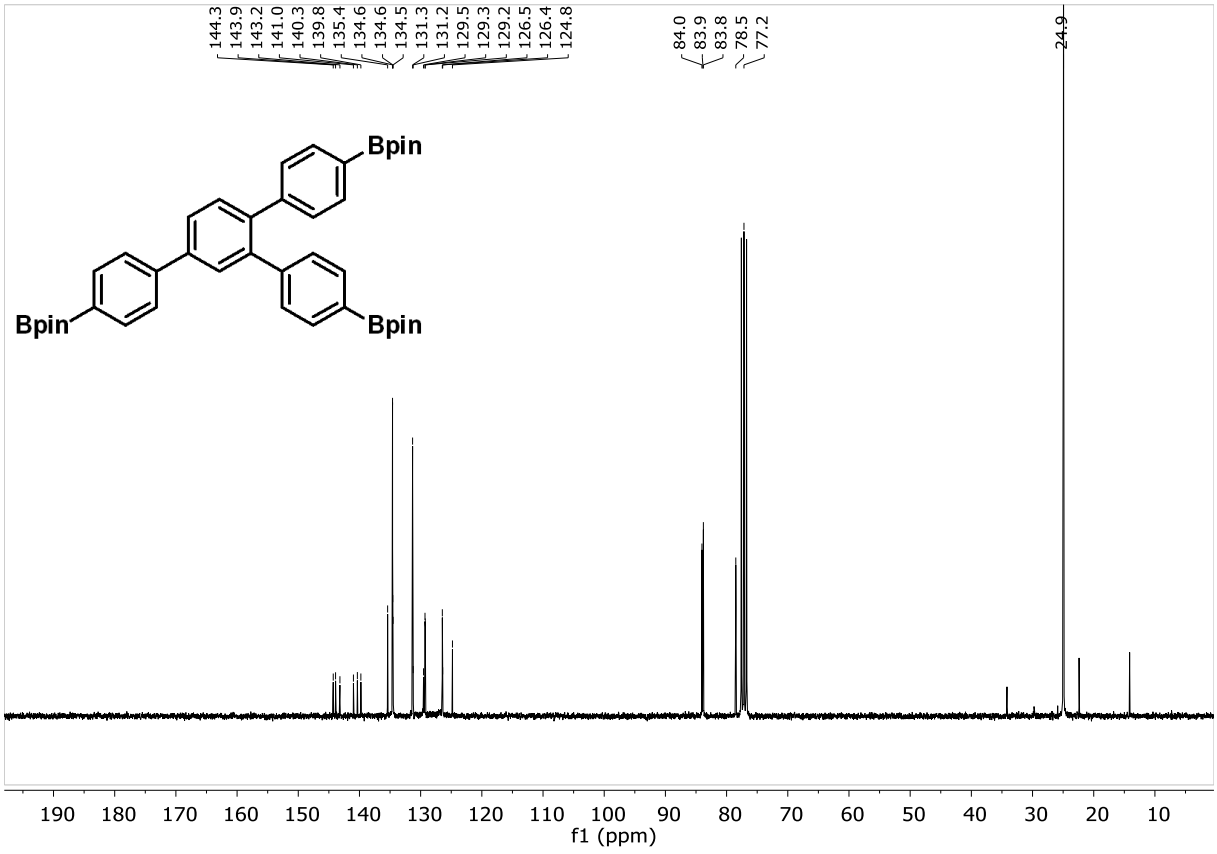
144.3
143.9
143.2
141.0
140.3
139.8
135.4
134.6
134.6
134.5
131.3
131.2
129.5
129.3
129.2
126.5
126.4
124.8
84.0
83.9
83.8
78.5
77.2
24.9
Bpin
Bpin
Bpin
190 180 170 160 150 140 130 120 110 100 90 80 70 60 50 40 30 20 10
f1 (ppm)

5.5 References

[1] a) J. Twilton, C. Le, P. Zhang, M. H. Shaw, R. W. Evans, D. C. W. MacMillan, *Nat. Rev. Chem.* **2017**, *1*, 0052. b) K. L. Skubi, T. R. Blum, T. P. Yoon, *Chem. Rev.* **2016**, *116*, 10035–10074. c) C. K. Prier, D. A. Rankic, D. W. C. MacMillan, *Chem. Rev.* **2013**, *113*, 5322–5363. d) N. A. Romero, D. A. Nicewicz, *Chem. Rev.* **2016**, *116*, 10075. e) V. Balzani, P. Ceroni, A. Juris, *Photochemistry and Photophysics: Concepts, Research, Applications*, Wiley-VCH, Weinheim, **2014**. f) T. P. Yoon, M. A. Ischay, J. Du, *Nat. Chem.* **2010**, *2*, 527–532.

[2] H. Hennig, R. Billing, *Coord. Chem. Rev.* **1993**, *125*, 89–100.

[3] J. Chen, W. R. Browne, *Coord. Chem. Rev.* **2018**, *374*, 15–35.

[4] H. G. Alt, *Angew. Chem. Int. Ed.* **1984**, *23*, 766–782.

[5] G. L. Geoffroy, M. S. Wrighton, *Organometallic Photochemistry*, Academic Press, **1979**.

[6] P. Chábera, Y. Liu, O. Prakash, E. Thyrhaug, A. E. Nahhas, A. Honarfar, S. Essén, L. A. Fredin, T. C. B. Harlang, K. S. Kjær, et al., *Nature* **2017**, *543*, 695–699.

[7] B. J. Shields, B. Kudisch, G. D. Scholes, A. G. Doyle, *J. Am. Chem. Soc.* **2018**, *140*, 3035–3039 and references therein.

[8] B. D. Ravetz, J. Y. Wang, K. E. Ruhl, T. Rovis, *ACS Catal.* **2019**, *9*, 200–204.

[9] C.-H. Lim, M. Kudisch, B. Liu, G. M. Miyake, *J. Am. Chem. Soc.* **2018**, *140*, 7667–7673.

[10] B. König, *Chemical Photocatalysis*, De Gruyter, **2013**, 139-149.

[11] H. Hennig, L. Weber, D. Rehorek, in *Photosensitive Metal-Organic Systems*, American Chemical Society, **1993**, pp. 351–375.

[12] Z. Zuo, D. T. Ahneman, L. Chu, J. A. Terrett, A. G. Doyle, D. W. C. MacMillan, *Science* **2014**, *345*, 437–440.

[13] E. R. Welin, C. Le, D. M. Arias-Rotondo, J. K. McCusker, D. W. C. MacMillan, *Science* **2017**, *355*, 380–385.

[14] K. E. Ruhl, T. Rovis, *J. Am. Chem. Soc.* **2016**, *138*, 15527–15530.

[15] M. Claros, F. Ungeheuer, F. Franco, V. Martin-Diaconescu, A. Casitas, J. Lloret-Fillol, *Angew. Chem. Int. Ed.* **2019**, *58*, 4869–4874.

[16] E. B. Corcoran, M. T. Pirnot, S. Lin, S. D. Dreher, D. A. DiRocco, I. W. Davies, S. L. Buchwald, D. W. C. MacMillan, *Science* **2016**, *353*, 279–283.

[17] a) H. Rao, L. C. Schmidt, J. Bonin, M. Robert, *Nature* **2017**, *548*, 74–77. b) H. Rao, C.-H. Lim, J. Bonin, G. M. Miyake, M. Robert *J. Am. Chem. Soc.* **2018**, *140*, 17830-17834.

[18] D. Brenna, M. Villa, T. N. Gieshoff, F. Fischer, M. Hapke, A. Jacobi von Wangelin, *Angew. Chem. Int. Ed.* **2017**, *56*, 8451–8454.

[19] C. Wang, X. Li, F. Wu, B. Wan, *Angew. Chem. Int. Ed.* **2011**, *50*, 7162–7166.

[20] A. Casitas, H. Krause, R. Goddard, A. Fürstner, *Angew. Chem. Int. Ed.* **2015**, *54*, 1521–1526.

[21] A. Fürstner, K. Majima, R. Martín, H. Krause, E. Kattnig, R. Goddard, C. W. Lehmann, *J. Am. Chem. Soc.* **2008**, *130*, 1992–2004.

[22] K. Ferré, L. Toupet, V. Guerchais, *Organometallics* **2002**, *21*, 2578–2580.

[23] U. Zenneck, W. Frank, *Angew. Chem. Int. Ed.* **1986**, *25*, 831–833.

[24] G. Lefevre, M. Taillefer, C. Adamo, I. Ciofini, A. Jutand, *Eur. J. Org. Chem.* **2011**, 3768-3780.

[25] a) A. Hu, Y. Chen, J.-J. Guo, N. Yu, Q. An, Z. Zuo, *J. Am. Chem. Soc.* **2018**, *140*, 13580-13585. b) M. Montalti, A. Credi, L. Prodi, M. T. Gandolfi, *Handbook of Photochemistry*, 3rd ed., CRC, Taylor & Francis, Boca Raton, **2006**.

[26] For further details: see the experimental section 5.4.

[27] N. Agenet, O. Buisine, F. Slowinski, V. Gandon, C. Aubert, M. Malacria, *Org. React.* **2007**, *68*, 1−302

[28] Y. Z. Voloshin, O. A. Varzatskii, T. E. Kron, V. K. Belsky, V. E. Zavodnik, N. G. Strizhakova, A. V. Palchik, *Inorg. Chem.* **2000**, *39*, 1907-1918. Contrary to the literature, elemental analysis suggested a molecular formula of $FeCl_2(MeCN)_{1.4}$ instead of $FeCl_2(MeCN)_4$.

[29] K. Costuas, F. Paul, L. Toupet, J.-F. Halet, C. Lapinte, *Organometallics* **2004**, *23*, 2053–2068.

[30] R. Birk, H. Berke, G. Huttner, L. Zsolnai, *Chem. Ber.* **1988**, *121*, 471–476.

[31] S. A. Stoian, Y. Yu, J. M. Smith, P. L. Holland, E. L. Bominaar, E. Münck, *Inorg. Chem.* **2005**, *44*, 4915–4922.

[32] Y. Yu, J. M. Smith, C. J. Flaschenriem, P. L. Holland, *Inorg. Chem.* **2006**, *45*, 5742–5751.

[33] D. Yang, S. Xu, Y. Zhang, Y. Li, Y. Li, B. Wang, J. Qu, *Inorg. Chem.* **2018**, *57*, 15198–15204.

[34] Y. Chen, L. Liu, Y. Peng, P. Chen, Y. Luo, J. Qu, *J. Am. Chem. Soc.* **2011**, *133*, 1147–1149.

[35] J. R. Cabrero-Antonino, A. Leyva-Pérez, A. Corma, *Chem. Eur. J.* **2012**, *18*, 11107–11114.

[36] A. Sagadevan, K. C. Hwang, *Adv. Synth. Catal.* **2012**, *354*, 3421-3427.

[37] T. Shida, *Electronic Absorption Spectra of Radical Ions*, Elsevier, Amsterdam, **1988**, pp. 159.

[38] G. Gamble, P. A. Grutsch, G. Ferraudi, C. Kutal, *Inorg. Chim. Acta* **1996**, *247*, 5–10.

[39] Y. Ohki, H. Sadohara, Y. Takikawa, K. Tatsumi, *Angew. Chem. Int. Ed.* **2004**, *43*, 2290–2293.

[40] V. Jakúbek, A. J. Lees, *Chem. Commun.* **1999**, 1631–1632.

[41] G. Pampaloni, *Coord. Chem. Rev.* **2010**, *254*, 402–419.

[42] D. R. Chrisope, K. M. Park, G. B. Schuster, *J. Am. Chem. Soc.* **1989**, *111*, 6195–6201.

[43] K. R. Mann, A. M. Blough, J. L. Schrenk, R. S. Koefod, D. A. Freedman, J. R. Matachek, *Pure Appl. Chem.* **1995**, *67*, 95–101.

[44] A. J. Lees, *Coord. Chem. Rev.* **2001**, *211*, 255–278.

[45] I. Fischler, E. A. Koerner von Gustorf, *Z. Naturforsch.* **1975***, 30b,* 291

[46] J. A. Widegren, R. G. Finke, *J. Mol. Cat. A* **2003**, *198*, 317-341.

[47] D. R. Anton, R. H. Crabtree, *Organometallics* **1983**, *2*, 855-859.

6 Appendix

6.1 List of abbreviations

Ac	acetyl
acac	acetylacetonate
APA	anthracenepropionate
Ar	aryl
ATR	attenuated total reflection
BA	biacetyl
Bn	benzyl
bpy	2,2'-bipyridine
Bu	butyl
CFL	compact fluorescent lightbulb
CT	charge transfer
CV	cyclic voltammetry
Cy	cyclohexyl
DABCO	1,4-diazabicyclo[2.2.2]octane
DBU	1,8-diazabicyclo[5.4.0]undec-7-ene
DCA	9,10-dicyanoanthracene
dct	dibenzo[*a*,*e*]cyclooctatetraene
DPA	9,10-diphenylanthracene
DFT	density functional theory
DIBAL-H	diisobutylaluminium hydride
DMA	*N*,*N*-dimethylaniline
DMF	*N*,*N*-dimethylformamide
DMSO	dimethylsulfoxide
DOI	digital object identifier
EI	electron impact
equiv.	equivalent
ESI	electron spray ionization
Et	ethyl
FcH	ferrocene
FDPP	furanyldiketopyrrolo-pyrrole
FID	flame ionization detector
FT-IR	Fourier-Transformed Infrared Spectroscopy
GC	gas chromatography
HAT	hydrogen atom transfer
HR-MS	high resolution mass spectroscopy
HOMO	highest occupied molecular orbital
***i*-Pr**	*iso*-propyl
ISC	intersystem crossing
LED	light emitting diode
LRMS	low resolution mass spectroscopy
LUMO	lowest unoccupied molecular orbital
MMA	methyl methacrylate

Me	methyl
NMP	*N*-methyl-2-pyrrolidone
NMR	nuclear magnetic resonance
PDI	perylenediimine
PET	photo-induced electron transfer
Ph	phenyl
ppm	parts per million
PPO	2,5-diphenyloxyzole
ppy	2-phenylpyridine
Pr	propyl
PtOEP	platinum(II)-octaethylporphyrin
PtTPBP	platinum(II)tetraphenyl-tetrabenzoporphyrin
PTZ	10-phenyl-10*H*-phenothiazine
py	pyridine
R	organic rest
r.t.	room temperature
SCE	standard calomel electrode
SDS	sodium dodecylsulfate
SET	single electron transfer
***t*-Bu**	*tert*-butyl
TEMPO	2,2,6,6-tetramethylpiperidine *N*-oxide
thf	tetrahydrofuran
TLC	Thin layer chromatography
TMS	trimethylsilyl
TOF	turnover frequency
***p*-TSA**	*para*-toluenesulfonic acid
TTA	triplet-triplet annihilation
TTET	triplet-triplet energy transfer
UC	upconversion
UV	ultraviolet radiation
VIS	visible radiation

6.2 Summary

The introductory chapter offers the reader a short overview about the history and most important concepts in photo(redox) catalysis.

In the second chapter, the recent advances of a young photoredox catalysis branch that makes use of multiple photon processes for synthetic organic chemistry are summarized in a review. The general concept of energy upconversion has been developed and investigated by physicists since decades. However, only over the last five years this approach found an echo in the synthetic chemistry community. Special attention is given to biphotonic catalyst activations such as triplet-triplet-annihilation (TTA) upconversion, consecutive photoinduced SET cascades and photoionizations.

Chapter three provides an efficient, convenient and mild methodology for the first photocatalytic aromatic chlorosulfonylation. The protocol features simple *in situ* formations of radical traps (SO_2 and HCl from $SOCl_2$ and H_2O) as well as the electrophile (diazonium salt from anilines), low catalyst loadings of commercial $Ru(bpy)_3Cl_2$, blue light irradiation and a wide functional group tolerance. Compared to the literature, our system distinguishes itself in a remarkable photostability of the generated arenesulfonyl chlorides. The proposed reaction mechanism is supported by DFT calculations and photochemical studies.

9,10-Dicyanoanthracene is introduced in chapter four as a simple, commercial and small organic dye for the mild activation of aryl halides under visible light irradiation. Absorption of a blue photon, followed by an electron transfer and absorption of a green photon affords $DCA^{\bullet-*}$. This excited doublet state lives long enough to transfer an electron to unactivated aryl-halides in order to generate an aryl radical. Various C-, S-, P- and B-nucleophiles are applied to this aromatic substitution reaction. Detailed spectroscopic investigations as well as DFT calculations corroborate a biphotonic mechanism in which the $DCA^{\bullet-*}$ acts as the reducing catalyst species.

Chapter five is devoted to the first metallaphotoredox protocol that employes a simple iron precursor ($FeCl_2$) in combination with a photoredox catalyst system for a synthetic application. In this ligand-free and light-gated arene assembly, cyclotrimerization reactions of terminal alkynes into the corresponding 1,2,4-trisubstituted benzenes are achieved under mild conditions and visible light irradiation. With no need for ligands, external reductants, expensive or toxic transition metals (Ir, Ni, etc.) this procedure is not only most user-friendly, but also highly sustainable compared to other protocols in this field. Additionally, detailed insights into the reaction mechanism via spectroscopy, kinetic monitorings and poisoning studies are provided.

6.3 Zusammenfassung

Das Einführungskapitel bietet dem Leser einen kurzen Überblick über die Geschichte und die wichtigsten Konzepte der Photo(redox)katalyse.

Im zweiten Kapitel sind die aktuellen Fortschritte eines jungen Teilgebiets der Photoredoxkatalyse, das sich mit der Verwendung von Mehrphotonenprozessen für die organische Synthesechemie beschäftigt, in einem Übersichtsartikel zusammengefasst. Das allgemeine Konzept der Energieaufkonversion wurde von Physikern schon vor Jahrzehnten entwickelt und untersucht. Allerdings fand dieser Ansatz erst über die letzten fünf Jahre hinweg Anklang in der synthetisch orientierten chemischen Gemeinde. Ein besonderer Fokus liegt hier auf biphotonischen Katalysatoraktivierungen, wie z.B. der Triplett-Triplett-Annihilierung (TTA), konsekutiven lichtinduzierten SET-Kaskaden und der Photoionisierung.

Kapitel drei stellt eine effiziente, praktische und milde Methode zur ersten photokatalytischen aromatischen Chlorosulfonylierung vor. Die Vorschrift umfasst die einfache *in situ* Erzeugung sowohl der Radikalfänger (SO_2 und HCl aus $SOCl_2$ und H_2O), als auch des Elektrophils (Diazoniumsalz aus Anilinen), geringere Katalysatorbeladung mit kommerziellem $Ru(bpy)_3Cl_2$, Belichtung mit blauem Licht und eine breite Funktionellegruppentoleranz. Im Vergleich zur Literatur zeichnet sich unser System durch die beachtliche Photostabilität der erzeugten aromatischen Sulfonylchloride aus. Der vorgeschlagene Reaktionsmechanismus wird durch DFT-Berechnungen und photochemische Studien unterstützt.

9,10-Dicyanoanthracen wird in Kapitel vier als einfacher, kommerzieller und kleiner organischer Farbstoff für eine milde Aktivierung von Arylhaliden unter Bestrahlung mit sichtbarem Licht vorgestellt. Absorption eines blauen Photons, gefolgt von einem Elektronentransfer und der Absorption eines grünen Photons erzeugt $DCA^{\bullet -*}$. Dieser angeregte Doublettzustand lebt lang genug, um ein Elektron auf nicht-aktivierte Aryl-Halide zu übertragen und so ein Arylradikal zu erzeugen. Verschiedene Nukleophile werden auf diese aromatische Substitutionsreaktion angewendet. Spektroskopische Untersuchungen, sowie DFT-Berechnungen untermauern einen biphotonischen Mechanismus in dem das $DCA^{\bullet -*}$ als reduzierende Katalysatorspezies agiert.

Kapitel fünf widmet sich dem erstem Metallaphotoredoxprotokoll, welches einen einfachen Eisen-Precursor ($FeCl_2$) in Kombination mit einem Photoredoxkatalysesystem für eine synthetische Anwendung verwendet. In dieser ligandfreien und lichtgesteuerten Aromatenherstellung werden Cyclotrimerisierungsreaktionen von terminalen Alkinen zu den entsprechenden 1,2,4-substituierten Benzolen unter milden Bedingungen und Bestrahlung mit sichtbarem Licht ermöglicht. Ohne Bedarf für Liganden, externe Reduktionsmittel, teure oder giftige Übergangsmetalle (Ir, Ni, etc.) ist diese Prozedur nicht nur äußerst anwenderfreundlich, sondern auch höchst nachhaltig im Vergleich zu anderen Vorschriften auf diesem Gebiet. Außerdem werden detaillierte Einblicke in den Reaktionsmechanismus durch Spektroskopie, Kinetisches Monitoring und Vergiftungstudien bereitgestellt.

6.4 Acknowledgements

In this section I would like to express my infinite gratitude to all the people that helped, assisted and supported me over this three year PhD period. Sincerest thanks to every single one of you! Danke!

An erster Stelle möchte ich mich bei Prof. Dr. Axel Jacobi von Wangelin für die Aufnahme in seine Gruppe, die interessante Themenstellung, die exzellente Betreuung und den immer sehr offenen Umgang bedanken. Die letzten Jahre in deiner Arbeitsgruppe waren mit Blick auf meine persönliche und wissenschaftliche Entwicklung eine große Bereicherung.

Dem Fonds der Chemischen Industrie danke ich für das Vertrauen und die finanzielle Unterstützung, die sie mir durch das Kekulé-Stipendium ermöglicht haben.

Prof. Dr. Julia Rehbein, Prof. Dr. Arno Pfitzner und Apl. Prof. Dr. Rainer Müller danke ich für die Übernahme des Zweitgutachtens, des Drittprüfers und des Kommissionsvorsitzes.

Mein herzlichster Dank geht natürlich an die zahlreichen Weggefährten der letzten Jahren - die aktuellen und ehemaligen Gruppenmitglieder:
Dr. Raúl Perez-Ruíz, Dr. Michal Májek, Dr. Matteo Villa, Dr. Tim Gieshoff, Dr. Efrain Reyes-Rodriguez and Dr. Davide Brenna vielen Dank für euere Hilfe, Unterstützung, Anleitung und natürlich die herausragende gemeinsame Zeit in Regensburg.
Erwähnen möchte ich hier auch die zwei besten Laborantinnen aus Regensburg Michaela Lutz und Veronika Scheidler.
Ich möchte mich besonders bei Patrick Bayer, Josef Bernauer, Bernhard Gregori, Sebastian Sandl, Dr. Dieter Schaarschmidt, Dr. Uttam Chakrabortry und Dr. Guojiao Wu für die unvergessene Zeit in Regensburg wie auch Hamburg bedanken. Der Umzug war für uns alle eine aufreibende Sache, aber ihr wart immer eine große Hilfe. Zusammen konnten wir zur rechten Zeit abschalten und ein bisschen Bayern in den hohen Norden einkehren lassen.
Vielen Dank auch an die neuen Leute in Hamburg, Matea Sršen, Javier Recío-Ramos, Luana Cardinale, Jennifer Börger, Andrey Fedulin, Dr. Pradip Gosh, Nils Nun, Kevin Schlüter, Christoph Alberti und Dr. Stephan Enthaler für die gemeinsame Zeit und die schönen Momente.

Zu guter Letzt, möchte ich im Speziellen meinen Eltern Josef und Rosa-Maria Neumeier und meiner Schwester Nicole Neumeier, sowie allen übrigen Familienmitgliedern für ihre unentwegte Unterstützung und das Vetrauen in und auf meinem Weg danken.

6.5 Curriculum vitae

Michael Neumeier

(Master of Science)

Personal Data

Date, Place of birth	May 8th, 1991 in Friedberg (Bavaria, Germany)
Nationality	German

Education

Since 02/2016	**Doctoral studies** in Organic Chemistry with Prof. Dr. Axel Jacobi von Wangelin at the University Regensburg (until 03/2018) and the University of Hamburg (since 04/2018) "Visible-light photoredox catalysis: a versatile tool for the activation and formation of aromatic compounds"
10/2013-09/2015	**Master of Science** in chemistry, TU Munich (**1.0**) "Anionic ring-opening polymerization of terpene-based lactams and characterization of novel oligoamide structures" (**1.0**) (with Prof. Dr. B. Rieger)
10/2010-09/2013	**Bachelor of Science** in chemistry, TU Munich (**1.7**) "Determination of the reversible absorption of CO_2 on polymer systems in a stirred tank reactor" (**1.0**) (with Prof. Dr. B. Rieger)
06/2010	Abitur, Rudolf-Diesel-Gymnasium Augsburg (**1.3**)

Fellowships and Memberships

Since 02/2016	Member of the graduate school “ChemPharm”, Regensburg
02/2016-03/2019	Member of the graduate school “Chemical Photocatalysis GRK 1626”, Regensburg
09/2016-08/2018	“Kekulé”-fellowship of the “Fonds der Chemischen Industrie”

List of publications

1) “Sustainable ligand-free iron-catalyzed visible light-gated photoredox cycloaddition”
M. Neumeier, U. Chakhraborty, D. Schaarschmidt, V. de la Pena O’Shea, R. Pérez-Ruíz, A. Jacobi von Wangelin, *manuscript submitted*.

2) “Electrochemiluminescence Bioassays can outperform Fluorescence Assays using a New Water-soluble Luminol Derivative”
M. Mayer, S. Takegami, M. Neumeier, S. Rink, A. Jacobi von Wangelin, S. Schulte, M. Vollmer, A. G. Griesbeck, A. Duerkop, A. J. Baeumner, *Angew. Chem. Int.*, **2018**, *57*, 408-411.

3) “Dichromatic Photocatalytic Substitutions of Aryl Halides with a Small Organic Dye”
M. Neumeier, D. Sampedro, M. Májek, V. de la Pena O’Shea, A. Jacobi von Wangelin, R. Pérez-Ruíz, *Chem. Eur. J.* **2018**, *24*, 105-108.

4) “Aromatic Chlorosulfonylation by Photoredox Catalysis“
M. Májek, M. Neumeier, A. Jacobi von Wangelin, *ChemSusChem* **2017**, *10*, 151-155.

5) “Sustainable Chiral Polyamides with High Melting Temperature via Enhanced Anionic Polymerization of a Menthone-Derived Lactam”
M. Winnacker, M. Neumeier, X. Zhang, C. M. Papadakis, B. Rieger, *Macromol. Rapid Commun.* **2016**, *37*, 851-857.

6) “New insights into synthesis and oligomerization of ε-lactams derived from the terpenoid ketone (−)-menthone”
M. Winnacker, A. Tischner, M. Neumeier, B. Rieger, *RSC Advances* **2015**, *5*, 77699-77705.

Presentations (Poster, Oral)

1) Posters: “Aromatic Chlorosulfonylation by Photoredox Catalysis” and “Overview of photocatalysis in the AJVW group” (special session of the GRK)
26th Lecture Conference on Photochemistry 2018 (GDCh), Jena (Germany)

2) Poster: “Aromatic substitutions of aryl halides enabled by dual photoactivation of 9,10-dicyanoanthracene”
Beistein Symposium on Photoredox Catalysis 2018, Potsdam (Germany)

3) Poster: “Aromatic substitutions of aryl halides enabled by dual photoactivation of 9,10-dicyanoanthracene”
GDCh-Wissenschaftsforum Chemie 2017, Berlin (Germany)

4) Poster: “Aromatic substitutions of aryl halides enabled by dual photoactivation of 9,10-dicyanoanthracene”
26th ISHC Congress 2017, Regensburg (Germany)

5) Oral communication: “Aromatic Chlorosulfonylation by Photoredox Catalysis”
ISOS 2017, “A. Corbella, Gargnano (Italy)

6) Poster: “Aromatic substitutions of aryl halides enabled by dual photoactivation of 9,10-dicyanoanthracene”
ISOS 2017, “A. Corbella”, Gargnano (Italy)

7) Lecture: “14 open doors”
“**Christmas Colloquium 2016**” of the Department of Organic Chemistry, Universität Regensburg (Germany)

8) Poster: “First Photoredox-Catalyzed Arene Chlorosulfonylation”
25th Lecture Conference on Photochemistry 2016 (GDCh), Jena (Germany)

9) Poster: “First Photoredox-Catalyzed Arene Chlorosulfonylation”
ORCHEM 2016 (GDCh), Weimar (Germany)

6.6 Eidesstattliche Erklärung

(1) Ich erkläre hiermit an Eides statt, dass ich die vorliegende Arbeit ohne unzulässiger Hilfe Dritter und ohne Benutzung anderer als der angegebenen Hilfsmittel angefertigt habe; die aus anderen Quellen direkt oder indirekt übernommenen Daten und Konzepte sind unter Angabe des Literaturzitats gekennzeichnet.

(2) Bei der Auswahl und Auswertung haben mir die in den jeweiligen Kapiteln aufgeführten Personen in der beschriebenen Art und Weise unentgeltlich geholfen.

(3) Weitere Personen waren an der inhaltlich-materiellen Herstellung der vorliegenden Arbeit nicht beteiligt. Insbesondere habe ich hierfür nicht die entgeltliche Hilfe eines Promotionsberaters oder anderer Personen in Anspruch genommen. Niemand hat von mir weder unmittelbar noch mittelbar geldwerte Leistungen für Arbeiten erhalten, die im Zusammenhang mit dem Inhalt der vorgelegten Dissertation stehen.

(4) Die Arbeit wurde bisher weder im In- noch im Ausland in gleicher oder ähnlicher Form einer anderen Prüfungsbehörde vorgelegt.

Regensburg, den .....